

MINERAL INCLUSIONS IN SAPPHIRE FROM BASALT -
RELATED DEPOSIT IN SOUTHERN VIETNAM



Mrs. Vu Doan Thi Anh

A Dissertation Submitted in Partial Fulfillment of the Requirements
for the Degree of Doctor of Philosophy in Geology
Department of Geology
FACULTY OF SCIENCE
Chulalongkorn University
Academic Year 2020
Copyright of Chulalongkorn University

มลทินแร่ในพลอยแซปไฟร์จากแหล่งที่สัมพันธ์กับหินบะซอลต์บริเวณเวียงคานมตอนใต้



วิทยานิพนธ์นี้เป็นส่วนหนึ่งของการศึกษาตามหลักสูตรปริญญาวิทยาศา
สตรดุษฎีบัณฑิต
สาขาวิชาธรณีวิทยา ภาควิชาธรณีวิทยา
คณะวิทยาศาสตร์ จุฬาลงกรณ์มหาวิทยาลัย
ปีการศึกษา 2563
ลิขสิทธิ์ของจุฬาลงกรณ์มหาวิทยาลัย

Thesis Title MINERAL INCLUSIONS IN SAPPHIRE FROM
 BASALT - RELATED DEPOSIT IN SOUTHERN
 VIETNAM
By Mrs. Vu Doan Thi Anh
Field of Study Geology
Thesis Advisor Professor Doctor CHAKKAPHAN SUTTHIRAT
Thesis Co Advisor Doctor ABHISIT SALAM

Accepted by the FACULTY OF SCIENCE, Chulalongkorn University in
Partial Fulfillment of the Requirement for the Doctor of Philosophy

..... Dean of the FACULTY OF
 SCIENCE
(Professor Doctor POLKIT SANGVANICH)

DISSERTATION COMMITTEE

..... Chairman
(Assistant Professor VICHAI CHUTAKOSITKANON)
..... Thesis Advisor
(Professor Doctor CHAKKAPHAN SUTTHIRAT)
..... Thesis Co-Advisor
(Doctor ABHISIT SALAM)
..... Examiner
(Assistant Professor PITSANUPONG
KANJANAPAYONT)
..... Examiner
(Associate Professor PIYAPHONG CHENRAI)
..... External Examiner
(Assistant Professor Somruedee Satitkune)

CHULALONGKORN UNIVERSITY

ว โด น ธิ อ น ्ह :

ม ล ทิน แร่ ใน พ ลอย แชนป์ ไฟร์ จาก แหล่ง ที่ สัม พันธ์ กับ หิน บะซอลต์ บริเวณ เวียดนาม ตอน
ใต้. (MINERAL INCLUSIONS IN SAPPHIRE FROM BASALT -
RELATED DEPOSIT IN SOUTHERN VIETNAM) อ. ที่ ป รึกษา ห ลั ก :
จักรพันธ์ สุทธิรัตน์, อ. ที่ ป รึกษา ร่ว ม : อภิสหิ ชาล ำ

พ ลอย แชนป์ ไฟร์ จาก ประเทศ เวียดนาม ตอน ใต้ ใน แหล่ง สะสม ตัว แบบ ตะกอน น้ำ ฟัด ผุ พัง
มา จาก หิน บะซอลต์ ใน ช่วง มหา ยุค ซี โน โซ อิก
ในการ ศึกษา ใน ครั้ง นี้ เก็บ มา จาก แหล่ง พ ลอย ที่ สำคัญ ประกอบ ด้วย แหล่ง ครอง น้ ง แหล่ง เพลี้ย คุ
แหล่ง ดัก นอง แหล่ง ดิลิน ฮ์ แหล่ง บิน ฮ์ ธวน แร่ ม ล ทิน ที่ พบ ใน ตัวอย่าง พ ลอย แชนป์ ไฟร์ ใต้ แก
อัลคาไล เฟลด์สปาร์ เซอร์คอน เพอร์โรโคสไมท์ ไพโรคลอร์ และ แร่ เหล็ก ออกไซด์
ลักษณะ ทาง เคมี แร่ ของ ม ล ทิน เหล่า นี้ บ่ง ชี้ วิวัฒนาการ จาก กลุ่ม หิน หนืด อัลคาไลน์ เฟลสิก

แร่ ออกไซด์ ชนิด ต่าง ๆ ใต้ แก แร่ เฮอไรไซไนต์ แร่ วัสไซต์
และ แร่ อิลเมไนต์ โดย แร่ อิลเมไนต์ มี สัดส่วน ของ องค์ ประกอบ ระหว่าง $\text{Il}_{49-54}\text{He}_{34-40}\text{Mt}_{7-10}$ และ
 $\text{Il}_{24-30}\text{He}_{36-38}\text{Mt}_{35-40}$ ต ก อ ยู่ ใน ชุด อิลเมไนต์-ฮีมาไทต์
สำหรับ แร่ วัสไซต์ พบ มี องค์ ประกอบ ใน ปริมาณ ไม่ สัม พันธ์ ดัง นี้
 $(\text{Fe}^{2+}_{0.3-0.9})(\text{Ti}^{3+}_{<0.179}\text{Al}^{3+}_{\leq 0.6}\text{Cr}^{3+}_{<0.1}\text{Fe}^{3+}_{\leq 0.46})\text{E}_{\leq 0.23}\text{O}$ มัก พบ ร่ว ม กับ แร่ เฮอไรไซไนต์
ซึ่ง บ่ง ชี้ ก ำ ร เ กิ ด ร่ว ม กับ แชนป์ ไฟร์
ซึ่ง แร่ วัสไซต์ และ แชนป์ ไฟร์ น่า จะ เกิด จาก ปฏิกิริยา สลาย ตัว ของ แร่ เฮอไรไซไนต์ (เฮอไรไซไนต์ =
แชนป์ ไฟร์ + วัสไซต์) จาก ก ำ ร ศึ ก ษา ยั ง พบ ว่า
ชุด แร่ ไทเทโนฮีมาไทต์ และ ชุด แร่ ไทเทโนแมกนีไทต์ ควร ต ก ผลิ ก ใน ช่วง การ ป รื บ ส ม ด ล ของ ธาตุ
เหล็ก และ ไทเทเนียม แบบ แยก ส่วน ใน สภาวะ ของ แข็ง

การหาอายุ ด้วย เทคนิค ยูเรเนียม-ตะกั่ว จาก แร่ ม ล ทิน เซอร์คอน ใน ตัวอย่าง แชนป์ ไฟร์
ได้ อายุ อยู่ ใน ช่วง 35.5 ± 1.6 ล้านปี (ประมาณ 35 ล้านปี) ถึง 14.73 ± 0.29 ล้านปี (ประมาณ
15 ล้านปี) สำหรับ แชนป์ ไฟร์ จาก แหล่ง ครอง น้ ง 5.94 ± 0.13 ล้านปี (ประมาณ 6 ล้านปี)
สำหรับ แชนป์ ไฟร์ จาก แหล่ง บิน ฮ์ ธวน และ แหล่ง ดัก นอง และ 5.491 ± 0.077 ล้านปี
สำหรับ แชนป์ ไฟร์ จาก แหล่ง ดิลิน ฮ์
ซึ่ง อายุ เหล่า นี้ สัม พันธ์ กับ ช่วง เวลา การ ป ระ ห ลั ก ของ หิน บะซอลต์ ใน ยุค ซี โน โซ อิก ใน ภูมิภาค นี้
ซึ่ง มี อุ น ห ภู มิ ใน ก ำ ร ต ก ผลิ ก อ ยู่ ที่ 561 ถึง 781
องศาเซลเซียส จากการ ค ำ นวณ โดย ใช้ ปริมาณ ไทเทเนียม ใน เซอร์คอน

สาขาวิชา ธรณีวิทยา

ลายมือชื่อนิสิต

ปีการศึกษา 2563

.....
ลายมือชื่อ อ.ที่ปรึกษาหลัก

๑

.....
ลายมือชื่อ อ.ที่ปรึกษาร่วม

.....

5972893123 : MAJOR GEOLOGY

KEYWOR Alkaline basalt, mineral inclusion, wüstite, sapphire, U-Pb zircon
D:

Vu Doan Thi Anh : MINERAL INCLUSIONS IN SAPPHIRE FROM
BASALT - RELATED DEPOSIT IN SOUTHERN VIETNAM. Advisor:
Prof. Dr. CHAKKAPHAN SUTTHIRAT Co-advisor: Dr. ABHISIT
SALAM

Sapphires in Southern Vietnam have been discovered in alluvial deposit derived from Cenozoic basalts. Sample collections for this study were taken from the most significant gem fields including Pleiku, Dak Nong, Di Linh, Binh Thuan, and Krong Nang. Several syngenetic mineral inclusions in these sapphires were classified as alkali feldspar, zircon, ferrocolumbite, pyrochlore, and iron oxides. Mineral chemical characteristics of these inclusions appeared to have evolved from alkaline felsic suite.

Oxide mineral inclusions occurred in sapphire included hercynite, wüstite, and ilmenite. Ilmenite ranged in composition between $\text{Il}_{49-54}\text{He}_{34-40}\text{Mt}_{7-10}$ and $\text{Il}_{24-30}\text{He}_{36-38}\text{Mt}_{35-40}$ falling in ilmenite-hematite series. Wüstite with nonstoichiometry, $(\text{Fe}^{2+}_{0.3-0.9})(\text{Ti}^{3+}_{<0.179}\text{Al}^{3+}_{\leq 0.6}\text{Cr}^{3+}_{<0.1}\text{Fe}^{3+}_{\leq 0.46})_{\leq 0.23}\text{O}$, was usually associated with hercynite inclusion clearly indicating cogenetic sapphire formation. Wüstite and sapphire appeared to have formed from the breakdown reaction of hercynite (hercynite = sapphire+wüstite). Titanohematite series and titanomagnetite series might have crystallized during iron-titanium reequilibration via subsolidus exsolution.

U-Pb geochronology of zircon inclusion in these sapphires yielded between 35.5 ± 1.6 Ma (~35 Ma) and 14.73 ± 0.29 Ma (~15 Ma) for Krong Nang sapphire, 5.94 ± 0.13 Ma (~6 Ma) for Binh Thuan and Dak Nong sapphire, and 5.491 ± 0.077 Ma (~5.5 Ma) for Di Linh sapphire. These age constraints relate to the main Cenozoic basaltic eruptions in this region. Crystallization temperature of sapphire formation was estimated at about 561- 781⁰C using Ti-in-zircon thermometry.

Field of Study: Geology

Student's Signature

Academic 2020

.....
Advisor's Signature

Year:

.....
Co-advisor's Signature

.....

ACKNOWLEDGEMENTS

I would like to express deep gratitude to my advisors, Professor Dr. Chakkaphan Sutthirat and Dr. Abhisit Salam, for their generous support and scientific contribution leading to the completion of this thesis.

I am truly grateful to Associate Professor Dr. Pisanupong Kanjanapayont and Assistant Professor Dr. Piyapong Chenrai, thesis committee, who have handled thesis defense as well as Assistant Professor Dr. Somruedee Sakkaravej kindly served as external committee.

Special thanks are sincerely delivered to all staff members of the Geology Department, Faculty of Science, Chulalongkorn University for their assistances, particularly Miss Sopit Poompuang for EPMA analysis. The Gem and Jewelry Institute of Thailand (Public Organization), GIT, has provided basic equipment and advanced analytical instruments such as the gemological microscope, Laser Raman Spectroscopy, Fourier Transform spectrophotometer (FTIR), and UV-Vis-NIR spectrophotometer during this research project. Associate Professor Dr. Elena Belousova, Macquarie University, Sydney, Australia facilitated in Laser Ablation-Inductively Coupled Plasma Mass-Spectrometry (LA-ICP-MS) of trace element analysis and U-Pb dating of zircon inclusion.

This dissertation would not be possible without the Scholarship Program for ASIAN Countries of Chulalongkorn University.

Last but not least, I must thank my parents (Mr. Doan Dai Tien and Mrs. Tran Thi An), husband (Mr. Nguyen Vu Thien), and son (Doan Thien Tam) who have encouraged during my PhD study.

Vu Doan Thi Anh

TABLE OF CONTENTS

	Page
.....	iii
ABSTRACT (THAI)	iii
.....	iv
ABSTRACT (ENGLISH).....	iv
ACKNOWLEDGEMENTS	v
TABLE OF CONTENTS.....	vi
LIST OF TABLES	ix
LIST OF FIGURES	xi
CHAPTER 1 INTRODUCTION.....	1
1.1 Background	1
1.2 Objectives.....	2
1.3 Brief Literature Reviews.....	2
1.4 Organization of Result and Chapter	4
CHAPTER 2 MINERAL INCLUSIONS IN SAPPHIRE FROM BASALTIC TERRANES IN SOUTHERN VIETNAM: INDICATOR OF ORIGINAL FORMATION.....	7
2.1 Introduction	7
2.2 Geological setting	10
2.3 Materials and Methods.....	10
2.4 Results.....	11
2.4.1 Columbite inclusion.....	13
2.4.2. Zircon inclusion.....	16
2.4.3 Alkali feldspar inclusion	17
2.4.4 Spinel inclusion	19
2.2.5 Ilmenite inclusion	19
2.4.6 Unidentified iron-bearing mineral inclusions.....	20

2.4.7 Pyrochlore inclusion	21
2.5 Disussion	27
2.6 Conclusions	28
CHAPTER 3 VARIETY OF IRON OXIDE INCLUSIONS IN SAPPHIRE FROM SOUTHERN VIETNAM: INDICATION OF ENVIRONMENTAL CHANGE DURING CRYSTALLIZATION.....	30
3.1 Introduction	30
3.2 Geological setting	30
3.3 Materials and methods	32
3.4 Results	32
3.4.1 Morphology of iron oxide inclusions.....	32
3.4.2 Raman spectroscopy of iron oxide inclusions	33
3.4.3 Mineral chemistry of iron oxide inclusions.....	42
3.5 Discussion	44
3.6 Conclusion.....	45
CHAPTER 4 TRACE ELEMENT GEOCHEMISTRY AND U-Pb DATING OF ZIRCON INCLUSIONS IN SAPPHIRES FROM SOUTHERN VIETNAM	47
4.1 Introduction	47
4.2 Geological setting	47
4.3 Material and methods.....	48
4.4 Results.....	50
4.4.1 Crystal habit and morphology	50
4.4.2 Mineral chemistry	52
4.4.3 Ti-in Zircon Thermometer	59
4.4.4 U-Pb dating.....	59
4.5 Discussion	60
4.5.1 Sequences of sapphire/zircon crystallization and basaltic eruption.	60
4.5.2 Original sapphire formation	61
4.6 Conclusion.....	68
CHAPTER 5 CONCLUSION.....	70

APPENDIX A RAMAN SPECTRUMS OF MINERAL INCLUSIONS	71
APPENDIX B BACK SCATTERED ELECTRON (BSE) IMAGES OF MINERAL INCLUSIONS	120
APPENDIX C EPMA DATA	141
APPENDIX D TRACE ELEMENT DATA OF ZIRCON INCLUSIONS	165
REFERENCES.....	169
VITA.....	179



จุฬาลงกรณ์มหาวิทยาลัย
CHULALONGKORN UNIVERSITY

LIST OF TABLES

Table 2.1 Summary of mineral inclusions found in sapphire from Southern Vietnam, compared to those reported from basaltic gem fields at Southeast Asia....	13
Table 2.2 Representative EPMA analyses of columbite inclusions found in sapphires from Southern Vietnam, Thailand, and Australia.....	15
Table 2.3 Representative EPMA analyses of zircon inclusions found in sapphires from Southern Vietnam, Laos, Thailand, and Australia.....	18
Table 2.4 REE analyses (ppm) of some zircons found in sapphire from Southern Vietnam	19
Table 2.5 Representative EPMA analyses of feldspar inclusions in sapphires from Southern Vietnam, Laos, Thailand, and Australia.....	22
Table 2.6 Representative EPMA analyses of spinel inclusions in sapphires from Southern Vietnam, Laos, Thailand, and Australia.....	23
Table 2.7 Representative EPMA analyses of ilmenite inclusions in sapphires from Southern Vietnam, Thailand, and Australia	24
Table 2.8 Representative EPMA analyses of unidentified iron-rich inclusions in sapphires from Southern Vietnam.....	25
Table 2.9 Representative EPMA analyses of pyrochlore inclusions in sapphires from Southern Vietnam	26
Table 3.1 Representative EPMA analyses of wüstite inclusions in sapphires from Southern Vietnam	39
Table 3.2 Representative EPMA analyses of spinel inclusions in sapphire from Southern Vietnam	40
Table 3.3 Representative EPMA analyses of ilmenite inclusions in sapphire from Southern Vietnam	41
Table 4.1 Representative EPMA analyses of zircon inclusions found in sapphire from Southern Vietnam	52
Table 4.2 Trace element contents (ppm) of zircons found in sapphire from Southern Vietnam compared with those reported from Southeast Asia basaltic gem fields and various sources.....	56

Table 4.3 Ti-in-zircon temperatures for zircon inclusions in sapphire from Southern Vietnam	62
Table 4.4 Summary of U-Pb dating results of the zircon inclusions in sapphire from Southern Vietnam	63
Table 4.5 Geochronological scale with respect to radiometric dating of basalts and mineral zircon inclusion found in sapphire from Southern Vietnam, compared with zircon and other in sapphire from Southeast Asia.....	65



LIST OF FIGURES

- Figure 1.1 Distribution of sapphire placers in Southern Vietnam (Modified from Izokh et al., 2010; Vu, 2018)..... 2
- Figure 2.1 High quality sapphires from Southern Vietnam: (left photo) intense blue sapphires (about 2 to 3 cts each stone) from Di Linh set in ear-rings; (right photo) a pendant with nearly 24 cts yellow sapphire surrounded by small bluish-green sapphires (<1 ct each) from Binh Thuan. These sapphires were heated to improve their colors. Photos by Doan Thi Anh Vu. 7
- Figure 2.2 Map of Vietnam showing distribution of Cenozoic basalts and main sapphire mining areas in Southern Vietnam; modified after Anh et al. (2018), Lepvrier et al. (2008), and Hoa et al. (2005). 8
- Figure 2.3 Artisanal miners used crowbars and shovels to remove topsoil and dig through the gem-bearing layer in Binh Thuan gem field (left). Gem-bearing gravels were washed and sieved along the local stream in Dak Nong gem field (right). Photos by Doan Thi Anh Vu..... 9
- Figure 2.4 Backhoe was used in a machinery mine to remove topsoil and reach the gem-bearing gravel layers prior to washing and dressing using water pump in Binh Thuan gem field (left) and Krong Nang gem field (right). Photos by Doan Thi Anh Vu..... 9
- Figure 2.5 Trapiche sapphires, about 10 cts (left) and 9cts (right), from Binh Thuan gem field. Photo by Doan Thi Anh Vu. 9
- Figure 2.6 Typical internal features observed in sapphire from Southern Vietnam: **(a)** strong color zones; **(b)** needle-like inclusions; **(c)** liquid-filled inclusions; **(d)** negative crystals situated in healed fractures; all photos were taken in darkfield illumination. Photos by Doan Thi Anh Vu..... 12
- Figure 2.7 **(a)** a bigger prismatic columbite inclusion; **(b)** two truncated-rhombic columbite inclusions surrounded by healed fractures; **(c)** cluster of several tiny columbites with colorless feldspar and zircon inclusions; they were observed in darkfield illumination. Photos by Doan Thi Anh Vu..... 14
- Figure 2.8 Quadrilateral compositional plots show ferrocolumbite inclusion found in sapphires from Southern Vietnam. Various compositional fields and

columbite–tapiolite miscibility gap were proposed by Černý and Ercit (1985).	14
Figure 2.9 Photomicrographs showing: (a) prismatic orange zircon inclusion; (b) colorless dipyramidal zircon inclusion surrounded by radial cracks, associated with black columbite inclusions; (c) tiny euhedral feldspar inclusions; All photos were taken in darkfield illumination by Doan Thi Anh Vu.	16
Figure 2.10 Ternary An-Ab-Or plots of alkali feldspar inclusions in the sapphires from Southern Vietnam.	17
Figure 2.11 Photomicrographs were taken in darkfield illumination by Doan Thi Anh Vu showing: (a) black octahedral hercynite spinel inclusion and (b) euhedral rhombohedral ilmenite inclusion.	20
Figure 2.12 (a) several tiny unidentified iron oxides with cubic shape; photo was taken in darkfield illumination by Doan Thi Anh Vu. (b) black scattered electron image of unidentified cubic iron oxides and euhedral hercynite-spinel.....	21
Figure 2.13 A red cubic pyrochlore inclusion displaying halo and radial cracks; darkfield illumination by Doan Thi Anh Vu.	21
Figure 2.14 The model for sapphire origin alkaline felsic melt, based on the alkaline basalt and crust growth models for Southern Vietnam (Anh et al., 2018; Hoang and Flower, 1998; Tri and Khuc, 2011).	29
Figure 3.1 This geological map shows distribution of Cenozoic basalts and locations of sapphire occurrences in Southern Vietnam, modified after Hoa et al., (2005).	31
Figure 3.2 Photomicrographs showing: (a) a small octahedral wüstite inclusion; (b) a bigger octahedral hercynite inclusion; (c) aggregate crystals of octahedral wüstite inclusions, and (d) aggregate crystals of octahedral hercynite inclusions. They were observed in darkfield illumination. Photo by Doan Thi Anh Vu.	35
Figure 3.3 Photomicrographs of rhombohedral hematite-ilmenite inclusions found in sapphires from Southern Vietnam: (a) a single crystal and (b) several single crystals. All photos were taken in darkfield illumination by Doan Thi Anh Vu.	35

Figure 3.4 Raman spectra of wüstite in laser power at 0.5 mW (a) and 5 mW (b and c)	36
Figure 3.5 Raman spectra of hercynite spinel: 0.5 mW (a) and 5 mW (b)	37
Figure 3.6 Raman spectra of ilmenite: 0.5 mW (a) and 5 mW (b)	38
Figure 3.7 Spinel compositions in sapphires from southern Vietnam are plotted on the Spinel-Hercynite-Magnetite diagram. This diagram is taken from Haggerty (1991).	42
Figure 3.8 Black scattered electron image (BSI) of hercynite and wüstite inclusions found in sapphires from Southern Vietnam: (a) Raman, (b) EPMA.	43
Figure 3.9 Chemical composition of ilmenite-hematite inclusions in sapphire from Southern Vietnam, represented on a FeO-Fe ₂ O ₃ -TiO ₂ diagram. The diagram is taken from Buggington and Lindsley (1964).	43
Figure 4.1 Map showing the distribution and ages of Cenozoic basalt in Southeast Asia; dating data in Thailand from modified after Barr and MacDonald, (1981); dating data in Cambodia modified after Sutherland et al., (2015b); dating data in Vietnam from (1998), Hoang et al., (2013), and (2005).	50
Figure 4.2 Zircon inclusions in sapphire from Southern Vietnam shows the forms of prism {110} plus pyramid {101} or dipyrmaid {101}. (a) G ₁ type of red- orange zircon inclusion. (b) G ₃ type of small colorless zircon inclusion. (c) L ₅ type of colorless zircon inclusion. (d) P ₁ type of colorless zircon inclusion. (e) S ₅ type of colorless zircon inclusion. (f) S ₇ type of colorless zircon inclusion.	51
Figure 4.3 Cathodoluminescence images of zircon from Southern Vietnam showing both oscillatory and sector zonation: concentric zoning (a) , sector and concentric zoning (b, c, and d) , and sector zoning (e and f)	53
Figure 4.4 The Y-U plots of zircon inclusions in sapphire from Southern Vietnam (data from Belousova et al., 2002).	57
Figure 4.5 The Y-Nb/Ta plots of zircon inclusions in sapphire from Southern Vietnam (data from Belousova et al., 2002).	57
Figure 4.6. The Y-U/Yb plots of zircon inclusions in sapphire from Southern Vietnam (data from Grimes et al., 2007).	58

- Figure 4.7 Chondrite-normalized REE patterns (chondrite's data from Taylor and McLennan, 1985) of studied zircons compared with patterns of zircon from various rocks (data from Belousova et al., 2002). 58
- Figure 4.8 Mean weight diagrams for zircons in sapphire from Southern Vietnam. These red vertical columns represent individual $^{206}\text{Pb}/^{238}\text{U}$ ages in Ma with their associated uncertainty; the green horizontal line is the calculated mean age for these values. 64
- Figure 4.9 Genetic model of sapphire from Southern Vietnam based on mineral chemistry and chronological data of zircon inclusion described in the study. 69



CHAPTER 1

INTRODUCTION

1.1 Background

Sapphires in secondary gem deposits have been reported in association with Late Cenozoic basalts in Australia, China, and Southeast Asia regions, such as New South Wales and Queensland in Australia (Coldham, 1985), Fujian in China (Keller and Keller, 1986), Chanthaburi-Trat in Thailand (Keller, 1982); Pailin in Cambodia (Jobbins and Berrangé, 1981); Ban Huai Sai in Laos (Bosshart, 1995). In Southern Vietnam, the main basaltic sapphire deposits have been discovered in Dak Nong, Di Linh, Binh Thuan, Krong Nang, and Pleiku (Figure. 1.1) (Garnier et al., 2005; Izokh et al., 2010; Long et al., 2004; Smith et al., 1995; Vu, 2010; 2018). These sapphires appear to be xenocrysts in alkaline basalts. They are unlikely to direct crystallization from the basalt magma, but the magma transported these sapphires and associated materials to the surface (Barr and MacDonald, 1981; Garnier et al., 2005; Izokh et al., 2010; Levinson and Cook, 1994; Smith et al., 1995). However, understanding of initial sapphire formation has been still unclearly recognized. General gemological techniques with carefully visual observation to identify growth features, inclusions, and other properties (such as color, specific gravity, and refractive indexes) may not be sufficient to determine the original sapphire formation. Mineral chemical analyses should provide significant information for this aspect. The study of inclusions in sapphire has become more concern since the last decade because these inclusions may preserve the valuable information of the chemical environment, physical condition and perhaps leading to a geological process that related to the initial formation of host sapphire.

Therefore, this study is focused on a wide range of mineral inclusions found in sapphire from the basalt-related deposit in Southern Vietnam, including Dak Nong, Di Linh, Binh Thuan, Krong Nang, and Pleiku deposits. They may yield crucial information leading to the interpretation of the genesis and age of sapphire formation.

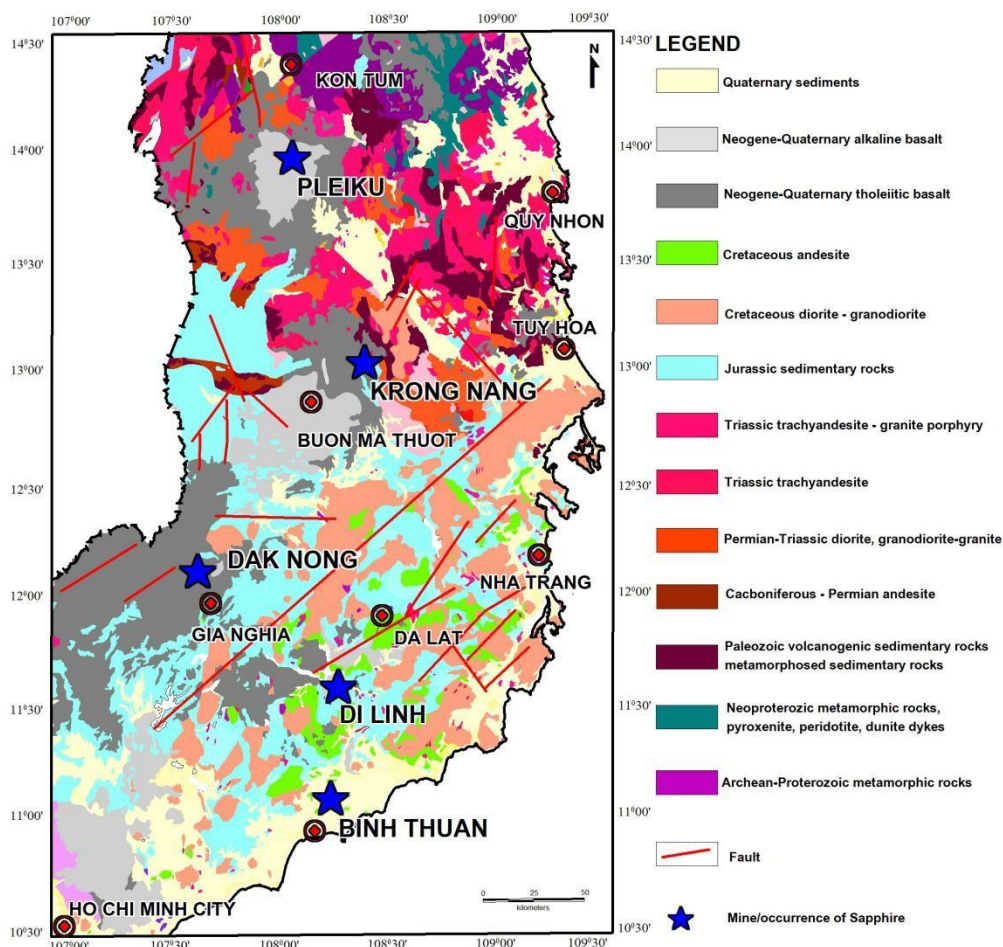


Figure 1.1 Distribution of sapphire placers in Southern Vietnam (Modified from Izokh et al., 2010; Vu, 2018)

1.2 Objectives

The main aim of this study is focused on mineral chemistry of inclusions, and U-Pb zircon geochronology of sapphires in Southern Vietnam, comprising Dak Nong, Di Linh, Binh Thuan, Krong Nang, and Pleiku.

1.3 Brief Literature Reviews

The early studies related to basaltic sapphire in Southern Vietnam were focused on basaltic rocks, xenoliths, and xenocrysts embedded in basaltic hosts (Anh et al., 2018; Hoang and Flower, 1998; 2013), hence understanding of the initial formation of sapphire remains surmises. In the jewelry industry, the origin determination of sapphire has become very important, recently; therefore, some investigators have worked on surface features and gemological characteristics of sapphire associated with basalts.

They believed that alkali basalts carried sapphires from their initial provenances to the earth's surface (Coenraads, 1992; Garnier et al., 2005; Smith et al., 1995). Alkali basalts and similar rocks are meta-aluminous to sub-aluminous which sapphire cannot crystallize directly from these magmas. Besides, sapphire-bearing xenoliths were seldom found in some gem fields, they contain important mineral assemblages of original sapphire formation. Recently, many researchers have been studied the genetic model of basaltic sapphire worldwide based on their mineral inclusions (Guo et al., 1996b; Khamloet et al., 2014; Sutherland et al., 1998a) because these inclusions provide valuable information of physical condition and chemical environment which lead to an interpretation of geological process and sapphire formation (Gübelin, 1983).

Mineral chemistry of inclusion found in sapphire has led to several genetic models which have been proposed as the initial formation of basaltic sapphires. For example, a cobalt-rich spinel inclusion was determined by Guo et al. (1994) and then they suggested a complex magma mixing process in the lower crust for the sapphire origin from Bo Ploi, Thailand. Subsequently, many types of mineral inclusion were published by Khamloet et al. (2014), genetic model was clearly reconstructed for the sapphire formation of the same area as a combination between felsic alkaline inclusion formation (e.g., feldspar, nepheline, zircon, manganiferous ilmenite, and monazite) and contact-metamorphic inclusion formation (e.g., Si-rich enstatite, almandine-pyrope garnet, sapphirine, staurolite, and biotite-phlogopite mica). For basaltic sapphires in Australia, Guo et al. (1996c) reported a carbonatitic inclusion group (i.e., titaniferous columbite, uranpyrochlore, and fersmite) combined with an alkaline felsic inclusion group (e.g., alkali feldspar, low-Ca plagioclase, zircon, uraninite, and ilmenorutile) and consequently proposed a genetic model related to interactions of carbonatitic magmas with alkaline felsic rocks. Besides, Sutherland et al. (1998a) presented a silica melt origin, based on inclusion suit (including feldspar, zircon, columbite, hercynite-magnetite, gahnospinel, rutile-ilmenite, and Ca-plagioclase).

Mineral inclusions also can provide temperature conditions for the crystallization of basaltic sapphires. Occurrences of co-existing albite and K-feldspar inclusion gave a minimum exsolution temperature of 400 °C for this inclusion and host corundum (sapphire) in New England (Guo et al., 1996b). Sutherland et al. (1998a) used mineral inclusions such as hercynite-magnetite and feldspar to estimate the

temperature about 685-900 °C for the formation of corundum (sapphire) from New England and Australia. The temperature between 860 and 1000 °C was suggested for basaltic sapphires from Den Chai and Bang Kha Cha, Thailand, based on sanidine and iron-rich spinel inclusions (Saminpanya and Sutherland, 2011) whereas a temperature < 700 °C was proposed for Bo Ploi sapphires from Thailand due to cobalt-rich spinel inclusion (Guo et al., 1994).

Therefore, mineral chemistry of inclusions in basaltic sapphires from Southern Vietnam is necessary to provide information about the genesis and geochronology of the original sapphire formation. This information can also support the gem and jewelry industry in the aspect of origin determination and certification.

1.4 Organization of Result and Chapter

The results of this study were grouped into three main aspects and then prepared as manuscript template which are ready to be submitted in international journals. Moreover, all analytical results are fully reported in the Appendices. Raman spectra of mineral inclusions are described in Appendix A. Back scattered electron (BSE) images of mineral inclusions are shown in Appendix B. Electron Probe Micro-Analyses (EPMA) of mineral inclusions and sapphires are collected in Appendix C. Trace element data of zircon inclusions are listed in Appendix D. The main results and discussions are arranged and presented in the drafts of three manuscripts as reported in Chapters 2 to 4. Specific finding in some aspect is concluded in Chapter 5.

Chapter 2: Mineral inclusions in sapphire from basaltic terranes in Southern Vietnam: indicator of original formation

Results summary: Sapphires in Southern Vietnam have been discovered in alluvial gem fields derived from Cenozoic basalts. Several syngenetic mineral inclusions were identified by Raman spectroscopy and Electron Probe Micro-Analyzer (EPMA); consequently, they were classified as ferrocolumbite, zircon, alkali feldspar (albite-anorthoclase-oligoclase), pyrochlore, hercynite spinel, and ilmenite (titano hematite series). Geochemical characteristics of these inclusions appear to have evolved from an alkaline felsic suite. Consequently, the original formation of these sapphires should have been related to the alkaline felsic magmatic process before basaltic magma, which was derived from the deeper upper mantle, had passed through

and transported sapphires and their associated minerals onto the surface via a volcanic eruption.

Status: Some information of this manuscript was present in the 15th Asia Oceania Geosciences Society. The revised manuscript was resubmitted to Gem and Gemology which is under reviewing process.

Chapter 3: Variety of iron oxides inclusions in sapphire from Southern Vietnam: indication of environmental change during crystallization

Results summary: In this report, syngenetic iron oxide inclusions with various compositions were focused on detailed mineral chemistry using Raman Spectroscopy and Electron Probe Micro-Analyzer. Consequently, varieties of iron oxide inclusions were recognized as wüstite, hercynite, and ilmenite. Ilmenite ranged between $\text{Il}_{49-54}\text{He}_{34-40}\text{Mt}_{7-10}$ and $\text{Il}_{24-30}\text{He}_{36-38}\text{Mt}_{35-40}$ falling in ilmenite-hematite series. Wüstite with nonstoichiometry, $(\text{Fe}^{2+}_{0.3-0.9})(\text{Ti}^{3+}_{<0.179}\text{Al}^{3+}_{\leq 0.6}\text{Cr}^{3+}_{<0.1}\text{Fe}^{3+}_{\leq 0.46})\square_{\leq 0.23}\text{O}$, is usually associated with hercynite inclusion clearly indicating cogenetic sapphire formation. Wüstite and sapphire appear to have formed from the breakdown reaction of hercynite (hercynite = sapphire+wüstite). Titanohematite series and titanomagnetite series might have crystallized during iron-titanium re-equilibration via subsolidus exsolution.

Status: This manuscript was submitted to Journal of Minerals which is now reviewing for publication in a special issue: Fluid, Melt and Solid Inclusions as Petrogenetic Indicators.

Chapter 4: Trace element geochemistry and U-Pb dating of zircon inclusion in sapphire from Southern Vietnam

Results summary: Trace element geochemistry of zircon inclusion in sapphire from Southern Vietnam shows a large variation of Hf (18200-34100 ppm), Y (779-4220 ppm), Th (329-5199 ppm), U (224-3587 ppm), and REE (705-2710 ppm) with positive Ce and negative Eu-anomalies observed in chondrite-normalized REE patterns. They indicate the majority of the host sapphires appear to have crystallized in an environment related to alkaline felsic melt at the lower crust. U-Pb zircon datings yields the ages ranging between 35.5 ± 1.6 Ma (~35 Ma) and 14.73 ± 0.29 Ma (~15 Ma) for Krong Nang sapphire, 5.94 ± 0.13 Ma (~6 Ma) for Binh Thuan sapphire, 5.598 ± 0.074 Ma for Dak Nong sapphire, and 5.491 ± 0.077 Ma for Di Linh sapphire which most of

them, except the Krong Nang sapphire, fall within the same period of the alkali-basalt eruptions in Southern Vietnam ($\leq 5\text{Ma}$). Hence, crystallization of sapphire could have occurred in the same thermal process when partial melting in both asthenosphere and a lower crust which the crustal basement appears significantly to have been occupied by late Eocene and Oligocene-Pleistocene granitoid rocks. Partial melting of the lower crust forming alkaline felsic melts led to the original formation of sapphire as well as basaltic melt extensively in this region. Temperature estimates from Ti-in-zircon thermometry suggest that the sapphire was crystallized at about 561-781 $^{\circ}\text{C}$.

Status: This manuscript has been prepared and is expected to submit to Journal of Asian Earth Sciences soon.



CHAPTER 2

MINERAL INCLUSIONS IN SAPPHIRE FROM BASALTIC TERRANES IN SOUTHERN VIETNAM: INDICATOR OF ORIGINAL FORMATION

2.1 Introduction

For a few decades, sapphire mines in Southern Vietnam have been under operation and significantly supplied gem materials to the jewelry industry (figure 2.1). Commercial gem mines have recently been located in four main areas including Dak Nong, Di Linh, Binh Thuan, and Krong Nang (figure 2.2) (Garnier et al., 2005; Izokh et al., 2010; Long et al., 2004; Smith et al., 1995; Vu, 2010; 2018). Specifically, the first discovery of abundant gem sapphires begun in Dak Nong and subsequently Di Linh, Binh Thuan, and Krong Nang, respectively. These sapphires accumulated in the Upper-Pleistocene to Quaternary alluvial deposits. Their gemological properties and chemical fingerprints have been reported as basaltic-type sapphires (Garnier et al., 2005; Izokh et al., 2010; Long et al., 2004; Smith et al., 1995; Vu, 2010; 2018).



Figure 2.1 High quality sapphires from Southern Vietnam: (left photo) intense blue sapphires (about 2 to 3 cts each stone) from Di Linh set in ear-rings; (right photo) a pendant with nearly 24 cts yellow sapphire surrounded by small bluish-green sapphires (<1 ct each) from Binh Thuan. These sapphires were heated to improve their colors. Photos by Doan Thi Anh Vu.

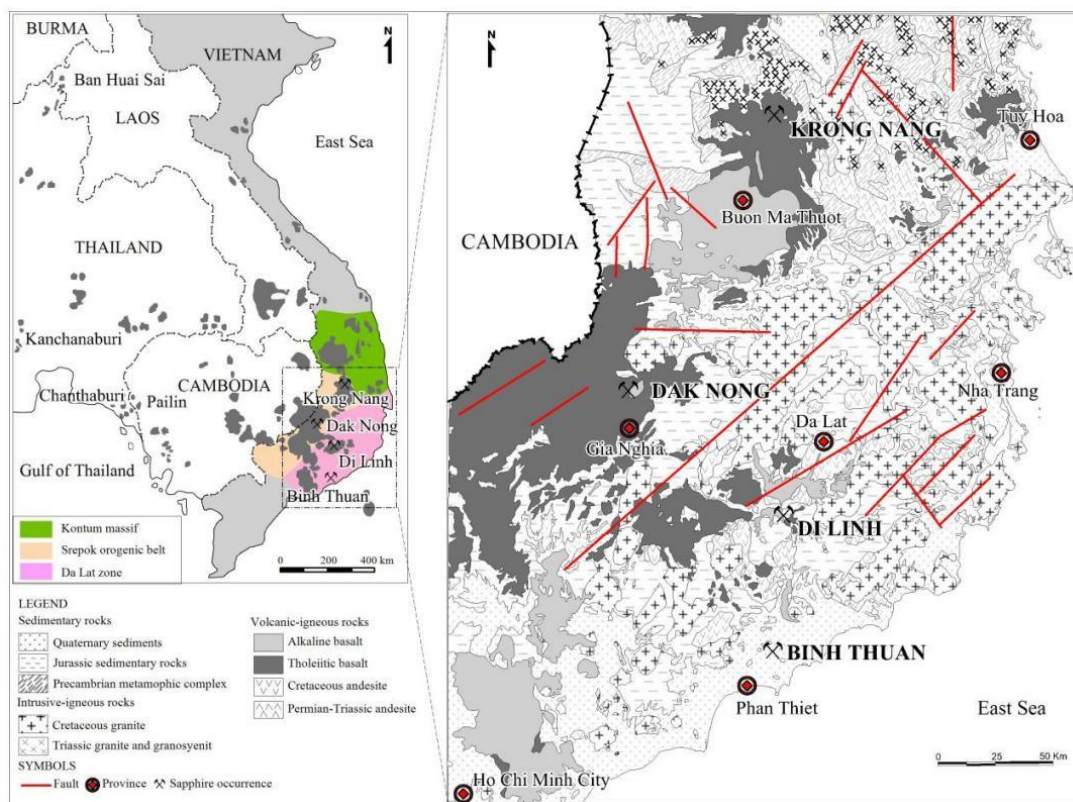


Figure 2.2 Map of Vietnam showing distribution of Cenozoic basalts and main sapphire mining areas in Southern Vietnam; modified after Anh et al. (2018), Lepvrier et al. (2008), and Hoa et al. (2005).

In 2017, we carried out field trips in Southern Vietnam encompassing the vicinities of Binh Thuan province, Di Linh (Lam Dong province), Dak Nong province, and Krong Nang (Dak Lak province) where sapphire samples were collected (see figure 2.2). Gem mining activities in these areas have been operated by a few local miners. Pitting with basic tools before washing and hand picking along streams by artisanal miners (figure 2.3) as well as machinery mines (figure 2.4) can also be found. Sapphires in this region usually range from dark blue to bluish-green, yellowish-green to green colors with rare yellow sapphire. The natural intense blue sapphire is the most famous one which has been specifically produced from Dak Nong and Di Linh gem fields (figure 2.1). Other colors, such as bluish-green and yellowish-green to green are commonly mined, particularly in Binh Thuan and Krong Nang gem fields, respectively (figure 2.1). However, these sapphire varieties are generally heat-treated for color enhancement. In addition, trapiche sapphires (figure 2.5) are sometimes found in these gem fields.



Figure 2.3 Artisanal miners used crowbars and shovels to remove topsoil and dig through the gem-bearing layer in Binh Thuan gem field (left). Gem-bearing gravels were washed and sieved along the local stream in Dak Nong gem field (right). Photos by Doan Thi Anh Vu.



Figure 2.4 Backhoe was used in a machinery mine to remove topsoil and reach the gem-bearing gravel layers prior to washing and dressing using water pump in Binh Thuan gem field (left) and Krong Nang gem field (right). Photos by Doan Thi Anh Vu.



Figure 2.5 Trapiche sapphires, about 10 cts (left) and 9cts (right), from Binh Thuan gem field. Photo by Doan Thi Anh Vu.

In this study, sapphire collections from Southern Vietnam were focused on detailed mineral chemistry of inclusions. The type of data was able to construct the potential genetic model of the original sapphire formation related to basaltic volcanism in this region, which may in turn be a crucial characteristic and indicator for origin determination by the gem testing laboratories.

2.2 Geological setting

Southern Vietnam geologically belongs to a large-scale structure of DaLat active continental margin (Da Lat zone) and Indosinian polyepisodic orogenic belt (Srepok orogenic belt) (Tri and Khuc, 2011), which is separated from Gondwana in Devonian (Hutchison, 2014; Metcalfe, 1988; 1996; 2009; 2011). Rock formations range widely from Precambrian basement rocks, Jurassic sediments, late Mesozoic rocks, and Cenozoic basaltic rocks (Hoa et al., 2005). The basement rocks in this area are composed of metamorphic complexes of granulites and gneiss granulite. A thick pile of Jurassic sediments covering the basement rocks is sandstone, siltstone, and shale. These basement rocks and Jurassic rocks are intruded by a number of late Mesozoic rocks, including Triassic granite and granosyenite and Cretaceous granite. The uppermost part of the study area was eventually covered by Cenozoic basalts which are directly associated with sapphires in Southern Vietnam. These Cenozoic (Neogene-Quaternary) basalts range in age from 0.8-17.6 Ma (Garnier et al., 2005; Hoang and Flower, 1998) which appear to have been related to the latest tectonic event, opening of East Sea after Indian-Eurasian collision (from 35 to 17 Ma) (Barr and MacDonald, 1981; Hoang and Flower, 1998; Lee et al., 1998; Rangin et al., 1995). According to Hoang and Flower (1998), these basalts covering about 23,000 km² with a thickness of several hundred meters erupted within two main episodes. The early stages mostly include tholeiite basalts (without xenoliths), which erupted from extensional N50⁰E- and N160⁰E-trending fissures, derived from lithosphere. On the other hand, the latter alkali basalts often bear mantle xenoliths and 'exotic' xenocrysts such as sapphire and zircon, usually flowed along conjugate strike-slip faults, originating from the asthenosphere.

2.3 Materials and Methods

Over a thousand rough sapphire samples from the gem fields in Southern Vietnam (i.e., Dak Nong, Di Linh, Krong Nang, and Binh Thuan) were collected for

this study. They were initially investigated under a gemological microscope to pick up suitable samples holding lots of mineral inclusions; subsequently, a total of 274 sapphire samples were then selected and polished to expose the inclusions. These inclusions were then identified by a laser Raman spectroscope, model 1000 Renishaw, based at the Gem and Jewellery Institute of Thailand (Public Organization) (GIT). Subsequently, they were analyzed for major and minor compositions using an Electron Probe Micro-Analyzer (EPMA) (JEOL JXA-8100) at the Department of Geology, Faculty of Science, Chulalongkorn University; operating conditions were set at 15 kV acceleration voltage and 24 nA filament current with 30 seconds of peak and background counts for each element prior to automatic ZAF calculation and reporting in oxide forms. Various natural minerals and artificial standards were used for calibration; they included quartz, corundum, eskolaite, fayalite, manganosite, periclase, nickel oxide, wollastonite, jadeite, potassium titanium phosphate, strontium barium niobate, zirconium, yttrium phosphate, cerium phosphate, and neodymium phosphate for SiO₂, Al₂O₃, Cr₂O₃, FeO, MnO, MgO, NiO, CaO, Na₂O, K₂O, Nb₂O₅, ZrO₂, Y₂O₃, Ce₂O₃, and Nd₂O₃, respectively. Fe²⁺ and Fe³⁺ ratios of some specific minerals (e.g., spinel and ilmenite) were estimated by stoichiometric calculation as suggested by Droop (1987). Moreover, rare earth elements of representative zircon inclusions were measured using a LA-ICP-MS system combination between an Agilent 7700 quadrupole ICP-MS (Agilent Technologies, Santa Clara, CA, USA) and a Photon Machines Excimer 193 nm laser system (Excite, Photon machines Inc., Redmond, WA, USA), based at Macquarie University, Australia. The analytical and calibration procedures for trace elements were similarly reported by Belousova et al. (2002). The NIST 610 standard glass and the GEMOC GJ-1 and Mud Tank zircon standards were used as the external calibration standard (Elhlou et al., 2006).

2.4 Results

The most common internal feature of sapphire from Southern Vietnam was strong color zoning (figure 2.6a). Other features include parallel twin planes, needle-like inclusions (figure 2.6b), liquid-filled inclusions (figure 2.6c), and negative crystals (figure 2.6d). Based on Raman spectroscopic and EPMA analyses, 275 mineral inclusions were identified as summarized in Table 2.1. Mineral inclusions previously reported in sapphires from Thailand, Laos, and Cambodia are also compared in the

same table. Columbite and zircon were the most often found inclusions in these sapphire samples whereas alkali feldspar and spinel were subsequently observable. Moreover, ilmenite, pyrochlore and unidentified iron minerals were rarely exposed. Details of these inclusions are described below.

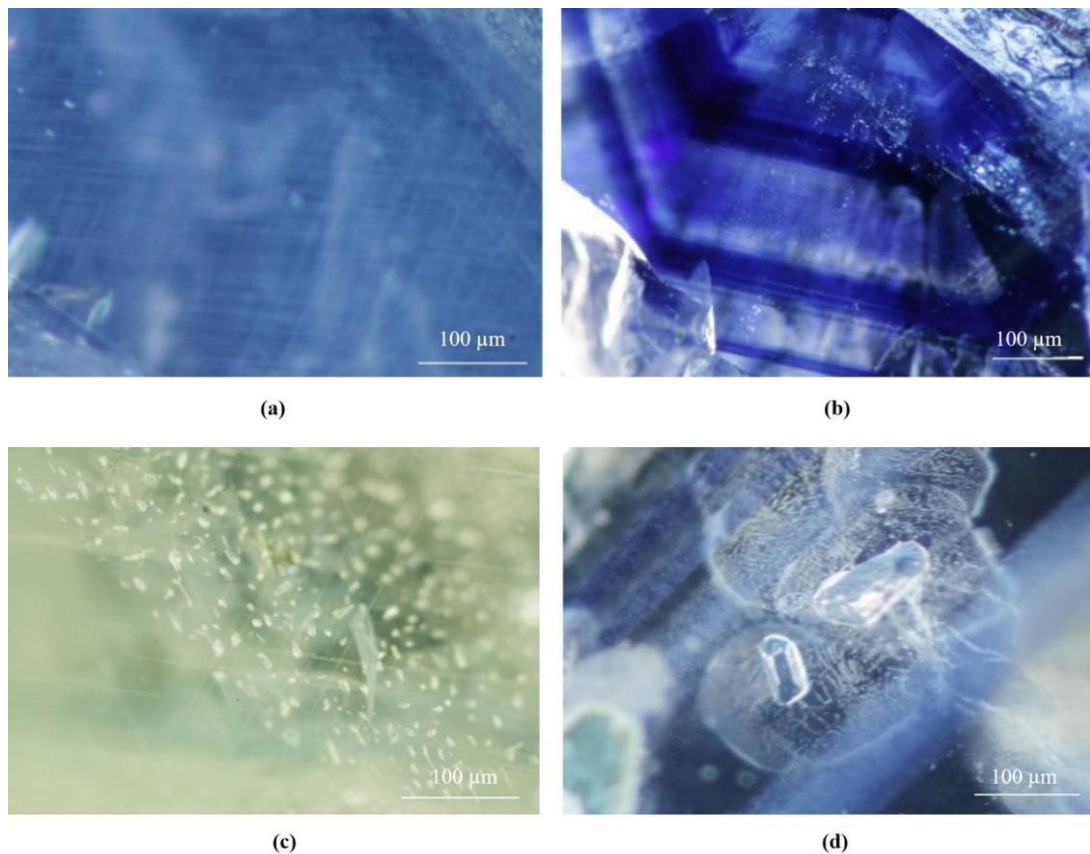


Figure 2.6 Typical internal features observed in sapphire from Southern Vietnam: **(a)** strong color zones; **(b)** needle-like inclusions; **(c)** liquid-filled inclusions; **(d)** negative crystals situated in healed fractures; all photos were taken in darkfield illumination. Photos by Doan Thi Anh Vu.

Table 2.1 Summary of mineral inclusions found in sapphire from Southern Vietnam, compared to those reported from basaltic gem fields at Southeast Asia.

Mineral group	Mineral inclusions	Southern Vietnam				Southeast Asia			
		Dak Nong	Di Linh	Krong Nang	Binh Thuan	Chanthaburi-Thailand	Kanchanaburi-Thailand	Ban Huai Sai-Laos	Paolin-Cambodia
Nb-Ta oxides	Columbite	xxx ^{*1}	xxx ^{*3}	xxx [*]	xxx ^{*3}	xx ⁴	-	x ⁸	-
	Pyrochlore	x [*]	x ³	x [*]	x ³	-	-	-	x ⁹
Silicates	Zircon	xxx ^{*12}	xxx ^{*3}	xxx [*]	xxx ^{*23}	xxx ⁴	xxx ⁶	x ⁵⁷	-
	Alkali feldspar	xx ^{*1}	xx ^{*3}	xx [*]	xx ^{*3}	xxx ⁴	xxx ⁶	x ⁷	-
Oxides	Spinel	x [*]	x ^{*3}	x [*]	x ^{*3}	x ^{*3} x ⁴⁵	xx ⁶	x ⁵	x ⁸
	Ilmenite	x [*]	x ^{*3}	x [*]	x ³	-	x ⁶	-	-
	Unidentified iron	x [*]	x [*]	x [*]	x [*]	-	-	-	-

xxx commonly found.

xx moderately found.

x rarely found.

*This study, using Raman and EPMA.

¹Izokh et al. (2010), using EPMA.

²Long et al. (2004), using SEM-EDS.

³Smith et al. (1995), using SEM-EDS.

⁴Promwongnan and Sutthirat (2019b), using Raman and EPMA.

⁵Sampanya and Sutherland (2011), using EPMA.

⁶Khamloet et al (2014), using EPMA.

⁷Sutherland et al. (2002), using EPMA.

⁸Sutherland et al. (1998b), using EPMA.

⁹Palke et al. (2019), using Raman.

2.4.1 Columbite inclusion

This inclusion was the most dominant mineral inclusion (nearly 47%) observed in sapphires from all gem fields in Southern Vietnam. They generally formed as opaque black euhedral crystals with a rhombic prism pyramid shape and a truncated rhombic pyramid shape, ranging in sizes from 1-2 μm up to several millimeters (figures 2.7a and 2.7b). They were often associated with zircon with/ without feldspar (figures 2.7c and 2.9b). Representative EPMA analyses of columbite inclusions moderately ranged between 65-77% Nb_2O_5 , $\leq 4.5\%$ Ta_2O_5 , $\leq 12\%$ TiO_2 , $\leq 3\%$ MgO , and 12-21% FeO (table 2) which were fit very well within the compositional range of ferrocolumbite (figure 2.8). Their compositions were also equivalent to those previously reported from Dak Nong sapphires by Izokh et al. (2010) as well as from Lava Plains and New England sapphires in Australia (Guo et al., 1996b; Sutherland et al., 1998b); however, the lower

FeO content of columbite inclusions in Bo Welu sapphires, Chanthaburi, Thailand has been reported by Promwongnan and Sutthirat (2019b). Ferrocolumbite inclusions in sapphire from Southern Vietnam contained low Ta content yielding $Ta/(Ta+Nb)$ less than 0.05 within a wide range of Mn contents ($<15\%$ MnO and <0.5 Mn/(Mn+Fe)) (figure 2.8) which may have derived from peralkaline complexes (peralkaline granite/syenite) (Mackay and Simandl, 2015).

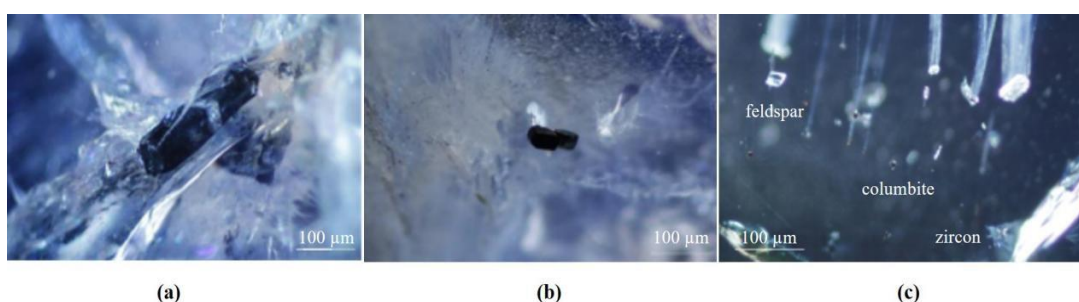


Figure 2.7 (a) a bigger prismatic columbite inclusion; (b) two truncated-rhombic columbite inclusions surrounded by healed fractures; (c) cluster of several tiny columbites with colorless feldspar and zircon inclusions; they were observed in darkfield illumination. Photos by Doan Thi Anh Vu.

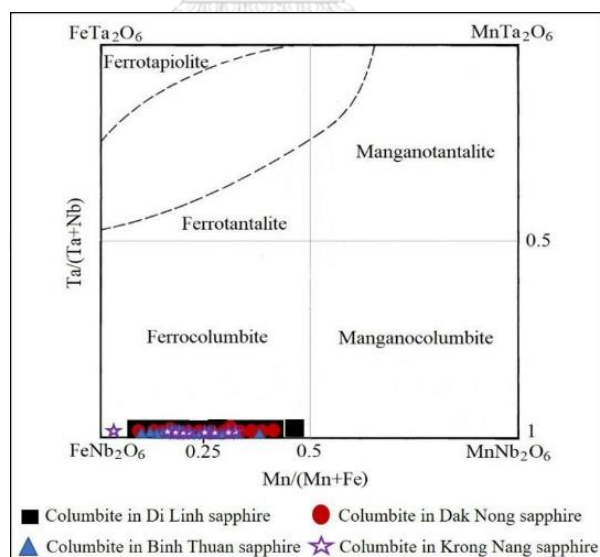


Figure 2.8 Quadrilateral compositional plots show ferrocolumbite inclusion found in sapphires from Southern Vietnam. Various compositional fields and columbite–tapiolite miscibility gap were proposed by Černý and Ercit (1985).

Table 2.2 Representative EPMA analyses of columbite inclusions found in sapphires from Southern Vietnam, Thailand, and Australia

	Southern Vietnam									Thailand	Australia	
	Dak Nong		Di Linh		Krong Nang		Binh Thuan		Dak Nong ¹	Chanthaburi ²	Lava Plains ³	New England ⁴
	DN63	DN68	DL65	DL73	KN25	KN29	PT10	PT19				
TiO ₂	2.85	4.06	6.94	6.56	4.78	1.95	7.86	6.33	na	0.43	3.57	3.03
FeO	12.32	12.73	14.41	15.86	21.35	13.78	16.34	15.01	15.90	9.79	16.59	17.44
MnO	6.45	6.81	5.74	4.54	0.70	3.75	2.45	3.08	2.93	1.58	2.99	2.19
MgO	0.52	1.38	1.32	1.00	0.77	1.32	1.08	0.13	na	0.08	1.18	0.54
CaO	0.00	0.05	0.02	0.00	0.00	0.03	0.02	0.35	na	0.42	0.03	0.00
Nb ₂ O ₅	75.92	70.02	68.03	67.62	70.80	77.23	68.98	67.8	77.10	74.37	71.98	73.95
Ta ₂ O ₅	0.74	4.45	1.80	3.67	0.50	1.30	0.92	4.39	3.61	0.25	2.98	2.38
ThO ₂	0.00	0.02	0.06	0.00	0.02	0.00	0.05	0.00	na	0.85	0.01	na
UO ₂	0.00	0.08	0.00	0.03	0.13	0.02	0.01	0.37	na	3.50	0.12	na
ZrO ₂	0.41	0.17	2.56	0.81	1.23	0.09	1.01	0.87	0.79	0.78	0.40	0.52
Y ₂ O ₃	0.00	0.00	0.06	0.03	0.00	0.00	0.04	0.02	na	2.76	0.01	na
Nd ₂ O ₃	0.00	0.00	0.00	0.00	0.00	0.00	0.00	1.06	na	1.42	na	na
Sm ₂ O ₃	0.00	0.00	0.00	0.00	0.01	0.00	0.02	0.00	na	0.72	na	na
Total	99.2	99.78	100.93	100.12	100.28	99.46	98.77	99.42	100.4	98.61	99.94	100.43
Formula 6(O)												
Ti	0.120	0.171	0.285	0.274	0.199	0.081	0.326	0.268	0.000	0.019	0.150	0.127
Fe	0.575	0.597	0.657	0.736	0.988	0.641	0.753	0.707	0.752	0.481	0.774	0.814
Mn	0.305	0.324	0.265	0.213	0.033	0.177	0.115	0.147	0.140	0.079	0.141	0.104
Mg	0.043	0.116	0.107	0.082	0.064	0.109	0.088	0.010	-	0.007	0.098	0.045
Ca	0.000	0.003	0.001	0.000	0.000	0.002	0.001	0.021	-	0.026	0.002	0.000
Nb	1.915	1.776	1.677	1.695	1.771	1.942	1.719	1.725	1.970	1.970	1.816	1.866
Ta	0.011	0.068	0.027	0.055	0.008	0.020	0.014	0.067	0.055	0.000	0.045	0.036
Th	0.000	0.000	0.001	0.000	0.000	0.000	0.001	0.000	-	0.011	0.160	-
U	0.000	0.001	0.000	0.000	0.002	0.000	0.000	0.005	-	0.046	0.002	-
Zr	0.011	0.005	0.068	0.022	0.033	0.003	0.027	0.024	0.022	0.022	0.011	0.014
Y	0.000	0.000	0.002	0.001	0.000	0.000	0.001	0.001	-	0.086	0.001	-
Nd	0.000	0.000	0.000	0.000	0.000	0.000	0.000	0.027	-	0.030	-	-
Sm	0.000	0.000	0.000	0.000	0.000	0.000	0.000	0.000	-	0.015	-	-
Total*	2.980	3.061	3.090	3.078	3.098	2.974	3.046	3.002	2.940	2.847	3.044	3.006
Mn/Mn+Fe	0.35	0.35	0.29	0.22	0.03	0.22	0.13	0.17	0.16	0.14	0.15	0.11
Ta/Ta+Nb	0.01	0.04	0.02	0.03	<0.01	0.01	0.01	0.04	0.03	<0.01	0.02	0.02

na = not analyzed.

¹Izokh et al. (2010).

²Promwongnan and Sutthirat (2019b).

³Guo et al. (1996b).

⁴Sutherland et al. (1998a).

2.4.2. Zircon inclusion

It often occurred in sapphires from all gem fields in Southern Vietnam but its abundance (about 22%) was less than columbite inclusion. This zircon commonly formed as euhedral tetragonal prismatic or dipyramidal crystals (figures 2.9a and b). It was mostly transparent colorless with some orange to orange-red grains. Their chemical compositions varied within narrow ranges of approximately 31-34% SiO₂ and 61-65% ZrO₂ (Table 2.3). The Hafnium contents showed a slightly wider range of about 1-4% wt leading to Hf/Zr ratios of 0.01 to 0.04 falling within the range of magmatic zircon, particularly syenite and granite (Deer et al., 2013). Significant trace elements included <1.5% ThO₂, <1.8% UO₂, and <0.6% Y₂O₃ which these elements appeared to be higher in zircon inclusions of Di Linh sapphire. On the other hand, these zircon inclusions yielded Th/U ratios > 0.2, indicating magmatic source (Huong et al., 2016; Rubatto and Gebauer, 2000; Williams and Claesson, 1987). In comparison with zircon analyses previously reported from Dak Nong (Izokh et al., 2010) and other basalt-associated sources such as Ban Huai Sai in Laos, Kanchanaburi in Thailand, Kings Plains and New England in Australia (Guo et al., 1996b; Khamloet et al., 2014; Sutherland et al., 2002; 1998a), they were similar in composition; although, the Y₂O₃ content of zircon inclusions from Bo Welu, Chanthaburi, Thailand (Promwongnan and Sutthirat, 2019b) has recently been reported with a higher content. Total REE contents of represent zircon inclusions range from 1156 - 2710 ppm (Table 2.4), more similar to those from syenite pegmatite (2043 ppm) and granitoid (1813 ppm) than those from carbonatite (600-700 ppm) (Belousova et al., 2002).

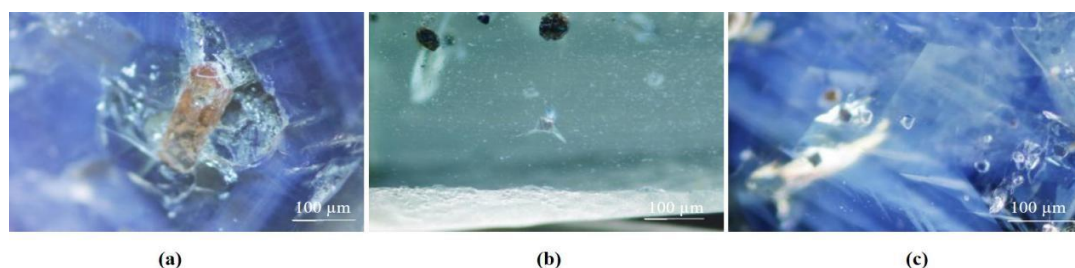


Figure 2.9 Photomicrographs showing: **(a)** prismatic orange zircon inclusion; **(b)** colorless dipyramidal zircon inclusion surrounded by radial cracks, associated with black columbite inclusions; **(c)** tiny euhedral feldspar inclusions; All photos were taken in darkfield illumination by Doan Thi Anh Vu.

2.4.3 Alkali feldspar inclusion

They were sometimes observed in sapphire samples (about 13%). They generally presented oval or euhedral grains with small sizes ranging from about 1-20 μm with rarely reaching 1 mm. They commonly showed transparent colorless (figures 2.7c and 2.9c). Their chemical compositions yielded rather uniform towards Na-rich feldspar between albite-anorthoclase-oligoclase ($\text{Ab}_{77-98}\text{An}_{<15}\text{Or}_{1-11}$, see table 2.5 and figure 2.10). However, feldspar in Krong Nang sapphires was mostly plotted close to the junction of albite-anorthoclase-oligoclase compositions ($\text{Ab}_{82-86}\text{An}_{6-11}\text{Or}_{6-11}$) whereas Di Linh feldspar was divided into two groups, the first group was close to the albite-anorthoclase boundary ($\text{Ab}_{82-85}\text{An}_{6-9}\text{Or}_{8-11}$) and the second one contained a lower K-content lying around the albite-oligoclase boundary ($\text{Ab}_{85-87}\text{An}_{7-11}\text{Or}_{4-5}$). Binh Thuan feldspar ranged between albite and oligoclase compositions while most of Dak Nong feldspar fell within albite composition ($\text{Ab}_{83-98}\text{An}_{1-10}\text{Or}_{1-8}$). These compositional ranges were wider than that previously reported as only oligoclase in Dak Nong sapphires (Izokh et al., 2010) as well as those in Ban Huai Sai sapphires from Laos (Sutherland et al., 2002), but narrower than those in sapphires from Kanchanaburi ($\text{Ab}_{70-77}\text{An}_{9-23}\text{Or}_{6-14}$) and Chanthaburi ($\text{Ab}_{80-91}\text{An}_{<14}\text{Or}_{7-17}$) in Thailand, Kings Plains ($\text{Ab}_{80-91}\text{An}_{<14}\text{Or}_{7-17}$) and New England ($\text{Ab}_{6-77}\text{An}_{<53}\text{Or}_{22-94}$) in Australia (Guo et al., 1996b; Khamloet et al., 2014; Promwongnan and Sutthirat, 2019b; Sutherland et al., 1998a).

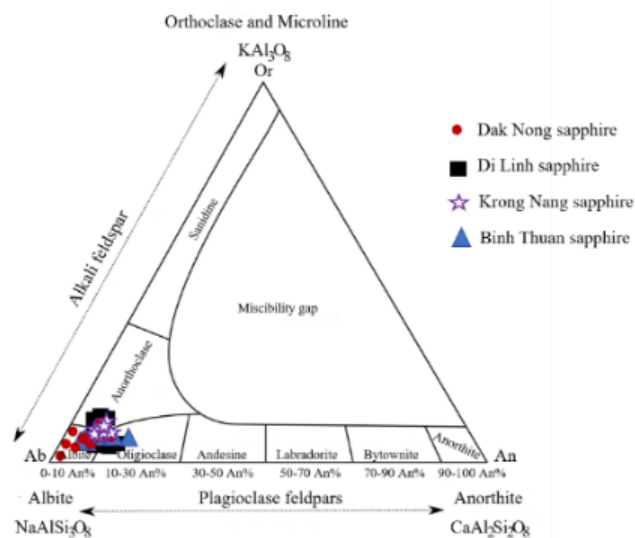


Figure 2.10 Ternary An-Ab-Or plots of alkali feldspar inclusions in the sapphires from Southern Vietnam.

Table 2.3 Representative EPMA analyses of zircon inclusions found in sapphires from Southern Vietnam, Laos, Thailand, and Australia

	Southern Vietnam								Laos	Thailand		Australia		
	Dak Nong		Di Linh		Krong Nang		Binh Thuan		Dak Nong ¹	Ban Huai Sai ²	Chanthaburi ³	Kanchanaburi ⁴	Kings Plains ⁵	New England ⁶
	DN23	DN31	DL60	DL44	KN15	KN13	PT69	PT65						
SiO ₂	32.16	32.43	33.36	32.59	33.84	33.43	34.44	33.86	32.34	31.23	33.63	34.14	32.12	31.48
TiO ₂	0.03	0.02	0.00	0.01	0.01	0.00	0.00	0.00	na	na	na	na	nd	0.00
Al ₂ O ₃	0.27	0.30	0.01	0.00	0.00	0.00	0.01	0.01	na	0.01	0.01	0.17	0.02	0.44
FeO	0.00	0.02	0.10	0.00	0.00	0.10	0.00	0.00	na	na	0.07	0.04	0.20	0.13
MgO	0.02	0.01	0.01	0.00	0.00	0.00	0.02	0.01	na	0.01	na	na	nd	0.00
CaO	0.06	0.05	0.00	0.00	0.00	0.01	0.00	0.00	na	na	na	0.00	0.02	0.00
Na ₂ O	0.00	0.00	0.00	0.00	0.00	0.00	0.00	0.00	na	na	na	na	na	0.00
K ₂ O	0.02	0.00	0.00	0.00	0.00	0.05	0.00	0.00	na	na	na	na	na	0.00
ThO ₂	0.03	0.31	0.41	1.40	0.32	0.03	0.26	0.09	0.76	0.18	1.21	na	0.49	0.11
UO ₂	0.12	1.40	0.45	1.73	0.23	0.06	0.26	0.34	0.93	0.41	1.13	na	0.84	0.11
ZrO ₂	64.47	61.44	62.69	61.00	63.98	63.29	63.22	62.02	63.96	64.02	59.39	62.40	63.78	64.84
HfO ₂	1.62	3.70	1.82	3.08	2.00	2.82	1.13	3.85	2.44	3.58	2.62	3.50	2.88	2.58
P ₂ O ₅	0.13	0.16	0.00	0.22	0.08	0.09	0.09	0.23	na	0.25	0.57	na	0.34	na
Y ₂ O ₃	0.02	0.08	0.04	0.56	0.05	0.07	0.13	0.03	na	0.80	0.85	na	0.34	0.46
Total	98.93	99.91	98.88	100.5	100.52	99.96	99.56	100.4	100.4	100.5	99.57	100.2	101.0	100.1
Formula 4(O)														
Si	0.996	1.008	1.031	1.013	1.028	1.024	1.046	1.033	1.001	0.973	1.035	1.036	0.989	0.976
Ti	0.001	0.000	0.000	0.000	0.000	0.000	0.000	0.000	-	-	-	-	-	0.000
Al	0.010	0.011	0.000	0.000	0.000	0.000	0.000	0.000	-	0.000	0.000	0.006	0.001	0.016
Fe	0.000	0.000	0.003	0.000	0.000	0.003	0.000	0.000	-	-	0.002	0.001	0.046	0.003
Mg	0.001	0.001	0.001	0.000	0.000	0.000	0.001	0.000	-	0.000	-	-	-	0.000
Ca	0.002	0.002	0.000	0.000	0.000	0.000	0.000	0.000	-	-	-	0.000	0.001	0.000
Na	0.000	0.000	0.000	0.000	0.000	0.000	0.000	0.000	-	-	-	-	-	0.000
K	0.001	0.000	0.000	0.000	0.000	0.002	0.000	0.000	-	-	-	-	-	0.000
Th	0.000	0.002	0.003	0.010	0.002	0.000	0.002	0.001	0.005	0.001	0.008	-	0.003	0.001
U	0.001	0.010	0.003	0.012	0.002	0.000	0.002	0.002	0.006	0.003	0.008	-	0.006	0.001
Zr	0.974	0.931	0.945	0.924	0.948	0.945	0.936	0.923	0.965	0.972	0.891	0.923	0.957	0.980
Hf	0.014	0.033	0.016	0.027	0.017	0.025	0.010	0.033	0.022	0.032	0.023	0.036	0.025	0.023
P	0.003	0.004	0.000	0.006	0.002	0.002	0.002	0.006	-	0.007	0.013	-	0.009	-
Y	0.000	0.001	0.001	0.009	0.001	0.001	0.002	0.000	-	0.013	0.014	-	0.006	0.008
Total*	2.004	2.003	2.002	2.001	2.000	2.003	2.001	1.999	2.000	2.002	1.995	2.002	2.001	2.008
Th/U	0.29	0.23	0.94	0.83	1.42	0.51	1.01	0.26	0.84	0.45	1.10	-	0.60	1.02
Hf/Zr	0.02	0.04	0.02	0.03	0.02	0.03	0.01	0.04	0.02	0.03	0.03	0.03	0.03	0.02

na = not analyzed; nd = not detected.

¹Izokh et al. (2010); ²Sutherland et al. (2002); ³Promwongnan and Sutthirat (2019b); ⁴Khamloet et al (2014); ⁵Guo et al.; (1996b); ⁶Sutherland et al. (1998a).

Table 2.4 REE analyses (ppm) of some zircons found in sapphire from Southern Vietnam

	Dak Nong	Di Linh	Krong Nang	Binh Thuan
	DN05	DL46	KN08	PT05
Y	1468.21	4220.35	1194.74	2868.13
La	0.02	0.00	0.01	0.00
Ce	2.79	12.00	1.65	13.33
Pr	0.01	0.06	0.02	0.0523
Nd	0.27	1.11	0.26	1.451
Sm	1.23	5.62	0.68	5.62
Eu	0.96	5.12	0.59	2.177
Gd	12.91	54.66	5.74	44.06
Tb	7.23	27.58	3.91	21.66
Dy	122.00	416.17	76.25	310.13
Ho	50.02	152.71	38.25	104.29
Er	258.30	672.98	258.42	442.14
Tm	60.40	134.11	83.73	89.21
Yb	566.33	115.50	1081.3	721.34
Lu	80.77	140.18	179.34	81.68
Total REE	1155.94	2710.22	1762.23	1815.47

2.4.4 Spinel inclusion

They were occasionally found in sapphires (about 4%) from Southern Vietnam. They usually occurred as black cubic crystals (figure 2.11a). Spinel inclusions with compositions ranging between chromite-hercynite and magnetite-hercynite have been previously reported, on the basis of SEM-EDS analyses, in sapphires from Binh Thuan and Di Linh (Smith et al., 1995). However, EPMA analyses of spinel inclusions in this study revealed significant components of hercynite (Hc₇₈₋₁₀₀) and spinel (Sp_{<23}) whereas other components were negligible (Table 2.5). Their Mg:Fe²⁺ ratios were mostly less than 1:4 falling into hercynite spinel (Deer et al., 2013). In comparison, these hercynite spinel inclusions contained a moderately lower spinel composition than those spinels in sapphires from Kanchanaburi in Thailand, Pailin in Cambodia, and New England in Australia (see also Table 2.5).

2.2.5 Ilmenite inclusion

This inclusion was found in only two samples from Di Linh and one sample from Dak Nong. They formed euhedral rhombohedral crystals with black opaque (figure 2.11b) which were confirmed by Raman spectroscopic identification. A previous study, based on SEM-EDS analysis, also recognized ilmenite within sapphires

from Di Linh and Binh Thuan (Smith et al., 1995). The chemical compositions of ilmenite inclusion in this study clearly belonged to titanohematite series (ilmenite-hematite, $\text{Il}_{54-49}\text{He}_{40-34}$) (Table 2.7). The low Mn content (<0.15 %wt MnO) of these titanohematites were close to an igneous magma source (Lindsley, 1991) as reported from Sybille Monzosyenite (Fuhrman et al., 1988), which was different from ilmenite with higher Mn from metamorphic rocks from Western Australia (Cassidy et al., 1988). Moreover, their Mn contents were similar to those of ilmenite in New England sapphires originating from silicate melt (Sutherland et al., 1998a) and different from those of ilmenite in Kanchanaburi sapphires from metamorphic melt (Khamloet et al., 2014) (Table 2.7).

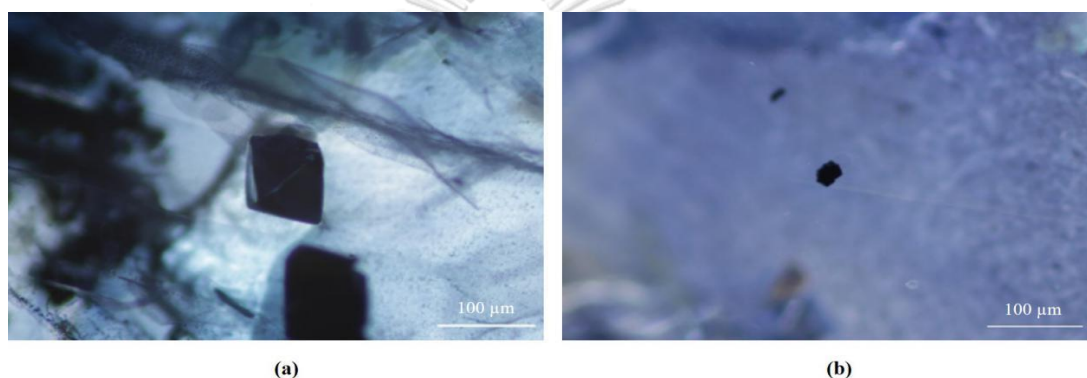


Figure 2.11 Photomicrographs were taken in darkfield illumination by Doan Thi Anh Vu showing: (a) black octahedral hercynite spinel inclusion and (b) euhedral rhombohedral ilmenite inclusion.

2.4.6 Unidentified iron-bearing mineral inclusions

They were also observed in these sapphire samples. They presented black tiny cubic crystals (figure 2.12a) which their morphological forms were similar to spinel inclusions. They were commonly associated with spinel inclusions and sometimes formed as composite inclusions (figure 2.12b). These iron-rich minerals contained up to 96% FeO with aluminum contents ranging from 0.1 to 13% Al_2O_3 (Table 2.8) and Raman spectra appeared to be magnetite, characteristic bands at 663 to 652 cm^{-1} (Faria et al., 1997). However, their atomic proportions, based on stoichiometric calculation as suggested by Droop (1987), yielded almost 1:1 of $\Sigma\text{R}^{3+}/\Sigma\text{R}^{2+}$, particularly $\text{Fe}^{3+}/\text{Fe}^{2+}$ (see Table 8) which seemed unlikely the formula of magnetite (Fe_3O_4) with $\text{Fe}^{3+}/\text{Fe}^{2+}$ ratio of 2:1. More details of these inclusions need to be worked out in the future.

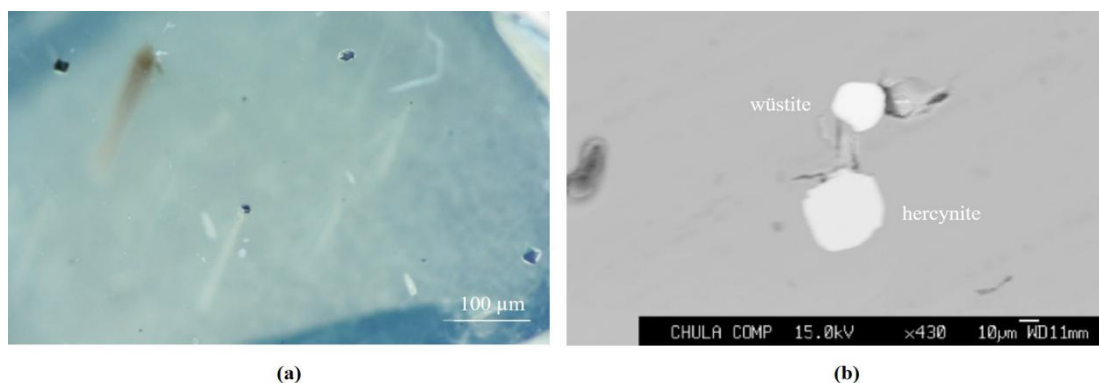


Figure 2.12 (a) several tiny unidentified iron oxides with cubic shape; photo was taken in darkfield illumination by Doan Thi Anh Vu. (b) black scattered electron image of unidentified cubic iron oxides and euhedral hercynite-spinel.

2.4.7 Pyrochlore inclusion

It was recognized as inclusions in a few sapphire samples from Dak Nong and a couple samples from Krong Nang. They formed similarly red cubic crystals which were commonly surrounded by radial cracks (figure 2.13). Based on SEM-EDS analysis, Smith et al. (1995) had previously reported uranpyrochlore in sapphires from Di Linh and Binh Thuan. EPMA analyses of pyrochlore in this study yielded a high U content (about 19-22% in ΣR^{2+}), a high Nb content leading to $Nb/Ta \geq 8$ and $(Nb+Ta)/Ti$ about 2 (table 2.9) which ranged within the compositional range of uranpyrochlore (Hogarth, 1977). These compositions were similar to those found in both Anakie sapphires (Guo et al., 1996b) and New England sapphires (Sutherland et al., 1998a) from Australia.

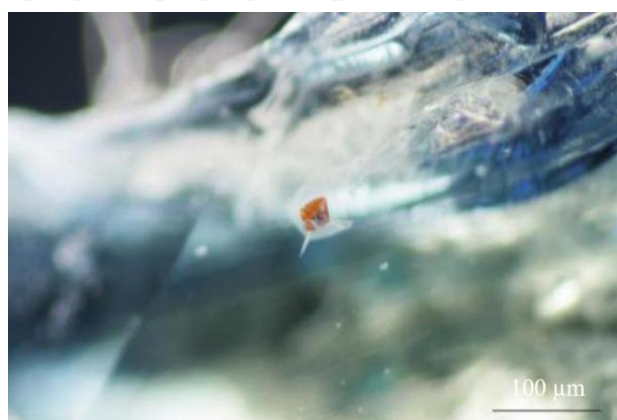


Figure 2.13 A red cubic pyrochlore inclusion displaying halo and radial cracks; darkfield illumination by Doan Thi Anh Vu.

Table 2.5 Representative EPMA analyses of feldspar inclusions in sapphires from Southern Vietnam, Laos, Thailand, and Australia.

	Southern Vietnam									Laos	Thailand		Australia	
	Dak Nong		Di Linh		Krong Nang		Binh Thuan		Dak Nong ¹	Ban Hwai Sai ²	Chanthaburi ³	Kanchanaburi ⁴	Kings Plains ⁵	New England ⁶
	DN41	DN34	DL27	DL34	KN53	KN37	PT01	PT23						
SiO ₂	67.93	64.13	65.66	62.30	65.83	64.38	68.89	64.31	64.20	64.83	65.60	66.97	64.81	2.425
TiO ₂	0.02	0.00	0.01	0.02	0.01	0.01	0.00	0.00	nd	na	0.01	0.02	na	0.000
Al ₂ O ₃	19.06	21.92	23.72	23.73	22.86	21.79	19.70	22.39	22.10	21.45	21.50	21.40	18.56	1.565
FeO	0.03	0.06	0.03	0.19	0.09	0.07	0.00	0.06	0.06	0.03	0.04	0.65	na	0.003
MnO	0.00	0.00	0.00	0.00	0.00	0.00	0.00	0.00	0.02	na	0.00	0.04	na	0.000
MgO	0.00	0.00	0.00	0.00	0.00	0.00	0.00	0.00	nd	na	0.05	nd	na	0.000
BaO	0.07	0.01	0.03	0.06	0.07	0.00	0.02	0.03	na	na	na	na	na	-
CaO	0.17	2.24	1.09	1.64	1.54	2.24	0.00	2.98	3.13	1.96	2.59	0.73	nd	0.544
Na ₂ O	11.33	9.65	7.63	10.76	8.73	9.22	11.37	9.02	9.71	9.37	4.31	2.69	0.73	0.484
K ₂ O	0.22	1.15	1.60	1.02	1.70	1.44	0.32	1.43	0.82	1.53	6.52	8.47	15.50	0.028
Total	98.83	99.16	99.76	99.72	100.84	99.15	100.3	100.2	100.1	99.17	100.6	100.9	99.60	100.0
Ti	0.001	0.000	0.000	0.001	0.000	0.000	0.000	0.000	-	-	0.000	0.001	-	0.000
Al	0.993	1.151	1.223	1.245	1.175	1.144	1.010	1.166	1.152	1.125	1.124	1.114	1.011	1.565
Fe	0.001	0.002	0.001	0.007	0.003	0.003	0.000	0.002	0.002	0.001	0.002	0.024	-	0.003
Mn	0.000	0.000	0.000	0.000	0.000	0.000	0.000	0.000	0.001	-	0.000	0.001	-	0.000
Mg	0.000	0.000	0.000	0.000	0.000	0.000	0.000	0.000	-	-	0.003	0.000	-	0.000
Ba	0.001	0.000	0.000	0.001	0.001	0.000	0.000	0.001	-	-	-	0.000	-	-
Ca	0.008	0.107	0.051	0.078	0.072	0.107	0.000	0.141	0.148	0.093	0.123	0.035	-	0.544
Na	0.971	0.833	0.647	0.929	0.738	0.796	0.959	0.772	0.833	0.808	0.371	0.230	0.065	0.484
K	0.012	0.065	0.089	0.058	0.095	0.082	0.018	0.081	0.046	0.087	0.369	0.477	0.914	0.028
Total*	4.991	5.016	4.884	5.095	4.957	4.999	4.986	5.003	5.023	5.000	4.899	4.893	4.988	5.048
Atomic (%)														
Ab	97.9	82.9	82.1	87.2	81.6	80.8	98.2	77.7	81.1	81.8	43.0	31.0	6.7	45.8
An	0.8	10.6	6.5	7.4	8.0	10.9	0.0	14.2	14.4	9.5	14.2	4.7	0.0	51.5
Or	1.3	6.5	11.3	5.4	10.5	8.3	1.8	8.1	4.5	8.8	42.8	64.3	93.3	2.7

na = not analyzed; nd = not detected.

¹Izokh et al. (2010).

²Sutherland et al. (2002).

³Promwongnan and Sutthirat (2019b).

⁴Khamloet et al. (2014).

⁵Guo et al. (1996b).

⁶Sutherland et al. (1998a).

Table 2.6 Representative EPMA analyses of spinel inclusions in sapphires from Southern Vietnam, Laos, Thailand, and Australia

	Southern Vietnam							Thailand	Cambodia	Australia
	Dak Nong		Di Linh	Krong Nang		Binh Thuan		Kanchanaburi ¹	Pailin ²	New England ³
	DN12	DN16	DL62	KN42	KN47	PT22	PT34			
SiO ₂	0.00	0.00	0.01	0.00	0.00	0.00	0.25	0.03	0.03	0.00
TiO ₂	0.12	0.08	0.70	0.13	0.18	0.00	1.91	0.07	0.26	0.13
Al ₂ O ₃	60.99	60.93	60.76	60.31	60.11	61.18	61.58	59.52	63.00	57.04
Cr ₂ O ₃	0.00	0.00	0.09	0.00	0.00	0.00	0.00	0.16	0.29	0.00
FeOtotal	33.99	34.18	33.87	34.96	33.77	33.35	35.53	35.39	21.77	34.66
MnO	0.00	0.89	0.34	0.05	1.18	0.53	1.44	0.22	0.15	0.48
MgO	4.02	4.29	4.62	3.17	4.31	4.60	0.08	5.85	13.50	6.09
ZnO	0.12	0.38	0.18	0.00	0.51	0.93	0.07	0.14	nd	0.69
CaO	0.06	0.00	0.00	0.00	0.00	0.00	0.00	0.00	nd	0.00
Total	99.29	100.74	100.58	98.61	100.06	100.58	100.95	101.36	99.00	99.15
Formula 32(O)										
Si	0.000	0.000	0.002	0.000	0.000	0.000	0.056	0.007	0.006	0.000
Ti	0.020	0.014	0.117	0.023	0.030	0.000	0.321	0.011	0.042	0.022
Al	16.134	15.975	15.886	16.153	15.881	16.018	16.194	15.570	15.774	15.364
Cr	0.000	0.000	0.016	0.000	0.000	0.000	0.000	0.028	0.049	0.000
Fe ³⁺	0.000	0.000	0.000	0.000	0.078	0.000	0.000	0.412	0.000	0.779
Fe ²⁺	6.380	6.359	6.285	6.645	6.253	6.196	6.630	6.157	3.868	5.846
Mn	0.000	0.168	0.064	0.009	0.224	0.100	0.272	0.041	0.027	0.093
Mg	1.344	1.421	1.529	1.072	1.440	1.524	0.026	1.934	4.276	2.075
Zn	0.020	0.062	0.030	0.000	0.122	0.152	0.012	0.023	-	0.116
Ca	0.015	0.000	0.000	0.000	0.000	0.000	0.000	0.000	-	0.000
Total*	23.913	23.999	23.929	23.901	24.029	23.991	23.526	24.183	24.041	24.296
ΣR ²⁺	7.759	8.010	7.907	7.726	8.040	7.973	6.956	8.155	8.171	8.131
ΣR ³⁺	16.154	15.989	16.022	16.175	15.989	16.018	16.571	16.028	15.870	16.165
Atomic (%)										
Sp	17.3	17.7	19.3	22.5	13.9	19.1	0.4	23.9	52.5	26.2
Hc	82.2	79.4	79.5	77.5	86.1	80.3	99.6	76.1	47.5	73.8

nd = not detected.

Fe²⁺ and Fe³⁺ were recalculated from total FeO after the method of Droop (1987).

ΣR²⁺ = Fe²⁺+Mn+Mg+Zn+Ca. ΣR³⁺ = Ti+Al+Cr+Fe³⁺.

¹Khamloet et al. (2014).

²Sutherland et al. (1998b).

³Sutherland et al. (1998a)

Table 2.7 Representative EPMA analyses of ilmenite inclusions in sapphires from Southern Vietnam, Thailand, and Australia

	Southern Vietnam			Thailand	Australia
	Dak Nong	Di Linh		Kanchanaburi ¹	New England ²
	DN39	DL23	DL85		
SiO ₂	0.11	0.10	0.00	0.00	0.70
TiO ₂	34.94	37.08	33.77	45.73	59.04
Al ₂ O ₃	0.02	1.50	0.58	6.90	0.45
Cr ₂ O ₃	0.00	0.04	0.12	na	0.00
FeO _{total}	61.43	61.58	63.48	27.64	32.05
MnO	0.14	0.06	0.05	17.59	0.40
MgO	0.00	0.18	0.64	0.98	1.85
ZnO	0.80	0.00	0.00	na	0.00
CaO	0.00	0.01	0.00	0.00	0.00
NiO	0.02	0.00	0.03	na	na
Total	97.46	100.54	98.67	98.84	94.57
Formula 6(O)					
Si	0.006	0.006	0.000	0.000	0.035
Ti	1.499	1.514	1.437	1.713	2.204
Al	0.001	0.096	0.039	0.405	0.026
Cr	0.000	0.002	0.005	-	0.000
Fe ³⁺	1.318	1.168	1.430	0.904	0.000
Fe ²⁺	1.612	1.629	1.573	0.248	1.330
Mn	0.007	0.003	0.002	0.742	0.017
Mg	0.000	0.014	0.054	0.073	0.137
Zn	0.000	0.000	0.000	-	0.000
Ca	0.049	0.000	0.000	0.000	0.000
Ni	0.001	0.000	0.001	-	-
Total*	4.494	4.431	4.541	4.085	3.748
ΣR ²⁺	1.669	1.646	1.630	1.063	1.484
ΣR ³⁺	2.818	2.780	2.911	3.022	2.230
Atomic (%)					
Il	53.1	54.5	49.4	56.7	98.8
Mt	6.8	6.9	8.3	0.0	0.0
He	38.7	33.7	39.8	29.9	0.0

na = not analyzed.

Fe²⁺ and Fe³⁺ were recalculated from total FeO after the method of Droop (1987).

ΣR²⁺ = Fe²⁺+Mn+Mg+Zn+Ca+Ni; ΣR³⁺ = Ti+Al+Cr+Fe³⁺.

¹Khamloet et al. (2014).

²Sutherland et al. (1998a).

Table 2.8 Representative EPMA analyses of unidentified iron-rich inclusions in sapphires from Southern Vietnam

	Dak Nong		Di Linh		Krong Nang		Binh Thuan	
	DN74	DN89	DL14	DL50	KN05	KN19	PT17	PT18
SiO ₂	0.03	0.02	0.00	0.02	1.58	0.06	0.27	0.34
TiO ₂	0.84	1.57	1.53	2.33	6.62	1.24	0.22	0.52
Al ₂ O ₃	9.85	8.78	6.66	0.21	10.82	11.84	0.12	10.14
Cr ₂ O ₃	0.01	0.00	0.04	0.02	0.33	0.03	0.03	0.06
FeO _{total}	88.13	87.90	89.29	96.45	75.75	86.30	95.46	86.45
MnO	0.20	0.14	1.49	0.41	0.08	0.18	1.81	1.57
MgO	0.35	0.18	0.29	1.36	0.15	0.37	0.88	0.05
ZnO	0.67	0.33	0.36	0.00	0.31	0.51	0.00	0.00
CaO	0.00	0.00	0.00	0.00	0.12	0.00	0.00	0.00
NiO	0.02	0.00	0.00	0.03	0.10	0.00	0.00	0.00
Total	100.11	98.92	99.66	100.84	95.86	100.52	98.78	99.13
Formula 32(O)								
Si	0.012	0.001	0.000	0.008	0.523	0.020	0.104	0.116
Ti	0.216	0.051	0.405	0.645	1.648	0.310	0.063	0.133
Al	3.967	3.598	2.769	0.091	4.218	4.641	0.053	4.104
Cr	0.002	0.000	0.011	0.006	0.086	0.008	0.010	0.016
Fe ³⁺	12.435	12.429	13.148	14.925	8.501	11.658	15.700	12.266
Fe ²⁺	12.744	13.121	13.183	14.740	12.460	12.349	14.788	12.571
Mn	0.058	0.041	0.446	0.128	0.023	0.051	0.585	0.457
Mg	0.178	0.092	0.150	0.748	0.073	0.183	0.498	0.026
Zn	0.170	0.085	0.095	0.000	0.075	0.125	0.000	0.000
Ca	0.000	0.000	0.000	0.000	0.041	0.000	0.000	0.000
Ni	0.006	0.000	0.000	0.008	0.027	0.000	0.000	0.000
Total*	29.788	29.784	30.206	31.299	27.676	29.345	31.801	29.690
ΣR ²⁺	13.156	13.339	13.874	15.624	12.699	12.708	15.871	13.054
ΣR ³⁺	16.620	16.078	16.333	15.667	14.453	16.617	15.826	16.519

Fe²⁺ and Fe³⁺ were recalculated from total FeO after the method of Droop (1987).

ΣR²⁺ = Fe²⁺+Mn+Mg+Zn+Ca+Ni. ΣR³⁺ = Ti+Al+Cr+Fe³⁺.

Table 2.9 Representative EPMA analyses of pyrochlore inclusions in sapphires from Southern Vietnam

	Southern Vietnam				Australia	
	Dak Nong		Krong Nang		Anakie ¹	New England ²
	DN35	DN77	KN18	KN36		
SiO ₂	0.23	0.37	0.55	0.33	na	0.00
TiO ₂	11.67	11.20	10.59	11.63	11.48	10.14
FeO	1.68	1.38	1.54	1.57	1.51	0.30
MnO	0.37	0.19	0.08	0.03	na	na
CaO	6.86	6.63	6.26	6.89	5.58	5.49
Na ₂ O	4.33	5.11	4.44	5.24	4.27	5.92
K ₂ O	0.04	0.05	0.06	0.09	na	na
Nb ₂ O ₅	33.61	32.24	33.88	33.03	32.99	38.48
Ta ₂ O ₅	6.05	6.50	5.97	6.34	6.58	4.44
ThO ₂	7.88	7.31	7.00	7.61	8.56	1.99
UO ₂	22.28	23.06	23.83	22.32	21.80	30.88
ZrO ₂	0.08	0.15	0.01	0.02	0.20	na
Y ₂ O ₃	0.00	0.08	0.12	0.08	0.66	na
Ce ₂ O ₃	0.12	0.35	0.34	0.28	0.48	na
Nd ₂ O ₃	0.14	0.17	0.00	0.06	0.54	na
Total	95.36	94.40	94.67	95.51	94.90	97.64
Formula 6(O)						
Si	0.016	0.026	0.039	0.023	-	0.000
Ti	0.605	0.591	0.557	0.601	0.607	0.518
Fe	0.097	0.081	0.090	0.090	0.089	0.017
Mn	0.022	0.011	0.005	0.002	-	-
Ca	0.506	0.498	0.469	0.508	0.420	0.400
Na	0.578	0.643	0.601	0.698	0.582	0.780
K	0.003	0.004	0.005	0.008	-	-
Nb	1.046	1.022	1.070	1.026	1.048	1.182
Ta	0.113	0.124	0.113	0.118	0.126	0.082
Th	0.123	0.117	0.111	0.119	0.137	0.031
U	0.341	0.360	0.370	0.341	0.341	0.467
Zr	0.003	0.005	0.000	0.001	0.007	0.000
Y	0.000	0.003	0.005	0.003	0.025	-
Ce	0.000	0.000	0.000	0.000	0.012	-
Nd	0.003	0.009	0.009	0.007	0.014	-
Total*	3.460	3.498	3.444	3.546	3.411	3.477
ΣR ²⁺	1.674	1.719	1.651	1.767	1.628	1.694
Nb/Ta	9	8	9	9	8	14
(Nb+Ta)/Ti	2	2	2	2	2	2
U/ΣR ²⁺	20	21	22	19	21	28

na = not analyzed.

ΣR²⁺ = Fe+Mn+Ca+Na+K+Th+U+Zr+Y+Ce+Nd.

¹Guo et al. (1996b).

²Sutherland et al. (1998a).

2.5 Discussion

Sapphire and ruby deposited within basaltic terranes have been suggested that they could not be crystallized directly from basaltic magma (Coenraads, 1992; Guo et al., 1996b; Khamloet et al., 2014; Levinson and Cook, 1994; Promwongnan and Sutthirat, 2019b; Sutherland et al., 2002; 1998a; 2015b). A corroded surface is typical feature observed in basalt-associated sapphires which clearly indicates transportation by the hot magma. This has also been reported for sapphires from Di Linh and Binh Thuan (Smith et al., 1995). A petrochemical study of sapphire-associated basalts from Dak Nong has also suggested that these xenocrystic sapphires may have formed in the boundary between the lower crust and upper mantle prior to corrosive transport in alkaline basaltic magma (Garnier et al., 2005). Moreover, a hypothesis has recently been proposed that the original crystallization of alluvial Dak Nong sapphires should have taken place in the shallow crust within an iron-rich syenite melt in collaboration with carbonate-H₂O-CO₂ fluid phases, based on geochemistry of syngenetic mineral inclusions (i.e., zircon, columbite, oligoclase, and Al-Ti-hematite) (Izokh et al., 2010).

Based on results of this detailed study, the most common syngenetic mineral inclusions, i.e., ferrocolumbite, alkali feldspar and zircon in sapphires under this study were similar in composition to those in Dak Nong sapphires (Izokh et al., 2010) as well as alkaline felsic inclusion groups in other alluvial basalt-related sapphires (Guo et al., 1996b). Although, hercynite spinel and ilmenite (titanohematite) inclusions observed in this study were quite different from Al-Ti-hematite (containing 85.6% Fe₂O₃, 11.9% Al₂O₃, 1.57% TiO₂ reported by Izokh et al., (2010) in Dak Nong sapphires, they still favored igneous sources instead of metamorphic sources. Although, columbite and pyrochlore in the studied sapphires were chemically close to the typical carbonatite assemblage in sapphire (Guo et al., 1996b), they were also similar to those found in alluvial basalt-associated sapphires from silicate melt origin (Sutherland et al., 1998a). Therefore, both columbite and pyrochlore may be controversial evidence to indicate the original source of these sapphires.

Consequently, a unique mineral inclusion suite including alkali feldspar, zircon, hercynitic spinel, and ilmenite appears most likely to have crystallized from alkaline felsic magma which is relevant to the original source of sapphires from Southern Vietnam. This magmatism should have been taken place extensively prior to

fractionated crystallization in the lower crust. This model agrees well with the genetic model proposed by Aspen et al., (1990); Pin et al., (2006); Upton et al., (2009); Sutherland et al., (1998a; 2009); Zaw et al., (2006), Khamloet et al., (2014); Promwongnan and Sutthirat (2019b).

Based on the geological setting in Southern Vietnam, granite and granosyenite occurred in Triassic and Cretaceous during orogenic periods due to Indosinian-Yangtze (South China) collision and Paleo-Pacific plate subduction, respectively (Carter et al., 2001; Nguyen et al., 2004; Shellnutt et al., 2013; Tri and Khuc, 2011). Subsequently, alkali basaltic magmas in Southern Vietnam had probably been derived from garnet peridotite of the asthenosphere at high pressure (<4 GPa) and high temperature (about 1470 °C) (Hoang and Flower, 1998), and mixed with recycling oceanic crustal materials from Paleo-Pacific plates that subducted beneath the Southeast Asian continental margin (Anh et al., 2018) during the early Tertiary Indian-Eurasian collision. Rising penetration at close to the Moho at about 50-60 km depth, the heat and volatility separated from these alkaline mafic melts caused the extensive melting of silicate rocks (granite and granosyenite) at lower-crust level with the formation of alkaline felsic melt (figure 2.14). Sapphires should have crystallized directly during the slow cooling of this alkaline felsic melt. Afterwards, the alkaline basaltic magma from the asthenosphere of mantle rose and then brought these sapphires onto the surface via volcanic eruption.

2.6 Conclusions

Mineral inclusions including ferrocolumbite, zircon, alkali feldspar, hercynite spinel, ilmenite (titanohematite), and pyrochlore were identified in sapphires from main gem deposits in Southern Vietnam. On the basis of mineral chemistry, they can be mostly grouped into alkaline felsic suites. A genetic model of “alkaline felsic melt” was proposed for the original formation of these sapphires. Detailed studies on U/Pb dating and trace analysis of zircon inclusions should be carried out to support time scale and original formation of the sapphire hosts; moreover, unidentified iron-bearing inclusions may give more significant information related to the crystallization environment.

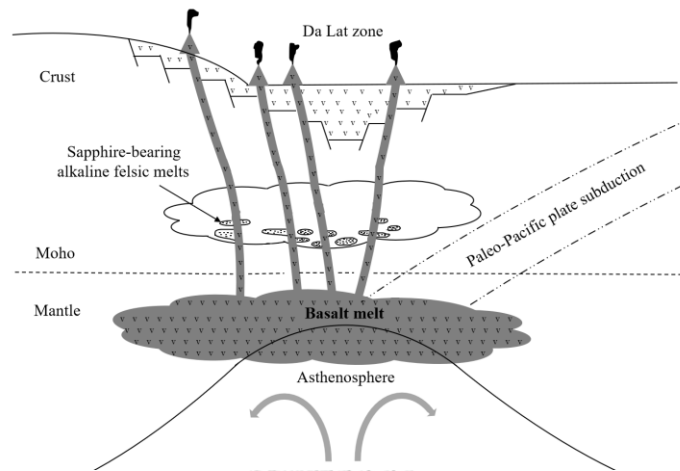


Figure 2.14 The model for sapphire origin alkaline felsic melt, based on the alkaline basalt and crust growth models for Southern Vietnam (Anh et al., 2018; Hoang and Flower, 1998; Tri and Khuc, 2011).

CHAPTER 3

VARIETY OF IRON OXIDE INCLUSIONS IN SAPPHIRE FROM SOUTHERN VIETNAM: INDICATION OF ENVIRONMENTAL CHANGE DURING CRYSTALLIZATION

3.1 Introduction

Iron-oxide minerals have been considered particularly as a significant geothermometer for their related assemblage as well as host rocks (Buddington and Lindsley, 1964; Coenraads, 1992; Karsli et al., 2008; Saminpanya and Sutherland, 2011; Sutherland and Coenraads, 1996; Turnock and Eugster, 1962). Previous investigations of gem sapphire from Southern Vietnam (i.e. Dak Nong, Di Linh, and Binh Thuan deposits) have recognized several iron-oxide inclusions (Izokh et al., 2010; Smith et al., 1995). Most of them were identified as ilmenite, magnetite-hercynite, and chromite-hercynite, using Scanning Electron Microscope-Energy Dispersive Spectrometer (SEM-EDS) and X-ray Diffractometer (XRD) (Smith et al., 1995). Moreover, Izokh et al. (2010) reported an iron-oxide inclusion namely Al-Ti-hematite that was chemically analyzed by EPMA; subsequently, they proposed that crystallization of host sapphire should relate to iron-rich syenitic melt and metasomatism between crustal rocks and contaminated basaltic melt in Dak Nong deposit. Although iron-oxide inclusions were previously reported, their mineral chemistry has never been completely analyzed.

This study was therefore designed to analyze most kinds of iron-oxide inclusion in sapphire from various basalt-related deposits in Southern Vietnam (i.e. Dak Nong, Di Linh, Binh Thuan, Krong Nang, and Pleiku). Detailed study of their mineral chemistry led to an interpretation of genesis and P-T condition of sapphire formation.

3.2 Geological setting

Late Cenozoic volcanism has related to regional tectonics, particularly after the end of East Sea opening in the Middle Miocene (Barr and MacDonald, 1981; Hoang et al., 2013; 1996) (Figure 3.1). Paleo-Pacific oceanic crustal material, previously subducted into the lower mantle, was subsequently entraining into the Hainan plume which was the main cause of basaltic magmatism in Southern Vietnam (Anh et al.,

2018). According to Hoang and Flow (1998), these volcanic activities have been exceeding over 100 km in diameter with thickness up to several hundred meters and covering a total area of approximately 23,000 km². The centers of volcanism appear to have developed during two main eruptive episodes. The early phases generated mainly quartz and olivine tholeiites with rare alkali basalt whereas the later phases produced olivine tholeiite, alkali basalt, basanite, and rare nephelinite. Tholeiite eruptions occurred significantly in the centers associated with the extensional rift. On the other hand, alkali basalt, olivine tholeiite, and basanite appear to have erupted along with conjugate strike-slip faults (Hoang et al., 1996). It should be notified that sapphire occurrences, mainly discovered in Quaternary and Upper-Pleistocene basaltic alluvials, have been related to alkali basalt (Garnier et al., 2005; Smith et al., 1995).

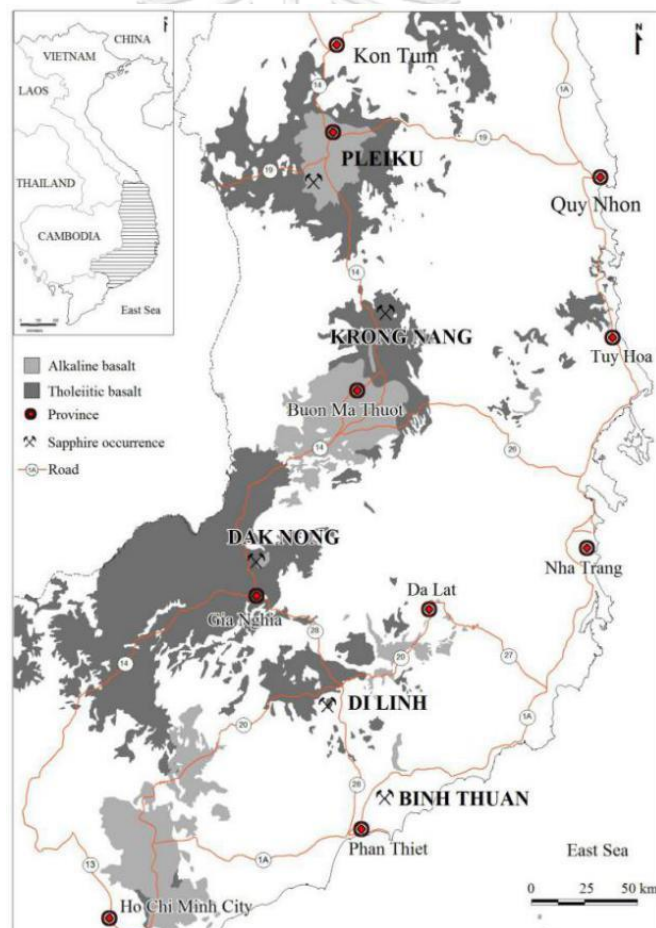


Figure 3.1 This geological map shows distribution of Cenozoic basalts and locations of sapphire occurrences in Southern Vietnam, modified after Hoa et al., (2005).

3.3 Materials and methods

Sapphire collections with a size of about 5 mm, were sampled from Dak Nong, Di Linh, Binh Thuan, Krong Nang, and Pleiku in Southern Vietnam (see Figure 3.1). Metallic opaque inclusions in the sapphire collection were specifically observed and picked up for further study. After mounting in epoxy, they were ground by a diamond wheel until inclusions were exposed; subsequently, they were polished using 6 μm , 3 μm , and 1 μm diamond pastes, respectively. These inclusions were initially identified by a Laser Raman spectroscope, Invia model, Renishaw equipped with a Leica optical microscope at the Gem and Jewellery Institute of Thailand (Public Organization) (GIT). The laser beam was generally set at about 5 μm with standard conditions including 532 nm radiation of NIR diode laser emitting at 785 nm and power of 15.7 mW (about 5 mW on the sample), at an approximate resolution of 0.5 cm^{-1} . However, Raman patterns of iron minerals may be quickly transformed by the excitation of the laser power (Hanesch, 2009). In this study, the laser power was therefore set at 0.5 and 5 mW on the sample, to observe detailed Raman patterns of these inclusions. Each spectrum was recorded in the spectral range from 200 cm^{-1} to 1500 cm^{-1} with 20 seconds exposure time, 6 accumulation, 50x magnification, at laboratory temperature of about 22 $^{\circ}\text{C}$.

Subsequently, these samples were carbon coated prior to major and minor analyses using an Electron Probe Microanalyzer (EPMA, JEOL model JXA-8100) at the Department of Geology, Faculty of Science, Chulalongkorn University. The operating condition was set up at 15 kV acceleration voltages with about 24 nA filament current; elements, appropriate standards and analytical crystals were selected for analyses with 30 seconds for peak counts and background counts of each element before automatic ZAF correction was applied to report as oxide contents. Finally, atomic proportions of these oxide analyses were recalculated on the basis of appropriate amount of oxygen as well as Fe^{2+} and Fe^{3+} ratios were also estimated using equation of Droop (1987).

3.4 Results

3.4.1 Morphology of iron oxide inclusions

Although, all of the studied iron-oxide minerals are similarly black opaque, their morphological affinities can be distinguished into two groups, i.e., octahedral and

rhombohedral shapes. Octahedral iron oxides form as single or aggregate crystals ranging in the size from 20-500 μm (Figure 3.2). On the other hand, rhombohedral iron oxides always show single crystals with size of about 80-600 μm length, and 40-300 μm width (Figure 3.3). Raman spectroscopic identification of these iron-oxide inclusions is reported below.

3.4.2 Raman spectroscopy of iron oxide inclusions

It should be notified again that the Raman pattern of iron minerals may be transformed rapidly by laser induction leading to Raman shift, which such effect can also be involved by the natural processes such as oxidation, recrystallization, order–disorder transitions (cation redistribution), phase transition or decomposition (Faria et al., 1997; Hanesch, 2009; Shebanova and Lazor, 2003). Therefore, low laser power about 0.5 and normal operation at 5 mW on the sample was applied in this study to observe Raman pattern and its alteration in each type of iron-oxide inclusions. As a results, three distinctive types were recognized by the Raman spectra; they were identified as wüstite, hercynite, and ilmenite groups. In comparison with morphological features, wüstite and hercynite inclusions belong to octahedral shape whereas ilmenite inclusions are characterized by rhombohedral shape.

Wüstite, Fe_{1-x}O with $0.04 < x < 0.12$, is stable at temperatures below 570 $^{\circ}\text{C}$ (Hazen and Jeanloz, 1984) which its destruction may lead to $\alpha\text{-Fe}$ and Fe_3O_4 (Jozwiak et al., 2007). Raman spectrum of wüstite appears to be transformed partly to magnetite (Fe_3O_4) even applying low power laser for excitation and it seems to be changed completely to the hematite spectrum with higher laser power (Faria et al., 1997; Hanesch, 2009; Raman et al., 1998; Thibeau et al., 1978). At the low laser power (0.5 mW), all wüstite inclusions clearly showed an only clear strong peak at 670 cm^{-1} of magnetite (Figure 3.4a). On the other hand, at high laser power (5 mW), some of Raman pattern of wüstite inclusions in the studied sapphire (e.g., DL50, DL56, PT17) were always composed of characteristic patterns of magnetite (weaker peak at around 670 cm^{-1}), hematite with higher intensity peaks at 247, 299, and 412, and wüstite assigned by the 595 cm^{-1} peaks as suggested by Hanesch (2009) (Figure 3.4b). These spectra match wüstite spectrums observed at low and high laser powers reported by Faria et al. (1997). Particularly, the others also showed similar to these Raman spectra but have a broader and higher band at the peak of magnetite (670 cm^{-1}) (Figure 3.4c), which may

be attributed to the Raman-active vibrations of spinel groups (Cynn et al., 1992), indicating more spinel group component in their structure. EPMA analysis will make more details on this type of spinel group. Comparison of the process of changing the wüstite spectrum under the effect of laser power in Figure 3.4 leads to the conclusion that magnetite peaks formed during the spectrum radiation were transformed into hematite peaks when increasing laser-power.

Raman spectrum of hercynite is displayed in Figure 3.5. The spectrum recorded at 0.5 mW yielded a strong band at 770 cm^{-1} which indicated vibration of AlO_4 tetrahedra, characteristic of spinel structure as suggested by (Cynn et al., 1992). In addition, another peak at 600 cm^{-1} was weaker and narrower than the first peak (Figure 3.5a). At 5 mW laser power, the characteristic spinel peak was broader and shifted at lower wavenumbers (753 cm^{-1}) with the appearances of additional weak peaks at 701 cm^{-1} and 593 cm^{-1} (Figure 3.5b). These spectra are similar to the hercynite spinel reported by Ospitali et al. (2005).

Ilmenite inclusion showed Raman spectrum indicating a mixture of minerals. Two main peaks observed using lower laser power were at 299, 498, and 683 cm^{-1} (Figure 6a). The highest intensity peak, 683 cm^{-1} , is due to ilmenite (Wang et al., 2004) whereas 299 and 498 cm^{-1} peaks are caused by hematite (Faria et al., 1997). Using higher laser power (5 mW), the Raman spectrum revealed broadened peaks at 247, 293, and 613 cm^{-1} matching the pattern of hematite; moreover, an additional characteristic peak of ilmenite still presented around 683 cm^{-1} as well as weak peaks at 430, 600, and 1370 cm^{-1} likely indicated oxidized titanomagnetite (Figure 6b) (Shebanova and Lazor, 2003; Wang et al., 2004). The Raman spectrum at high laser power (5 mW) appeared similarly ilmenite exsolution in the Ti-rich magnetite (titanomagnetite) in igneous intrusive rocks from Bijigou, Pazhuhua, and Xinjie in China (Tan et al., 2016).

In addition, mineral chemistry of iron oxide inclusion, based on EPMA, clearly supports Raman spectroscopic identification. Representative EPMA analyses of each iron-oxide type are present in Tables 3.1 to 3.3.

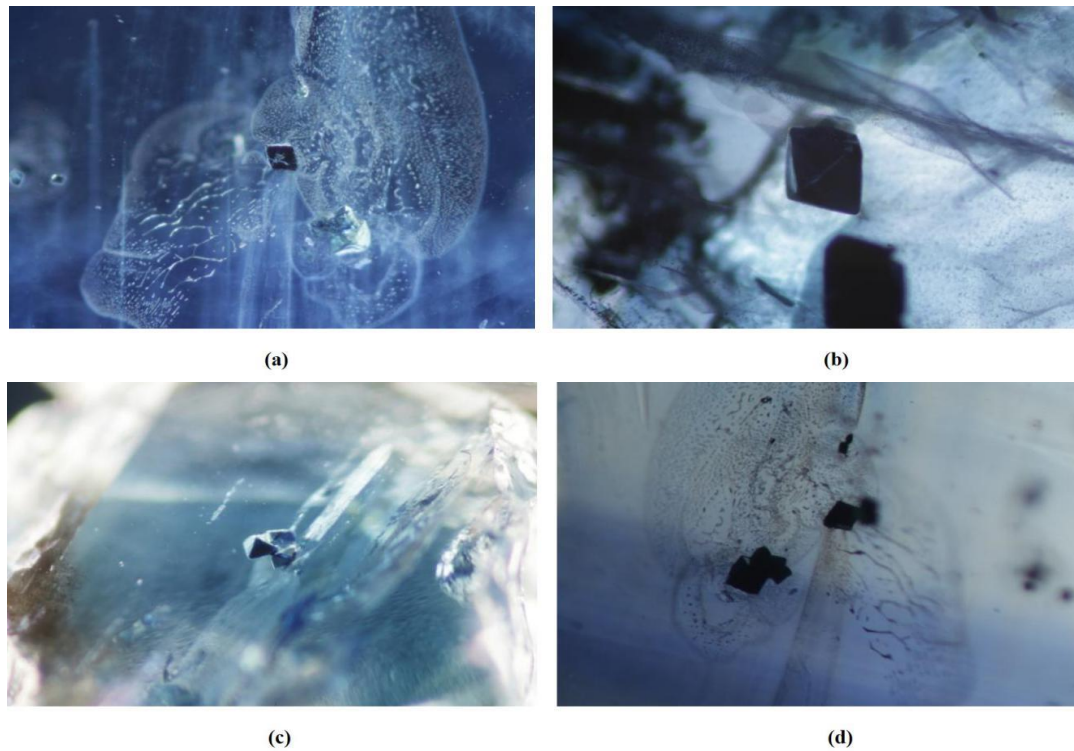
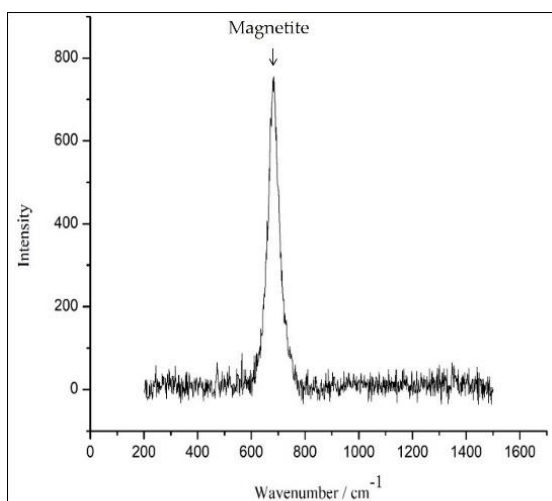


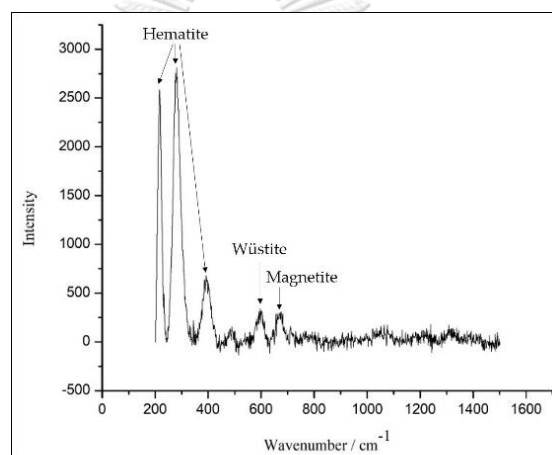
Figure 3.2 Photomicrographs showing: **(a)** a small octahedral wüstite inclusion; **(b)** a bigger octahedral hercynite inclusion; **(c)** aggregate crystals of octahedral wüstite inclusions, and **(d)** aggregate crystals of octahedral hercynite inclusions. They were observed in darkfield illumination. Photo by Doan Thi Anh Vu.



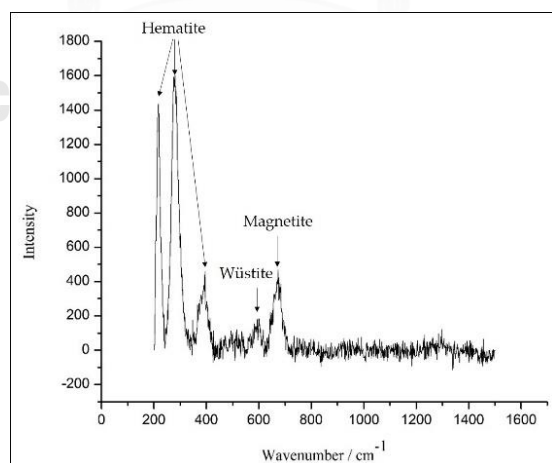
Figure 3.3 Photomicrographs of rhombohedral hematite-ilmenite inclusions found in sapphires from Southern Vietnam: **(a)** a single crystal and **(b)** several single crystals. All photos were taken in darkfield illumination by Doan Thi Anh Vu.



(a)



(b)



(c)

Figure 3.4 Raman spectra of wüstite in laser power at 0.5 mW (a) and 5 mW (b and c).

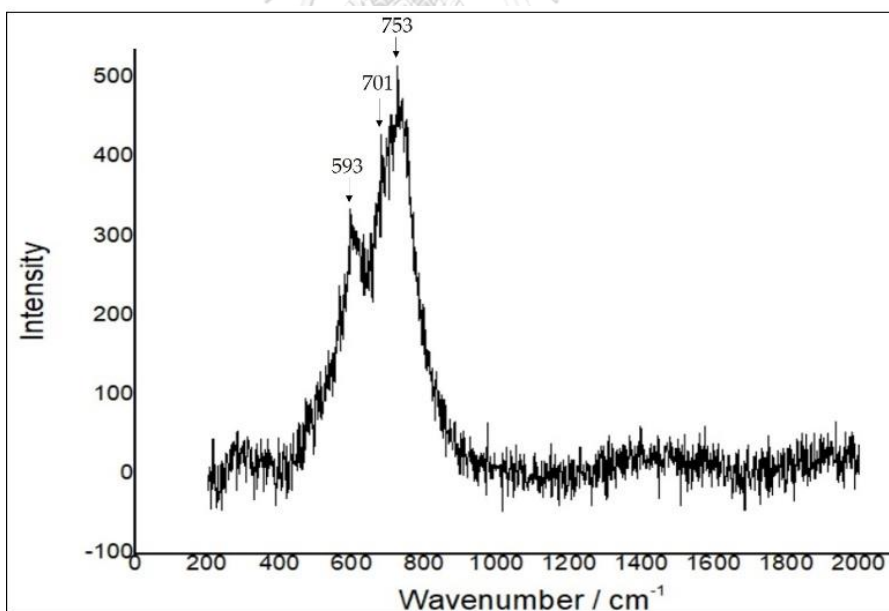
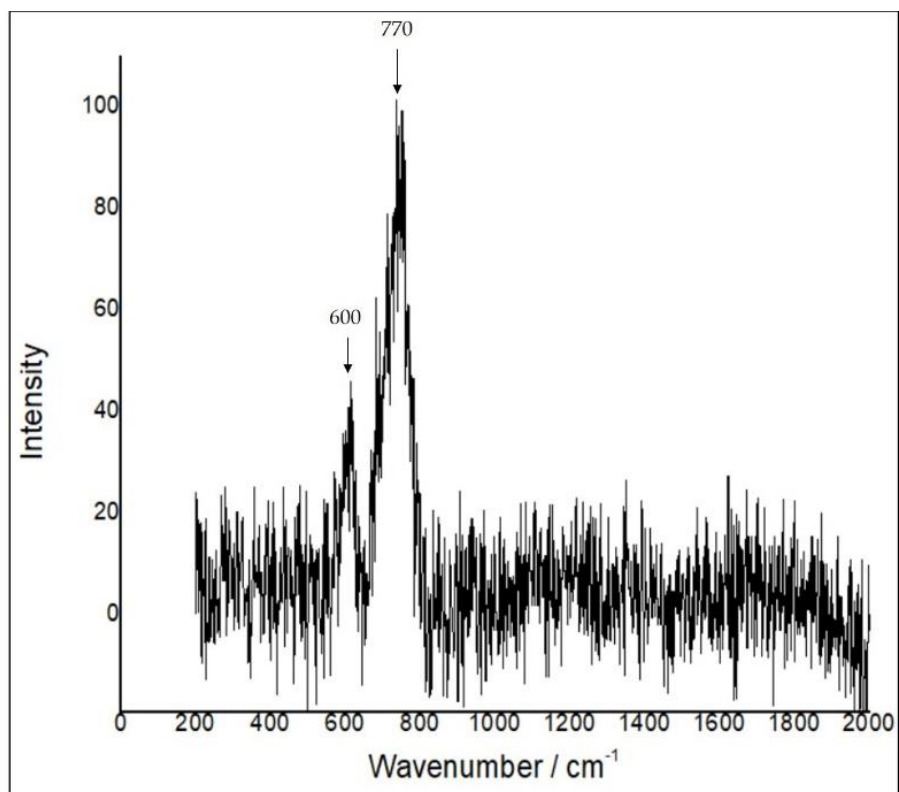
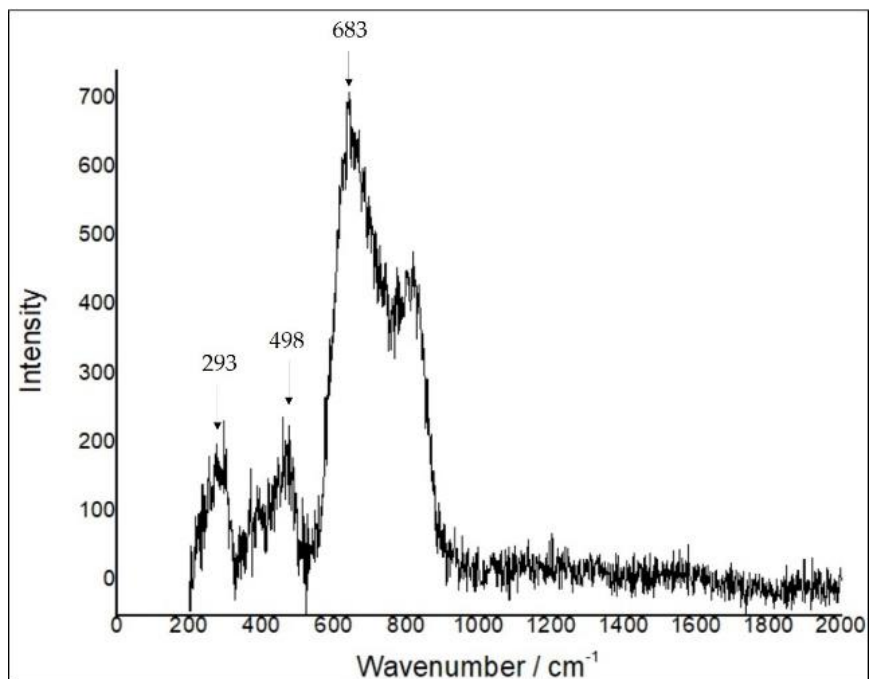
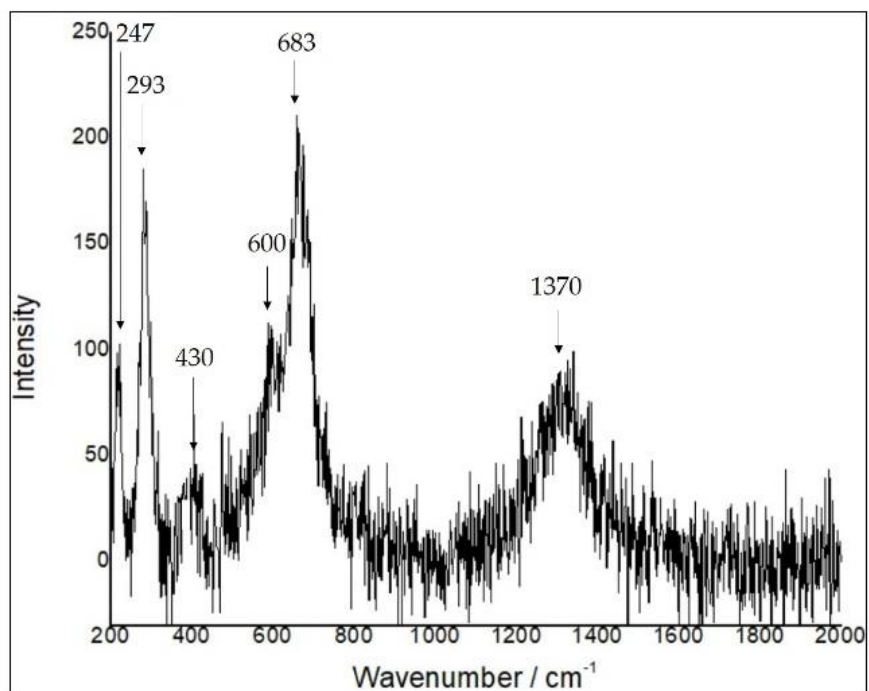


Figure 3.5 Raman spectra of hercynite spinel: 0.5 mW (a) and 5 mW (b).



(a)



(b)

Figure 3.6 Raman spectra of ilmenite: 0.5 mW (a) and 5 mW (b).

Table 3.1 Representative EPMA analyses of wüstite inclusions in sapphires from Southern Vietnam

Mineral phase analysis (wt%)	Wüstite (FeO)-Hercynite										Wüstite (FeO)			
	Southern Vietnam										Southern Vietnam			Germany
	Dak Nong		Di Linh		Krong Nang		Binh Thuan		Pleiku		Di Linh		Binh Thuan	Rumburk ¹
	DN74	DN89	DL14	DL63	KN20a	KN05	PT18	PT49	GL27	GL85	DL50	DL56	PT17a	
SiO ₂	0.03	0.02	0.00	0.00	0.00	1.58	0.34	0.44	0.34	0.00	0.02	0.15	0.27	0.85
TiO ₂	0.84	1.57	1.53	0.00	0.00	6.62	0.52	5.89	0.00	1.33	2.33	3.25	0.22	0.04
Al ₂ O ₃	9.85	8.78	6.66	10.17	5.61	10.82	10.14	12.88		6.18	0.21	0.27	0.12	0.29
Cr ₂ O ₃	0.01	0.00	0.04	0.06	0.00	0.33	0.06	0.03	0.03	0.00	0.02	0.04	0.03	na
FeO	88.13	87.90	89.29	86.83	85.30	75.75	86.45	77.29	86.25	82.50	96.45	95.31	95.46	91.94
MnO	0.2	0.14	1.49	0.00	2.25	0.08	1.57	2.38	0.00	0.88	0.41	0.35	1.81	0.14
MgO	0.35	0.18	0.29	0.00	0.13	0.15	0.05	0.15	0.00	0.30	1.36	0.40	0.88	0.12
ZnO	0.67	0.33	0.36	0.01	0.68	0.31	0.00	0.82	0.07	0.37	0.00	0.00	0.00	na
CaO	0.00	0.00	0.00	0.00	0.00	0.12	0.00	0.00	0.00	0.00	0.00	0.29	0.00	0.14
NiO	0.02	0.00	0.00	0.00	0.01	0.10	0.00	0.08	0.05	0.02	0.03	0.00	0.00	na
Total	100.11	98.92	99.66	97.07	93.97	95.86	99.13	99.47	98.12	91.58	100.84	100.06	98.78	93.52
Formula 4(O)														
Si	0.001	0.001	0.000	0.000	0.000	0.065	0.015	0.002	0.015	0.000	0.001	0.007	0.013	0.043
Ti	0.027	0.051	0.051	0.000	0.000	0.206	0.017	0.178	0.000	0.048	0.081	0.113	0.008	0.002
Al	0.496	0.450	0.346	0.529	0.315	0.527	0.513	0.612	0.577	0.349	0.011	0.015	0.007	0.017
Cr	0.000	0.000	0.001	0.002	0.000	0.011	0.002	0.001	0.001	0.000	0.001	0.001	0.001	-
Fe ²⁺	3.147	3.194	3.291	3.203	3.403	2.620	3.105	2.604	1.507	3.309	3.708	3.681	1.962	3.863
Mn	0.007	0.005	0.056	0.000	0.091	0.003	0.057	0.081	0.000	0.036	0.016	0.014	0.073	0.006
Mg	0.022	0.012	0.019	0.000	0.009	0.009	0.003	0.009	0.000	0.022	0.093	0.027	0.062	0.009
Zn	0.021	0.011	0.012	0.000	0.024	0.009	0.000	0.000	0.002	0.013	0.000	0.000	0.000	-
Ca	0.000	0.000	0.000	0.000	0.000	0.005	0.000	0.024	0.000	0.000	0.000	0.014	0.000	0.008
Ni	0.001	0.000	0.000	0.000	0.000	0.003	0.000	0.003	0.002	0.001	0.001	0.000	0.000	-
Total*	3.723	3.723	3.776	3.734	3.842	3.460	3.711	3.514	3.697	3.777	3.912	3.872	3.975	3.947
ΣR ²⁺	3.198	3.222	3.378	3.203	3.527	2.649	3.165	2.721	1.511	3.381	3.818	3.736	2.097	3.886
ΣR ³⁺	0.524	0.502	0.397	0.529	0.315	0.798	0.545	0.793	0.9.5	0.397	0.093	0.135	0.028	0.062
Wüstite%	86	87	89	86	92	77	85	77	84	89	98	96	99	98
Hercynite %	14	13	11	14	8	23	15	23	16	11	2	4	1	2

Not. na = not analyzed.

$$\Sigma R^{2+} = \text{Fe}^{2+} + \text{Mn} + \text{Mg} + \text{Zn} + \text{Ca} + \text{Ni}, \Sigma R^{3+} = \text{Si} + \text{Ti} + \text{Al} + \text{Cr} + \text{Fe}^{3+}.$$

¹Seifert et al. (2010).

Table 3.2 Representative EPMA analyses of spinel inclusions in sapphire from Southern Vietnam

Mineral phase analysis (wt%)	Dak Nong		Di Linh	Krong Nang		Binh Thuan		Pleiku
	DN12	DN16	DL62	KN20b	KN43	PT07	PT55	GL07
SiO ₂	0.00	0.00	0.01	0.00	0.00	0.02	0.00	0.02
TiO ₂	0.12	0.08	0.70	0.00	0.00	0.00	0.00	0.32
Al ₂ O ₃	60.99	60.93	60.76	61.07	60.68	61.12	60.94	60.02
Cr ₂ O ₃	0.00	0.00	0.09	0.07	0.02	0.01	0.00	0.00
FeO	33.99	34.18	33.87	33.84	32.24	33.40	34.62	33.87
MnO	0.00	0.89	0.34	0.81	0.28	0.06	0.46	0.98
MgO	4.02	4.29	4.62	4.61	5.26	4.55	4.07	5.23
ZnO	0.12	0.38	0.18	0.00	0.63	0.67	0.18	0.00
CaO	0.06	0.00	0.00	0.00	0.00	0.00	0.01	0.00
NiO	0.00	0.00	0.00	0.03	0.00	0.09	0.00	0.00
Total	99.29	100.74	100.58	100.43	99.11	99.91	100.27	100.45
Formula 32(O)								
Si	0.000	0.000	0.002	0.000	0.000	0.003	0.000	0.005
Ti	0.020	0.014	0.117	0.000	0.000	0.000	0.000	0.054
Al	16.134	15.975	15.886	16.003	16.025	16.071	16.040	15.763
Cr	0.000	0.000	0.016	0.012	0.004	0.002	0.000	0.000
Fe ³⁺	0.000	0.000	0.000	0.000	0.000	0.000	0.000	0.157
Fe ²⁺	6.380	6.359	6.285	6.292	6.042	6.232	6.466	6.155
Mn	0.000	0.168	0.064	0.152	0.053	0.012	0.087	0.186
Mg	1.344	1.421	1.529	1.529	1.758	1.514	1.355	1.739
Zn	0.020	0.062	0.030	0.000	0.104	0.111	0.030	0.000
Ca	0.015	0.000	0.000	0.000	0.000	0.000	0.002	0.000
Ni	0.000	0.000	0.000	0.006	0.000	0.017	0.000	0.000
Total*	23.913	23.999	23.929	23.993	23.986	23.960	23.980	24.059
ΣR ²⁺	7.759	8.010	7.907	7.979	7.957	7.885	7.940	8.080
ΣR ³⁺	16.154	15.989	16.022	16.014	16.029	16.076	16.040	15.979

Not. Fe²⁺ and Fe³⁺ were recalculated from total FeO after the method of Droop (1987).

ΣR²⁺ = Fe²⁺+Mn+Mg+Zn+Ca+Ni. ΣR³⁺ = Si+Ti+Al+Cr+Fe³⁺.

Table 3.3 Representative EPMA analyses of ilmenite inclusions in sapphire from Southern Vietnam

Mineral phase analysis (wt%)	Dak Nong		Di Linh	Krong Nang		Binh Thuan		Pleiku
	DN12	DN16	DL62	KN20b	KN43	PT07	PT55	GL07
SiO ₂	0.00	0.00	0.01	0.00	0.00	0.02	0.00	0.02
TiO ₂	0.12	0.08	0.70	0.00	0.00	0.00	0.00	0.32
Al ₂ O ₃	60.99	60.93	60.76	61.07	60.68	61.12	60.94	60.02
Cr ₂ O ₃	0.00	0.00	0.09	0.07	0.02	0.01	0.00	0.00
FeO	33.99	34.18	33.87	33.84	32.24	33.40	34.62	33.87
MnO	0.00	0.89	0.34	0.81	0.28	0.06	0.46	0.98
MgO	4.02	4.29	4.62	4.61	5.26	4.55	4.07	5.23
ZnO	0.12	0.38	0.18	0.00	0.63	0.67	0.18	0.00
CaO	0.06	0.00	0.00	0.00	0.00	0.00	0.01	0.00
NiO	0.00	0.00	0.00	0.03	0.00	0.09	0.00	0.00
Total	99.29	100.74	100.58	100.43	99.11	99.91	100.27	100.45
Formula 32(O)								
Si	0.000	0.000	0.002	0.000	0.000	0.003	0.000	0.005
Ti	0.020	0.014	0.117	0.000	0.000	0.000	0.000	0.054
Al	16.134	15.975	15.886	16.003	16.025	16.071	16.040	15.763
Cr	0.000	0.000	0.016	0.012	0.004	0.002	0.000	0.000
Fe ³⁺	0.000	0.000	0.000	0.000	0.000	0.000	0.000	0.157
Fe ²⁺	6.380	6.359	6.285	6.292	6.042	6.232	6.466	6.155
Mn	0.000	0.168	0.064	0.152	0.053	0.012	0.087	0.186
Mg	1.344	1.421	1.529	1.529	1.758	1.514	1.355	1.739
Zn	0.020	0.062	0.030	0.000	0.104	0.111	0.030	0.000
Ca	0.015	0.000	0.000	0.000	0.000	0.000	0.002	0.000
Ni	0.000	0.000	0.000	0.006	0.000	0.017	0.000	0.000
Total*	23.913	23.999	23.929	23.993	23.986	23.960	23.980	24.059
ΣR ²⁺	7.759	8.010	7.907	7.979	7.957	7.885	7.940	8.080
ΣR ³⁺	16.154	15.989	16.022	16.014	16.029	16.076	16.040	15.979

Not. Fe²⁺ and Fe³⁺ were recalculated from total FeO after the method of Droop (1987).

ΣR²⁺ = Fe²⁺+Mn+Mg+Zn+Ca+Ni. ΣR³⁺ = Si+Ti+Al+Cr+Fe³⁺.

3.4.3 Mineral chemistry of iron oxide inclusions

Wüstite varies in composition from about 76-97% FeO, <13% Al₂O₃, and <7% TiO₂ with traces of MnO (Table 3.1). Based on these compositions, they are mostly characterized by non-stoichiometric formula. Composition of these wüstite inclusions is similar to that forming in under strongly reducing conditions reported from Rumburk granite (see Table 3.1). Calculated atomic proportions show the existence of hercynite in wüstite composition with hercynite ranging from 1 to 23 per cent (see Table 1 again). For formula calculation, only one decimal should be used for formula. Based on the procedure of Smyth et al. (2000), the average chemical formula can be expressed for nonstoichiometry wüstite as $(\text{Fe}^{2+}_{0.3-0.9})(\text{Ti}^{3+}_{<0.179}\text{Al}^{3+}_{\leq 0.6}\text{Cr}^{3+}_{<0.1}\text{Fe}^{3+}_{\leq 0.46})\square_{\leq 0.23}\text{O}$, with $x=0.04-0.23$ implied a deficiency of Fe.

Spinel inclusions present narrow compositional ranges of 60-62% Al₂O₃, 32-36% FeO, and $\leq 5.3\%$ MgO (Table 3.2). Smith et al. (1995) previously reported composition of spinel inclusions in Di Linh and Binh Thuan sapphires, based on SEM-EDS analyses, varying between chromite-hercynite and magnetite-hercynite series. EPMA analyses of spinel inclusions in this study show almost pure hercynite composition $(\text{Fe}^{2+}_{6.0-6.8}\text{Mn}^{2+}_{<0.3}\text{Mg}^{2+}_{<1.8}\text{Zn}^{2+}_{<0.2}\text{Ca}_{<0.1})(\text{Ti}^{3+}_{<0.3}\text{Al}^{3+}_{15.8-16.4}\text{Fe}^{3+}_{<0.2})\text{O}_{32}$ (Figure 3.7). Besides, these analyses show some hercynites intergrowth with wüstites included in sapphire from Southern Vietnam in sample KN20 (see table 3.1 and 3.2 and Figure 3.8).

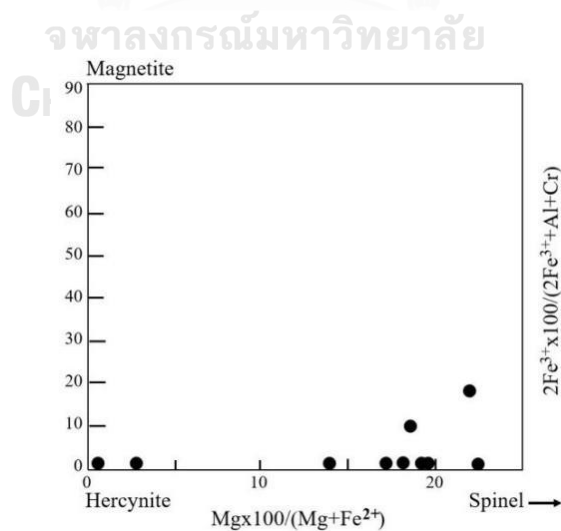


Figure 3.7 Spinel compositions in sapphires from southern Vietnam are plotted on the Spinel-Hercynite-Magnetite diagram. This diagram is taken from Haggerty (1991).

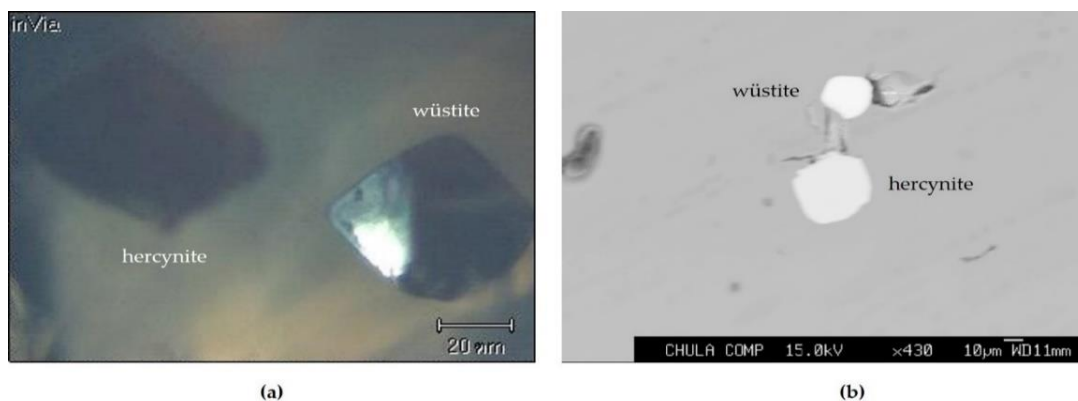


Figure 3.8 Black scattered electron image (BSI) of hercynite and wüstite inclusions found in sapphires from Southern Vietnam: **(a)** Raman, **(b)** EPMA.

Ilmenite inclusions yielded EPMA analyses as summarized in Table 3.3. Their compositions range within about 34-37% TiO_2 , 61-64% FeO , and $\leq 1.5\%$ Al_2O_3 . However, two ilmenite inclusions in Pleiku sapphire show higher Fe contents (75-76 % FeO) with lower Ti contents (19-20% TiO_2). Ternary diagram of FeO - Fe_2O_3 - TiO_2 system (Figure 3.9) shows clearly that most ilmenite inclusions fall within ilmenite-hematite series which GL25 and GL86 samples of Pleiku sapphire move towards hematite component. Consequently, their recalculated atomic proportions yielded different end-member ratios of ilmenite-hematite-magnetite as $\text{Il}_{49-54}\text{He}_{34-40}\text{Mt}_{7-10}$ and $\text{Il}_{24-30}\text{He}_{36-38}\text{Mt}_{35-40}$, respectively (see Table 3.3).

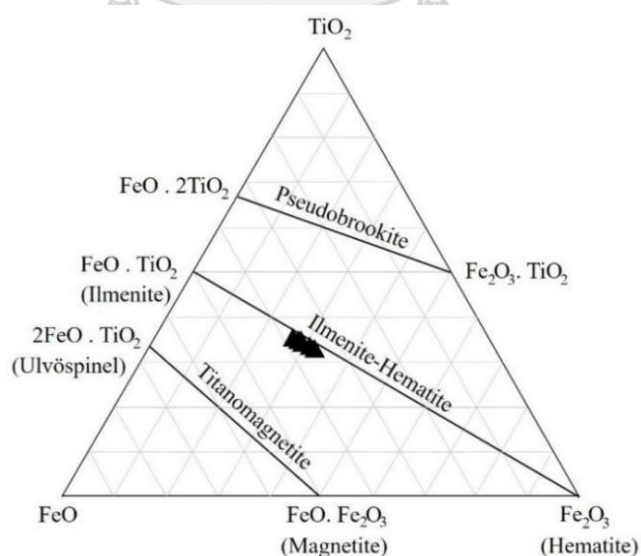
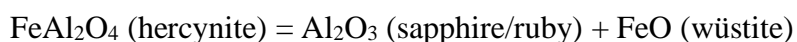


Figure 3.9 Chemical composition of ilmenite-hematite inclusions in sapphire from Southern Vietnam, represented on a FeO - Fe_2O_3 - TiO_2 diagram. The diagram is taken from Buggington and Lindsley (1964).

3.5 Discussion

Iron oxide inclusions in sapphire from Southern Vietnam are mostly characterized by euhedral rhombohedral and octahedral which appear to be syngenetic inclusion (Gübelin, 1983). Therefore, their chemical and physical conditions can be used to reconstruct the original formation of the host sapphire. In this study, based on morphological and Raman spectroscopic characteristics combined with EPMA analyze results, iron oxide minerals in sapphire from Southern Vietnam are determined as wüstite, hercynite, titanohematite, and titanomagnetite. These EPMA analyses are newly reported for mineral chemistry of inclusions in sapphires from Southern Vietnam. Especially, wüstite inclusion is firstly discovered in sapphire.

Raman spectroscopic features of iron oxide inclusions exhibit clearly ilmenite solid solutions (e.g., ilmenite-hematite and titanomagnetite), which are characteristic of rhombohedral solid solutions (Wang et al., 2004); on the other hand, hercynite spinel and wüstite belong to cubic and octahedral shapes (Smyth et al., 2000). EPMA show attribute of wüstite and hercynite in octahedral iron oxide inclusion whereas rhombohedral iron oxides favor ilmenite-hematite (titanohematite, and titanomagnetite). Hercynite components up to 23 percent obtained in nonstoichiometry wüstites (Table 1) may affect increasing of 610 cm^{-1} peaks (magnetite) in the Raman spectrum (Figure 4c). Nonstoichiometry wüstite appears to have formed under a strong reducing condition (Miyashiro, 1964; Seifert et al., 2010). Furthermore, the co-existing syngenetic wüstite and hercynite inclusions in sapphire from Southern Vietnam (Figure 8) may be involved by hercynite breakdown reaction process (Nestola et al., 2015; Schollenbruch et al., 2010):



Therefore, syngenetic wüstite and hercynite inclusions should be formed in a strongly reducing environment related to the hercynite breakdown reaction process. On the other hand, titanohematite and titanomagnetite inclusions should derive from sub-solidus re-equilibration (Buddington and Lindsley, 1964; Lattard, 1995) which suggests an oxidizing environment. Compositions of titanomagnetite inclusion are towards hematite component without ulvöspinel component (Table 3) which should be re-equilibrated under slow cooling oxidized sub-solidus environment (Buddington and Lindsley, 1964; Vincent, 1960). This supports the complete oxidation reaction of

spinel_{ss} by the re-equilibration: $4\text{Fe}_3\text{O}_4$ (in exsolution) + $\text{O}_2 = 6\text{Fe}_2\text{O}_3$ (in ilmenite) to ilmenite exsolution in titanomagnetite.

This information indicates environmental change during the formation of these oxide inclusions as well as their host sapphire. Initial crystallization should be taken place in a strong reducing (indicated by wüstite occurrences) magma chamber before the slow cooling sub-solidus stage under low oxidizing condition (based on phase transform from titanomagnetite to titanohematite). This process is related to oxygen fugacity and temperature changing towards slow cooling process.

Wüstite appears to have occurred in the continental crust as suggested by Seifert et al. (2010) who reported wüstite inclusion in fluorapatite crystallized from S-type granite melts. Furthermore, hercynite has been recognized as inclusion in magmatic sapphires formed in the crust (Sutherland et al., 2002; Sutherland et al., 1998a). Besides, titanomagnetite inclusion with Il_{24-30} component was observed in this study which this ilmenite composition may be formed in plutonic rocks under crustal environment as suggested by Buddington (1955). Therefore, coexisting wüstite, hercynite, titanohematite, and titanomagnetite clearly indicate crystallization directly from magma in the lower crust.

Under a silica-saturated condition, iron-oxide minerals (i.e., wüstite, hercynite, titanohematite, and titanomagnetite) are not stable; all Fe^{2+} atoms enter preferentially silicates' structure, instead. Therefore, wüstite, hercynite, titanohematite, and titanomagnetite may only be formed in the silica-undersaturated environment. Titanomagnetite was proposed higher temperature than the ilmenite-hematite miscibility gap at about 600-700 °C (Lindsley, 1991) because Fe^{3+} in ilmenite-hematite_{ss} tends to exsolve directly as hematite rather than magnetite. Titanomagnetite inclusion in this study should crystallize directly from magma before sub-solidus re-equilibration of iron-titanium oxides during slow cooling within low the oxidizing environment. This late state re-equilibration leads to magnetite decreasing in spinel_{ss} with $f\text{O}_2$ increasing, slightly.

3.6 Conclusion

Iron-oxide mineral inclusions provide useful indicators of crystallization conditions of their host sapphire from Southern Vietnam. They include wüstite, hercynite, titanohematite series, and titanomagnetite series. Titanohematite series and

titanomagnetite series could have been formed in sub-solidus re-equilibration within the slow cooling process. Whereas wüstite might have been crystallized from hercynite breakdown reaction ($\text{hercynite} = \text{sapphire} + \text{wüstite}$). These results indicate environmental change during the crystallization process of sapphire, wüstite, and hercynite under reducing environment in the magma chamber before slow cooling sub-solidus re-equilibrium of titanomagnetite to titanohematite under low oxidizing condition.



CHAPTER 4

TRACE ELEMENT GEOCHEMISTRY AND U-Pb DATING OF ZIRCON INCLUSIONS IN SAPPHIRES FROM SOUTHERN VIETNAM

4.1 Introduction

Zircon is a common inclusion occurred in most basalt-related sapphires from various locations, e.g., Vietnam, Australia, Thailand, Cambodia, Laos, and China (Coenraads et al., 1990; Izokh et al., 2010; Khamloet et al., 2014; Sutherland et al., 2002; 2015a; 2015b). Zircon confined to alteration domains within sapphire has normally assumed to be cogenetic with the host sapphire (Coenraads et al., 1990; Izokh et al., 2010; Khamloet et al., 2014; Sutherland et al., 2002; 2015a; 2015b). Hence, trace element geochemistry combined with dating data of zircon inclusion should be fingerprints and an important indication of the geological formation of the host sapphire. In Southern Vietnam, sapphire has been exploited in basalt-related alluvial deposits (Figure 2.1).

From previously published data, many researchers have carried out isotopic U-Pb dating of zircon using various techniques such as Sensitive High-Resolution Ion Microprobe (SHRIMP), Laser Ablation Inductively Coupled Plasma Mass Spectrometry (LA-ICP-MS), Secondary Ion Mass Spectrometry (SIMS), and an evaporation method (Akinin et al., 2017; Compston, 1999; Liu et al., 2015; Rosa et al., 2002). However, LA-ICP-MS has become popularly used for trace element analysis and age dating of zircon inclusion in basaltic sapphire due to its high sensitivity (Guo et al., 1996c; Khamloet et al., 2014; Mbih et al., 2016; Sutherland et al., 2002; 2015a; 2015b; Sutthirat et al., 2020).

This study presents the morphological features, trace element geochemistry, and U-Pb dating analysis by the LA-ICP-MS technique of zircon inclusion for interpretation of the crystallization environment of the host sapphire.

4.2 Geological setting

The significant tectonic events in Southeast Asia have induced several deformation episodes related to Indosinian and Cretaceous orogenies prior to the opening of the East Sea. The Indosinian and Cretaceous orogenies had induced silicic

intrusions caused by Indosinian-South China collision during Permo-Triassic at about 245-240 Ma and the Paleo-Pacific plate subduction, respectively (Hutchison, 2014; 1989; Metcalfe, 2011). Subsequently, Indosinian-Eurasian collision from 35 to 17 Ma had induced the opening of the East Sea (Barr and MacDonald, 1981). The last activity triggered extensional NW-SE strip-slip and N60°E- and N160°E-trending faults as well as lithospheric thinning; these processes caused melting and upwelling of the underlying asthenosphere forming basaltic melt rising from the lower mantle in Southeastern Asia (Flower et al., 1992). Consequently, Cenozoic basaltic series have erupted throughout this region, occupying over 70,000 km², with exceeding 100 km in diameter, up to several hundred meters thick, extensively during the East Sea opening in Middle Miocene (Barr and MacDonald, 1981) (Figure 2.1). These basalts have ranged in age from 24 Ma to recent when the 1923 eruption of the Ile des Cendres took place on the Vietnamese coast (Hoang and Flower, 1998).

Quaternary and Neogene basaltic rocks that occurred in the Southern and Central Vietnam crop out over an area of approximately 23,000km² (Hoang and Flower, 1998). These basalts have different ages such as in Da Lat (17.6-7.9 Ma), Phuoc Long (<8-3.4 Ma), Buon Ma Thuot (5.8-1.6 Ma), Pleiku (4.3-0.8 Ma), Xuan Loc (0.83-0.44 Ma), and Ile des Cendres (0.8-0. Ma) (Hoang and Flower, 1998), and in Dak Nong (1.1-7.1 Ma) (Garnier et al., 2005) (Figure 4.1). Their volcanic centers reflect two main eruptive episodes, shield-building phases mostly including quartz, olivine tholeiite, and less alkali basalt. The later phases are made up of small-volume flows of alkali basalt, basanite, and rare nephelinite; these basalts are associated with sapphire occurrences (Garnier et al., 2005; Smith et al., 1995). The tholeiite eruptions usually flow in extensional rift while the alkali basalt, olivine tholeiite, and basanite eruptions are associated with the conjugate strike-slip faults (Hoang et al., 1996). Sapphires have been found in Quaternary and Upper-Pleistocene alluvial deposits in Southern Vietnam.

4.3 Material and methods

Most sapphire samples containing zircon inclusion were collected directly from deposits at Binh Thuan and Di Linh in Lam Dong province, Dak Nong and Krong Nang in Dak Lak province (Figure 2.1). The zircon inclusions having good oval shapes with larger size (~200 μm) and lack of fracture were selected for analyses of trace and rare earth elements (REE), and U-Pb dating. These samples were carefully polished with

powder numbers 400 (60 μm), 800 (36-40 μm), 1500 (12 μm), 3000 (8-4 μm), before finishing with 6 μm , 3 μm , 1 μm diamond pastes, respectively. These preparations were carried out until zircon inclusions exposed. Subsequently, they were mounted in epoxy blocks and carbon-coated prior to analytical works. These zircon inclusions were initially observed for zoning patterns using cathodoluminescence (CL) and back-scattered electron (BSE) images.

Major-element composition of zircon inclusions was analyzed by a JEOL JXA-810 Electron Probe Micro-Analyzer (EPMA) at the Department of Geology, Faculty of Science, Chulalongkorn University. The operating condition was set at 15 kV acceleration voltages and 24 nA filament current.

The trace elements including rare earth elements were measured using an LA-ICP-MS system combination between an Agilent 7700 quadrupole ICP-MS (Agilent Technologies, Santa Clara, CA, USA) and a Photon Machines Excimer 193 nm laser system (Excite, Photon machines Inc., Redmond, WA, USA) based at Macquarie University, Australia. Most of these analyses were performed by the same laser conditions as for U-Pb dating. The analytical and calibration procedures for trace elements were similarly reported by Belousova et al. (2002). The NIST 610 standard glass and the GEMOC GJ-1 and Mud Tank zircon standards were used as the external calibration standard (Elhlou et al., 2006).

Zircon U-Pb dating was also carried out by the same LA-ICP-MS system reported above. They were performed with a 50 μm diameter spot, pulsing the laser at 5 Hz, and energy of 8 J/cm². The analytical procedures for U-Pb dating were given by Jackson et al. (2004). The acquisition time for each analysis was 3 minutes, including 1 minute background and 2 minutes signal measurement. Ablation was performed in a He atmosphere to improve the efficiency of ionic transportation. The GEMOC GJ-1 zircon and zircon 91500 were used as a standard for isotopic analysis and independent control on reproducibility and instrument stability, respectively. The data reduction was done with the online software package GLITTER (version 4.4.4, ARC National Key Center, Sydney, Australia) (Griffin et al., 2008). Measured compositions were corrected on the basis of the common-Pb correction method by Andersen, (2002), assuming recent Pb-lost with a common-Pb composition appropriating present-day

average orogenic Pb as the second-stage growth curve for $^{238}\text{U}/^{204}\text{Pb} \approx 9.74$ (Stacey and Kramers, 1975).

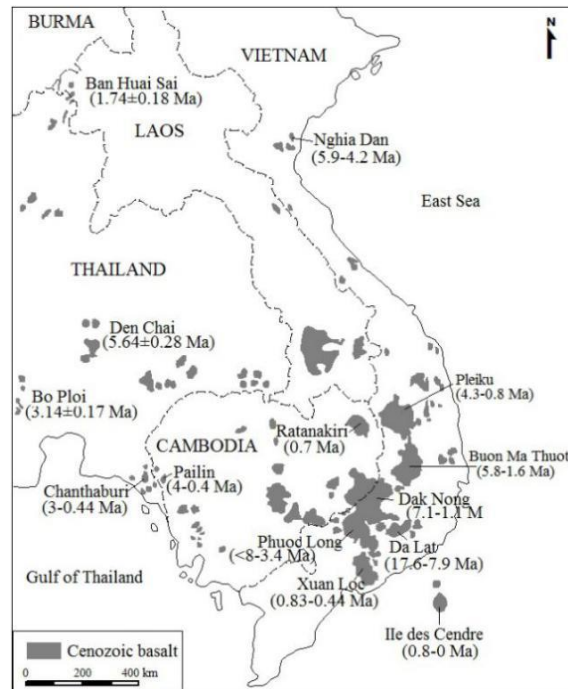


Figure 4.1 Map showing the distribution and ages of Cenozoic basalt in Southeast Asia; dating data in Thailand from modified after Barr and MacDonald, (1981); dating data in Cambodia modified after Sutherland et al., (2015b); dating data in Vietnam from (1998), Hoang et al., (2013), and (2005).

4.4 Results

4.4.1 Crystal habit and morphology

The crystallographic study shows that zircon inclusions have more developed {110} prisms than {100} prisms, which related to high U (Th), Y(REE), and P contents in the parental melt (Benisek and Finger, 1993; Guo et al., 1996c). The combinations of the {110} prisms and {101} bipyramids are a common form of these zircon inclusions. On the other hand, forms of {110} prism plus {211} dipyramids or {311} dipyramids are less pronounced. Crystal length-to-width of these zircon inclusions ranges mostly around 1:1-2, with the highest value of 1:4 (Figure 4.2). Based on the classification of Pupin (2000), these zircons fall in L₅, G₁, S₄, S₅, P₁, and S₇, which are typical crystallization from peralkaline and peraluminous melts (syenite and granite).

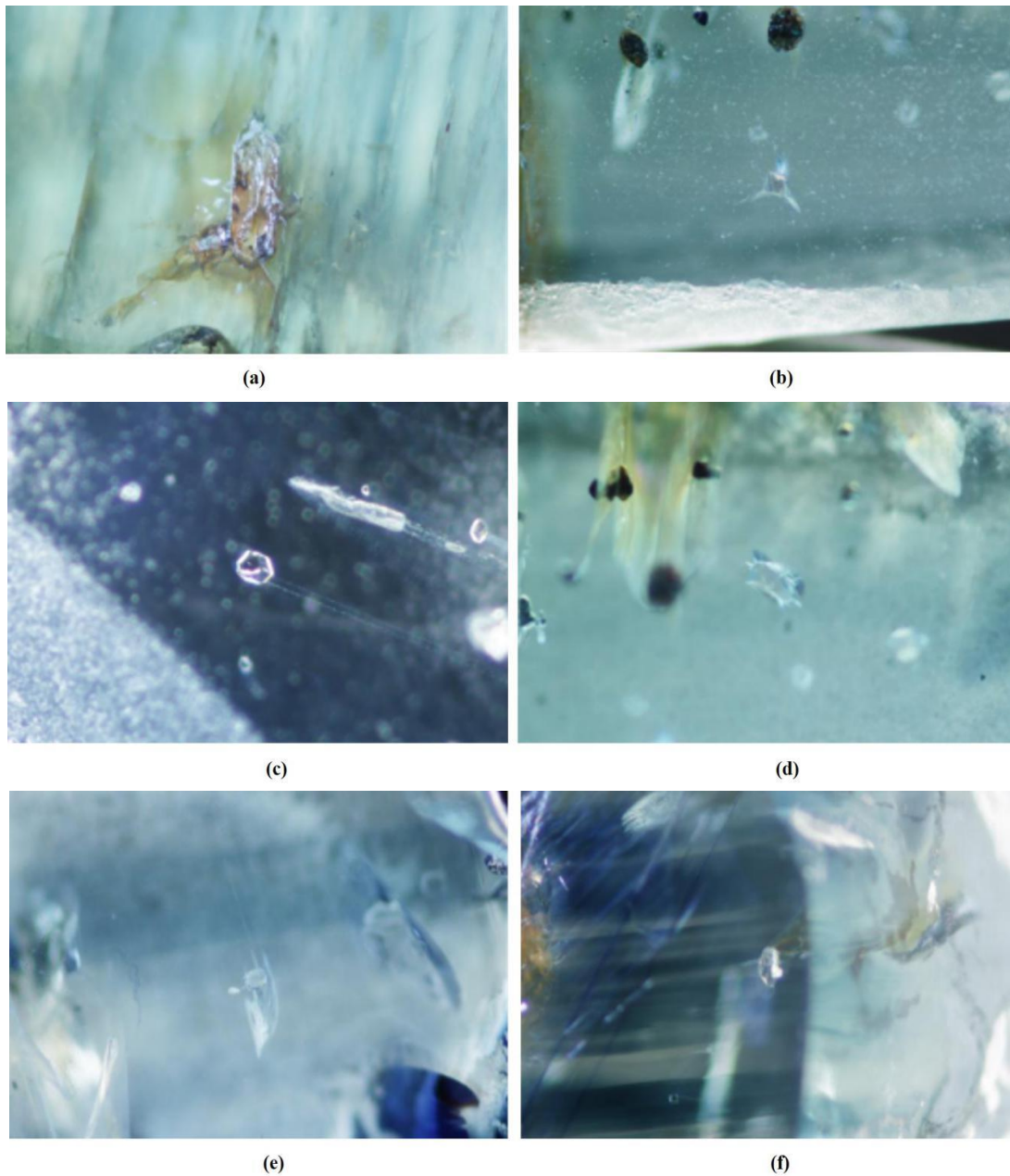


Figure 4.2 Zircon inclusions in sapphire from Southern Vietnam shows the forms of prism $\{110\}$ plus pyramid $\{101\}$ or dipyrmaid $\{101\}$. **(a)** G_1 type of red-orange zircon inclusion. **(b)** G_3 type of small colorless zircon inclusion. **(c)** L_5 type of colorless zircon inclusion. **(d)** P_1 type of colorless zircon inclusion. **(e)** S_5 type of colorless zircon inclusion. **(f)** S_7 type of colorless zircon inclusion.

Cathodoluminescent study indicates that all zircon inclusions display strong, primary, magmatic oscillatory polygonal zoning (Figure 4.3) evidenced for the non-equilibrium conditions during crystallization (Shore and Fowler, 1996). The oscillatory polygonal areas are very fine (Figure 4.3a, b, and c) which are sometimes imposed by distinctive sector zoning (Figures 4.3d and e). Besides, a few samples only show sector zoning (Figure 4.3f).

4.4.2 Mineral chemistry

Representative EPMA analyses of zircon inclusions from each area are present in Table 1. Their major compositions range from about 32 to 34% SiO₂ and 61-65% ZrO₂ whereas HfO₂ ranges moderately 1.8-3.4 %wt which Hf appears to be higher in Binh Thuan zircon. However, these zircons yield Zr/Hf ratios varying from 28 to 59 with an average of 41 that is close to those of continental zircon (36-45) than mantle zircon (60-68) (Pupin, 2000).

Table 4.1 Representative EPMA analyses of zircon inclusions found in sapphire from Southern Vietnam

Mineral phase analysis (wt.%)	Dak Nong			Di Linh			Krong Nang			Binh Thuan		
	DN05	DN20	DN32	DL44	DL46	DL60	KN08	KN13	KN15	PT05	PT13	PT26
SiO ₂	32.56	32.07	32.15	32.59	33.64	33.36	33.62	33.43	33.84	31.95	34.44	33.20
TiO ₂	0.01	0.05	0.00	0.01	0.05	0.00	0.01	0.00	0.01	0.00	0.00	0.00
Al ₂ O ₃	0.01	0.00	0.02	0.00	0.01	0.01	0.01	0.00	0.00	0.00	0.01	0.00
FeO	0.00	0.00	0.07	0.00	0.09	0.10	0.00	0.10	0.00	0.08	0.00	0.00
MgO	0.00	0.00	0.00	0.00	0.02	0.01	0.00	0.00	0.00	0.00	0.02	0.01
CaO	0.00	0.00	0.00	0.00	0.01	0.00	0.00	0.01	0.00	0.00	0.00	0.02
Na ₂ O	0.00	0.00	0.01	0.00	0.00	0.00	0.00	0.00	0.00	0.00	0.00	0.00
K ₂ O	0.00	0.00	0.01	0.00	0.00	0.00	0.00	0.05	0.00	0.00	0.00	0.00
ThO ₂	0.06	0.10	0.03	1.40	0.16	0.41	0.07	0.03	0.32	0.02	0.26	0.27
UO ₂	0.15	0.02	0.09	1.73	0.15	0.45	0.15	0.06	0.30	0.09	0.26	0.73
ZrO ₂	64.33	63.69	62.78	61.00	62.80	62.69	62.47	63.29	63.98	64.68	63.22	61.94
HfO ₂	2.89	3.03	3.27	3.08	2.27	1.82	2.42	2.82	2.26	2.87	2.13	3.41
P ₂ O ₅	0.02	0.01	0.00	0.22	0.04	0.00	0.13	0.09	0.08	0.01	0.09	0.15
Y ₂ O ₃	0.04	0.10	0.00	0.56	0.07	0.04	0.03	0.07	0.05	0.03	0.13	0.07
Total	100.07	99.07	98.42	100.58	99.31	98.88	98.91	99.96	100.86	99.74	100.56	99.80
Zr/Hf	46	36	33	34	47	59	44	38	55	44	51	39

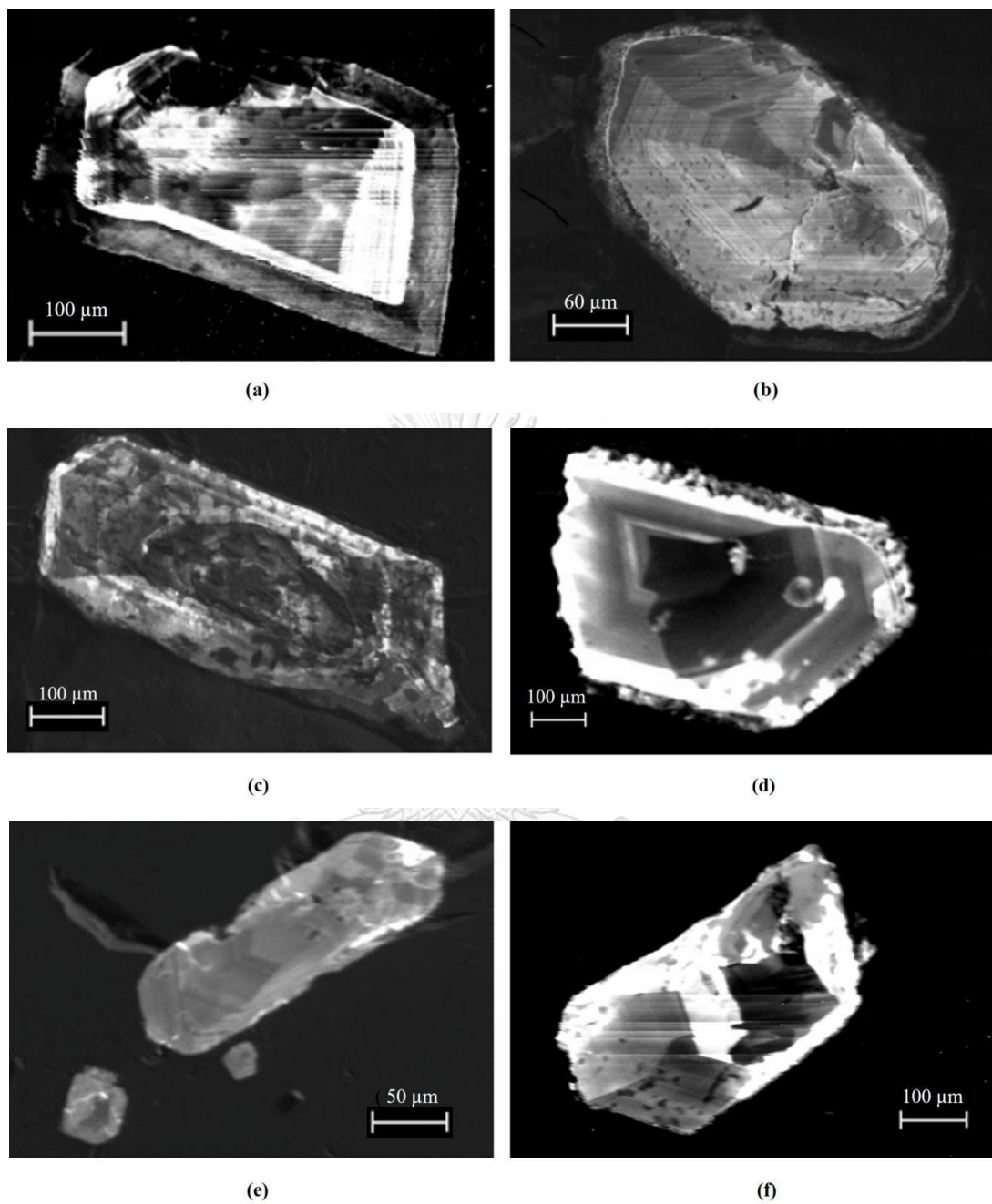


Figure 4.3 Cathodoluminescence images of zircon from Southern Vietnam showing both oscillatory and sector zonation: concentric zoning (a), sector and concentric zoning (b, c, and d), and sector zoning (e and f).

Trace element analyses of these zircon inclusions are representatively summarized in Table 4.2. REE of the studied zircons is normalized to chondrite values (reported by Taylor and McLennan, (1985). Yttrium contents fall within a wide range of hundreds to thousands of ppm (779-4220 ppm). The lowest Y content is found in Krong Nang zircon whereas the highest content is from Di Linh zircon. In comparison with zircon inclusions in sapphire from the previous report of Dak Nong (181-881 ppm, Izokh et al., 2010) and other basalt-related sapphires such as Bo Phloi in Thailand (2431 ppm, Sutthirat et al., 2020), Ratanakiri in Cambodia (117-631 ppm, Sutherland et al., 2015b), and New England in Australia (1218 ppm, Sutherland et al., 1998a), the zircon inclusions in Vietnamese sapphire appear to have higher Y contents; although, zircon inclusions in sapphire from Ban Huai Sai in Laos has been reported with higher content (3966-6275 ppm, Sutherland et al., 2002). However, the Y range of the studied zircons falls within the composition of crustal zircons reported by Belousova et al. (2002).

Uranium concentrations vary from 224 to 3587 ppm. The lowest and highest contents are found in zircon inclusion in Binh Thuan. Previous report of zircon inclusion in Dak Nong sapphire also introduced the similar U content (1252 ppm, Izokh et al., 2010). However, they are higher than kimberlitic zircons from mantle source (6-60 ppm, Belousova et al., 2002). Although, uranium in the studied zircons is lower than zircon inclusions in Ban Huai Sai sapphire from Laos (2855-6506 ppm, Sutherland et al., 2002), it shows similar range to those reported from Bo Phloi in Thailand (403 ppm, Sutthirat et al., 2020), Ratanakiri in Cambodia (average 714 ppm, Sutherland et al., 2015b), and New England in Australia (968-984 ppm, Sutherland et al., 1998a). In comparison with zircon from different source rocks (data from Belousova et al., 2002), it can be presented by plots of U versus Y which the studied zircons fall mostly within the overlapping ranges of syenite pegmatite, granitoid, and other uncommon rocks (e.g., lamproite, basic, larvikite) (Figure 4.4).

Thorium contents range from 329 to 5199 ppm. Likewise the uranium contents, the lowest and highest value is also found in Binh Thuan; these Th contents are similar to those previously reported from Dak Nong sapphire (1092 ppm, Izokh et al., 2010), Ratanakiri in Cambodia (150-1270 ppm, Sutherland et al., 2015b), and New England in Australia (832-850 ppm, Sutherland et al., 1998a), but higher than that from Bo Phloi in Thailand (132 ppm, Sutthirat et al., 2020) and lower than that from Ban Huai Sai in

Laos (1907-6496 ppm, Sutherland et al., 2002). However, the overall Th/U ratios of studied zircons are >0.5 (0.53-3.80) which fall closely into the range of magmatic zircons (Hoskin and Schaltegger, 2003).

Nb and Ta contents range from 11 to 268 ppm and from 4 to 93 ppm, respectively. Both elements are lower than zircon inclusions previously reported from Dak Nong (37-338 ppm Nb and 37-107 ppm Ta, Izokh et al., 2010). However, the Nb/Ta ratios of studied zircons (1.73-3.82) fall into the range of igneous zircon (Belousova et al., 2002). Y versus Nb/Ta discrimination diagram (Figure 4.5) indicates that the studied zircons fall in the overlapping compositional fields of zircons from various sources including syenite pegmatite, granitoid as well as some uncommon rocks such as lamproite, basic, and larvikite.

Yb contents range from 272 to 1145 ppm, with the lowest value is from Dak Nong sapphire and the highest one is obtained from Krong Nang sapphire. However, they appear to be higher than those of zircon inclusions previously reported from Dak Nong (39-368 ppm, Izokh et al., 2010), Ratanakiri in Cambodia (117-631 ppm, Sutherland et al., 2015b), and New England in Australia (563 ppm, Sutherland et al., 1998a), but lower than those of zircon inclusions from Bo Ploi in Thailand (1459 ppm, Sutthirat et al., 2020) and Ban Huai Sai in Laos (1612-3045 ppm, Sutherland et al., 2002). However, the overall U/Yb ratios of studied zircons are over 0.30 (0.31-4.97) which are close to composition of zircon from continental crust rather than that of recycled oceanic crusts shown in the Y against U/Yb classification diagram of Grimes et al. (2007) (Figure 4.6).

Total REE contents of these zircon inclusions range from 705 to 2710 ppm which zircon inclusions from Di Linh appear to have higher REE contents than the others. In comparison, these REE contents are lower than those of zircon inclusions previously reported from Dak Nong (1230-3487 ppm, Izokh et al., 2010), Ban Huai Sai in Laos (3321-5785 ppm, Sutherland et al., 2002), but they are similar to those from Bo Phloi in Thailand (2507 ppm, Sutthirat et al., 2020) and New England in Australia (1142 ppm, Sutherland et al., 1998a). Moreover, the total REE contents of studied zircons are close to those of zircons from syenite pegmatite (2043 ppm) and granitoid (1813 ppm) than carbonatite (600-700 ppm) and lamproite (600-700 ppm) (Belousova et al., 2002).

Table 4.2 Trace element contents (ppm) of zircons found in sapphire from Southern Vietnam compared with those reported from Southeast Asia basaltic gem fields and various sources

Analysis (ppm)	Southern Vietnam								Southeast Asia		Other rocks ³		
	Dak Nong		Di Linh		Krong Nang		Binh Thuan		Laos ¹	Thailand ²	Syenite pegmatite	Granitoid	Carbonatite
	DN05	DN32	DL04	DL46	KN08	KN15	PT05	PT13					
P	266.43	234.88	486.39	347.90	511.39	482.76	426.47	163.26	557.00	1315.57	233.00	763.00	52.00
Y	1468.21	1090.09	2152.97	4220.35	1.194.7	779.04	2868.13	1015.23	3966.00	2631.36	3062.00	2515.00	379.00
Nb	20.76	106.8	36.19	50.02	23.14	20.69	267.46	10.97	na	11.21	16.80	4.30	10.00
La	0.02	0.00	0.03	0.00	0.01	0.0428	0.00	bdl	0.24	bdl	0.15	12.00	0.17
Ce	2.79	9.29	6.79	12.00	1.65	1.221	13.33	2.611	40.00	0.84	34.00	61.00	4.50
Pr	0.01	0.04	0.03	0.06	0.02	0.019	0.05	0.0089	0.41	0.06	0.60	8.00	0.54
Nd	0.27	0.86	0.50	1.11	0.26	0.319	1.45	0.147	3.60	0.92	9.20	44.70	6.20
Sm	1.23	3.07	2.43	5.62	0.68	0.935	5.62	0.886	7.10	2.85	14.00	21.50	6.60
Eu	0.96	2.21	1.73	5.12	0.59	0.425	2.18	0.808	0.40	0.19	2.60	2.10	4.00
Gd	12.91	21.26	22.47	54.66	5.74	6.66	44.06	8.82	36.00	22.58	73.00	58.00	20.00
Tb	7.23	9.35	12.79	27.58	3.91	3.35	21.66	5.32	20.00	na	na	na	na
Dy	121.92	126.08	202.47	416.17	76.25	56.5	310.13	87.84	288.00	182.86	318.00	224.00	56.00
Ho	50.02	40.31	74.66	152.71	38.25	25.38	104.29	34.89	121.00	81.63	110.00	85.00	15.00
Er	258.30	165.94	344.21	672.98	258.42	158.25	442.14	175.47	658.00	467.28	482.00	378.00	53.00
Tm	60.40	32.92	73.64	134.11	83.73	46.01	89.21	40.67	166.00	na	na	na	na
Yb	566.33	271.81	640.79	1115.50	1081.30	538.72	721.34	373.51	1612.00	1458.97	836.00	769.00	64.00
Lu	80.77	32.06	76.52	140.18	179.34	101.69	81.67	52.01	368.00	289.09	164.00	150.00	11.00
Hf (wt%)	2.19	2.11	1.75	1.84	1.10	1.55	2.68	1.80	0.25	1.32	0.95	1.28	1.04
Ta	7.77	38.79	10.52	18.72	10.23	12.63	92.45	3.82	na	6.42	5.20	2.30	6.10
Th	753.05	4261.19	1100.88	3117.02	377.95	337.95	5198.78	328.52	1907.00	131.73	647.00	368.00	212.00
U	559.67	1856.08	500.22	1129.58	337.75	387.13	3586.87	223.5	2855.00	402.86	356.00	764.00	0.29
Total REE	1155.94	705.85	1446.27	2710.22	13446.51	936.17	1815.47	777.67	37561.75	2507.00	15863.55	1813.30	11300.40
Th/U	1.35	2.30	2.20	2.76	1.12	0.87	1.45	1.47	0.67	0.33	1.82	48.00	731.03
U/Yb	0.99	6.83	0.78	1.01	0.31	0.72	4.97	0.6	1.77	0.28	0.43	0.99	0.01
Nb/Ta	2.67	2.75	3.44	2.67	2.26	1.64	2.89	2.87	0.00	1.75	3.23	1.87	1.64
Eu/Eu*	0.24	0.27	0.23	0.29	0.30	0.17	0.14	0.29	0.22	0.02	0.08	0.06	0.35

bdl= below detection limit; na = not analyzed.

Eu/Eu*=Eu/(Sm+Gd)/2.

¹Sutherland et al. (2002).

²Sutthirat et al. (2020).

³Belousova et al. (2002).

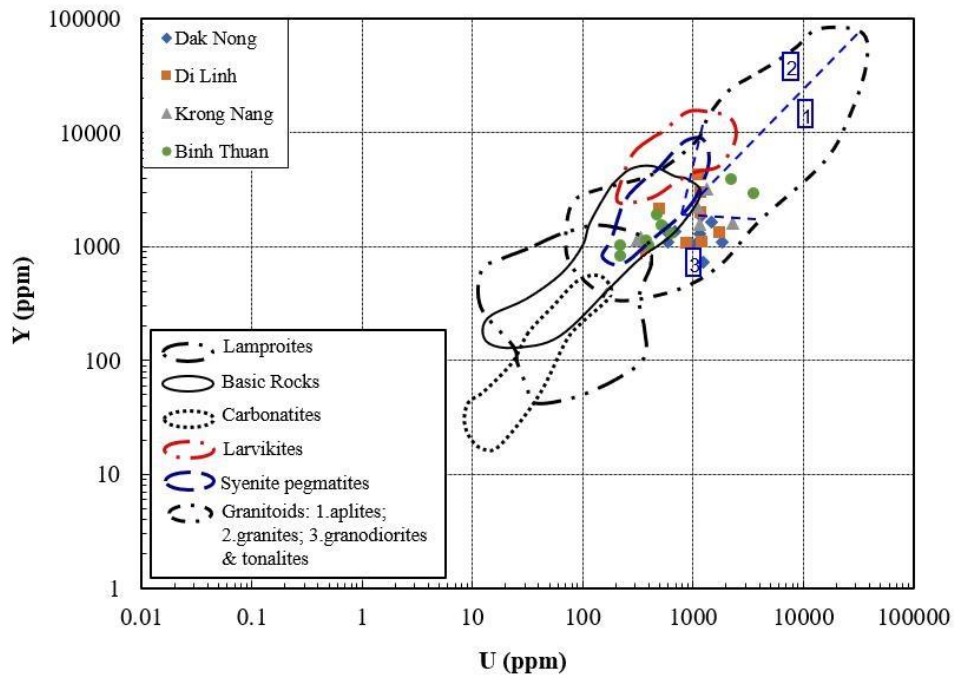


Figure 4.4 The Y-U plots of zircon inclusions in sapphire from Southern Vietnam (data from Belousova et al., 2002).

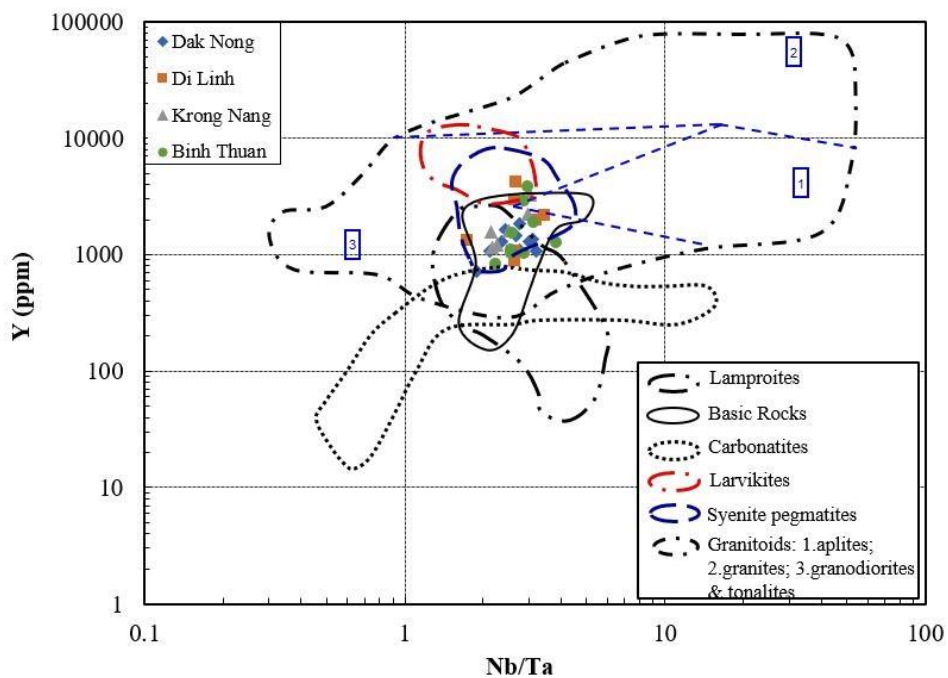


Figure 4.5 The Y-Nb/Ta plots of zircon inclusions in sapphire from Southern Vietnam (data from Belousova et al., 2002).

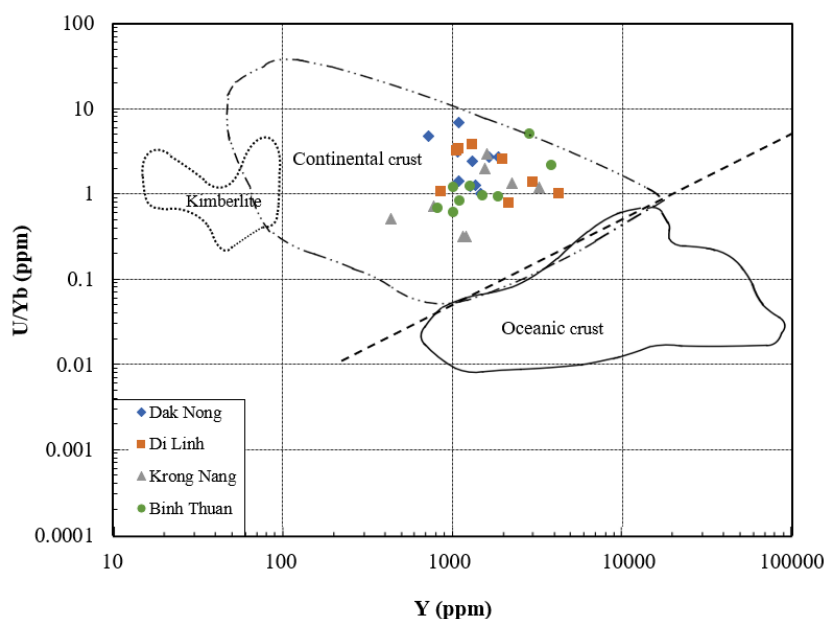


Figure 4.6. The Y-U/Yb plots of zircon inclusions in sapphire from Southern Vietnam (data from Grimes et al., 2007).

The chondrite-normalized REE patterns of studied zircons show higher LREE with pronounced positive Ce and negative Eu anomalies ($Eu/Eu^* = 0.14-0.32$) with rapidly rising towards HREE. These patterns are similar to those of zircons from syenite pegmatite rather than granitoid and carbonatite (Figure 4.7) (Belousova et al., 2002).

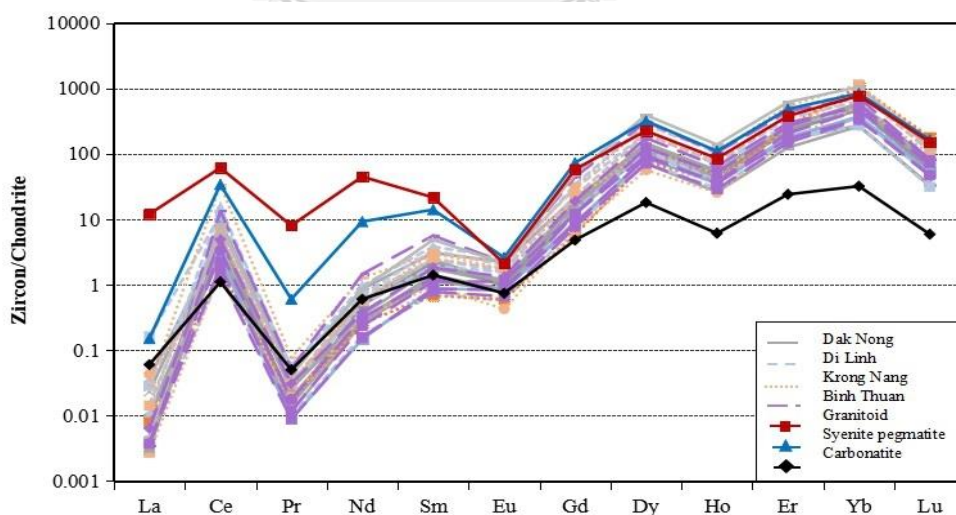


Figure 4.7 Chondrite-normalized REE patterns (chondrite's data from Taylor and McLennan, 1985) of studied zircons compared with patterns of zircon from various rocks (data from Belousova et al., 2002).

4.4.3 Ti-in Zircon Thermometer

Result study about the morphological features of zircon inclusions in sapphire from Southern Vietnam show that these inclusions and their host sapphire could form in the same formation environment, particularly physical condition (i.e., temperature and pressure). From EPMA data of zircon inclusions in sapphire from Southern Vietnam, it can be used to estimate the temperature of zircon inclusions which also represent for crystallization temperature of iron-oxide minerals and their host sapphire. The zircon inclusions having a range of 0.70-13.92 ppm Ti (Table 4.3) are selected to estimate for crystallization temperature of zircon based on equilibrium Ti concentration: $T (^{\circ}\text{C})_{\text{zircon}} = [5080 (\pm 30) / 6.01 (\pm 0.03) - \log(\text{Ti}_{\text{ppm}})] - 273$ (Watson et al., 2006). Thermometry for zircon inclusions in sapphire from Southern Vietnam gives an average temperature estimate between $551-771 \pm 10 ^{\circ}\text{C}$, within uncertainty thresholds of $561- 781^{\circ}\text{C}$. This estimation results of the crystallization temperature of zircon inclusions are also the crystallization temperature of their host sapphire from Southern Vietnam.

4.4.4 U-Pb dating

U-Pb isotopic age data of 16 zircon inclusions are summarized presented in Table 4.4 and Figures 8. All samples yield young ages reflecting from depleted ^{206}Pb , ^{207}Pb , and ^{208}Pb . Due to the $^{207}\text{Pb}/^{235}\text{U}$ and $^{208}\text{Pb}/^{232}\text{Th}$ ages obtain large errors, only the $^{206}\text{Pb}/^{238}\text{U}$ ages is considered as the most reliable.

These zircon inclusions present similar ages between core and rim (see Table 4.4). The youngest ages are observed from Di Linh (5.491 ± 0.077 Ma), Dak Nong (5.598 ± 0.074 Ma) and Binh Thuan (5.94 ± 0.13 Ma). On the other hand, zircon inclusions in Krong Nang sapphire yield 14.73 ± 0.29 Ma (~ 15 Ma) and 35.5 ± 1.6 Ma (~ 35 Ma) which are the oldest age of zircon inclusions in sapphire from basaltic terranes in Southern Vietnam (Figure 4.8). In comparison with other basaltic sapphire deposit in Southeast Asias, the studied zircon inclusions from Southern Vietnam are older than those from Laos and Cambodia but are similar to Thailand (see Table 4.4). Based on $^{40}\text{Ar}/^{39}\text{Ar}$ geochronological data previously reported by Hoang and Flower (1998), they determined basaltic activities in Central and Southern Vietnam ranging from 17.6 Ma to 1923. Therefore, the U-Pb zircon ages obtained from sapphires in Southern Vietnam fall within the main period of basaltic eruption in Central and Southern Vietnam, except

the oldest zircon age in Krong Nang sapphire (~35 Ma). However, this age still falls within the basaltic formation period related to Indosinian-Eurasian collision (35 to 17 Ma), reported by Barr and Macdonald (1981).

4.5 Discussion

4.5.1 Sequences of sapphire/zircon crystallization and basaltic eruption.

U-Pb dating on zircons in sapphire from Southern Vietnam gave the range ~35 to 5.5 Ma. This result indicated different age groups of crystallization periods of zircon inclusions and their hosted sapphire, with the early age group at ~35 Ma (late Eocene), then a moderate age group at ~15 Ma (middle Miocene), and late age group at ~6-5.5 Ma (late Pliocene). These groups were compared with the Cenozoic basaltic activities from Southern Vietnam (Table 4.5). The first age group (~35 Ma) found in Krong Nang is not coincided with peak eruptive basalt ages from Southern Vietnam (17.6- 0 Ma), suggesting that these zircon inclusions and their hosted sapphire were probably crystallized at earlier basaltic formation period at late Eocene that related to Indosinian-Eurasian collision event (Barr and MacDonald, 1981). The second age group (~15 Ma) found in Krong Nang coincided with the earlier basaltic eruptive events in Southern Vietnam that occurred in Da Lat (17.6-7.9 Ma). While the last age group (~6-5.5 Ma) distributed in Dak Nong, Di Linh, and Binh Thuan closed to basaltic eruptive events in Dak Nong (7.1-1.1 Ma). Hoang and Flower (1998) mentioned that basalt magma from Vietnam always erupted early phase with voluminous tholeiite basalts, then later phase with lesser amounts of alkali basalts that associated with sapphire. However, these alkali basalts only erupted from Pliocene to Quaternary (≤ 5 Ma) (Lee et al., 1998), the last age group (~6-5.5 Ma) should have coincided with alkali basaltic eruptive events in Dak Nong at the age ≤ 5 Ma.

The crystallization event difference between Krong Nang and other areas (i.e., Dak Nong, Di Linh, and Binh Thuan) may derive from the geological setting in Southern Vietnam. Silicate rocks from Southern Vietnam have formed in two different orogenic periods, including Triassic period due to Indosinian-Yangtze (South China) collision distributed mainly in north of Southern Vietnam such as Krong Nang and Cretaceous period due to Paleo-Pacific plate subduction occurred in central and south of Southern Vietnam (i.e., Dak Nong, Di Linh, and Binh Thuan) (Carter et al., 2001; Nguyen et al., 2004; Shellnutt et al., 2013; Tri and Khuc, 2011) (see Figure 2.1).

Subsequently, Indosinian-Eurasian collision from 35 to 17 Ma caused thinning of lithosphere and melting of asthenosphere, forming basalt melt afterward. Based on geographical location, the north of Southern Vietnam is affected clearly before Central and South of Southern Vietnam, hence basalt melt activities related to sapphire formation probably occurred in Krong Nang before Dak Nong, Di Linh, and Binh Thuan. As thus, the crystallization of sapphire from Krong Nang is probably earlier than that in Dak Nong, Di Linh, and Binh Thuan. This can occur in Bo Ploi sapphires from Thailand, where closes to Indosinian-Eurasian collision zone, that has recently recorded by Sutthirat et al. (2020). They reported that the Bo Ploi sapphires could firstly crystallize in the host melts at 24 Ma or event older before corrosive transport in 3-4 Ma alkaline basalts.

Base on $^{40}\text{Ar}/^{39}\text{Ar}$ geochronological data previously reported by Lee et al. (1998), alkaline basalts are commonly erupted in Southern Vietnam from Pliocene to Quaternary (≤ 5 Ma). As thus, all the ages data in this study indicate that zircon inclusions and their host sapphire were crystallized before they were brought up the surface by ascending alkaline basalts at the age of ≤ 5 Ma. These data also suggested that crustal residence time of sapphire and its associated zircon from Dak Nong, Di Linh, and Binh Thuan (~ 6 -5.5 Ma) before eruption is a shorter time than those from Krong Nang (~ 35 and 15 Ma).

4.5.2 Original sapphire formation

As the results from chapter 2 and 3 have proposed a genetic model of the original sapphire formation from Southern Vietnam before transportation by basaltic magma to the surface (see Figure 4.9). These results suppose that the fractionated crystallization of sapphire occurred in alkaline felsic melts melt. This model bases on the presence of mineral inclusions and their mineral chemistries recorded in sapphire varieties. A unique mineral inclusion suite was recorded, namely alkaline felsic suite - granite or syenite- (i.e., ferrocolumbite, pyrochlore, zircon, alkali feldspar, hercynite spinel, and ilmenite-hematite series, and wüstite).

Table 4.3 Ti-in-zircon temperatures for zircon inclusions in sapphire from Southern Vietnam

Locality	Sample No	Ti (ppm)	T °C
Dak Nong	DN04	3.22	650
	DN15	1.39	593
	DN20	11.03	750
	DN22	12.51	761
	DN23	6.53	705
	DN24	5.37	689
	DN31	3.51	657
Di Linh	DL01	5.65	693
	DL04	6.92	710
	DL20	2.8	640
	DL40	7.41	715
	DL43	4.16	669
	DL44	1.64	603
	DL46	11.78	756
Krong Nang	KN08	1.62	603
	KN12	8.59	728
	KN14	7	711
	KN15	2.51	633
	KN27	3.69	660
Binh Thuan	PT05	0.7	551
	PT13	8.29	725
	PT36	8.28	725
	PT59	13.65	769
	PT66	9.81	739
	PT70	3.17	649
Pleiku	GL02	2.08	619
	GL11	6.44	704
	GL12	5.27	688
	GL13	12.26	759
	GL16	1.37	592
	GL19	4.64	678
	GL22	7.27	714
	GL72	4.63	677
	GL73	5.54	692
GL74	13.92	771	

Table 4.4 Summary of U-Pb dating results of the zircon inclusions in sapphire from Southern Vietnam

Areas	Analysis No.	Th	U	207Pb/206Pb	$\pm 2\sigma$	207Pb/235U	$\pm 2\sigma$	206Pb/238U	$\pm 2\sigma$	208Pb/232Th	$\pm 2\sigma$
Dak Nong	DN05-1	5106.39	2024.07	137.7	188	6.2	0.5	5.6	0.1	5.5	0.2
	DN05-2	1047.08	724.62	834.7	267	9.1	1.2	6.0	0.3	6.8	0.4
	DN06-1	765.32	739.99	190.0	334	6.1	0.9	5.4	0.2	7.1	0.4
	DN06-2	2772.76	1878.31	431.0	166	7.0	0.5	5.5	0.1	5.5	0.2
	DN20-1	2125.81	1378.76	447.9	195	7.2	0.6	5.7	0.2	5.8	0.3
	DN20-2	767.19	726.32	626.7	263	8.3	1.0	6.0	0.2	6.8	0.4
	DN32-1	26683.32	6224.68	66.0	136	6.1	0.3	5.7	0.1	5.7	0.2
	DN46-1	3391.68	1761.05	531.4	206	7.4	0.7	5.6	0.2	5.2	0.3
	DN46-2	456.25	409.01	307.4	486	6.8	1.5	5.7	0.3	5.6	0.5
Di Linh	DL04-1	2104.91	7001.23	273.7	100	6.3	0.3	5.4	0.1	6.6	0.3
	DL04-2	970.38	629.40	679.1	420	8.3	1.7	5.7	0.4	6.2	0.5
	DL44-1	37267.99	17996.68	589.9	148	7.5	0.5	5.1	0.1	5.1	0.4
	DL44-2	31354.25	16313.65	588.7	65	7.9	0.2	5.9	0.1	6.0	0.2
	DL46-1	17987.08	2935.32	237.3	197	6.6	0.6	5.4	0.2	5.8	0.3
	DL46-2	15072.68	2838.33	181.7	174	6.4	0.5	5.5	0.1	5.8	0.2
	DL46-3	5313.24	1431.13	180.3	271	6.7	0.8	6.0	0.2	6.4	0.5
	DL48-1	8086.59	1943.90	274.7	265	6.7	0.8	5.5	0.2	5.8	0.4
	DL48-2	1195.64	537.25	0.1	449	6.3	1.5	6.1	0.4	6.3	0.5
	DL60-1	14824.82	5160.53	155.5	113	6.1	0.3	5.4	0.1	5.3	0.2
DL60-2	8236.51	3870.64	80.1	126	6.1	0.3	5.6	0.1	5.5	0.2	
Krong Nang	KN08-1	558.68	404.40	0.1	0.0	13.3	1.8	14.4	0.5	16.9	0.9
	KN08-2	481.63	412.69	1183.1	184	26.8	2.4	14.9	0.5	21.8	1.2
	KN13-1	1573.83	1841.15	34.6	87	34.8	1.2	34.8	0.5	37.0	1.5
	KN13-2	1228.47	1534.40	79.0	93	36.5	1.4	35.9	0.6	37.0	1.5
	KN13-3	1479.71	1783.74	197.1	112	38.4	1.8	35.9	0.7	35.2	1.8
	KN15-1	1388.20	1613.55	457.3	279	20.7	2.6	14.9	0.7	14.9	1.5
Binh Thuan	PT05-1	4010.85	2992.96	365.3	168	6.5	0.5	5.3	0.1	4.4	0.3
	PT05-2	6783.02	4476.22	41.0	134	5.7	0.3	5.4	0.1	5.9	0.2
	PT08-1	5696.36	1558.79	583.9	240	7.4	0.8	5.2	0.2	5.4	0.3
	PT08-2	834.94	367.34	15.8	514	6.5	1.4	6.3	0.4	6.4	0.5
	PT13-1	435.35	255.53	522.4	544	7.8	2.0	5.9	0.4	5.6	0.5
	PT13-2	719.52	288.24	85.1	600	6.5	1.8	5.9	0.3	6.8	0.4
	PT26-1	2302.15	1884.31	133.9	209	5.7	0.5	5.0	0.1	4.9	0.3
	PT26-2	739.64	933.82	69.1	492	5.4	1.2	4.7	0.3	5.6	0.6
	PT65-1	10388.79	5908.19	363.2	267	6.5	0.8	5.0	0.2	4.9	0.4
PT68-2	633.30	489.67	107.8	496	6.7	1.5	6.1	0.3	6.8	0.5	

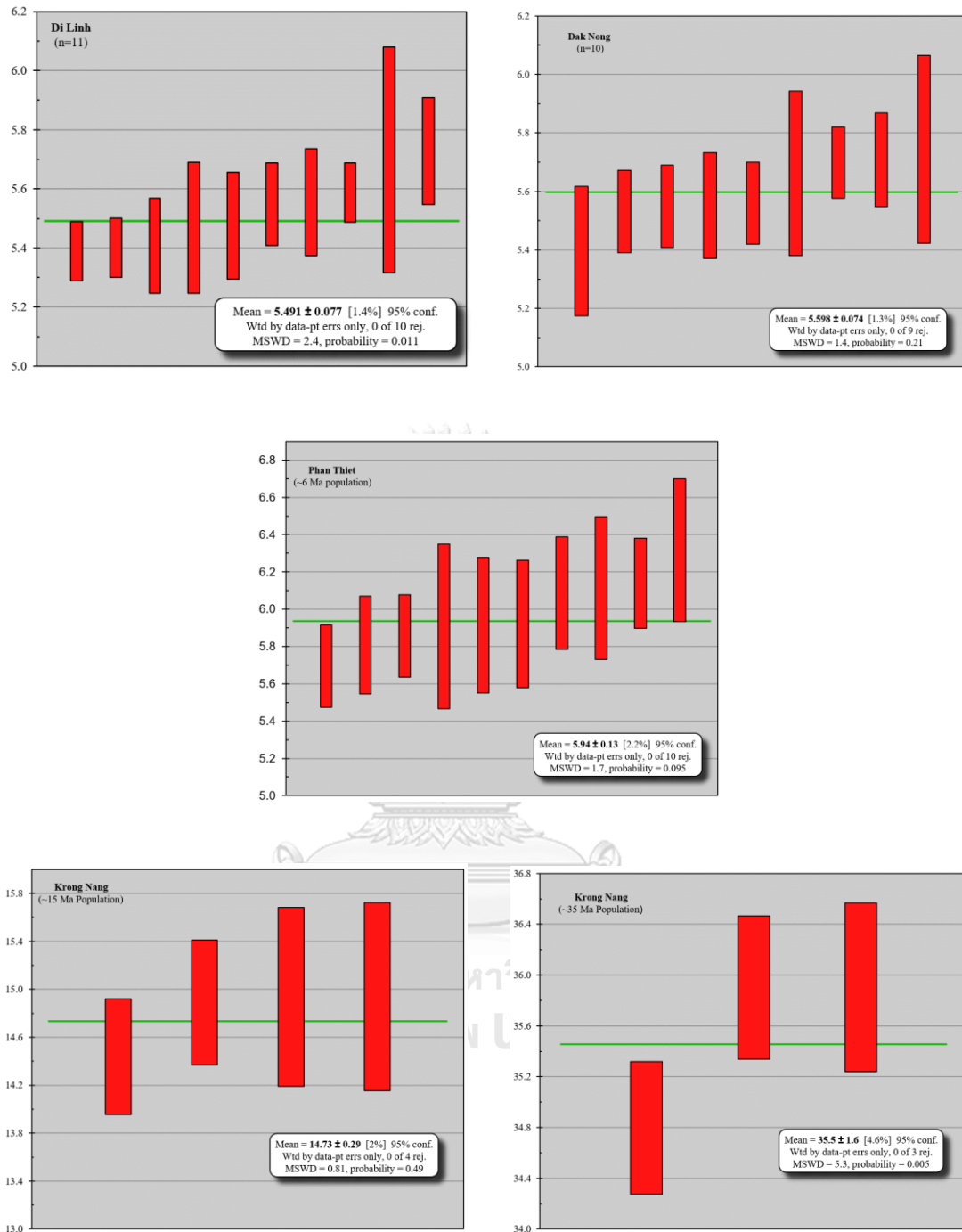


Figure 4.8 Mean weight diagrams for zircons in sapphire from Southern Vietnam. These red vertical columns represent individual $^{206}\text{Pb}/^{238}\text{U}$ ages in Ma with their associated uncertainty; the green horizontal line is the calculated mean age for these values.

Table 4.5 Geochronological scale with respect to radiometric dating of basalts and mineral zircon inclusion found in sapphire from Southern Vietnam, compared with zircon and other in sapphire from Southeast Asia

Geological Time Scale			Age (Ma)	Cenozoic basalt from Southern Vietnam (40Ar/39Ar) ¹						U-Pb zircon inclusions in sapphire from Southern Vietnam				U-Pb zircon inclusions in sapphire from Southeast Asia			U-Th-Pb other inclusions in sapphire from Thailand ⁵				
				Da Lat	Phuoc Long	Dak Nong	Buon Ma Thuot	Pleiku	Le des Cendres	Dak Nong	Di Linh	Krong Nang	Phan Thiet	Thailand ²	Laos ³	Cambodia ⁴	Zircon	Monazite			
Cenozoic	Quaternary	Holocene	<0.01																		
		Pleistocene	Upper	0.13																	
			Middle	0.8																	
			Lower	2.5										1.2-1.3	0.9						
		Pliocene	Upper	3.5																	
			Lower	5																	
	Neogene	Miocene	6																		
			7																		
			8																		
			9																		
			10																		
			11																		
			12																		
			13																		
			14																		
			15																		
			16																		
			17																		
			18																		
			19																		
			20																		
			Paleogene	Oligocene	25																
Eocene	35																				
Paleocene	55																				
	65																				

*This study; ¹Hoang and Flower (1998); ²Sutthirat et al., (2020); ³Sutherland et al., (2002); ⁴Sutherland et al., (2015); ⁵Khamlo et (2011).

Heaman et al. (1990) mentioned that trace element contents in zircon is useful in studies geochemical fingerprints leading to petrogenetic indicators. Base on the result in this study, the level of substitution of Σ REE, Th/U, Zr/Hf, Y versus U, Y versus Nb/Ta, and Y versus U/Yb of zircon inclusions have supported the formation of sapphire from Southern Vietnam related to felsic alkaline melt (granite or syenite).

The wide range of total REE contents (>700 to 2710 ppm) in zircons in sapphire from Southern Vietnam indicated that formations of Southern Vietnam sapphire derived from silicate rocks (i. e., granitoid and syenite) (Belousova et al., 2002). However, in discrimination diagrams of both Y versus U and Y versus Nb/Ta (see Figures 4.5 and 4.6, respectively), studied zircons entirely fall into rock varieties comprising syenite pegmatite, granitoid and slightly involved by lamproite, basic, and larvikite. In fact, syenite pegmatite, granitoid, lamproite, basic, and larvikite melts are similarly characterized by high alkaline compositions. Therefore, these data implied that the occurrence of studied zircon and their host sapphire should have closely related to felsic alkaline (silicate) melts. Moreover, the presences of negative Eu anomalies (see Figure 5b) in studied zircons suggested that studied zircon and their host sapphire appeared to have crystallized from more fractionated and evolved felsic rocks, as large reflects of Eu^{2+} partitioning into plagioclase at high redox conditions during magma evolution (Belousova et al., 2002; Li et al., 2000). Besides, the U versus Nb/Ta of zircon inclusions (see Figure 8) evidenced that Southern Vietnam sapphire should have crystallized from the continental crust source. In addition, Zr/Hf ratios in studied zircons also further favor a continental crust source. Futhermore, Th/U ratios in studied zircons close to magmatic origin. From the above information, the origin of sapphire from Southern Vietnam could have related to highly evolved alkaline felsic (silicate) melts in the continental crust. This agrees well with other authors reported of the Dak Nong sapphire (Izokh et al., 2010) and is compatible with Aspen et al., (1990); Pin et al., (2006); Upton et al., (2009); Sutherland et al., (2002; 1998a; 2015b; 2009), Zaw et al., (2006), Khamloet et al., (2014); Promwongnan and Sutthirat (2019b).

Base on the correlation between structure, geochemistry, and geochronological of zircon inclusions, the formation of sapphire can be divided into 3 scenarios as shown in Figure 4.9.

The first interval (Figure 4.9a) is marked by the early formation of sapphire in alkaline felsic melts at the age of ~35 Ma. This period is based on the presence of U-Pb age of Krong Nang zircon inclusion (35.5 ± 1.6 Ma). During this period, both basalt melt and silicate melt were formed by extension tectonics. The interplay between the India-Eurasia collision and Paleo-Pacific plate subduction beneath the East of Eurasia margin (i.e., South-Central Vietnam and East Asia) resulted in Cenozoic decompression setting in East Asia as well as Southern Vietnam capable of inducing thinning in lithosphere and melting in asthenosphere (Flower et al., 1992; Hoang et al., 2013). Consequently, thermally anomalous asthenosphere melt provided a potential driver for lithosphere extrusion, allowing transtensional asthenosphere melt. Subsequently, basaltic melts would have formed from the upwelling of the asthenosphere in the shallow mantle under this region during the crustal extension. At the same time, the alkaline felsic melt could also be formed by very low degree of partial melting of lower crustal rocks during the same period of thermal extension. Therefore, sapphire in Krong Nang would firstly crystallize from early-formed alkaline felsic melts at ~35 Ma while these melts were cooled in a short time afterward.

The second scenario (Figure 4.9b) was the main events of sapphire formation which span from ~35 to 5.5 Ma supported by the U-Pb age of Krong Nang zircon inclusion (35.5 ± 1.6 and 14.73 ± 0.29 Ma), Dak Nong zircon inclusions (5.598 ± 0.074 Ma), Binh Thuan zircon inclusions (5.94 ± 0.13 Ma), and Di Linh zircon inclusions (5.491 ± 0.077 Ma). During this scenario, several strike-slip and normal faultings setting into Southern Vietnam due to the effect of India-Eurasia collision (Rangin et al., 1995), supported upward penetration of basalt melts from asthenosphere in the shallow mantle. Hence, the alkaline felsic melts as well as basalt melts were extended. Most of sapphire from Southern Vietnam (i.e., Dak Nong, Di Linh, Binh Thuan, and Krong Nang) were crystallized directly in these alkaline felsic melts during this period.

Final scenario (Figure 4.9c) was the main eruption period (≤ 5 Ma) with volcanic activities of alkali basalts that brought up the sapphire on the surface. At the beginning of rising, alkali basalt melt from asthenosphere carried mantle xenoliths (i.e., garnet lherzolite, spinel lherzolites, and harzburgite) (Garnier et al., 2005), recycling oceanic crustal materials (i.e., gabbro, basalt, and sediment) (Anh et al., 2018), xenocrysts (olivine, Al-rich clinopyroxene, orthopyroxene, phlogopite) (Garnier et al., 2005), and

lower crustal xenoliths comprising sapphires forming directly in the alkaline felsic melts during the time of eruption ascending onto the surface. This scenario base on a range of eruption ages of alkali basalts from Southern Vietnam from Pliocene to Quaternary ($\leq 5\text{Ma}$) (Lee et al., 1998). Afterward, weathering and erosion processes released the sapphire from alkali basalt hosts from Southern Vietnam and resulted in the deposited and enrichment in the gem placers found today.

4.6 Conclusion

Trace-element geochemistry of zircons included in sapphire from Southern Vietnam indicated that the initial origin of sapphire from Southern Vietnam related to highly evolved alkaline felsic melts. The formation of sapphire occurred earlier during $\sim 35\text{-}5.5\text{ Ma}$ base on the U-Pb dates of Krong Nang zircon inclusions (35.5 ± 1.6 and $14.73 \pm 0.29\text{ Ma}$), Binh Thuan zircon inclusions ($5.94 \pm 0.13\text{ Ma}$), Dak Nong zircon inclusions ($5.598 \pm 0.074\text{ Ma}$), and Di Linh zircon inclusions ($5.491 \pm 0.077\text{ Ma}$). Then, the alkali basalts brought up sapphire along with other xenoliths and xenocrysts to the surface during Pliocene to Quaternary ($\leq 5\text{Ma}$). Temperature estimates from Ti-in-zircon thermometry suggest that the sapphire was crystallized about $561\text{-}781\text{ }^{\circ}\text{C}$.

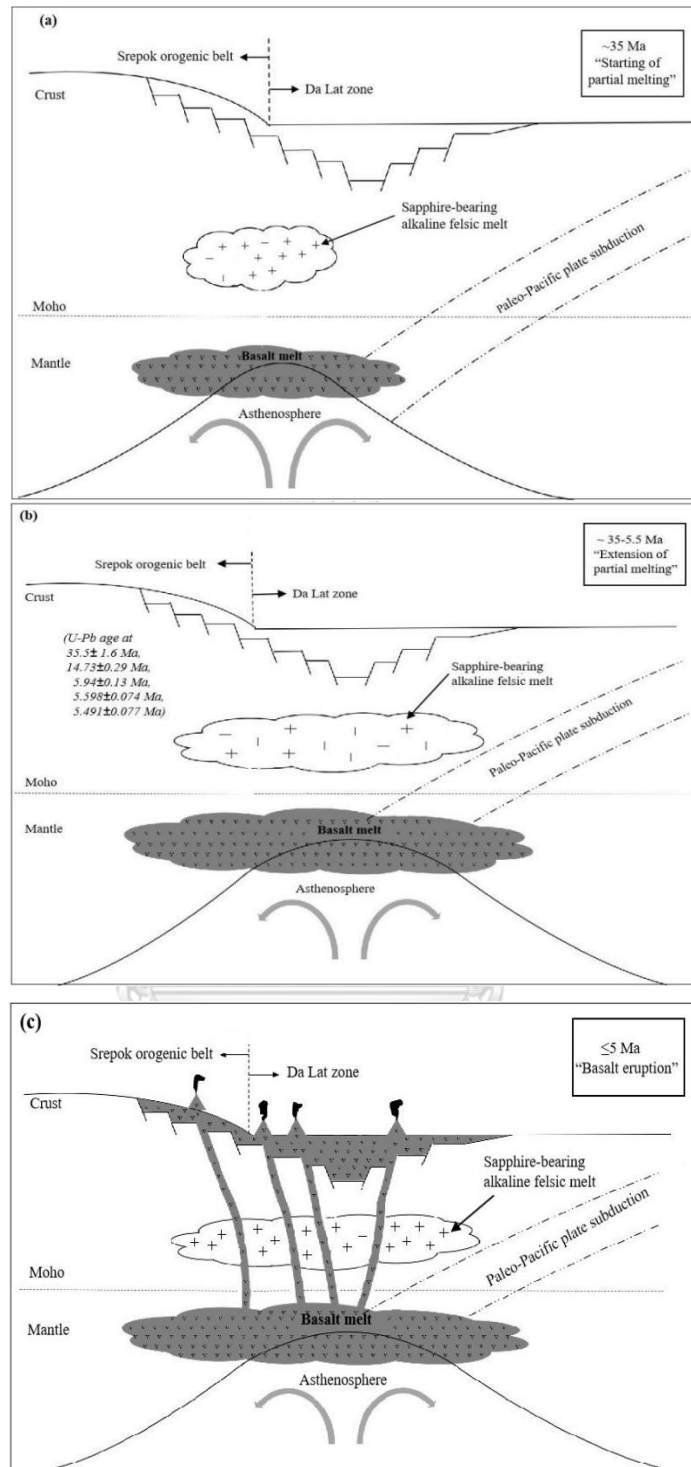


Figure 4.9 Genetic model of sapphire from Southern Vietnam based on mineral chemistry and chronological data of zircon inclusion described in the study.

CHAPTER 5

CONCLUSION

Blue-green-yellow sapphires have occurred in basaltic alluvial deposits in the Southern Vietnam. They were firstly discovered in Dak Nong and then Di Linh. Subsequently, other occurrences have reported in Binh Thuan, Krong Nang, and Pleiku. The analytical results of mineral inclusion in these sapphires can conclude below.

1) Several syngenetic mineral inclusions found in these sapphires are alkali feldspar, zircon, ferrocolumbite, uranpyrochlore, and various iron-oxide minerals.

2) Oxide mineral inclusions include wüstite, hercynite, and ilmenite. Ilmenite ranges between $\text{Il}_{49-54}\text{He}_{34-40}\text{Mt}_{7-10}$ and $\text{Il}_{24-30}\text{He}_{36-38}\text{Mt}_{35-40}$ falling in ilmenite-hematite series. Wüstite with nonstoichiometry, $(\text{Fe}^{2+}_{0.3-0.9})(\text{Ti}^{3+}_{<0.179}\text{Al}^{3+}_{\leq 0.6}\text{Cr}^{3+}_{<0.1}\text{Fe}^{3+}_{\leq 0.46})\square_{\leq 0.23}\text{O}$, is usually associated with hercynite inclusion clearly indicating cogenetic sapphire formation. Wüstite and sapphire appear to have formed from the breakdown reaction of hercynite (hercynite = sapphire+wüstite). Titanohematite series and titanomagnetite series might have crystallized during iron-titanium reequilibration via subsolidus exsolution.

3) Mineral chemical characteristics of these inclusions appear to have evolved from alkaline felsic magma. Consequently, the original formation of their host sapphires should have related to alkaline felsic magmatic process before basaltic magma, derived from the deeper upper mantle, had passed through and transported sapphires and their associated minerals onto the surface via volcanic eruption.

4) Temperature estimated from Ti in zircon inclusions indicates that sapphire crystallization at about 560- 780°C.

5) U-Pb zircon dating yields ages ranging between 35.5 ± 1.6 Ma (~35 Ma) and 14.73 ± 0.29 Ma (~15 Ma) for Krong Nang sapphire, 5.94 ± 0.13 Ma (~6 Ma) for Binh Thuan sapphire, 5.598 ± 0.074 Ma for Dak Nong sapphire, and 5.491 ± 0.077 Ma for Di Linh sapphire. Except the dating result of Krong Nang sapphire, the others fall within the same period of the alkali-basalt eruptions in Southern Vietnam (≤ 5 Ma).

APPENDIX A

RAMAN SPECTRUMS OF MINERAL INCLUSIONS

a. Columbite

1) Binh Thuan area in Southern Vietnam

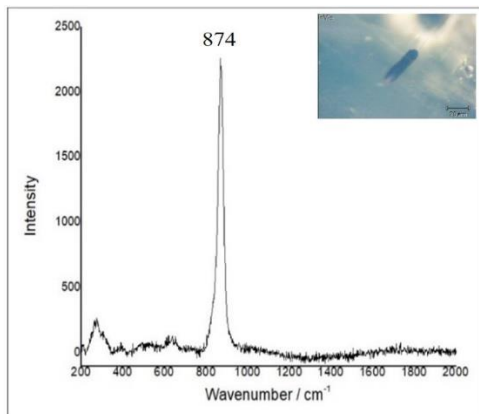


Figure A-01 Raman spectrum of a columbite observed in the sample PT02

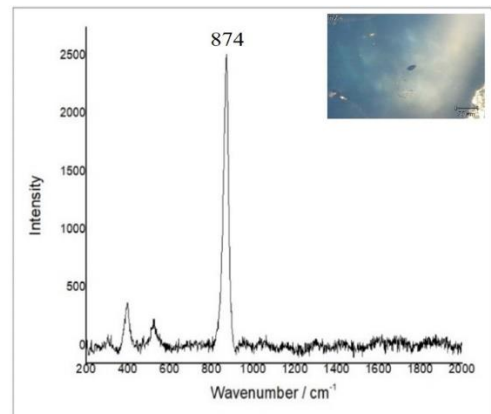


Figure A-02 Raman spectrum of a columbite observed in the sample PT03

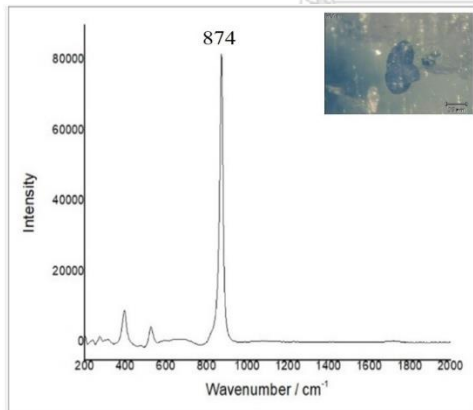


Figure A-03 Raman spectrum of a columbite observed in the sample PT09

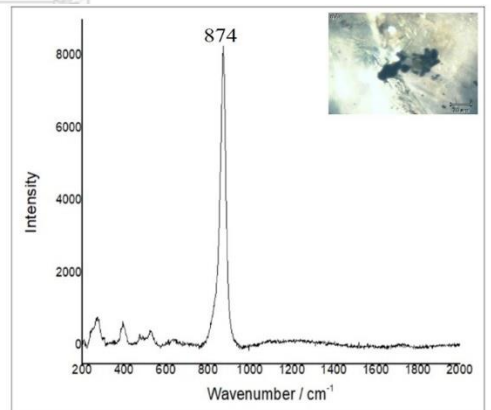


Figure A-04 Raman spectrum of a columbite observed in the sample PT10

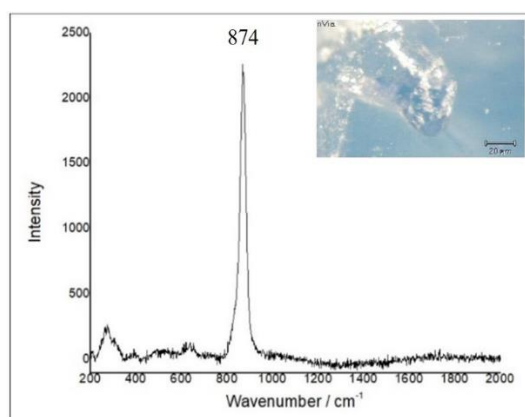


Figure A-05 Raman spectrum of a columbite observed in the sample PT11

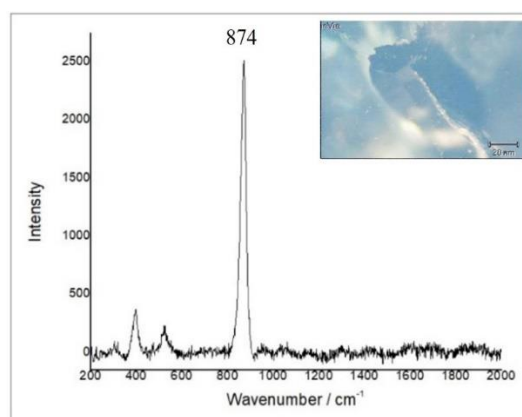


Figure A-06 Raman spectrum of a columbite observed in the sample PT14

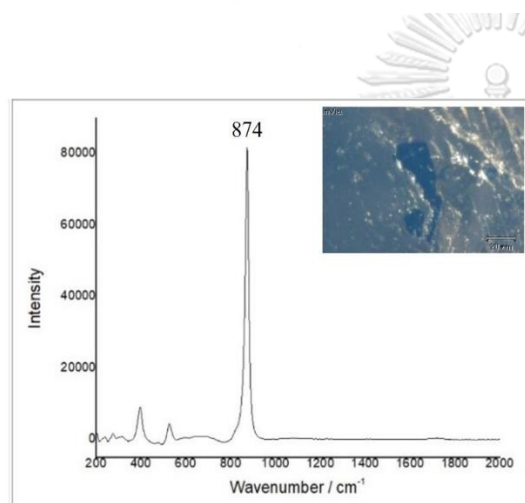


Figure A-07 Raman spectrum of a columbite observed in the sample PT19

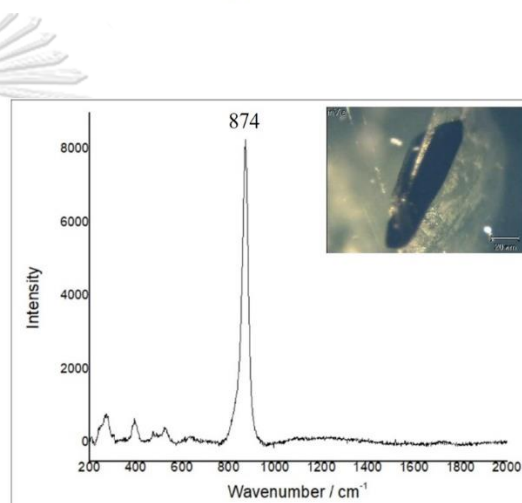


Figure A-08 Raman spectrum of a columbite observed in the sample PT20

CHULALONGKORN UNIVERSITY

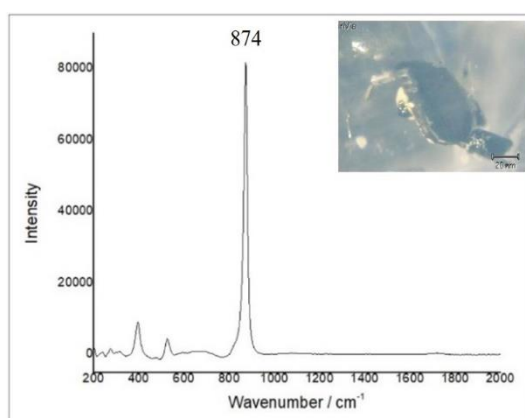


Figure A-09 Raman spectrum of a columbite observed in the sample PT21

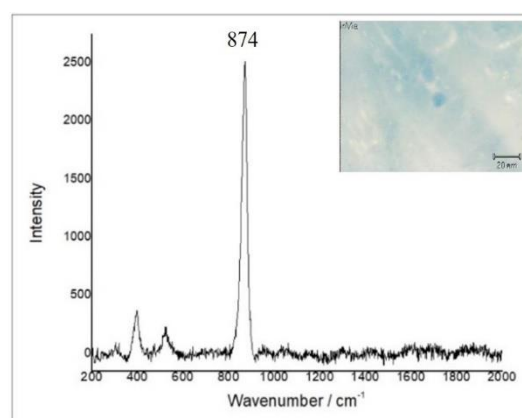


Figure A-10 Raman spectrum of a columbite observed in the sample PT24

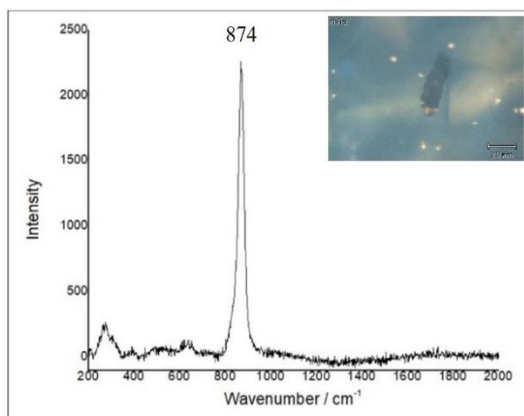


Figure A-11 Raman spectrum of a columbite observed in the sample PT25

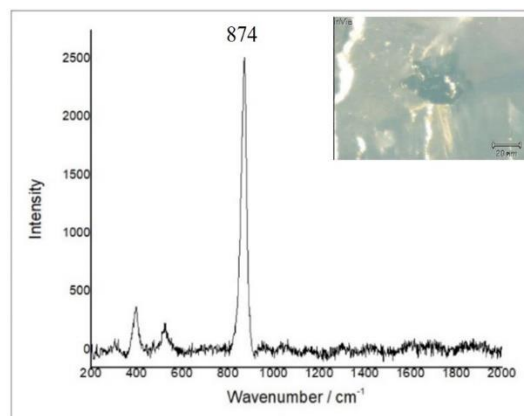


Figure A-12 Raman spectrum of a columbite observed in the sample PT27

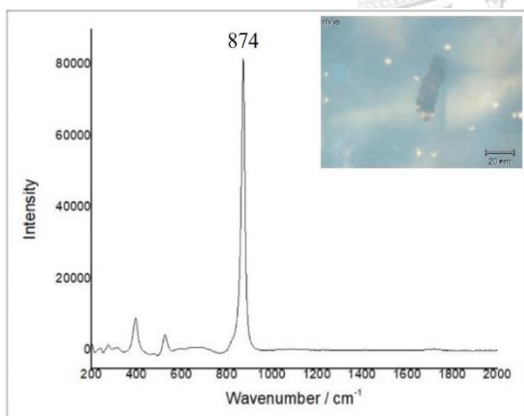


Figure A-13 Raman spectrum of a columbite observed in the sample PT28

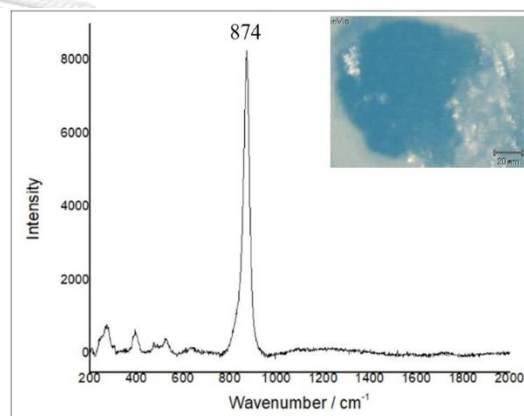


Figure A-14 Raman spectrum of a columbite observed in the sample PT29

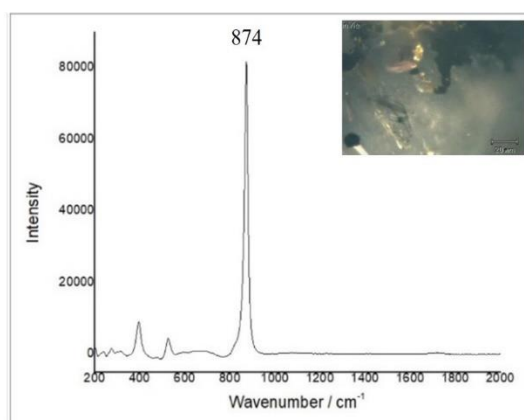


Figure A-15 Raman spectrum of a columbite observed in the sample PT30

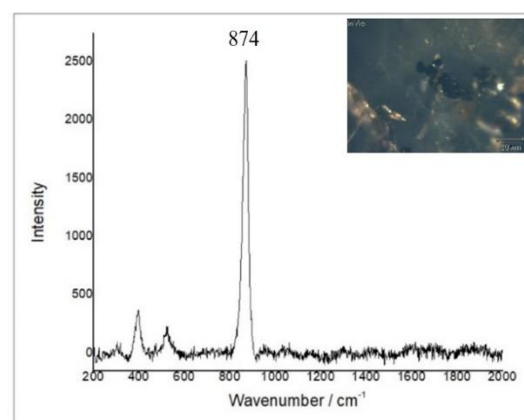


Figure A-16 Raman spectrum of a columbite observed in the sample PT32

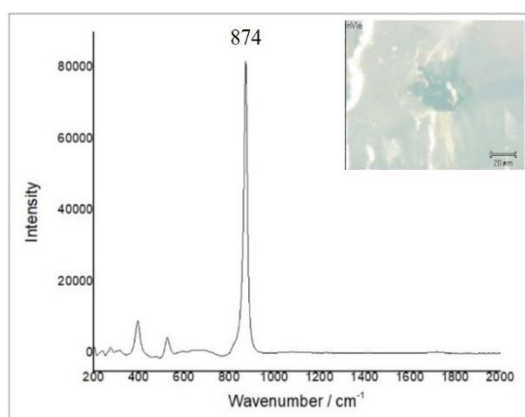


Figure A-17 Raman spectrum of a columbite observed in the sample PT35

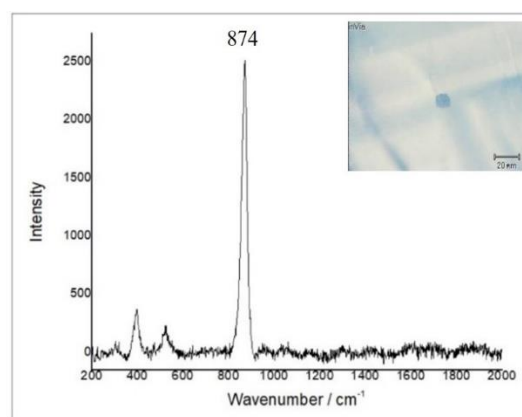


Figure A-18 Raman spectrum of a columbite observed in the sample PT37

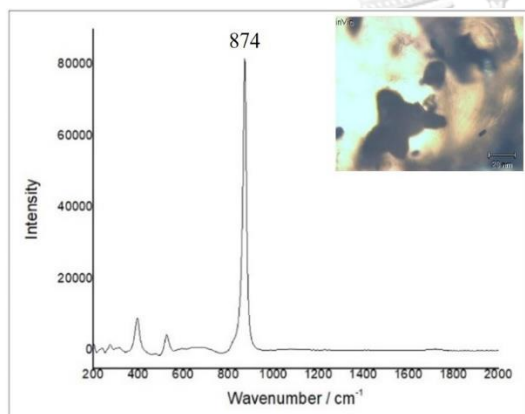


Figure A-19 Raman spectrum of a columbite observed in the sample PT39

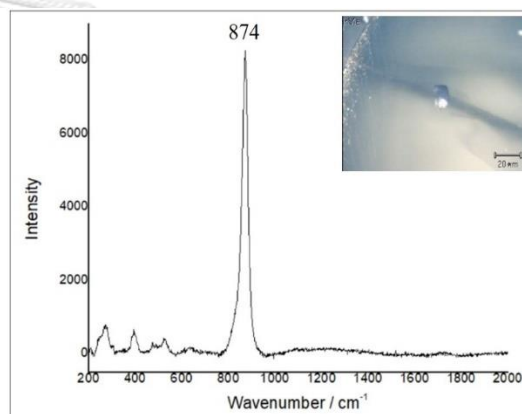


Figure A-20 Raman spectrum of a columbite observed in the sample PT40

CHULALONGKORN UNIVERSITY

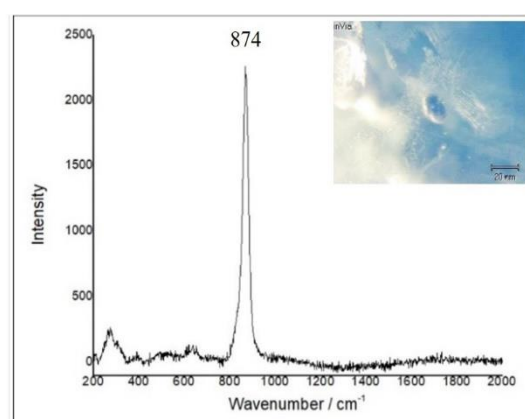


Figure A-21 Raman spectrum of a columbite observed in the sample PT41

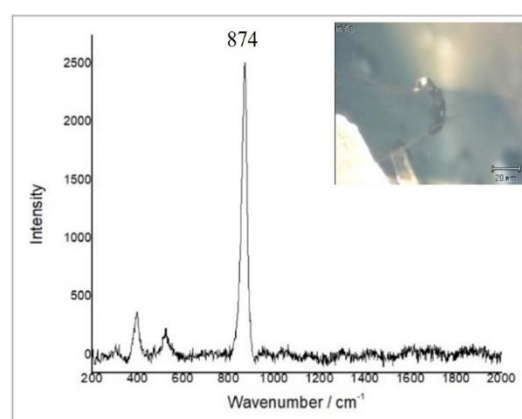


Figure A-22 Raman spectrum of a columbite observed in the sample PT42

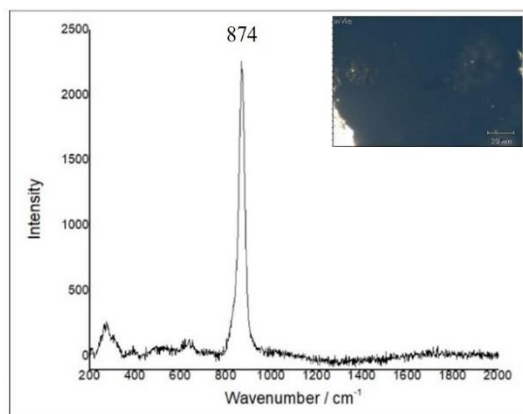


Figure A-23 Raman spectrum of a columbite observed in the sample PT50

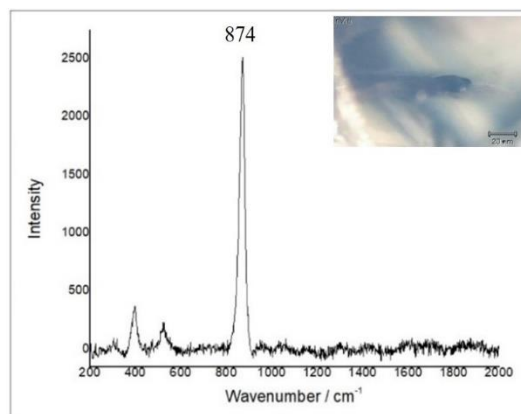


Figure A-24 Raman spectrum of a columbite observed in the sample PT57

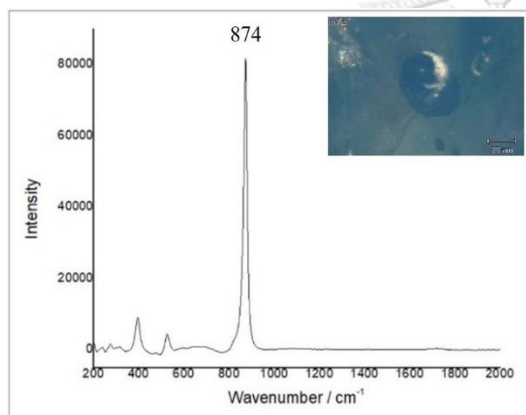


Figure A-25 Raman spectrum of a columbite observed in the sample PT58

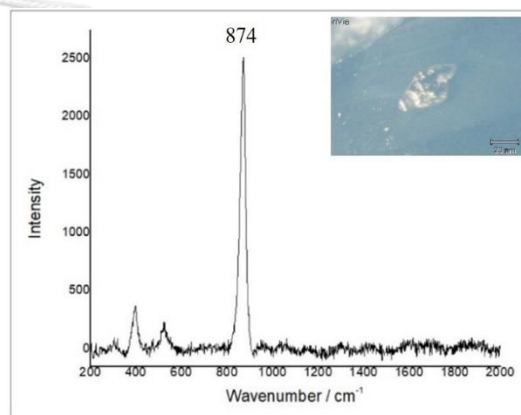


Figure A-26 Raman spectrum of a columbite observed in the sample PT64

CHULALONGKORN UNIVERSITY

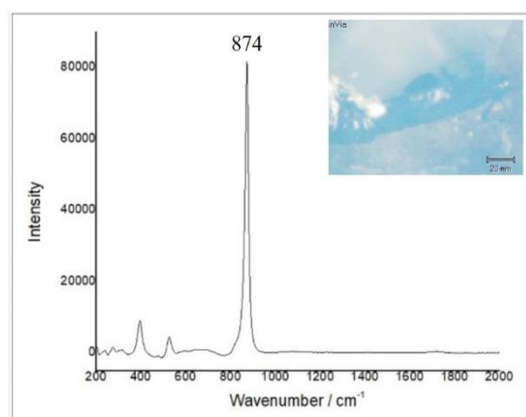


Figure A-27 Raman spectrum of a columbite observed in the sample PT72

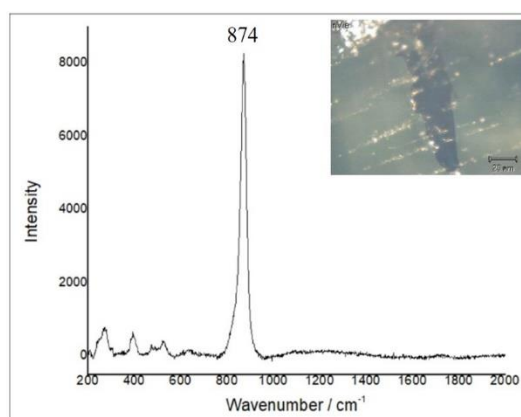


Figure A-28 Raman spectrum of a columbite observed in the sample PT73

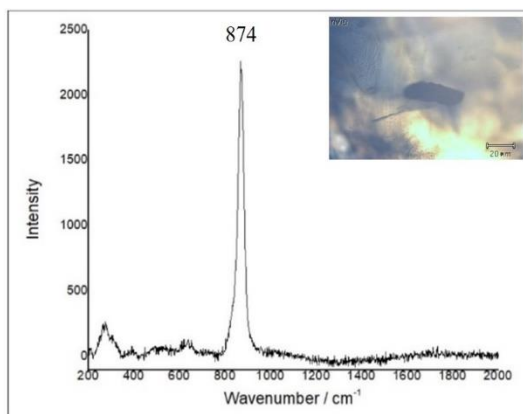


Figure A-29 Raman spectrum of a columbite observed in the sample PT74

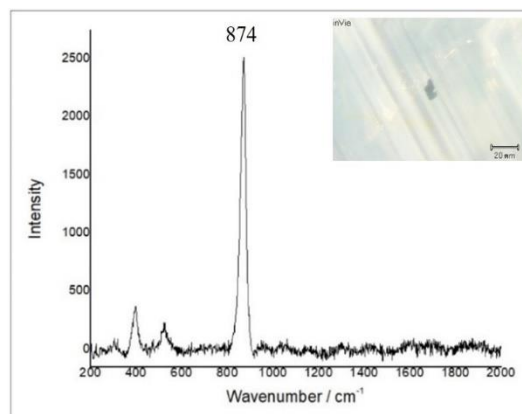


Figure A-30 Raman spectrum of a columbite observed in the sample PT75

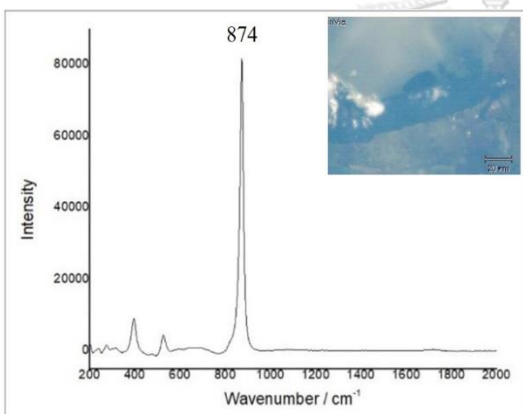


Figure A-31 Raman spectrum of a columbite observed in the sample PT76

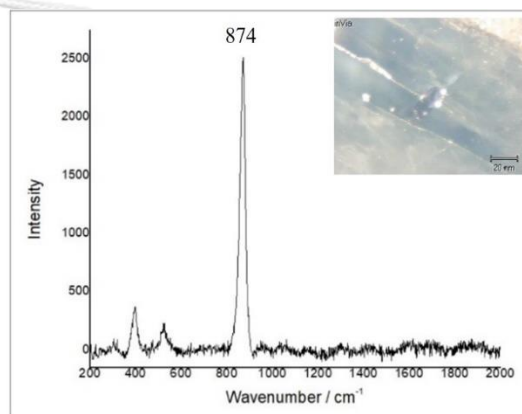


Figure A-32 Raman spectrum of a columbite observed in the sample PT77

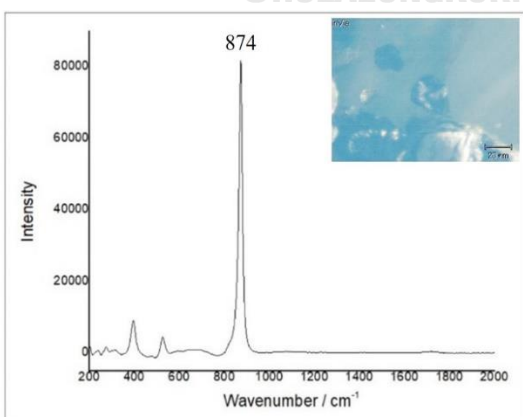


Figure A-33 Raman spectrum of a columbite observed in the sample PT78

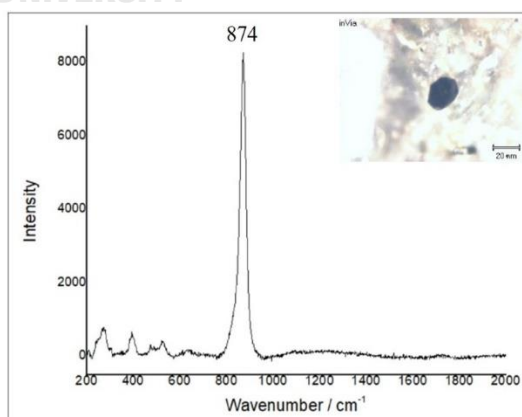


Figure A-34 Raman spectrum of a columbite observed in the sample PT79

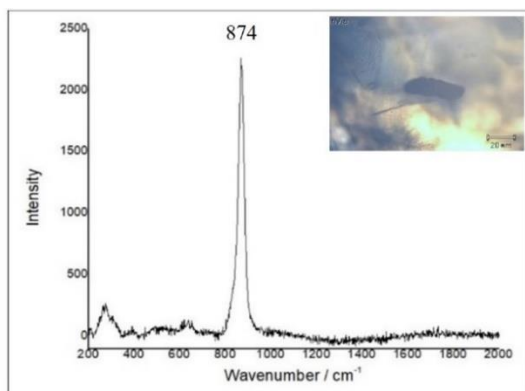


Figure A-35 Raman spectrum of a columbite observed in the sample PT82

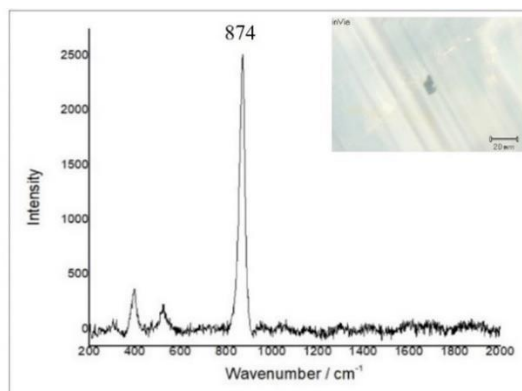


Figure A-36 Raman spectrum of a columbite observed in the sample PT83

2) Di Linh area in Southern Vietnam

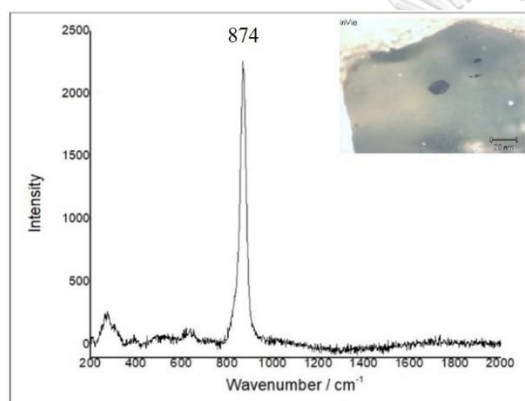


Figure A-37 Raman spectrum of a columbite observed in the sample DL03

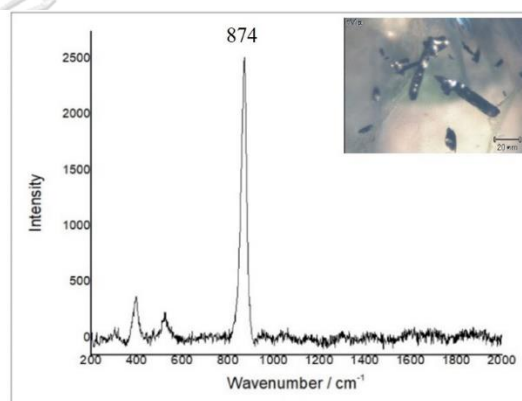


Figure A-38 Raman spectrum of a columbite observed in the sample DL06

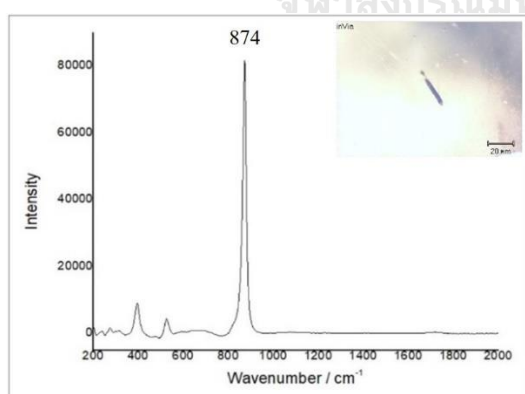


Figure A-39 Raman spectrum of a columbite observed in the sample DL07

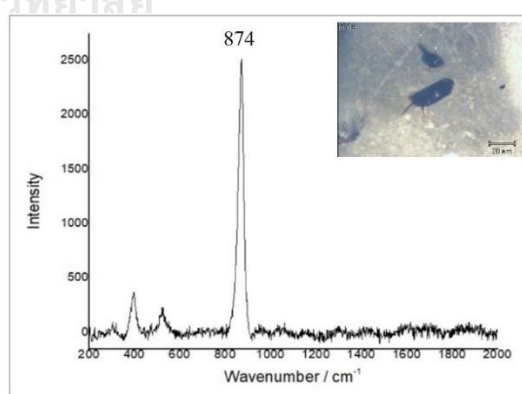


Figure A-40 Raman spectrum of a columbite observed in the sample DL10

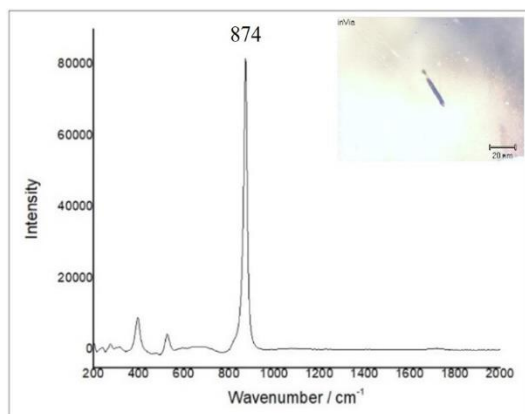


Figure A-39 Raman spectrum of a columbite observed in the sample DL07

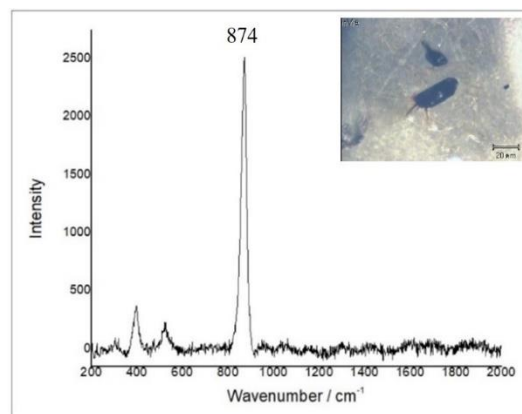


Figure A-40 Raman spectrum of a columbite observed in the sample DL10

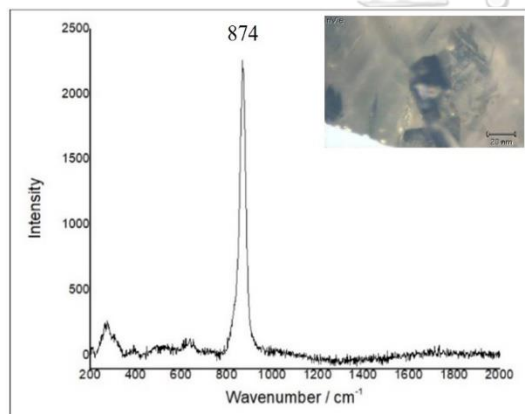


Figure A-43 Raman spectrum of a columbite observed in the sample DL16

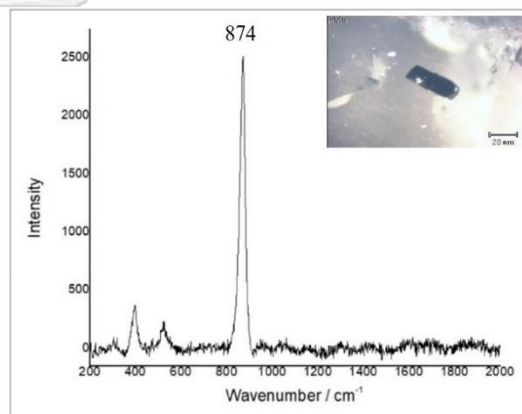


Figure A-44 Raman spectrum of a columbite observed in the sample DL19

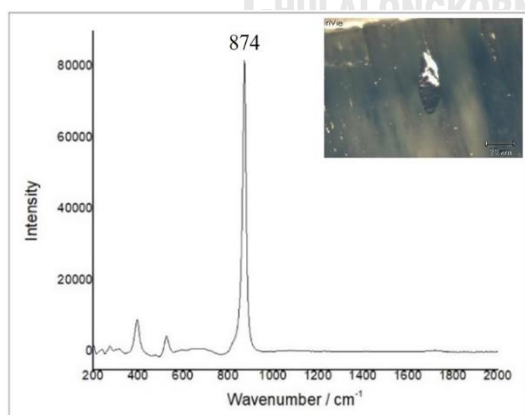


Figure A-45 Raman spectrum of a columbite observed in the sample DL21

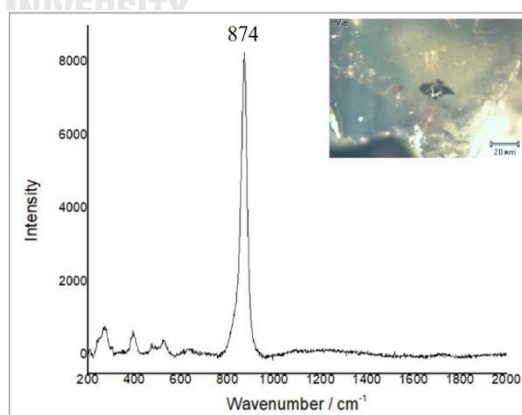


Figure A-46 Raman spectrum of a columbite observed in the sample DL26

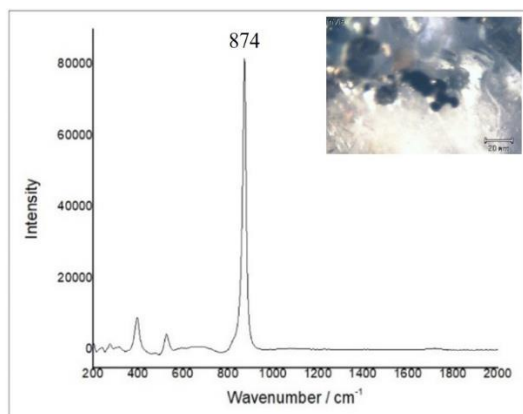


Figure A-47 Raman spectrum of a columbite observed in the sample DL29

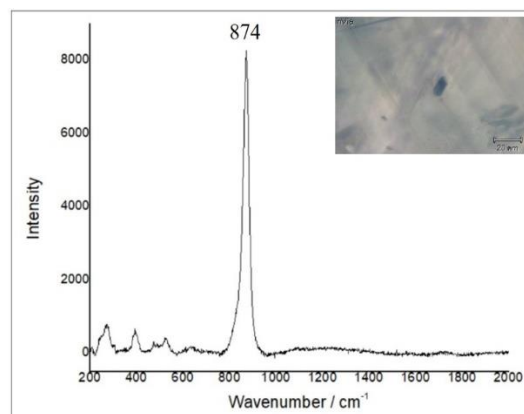


Figure A-48 Raman spectrum of a columbite observed in the sample DL30

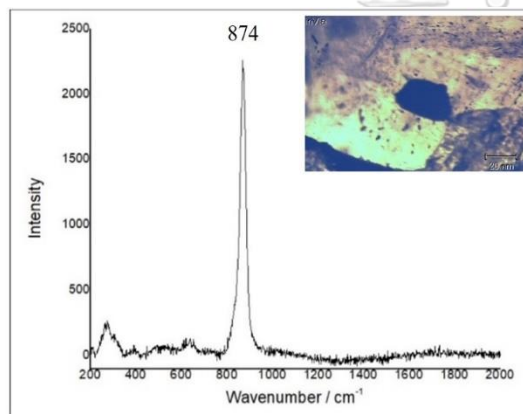


Figure A-49 Raman spectrum of a columbite observed in the sample DL32

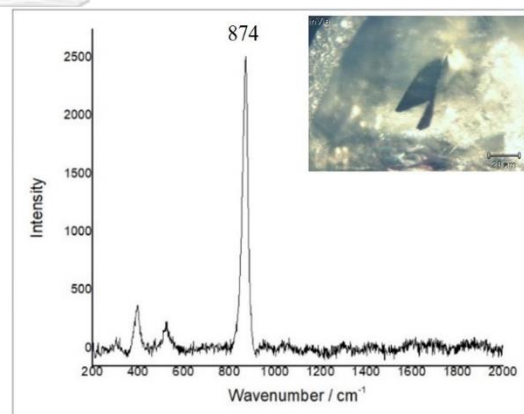


Figure A-50 Raman spectrum of a columbite observed in the sample DL35

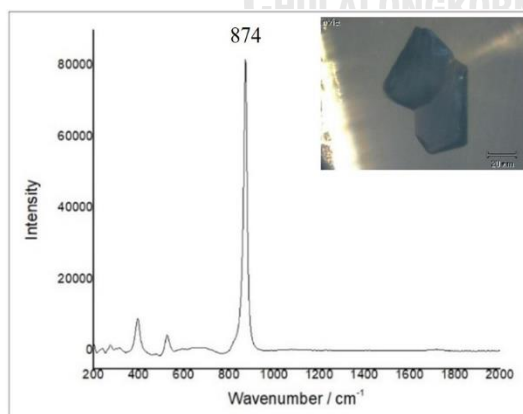


Figure A-51 Raman spectrum of a columbite observed in the sample DL38

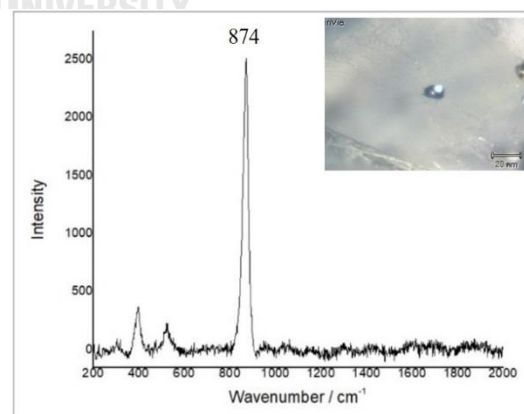


Figure A-52 Raman spectrum of a columbite observed in the sample DL52

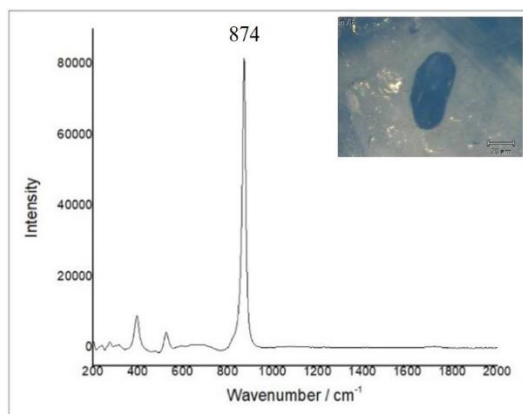


Figure A-53 Raman spectrum of a columbite observed in the sample DL54

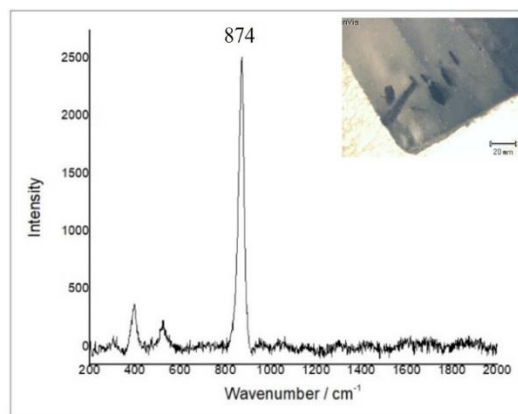


Figure A-54 Raman spectrum of a columbite observed in the sample DL55

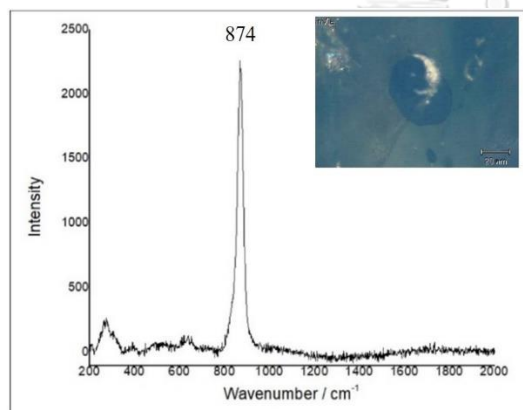


Figure A-55 Raman spectrum of a columbite observed in the sample DL64

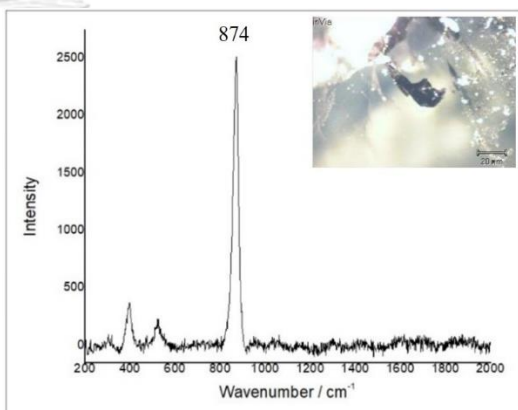


Figure A-56 Raman spectrum of a columbite observed in the sample DL65

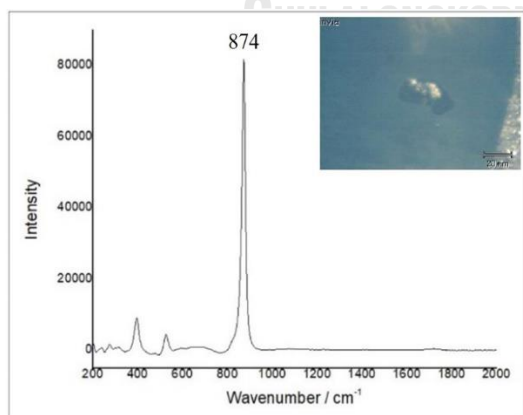


Figure A-57 Raman spectrum of a columbite observed in the sample DL66

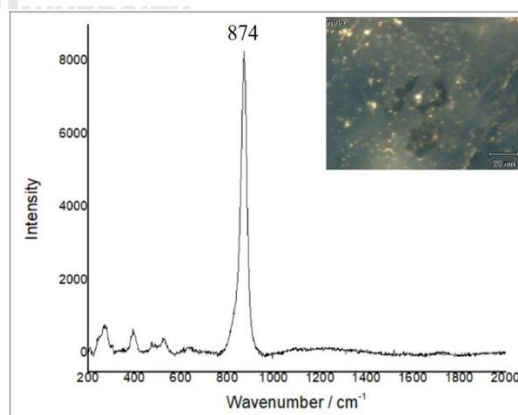


Figure A-58 Raman spectrum of a columbite observed in the sample DL67

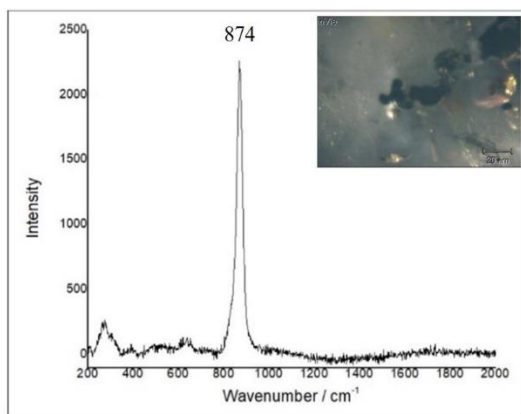


Figure A-59 Raman spectrum of a columbite observed in the sample DL68

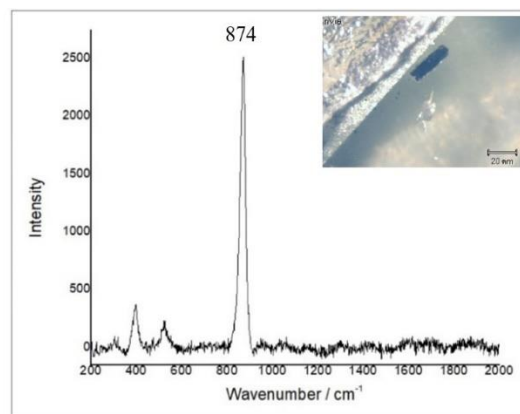


Figure A-60 Raman spectrum of a columbite observed in the sample DL69

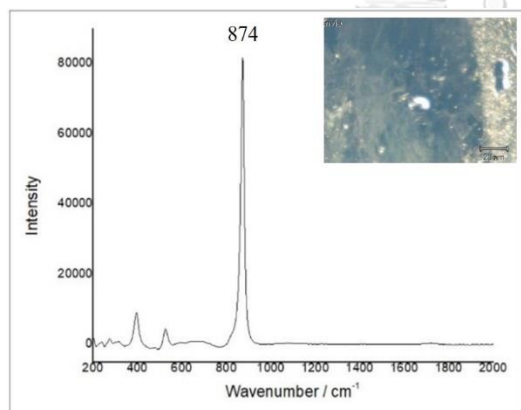


Figure A-61 Raman spectrum of a columbite observed in the sample DL70

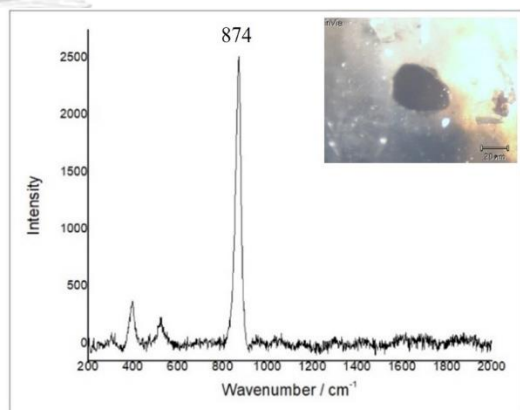


Figure A-62 Raman spectrum of a columbite observed in the sample DL72

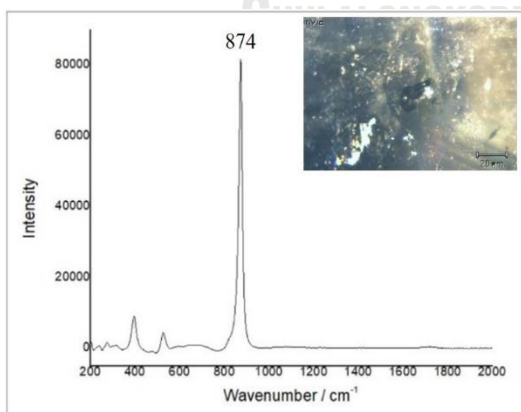


Figure A-63 Raman spectrum of a columbite observed in the sample DL73

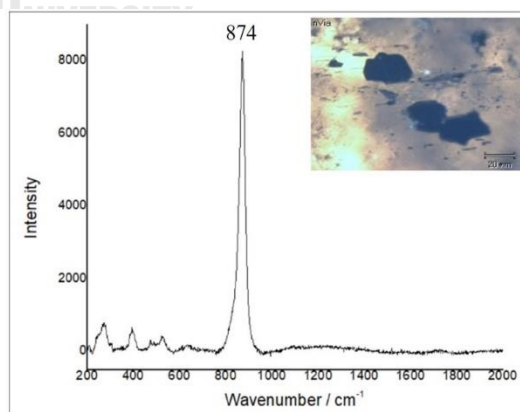


Figure A-64 Raman spectrum of a columbite observed in the sample DL74

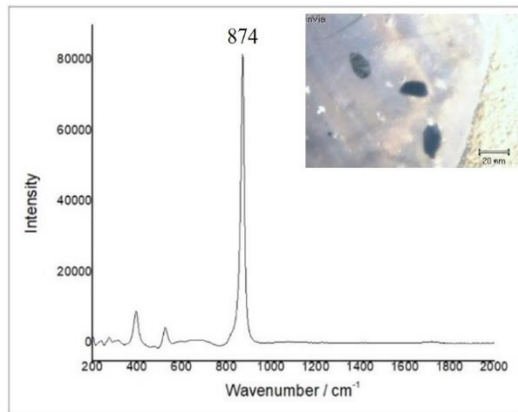


Figure A-65 Raman spectrum of a columbite observed in the sample DL76

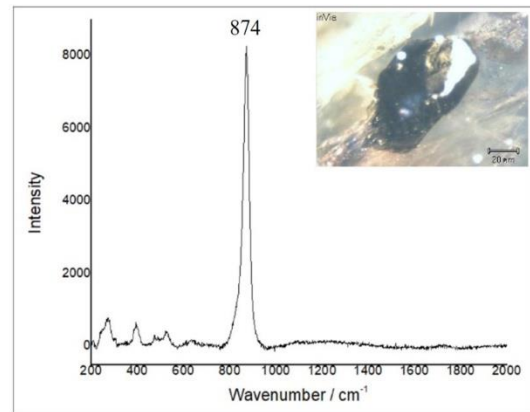


Figure A-66 Raman spectrum of a columbite observed in the sample DL77

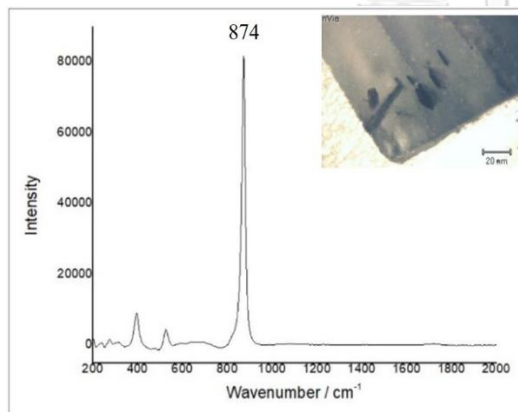


Figure A-67 Raman spectrum of a columbite observed in the sample DL78

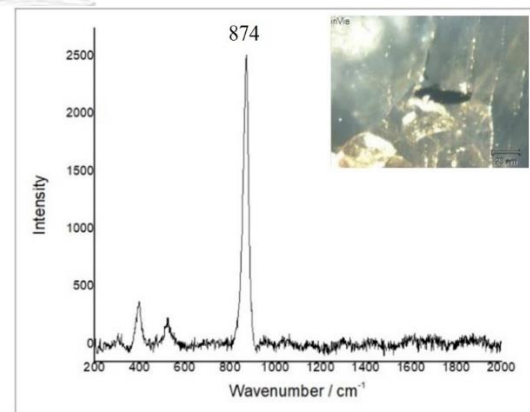


Figure A-68 Raman spectrum of a columbite observed in the sample DL79

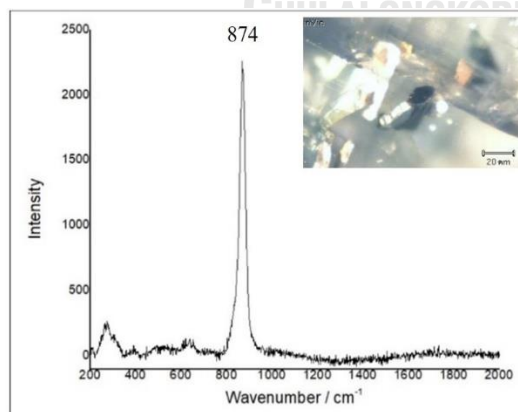


Figure A-69 Raman spectrum of a columbite observed in the sample DL80

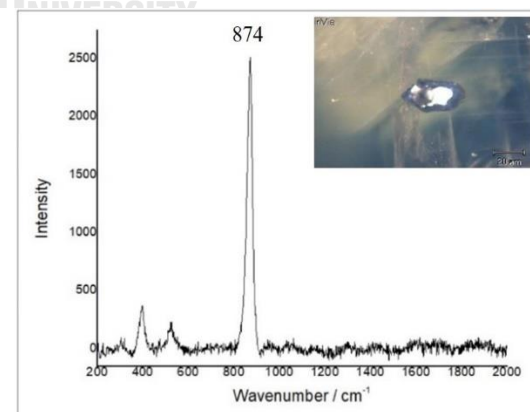


Figure A-70 Raman spectrum of a columbite observed in the sample DL81

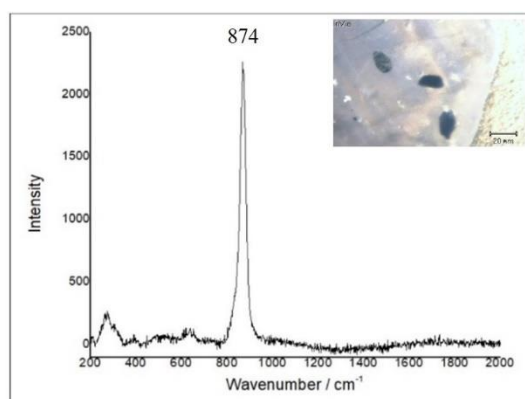


Figure A-71 Raman spectrum of a columbite observed in the sample DL82

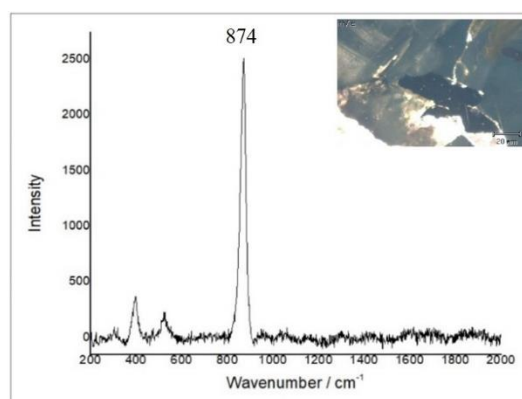


Figure A-72 Raman spectrum of a columbite observed in the sample DL83

3) Krong Nang area in Southern Vietnam

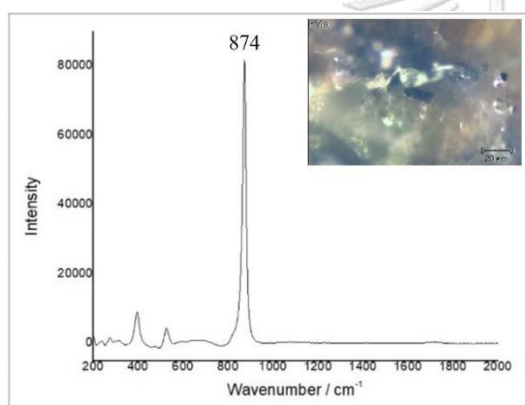


Figure A-73 Raman spectrum of a columbite observed in the sample KN17

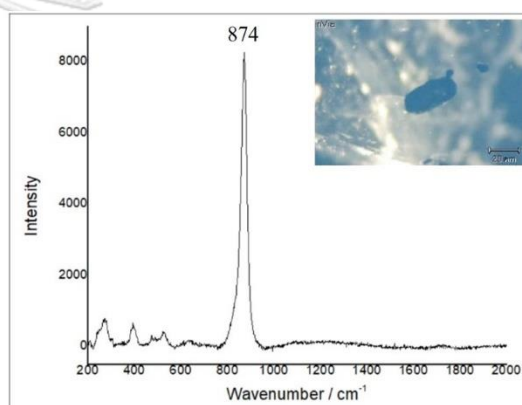


Figure A-74 Raman spectrum of a columbite observed in the sample KN25

CHULALONGKORN UNIVERSITY

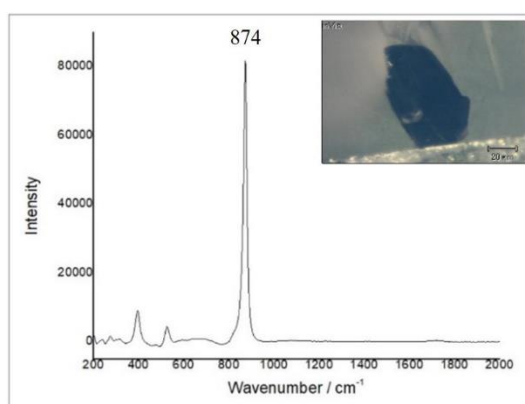


Figure A-75 Raman spectrum of a columbite observed in the sample KN29

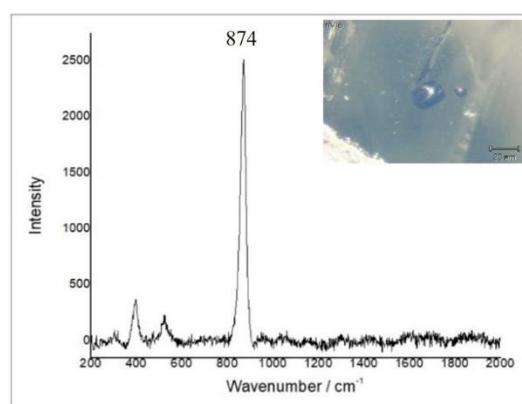


Figure A-76 Raman spectrum of a columbite observed in the sample KN30

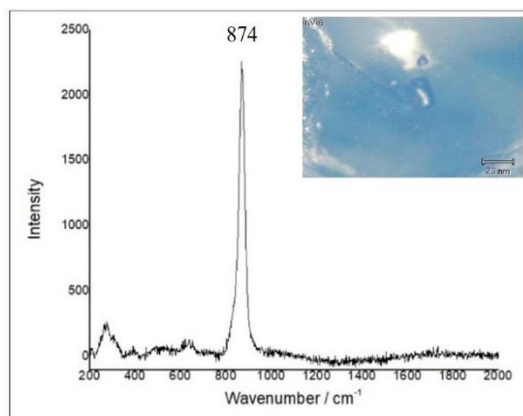


Figure A-77 Raman spectrum of a columbite observed in the sample KN32

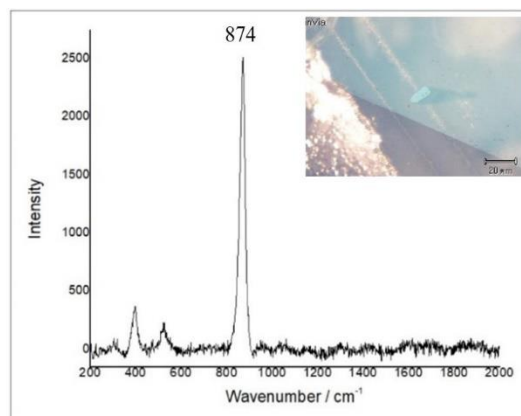


Figure A-78 Raman spectrum of a columbite observed in the sample KN38

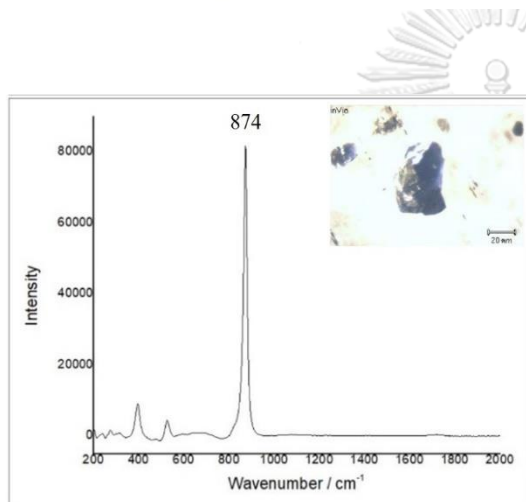


Figure A-79 Raman spectrum of a columbite observed in the sample KN39

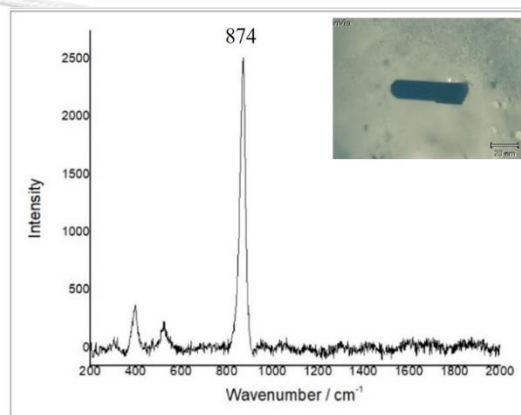


Figure A-80 Raman spectrum of a columbite observed in the sample KN40

CHULALONGKORN UNIVERSITY

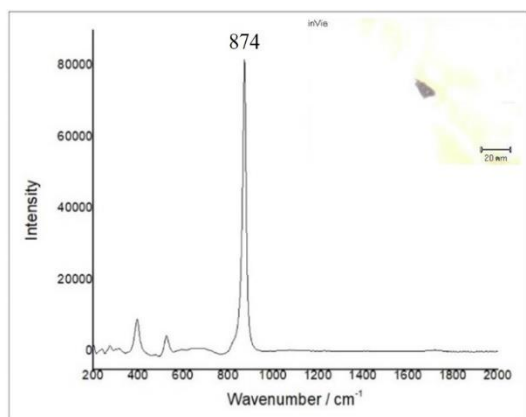


Figure A-81 Raman spectrum of a columbite observed in the sample KN41

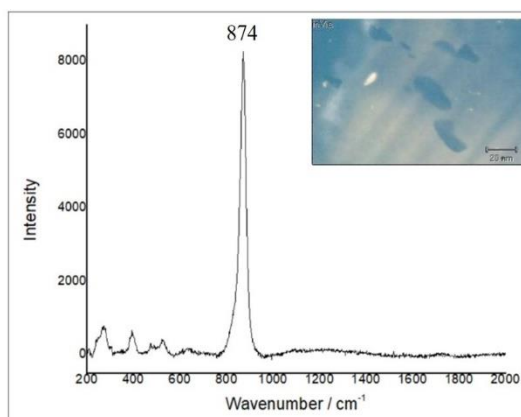


Figure A-82 Raman spectrum of a columbite observed in the sample KN44

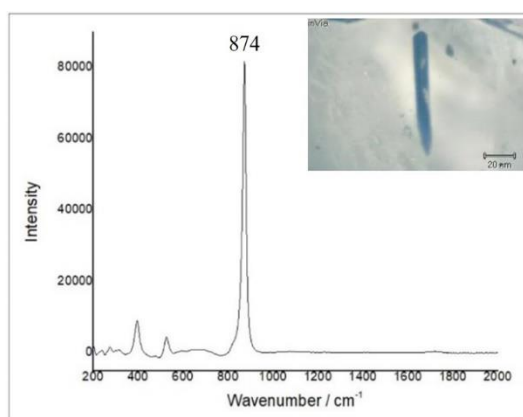


Figure A-83 Raman spectrum of a columbite observed in the sample KN46

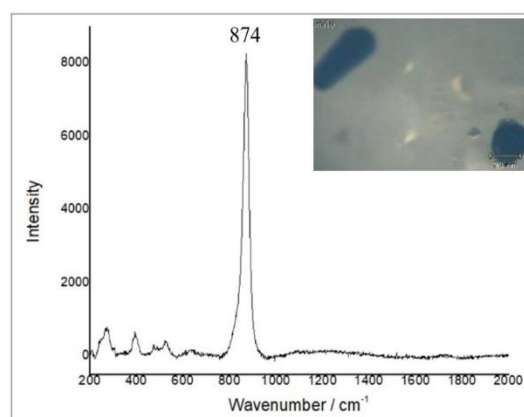


Figure A-84 Raman spectrum of a columbite observed in the sample KN48

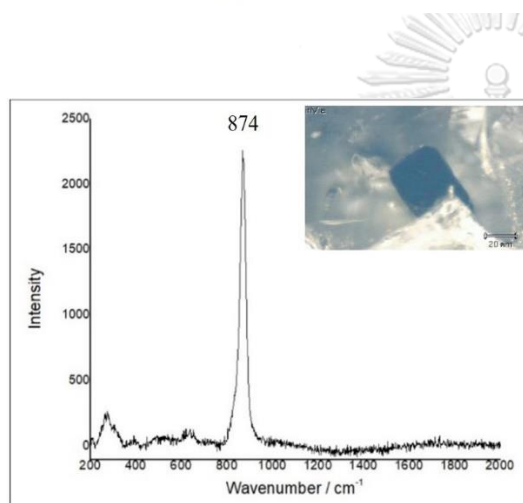


Figure A-85 Raman spectrum of a columbite observed in the sample KN49

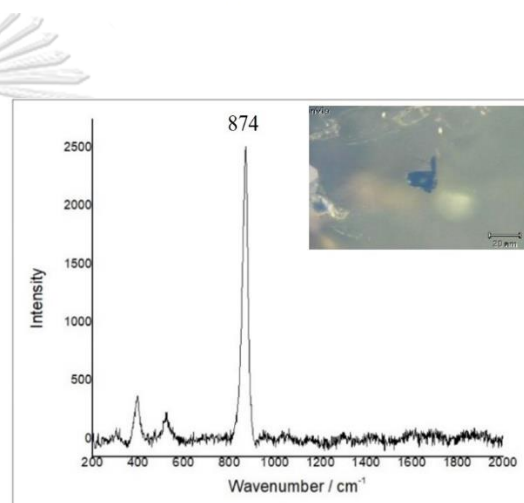


Figure A-86 Raman spectrum of a columbite observed in the sample KN50

CHULALONGKORN UNIVERSITY

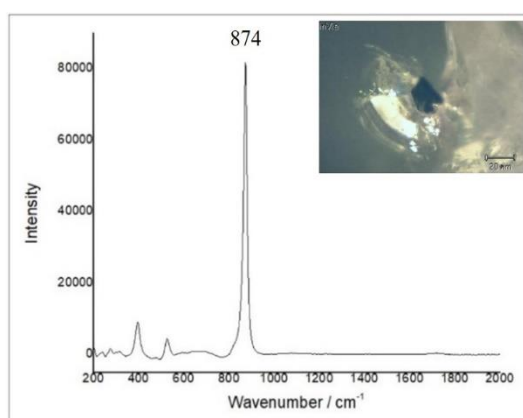


Figure A-87 Raman spectrum of a columbite observed in the sample KN54

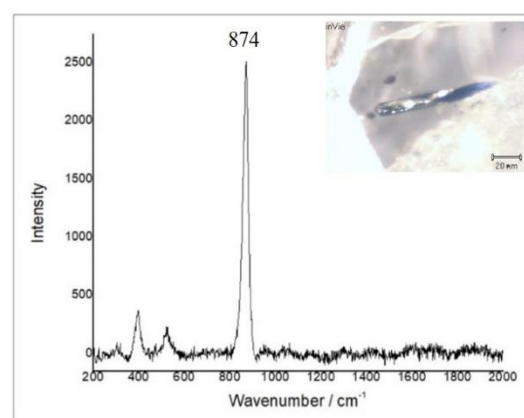


Figure A-88 Raman spectrum of a columbite observed in the sample KN55

4) Dak Nong area in Southern Vietnam

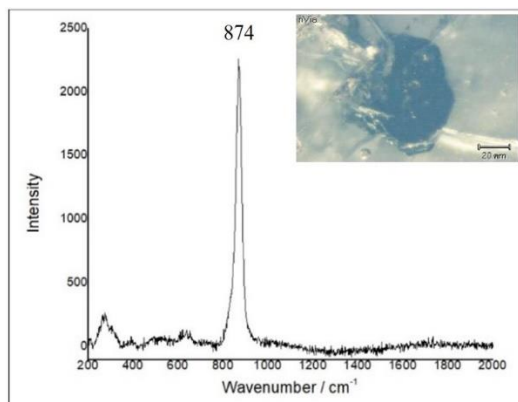


Figure A-89 Raman spectrum of a columbite observed in the sample DN01

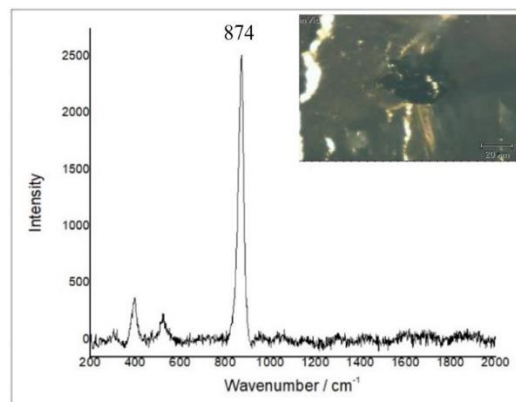


Figure A-90 Raman spectrum of a columbite observed in the sample DN02

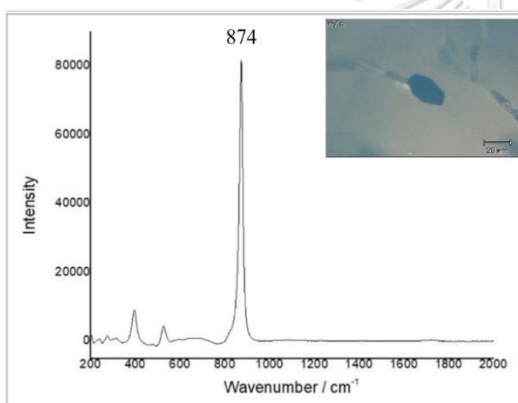


Figure A-91 Raman spectrum of a columbite observed in the sample DN07

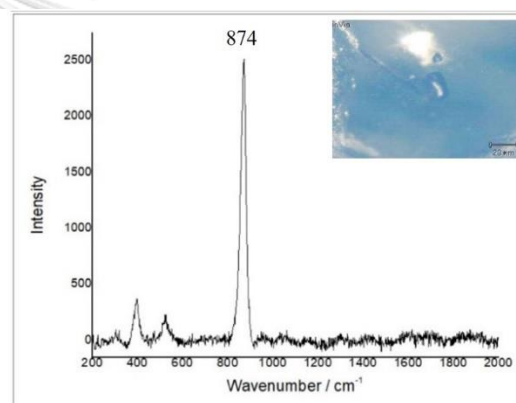


Figure A-92 Raman spectrum of a columbite observed in the sample DN09

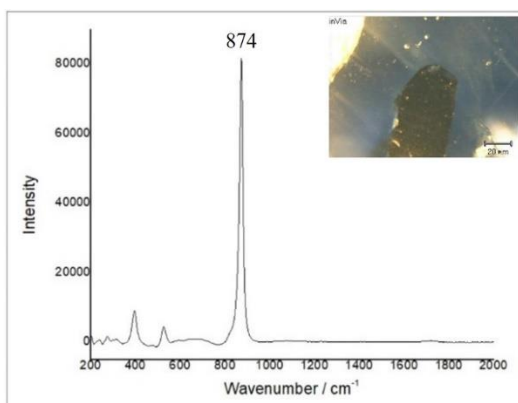


Figure A-93 Raman spectrum of a columbite observed in the sample DN11

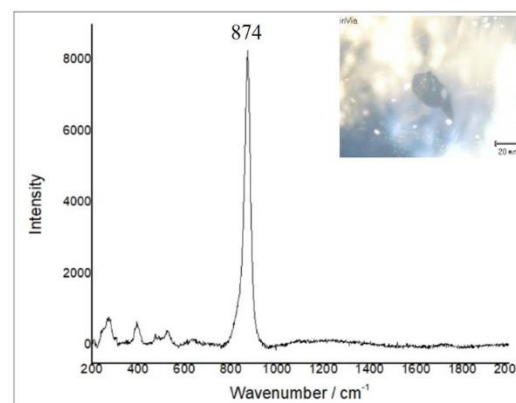


Figure A-94 Raman spectrum of a columbite observed in the sample DN17

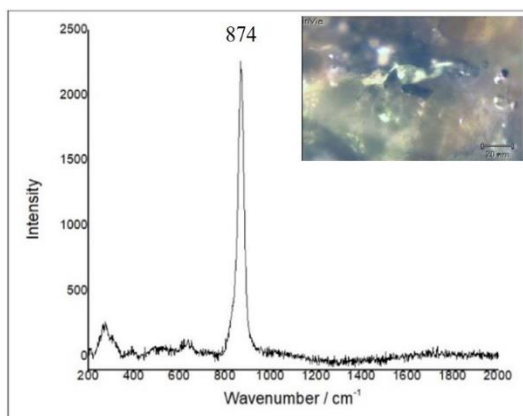


Figure A-95 Raman spectrum of a columbite observed in the sample DN18

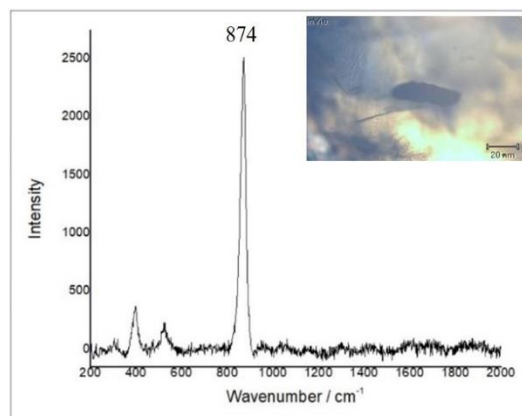


Figure A-96 Raman spectrum of a columbite observed in the sample DN19

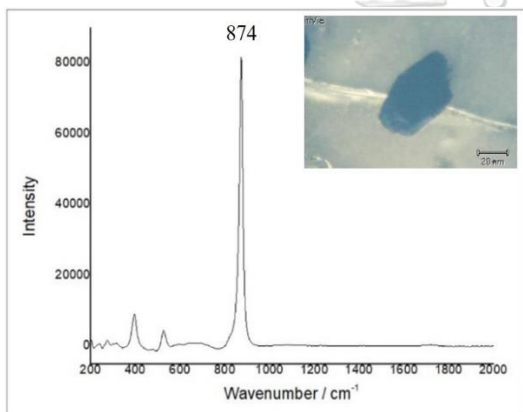


Figure A-97 Raman spectrum of a columbite observed in the sample DN28

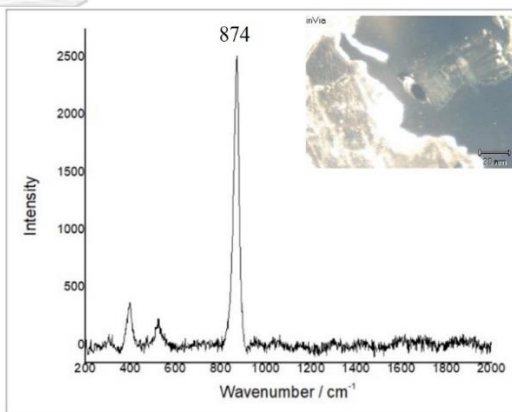


Figure A-98 Raman spectrum of a columbite observed in the sample DN30

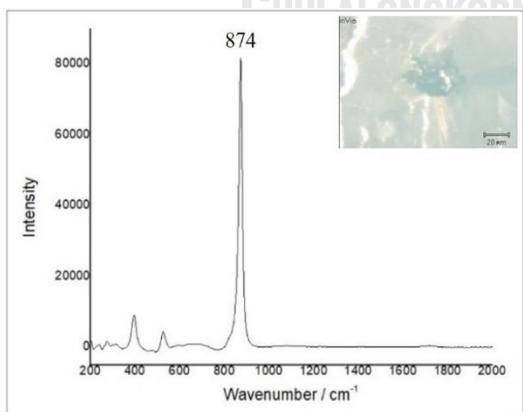


Figure A-99 Raman spectrum of a columbite observed in the sample DN38

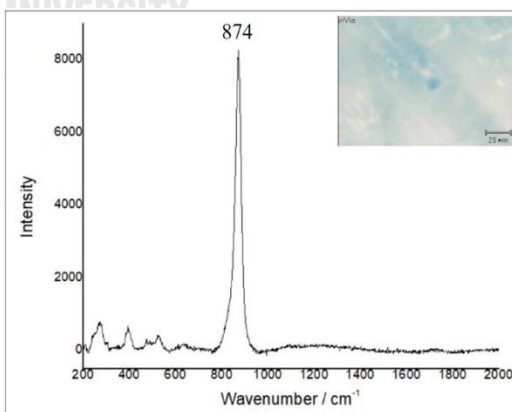


Figure A-100 Raman spectrum of a columbite observed in the sample DN43

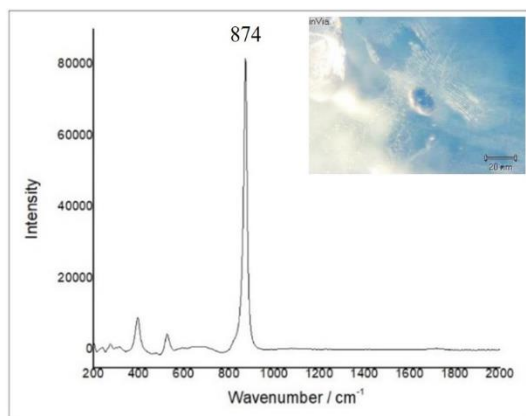


Figure A-101 Raman spectrum of a columbite observed in the sample DN44

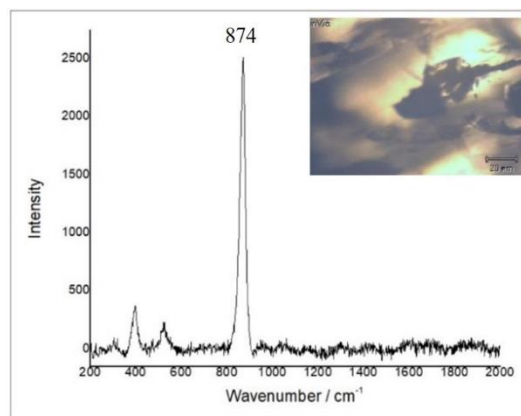


Figure A-102 Raman spectrum of a columbite observed in the sample DN45

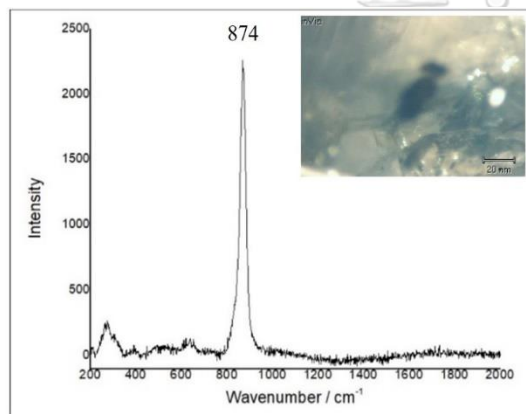


Figure A-103 Raman spectrum of a columbite observed in the sample DN47

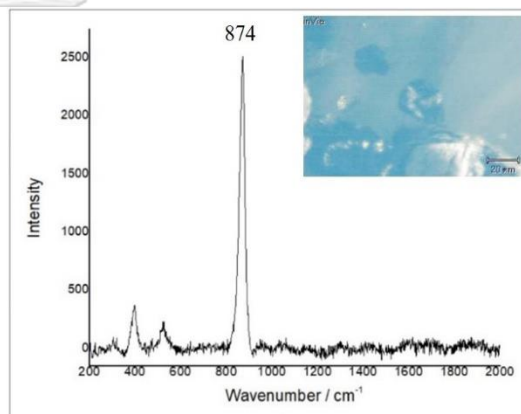


Figure A-104 Raman spectrum of a columbite observed in the sample DN48

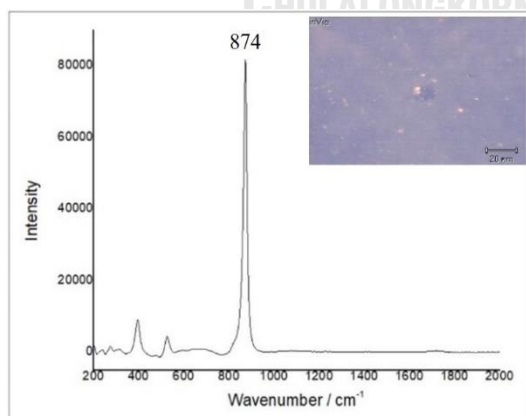


Figure A-105 Raman spectrum of a columbite observed in the sample DN49

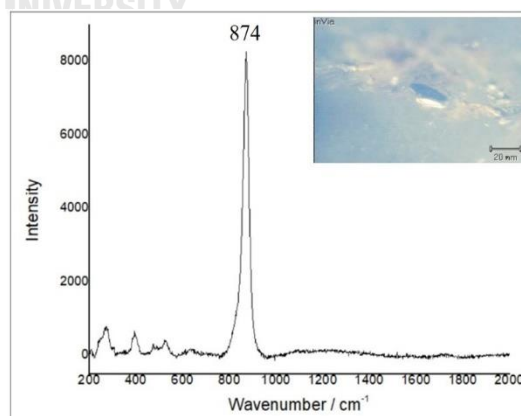


Figure A-106 Raman spectrum of a columbite observed in the sample DN50

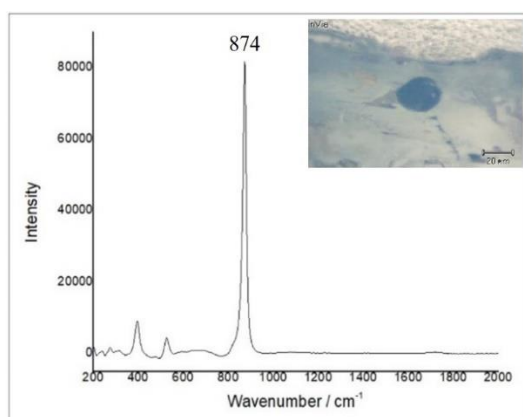


Figure A-107 Raman spectrum of a columbite observed in the sample DN51

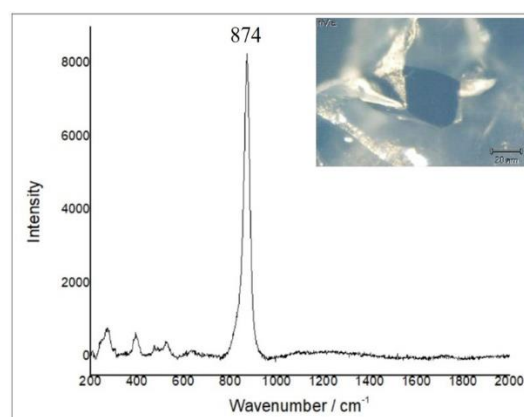


Figure A-108 Raman spectrum of a columbite observed in the sample DN52

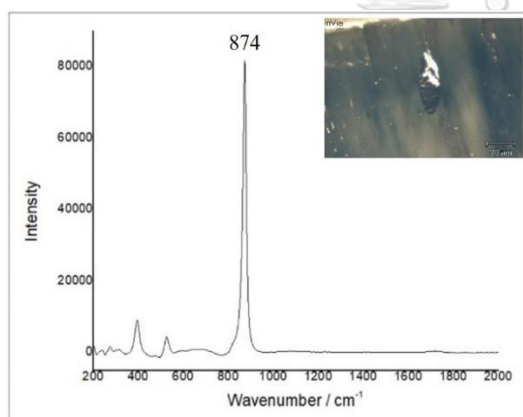


Figure A-109 Raman spectrum of a columbite observed in the sample DN53

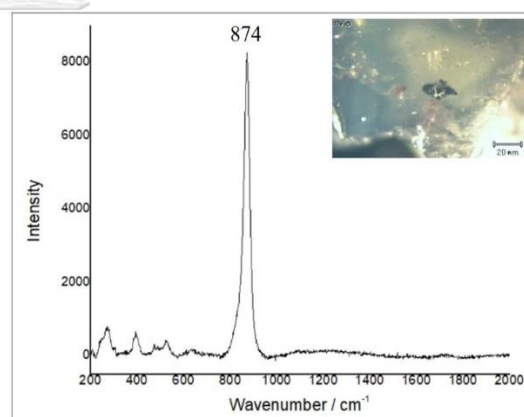


Figure A-110 Raman spectrum of a columbite observed in the sample DN54

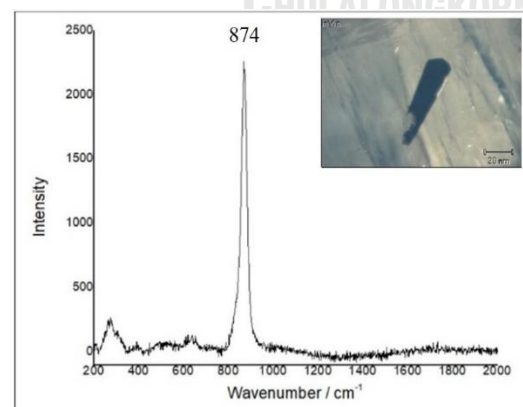


Figure A-111 Raman spectrum of a columbite observed in the sample DN55

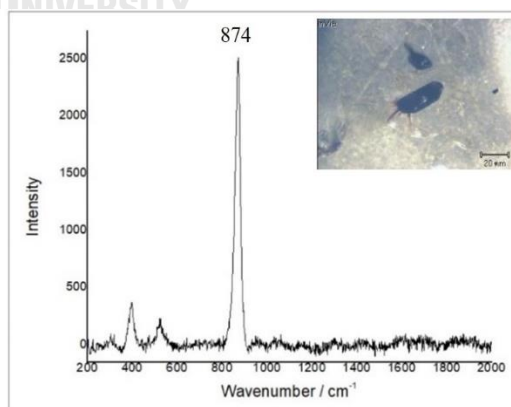


Figure A-112 Raman spectrum of a columbite observed in the sample DN57

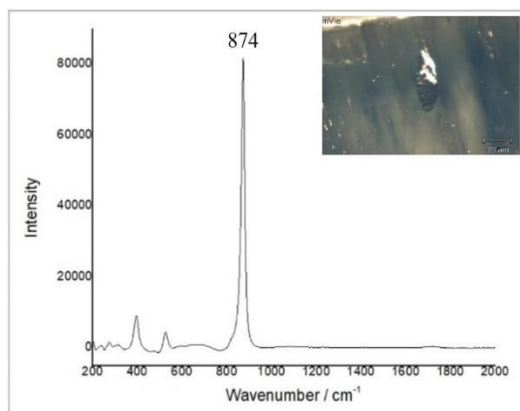


Figure A-113 Raman spectrum of a columbite observed in the sample DN58

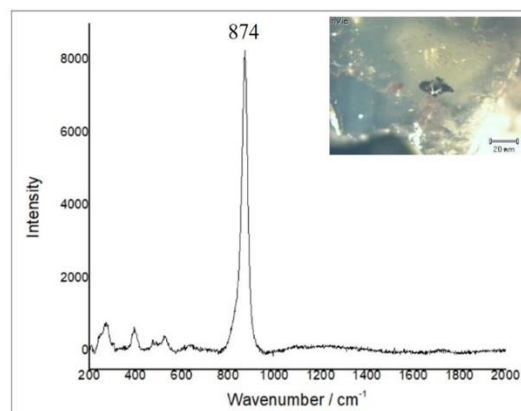


Figure A-114 Raman spectrum of a columbite observed in the sample DN59

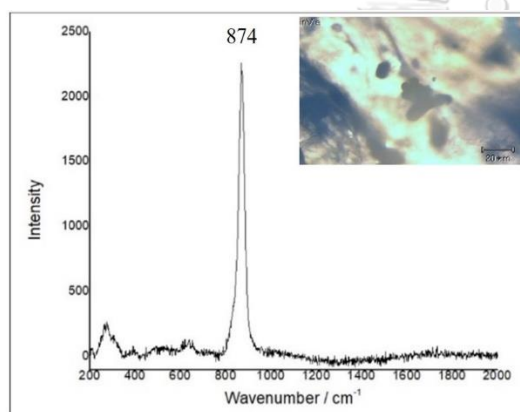


Figure A-115 Raman spectrum of a columbite observed in the sample DN60

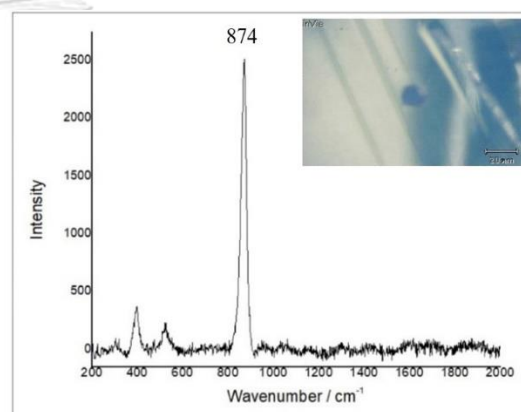


Figure A-116 Raman spectrum of a columbite observed in the sample DN61

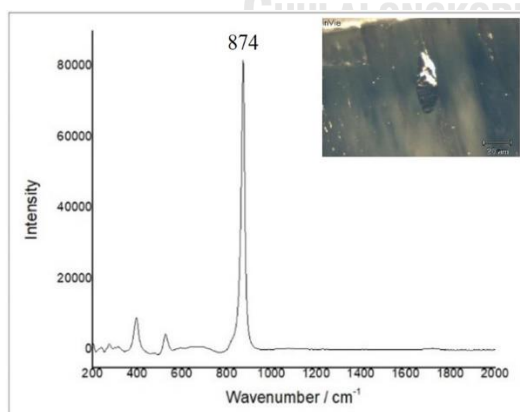


Figure A-117 Raman spectrum of a columbite observed in the sample DN62

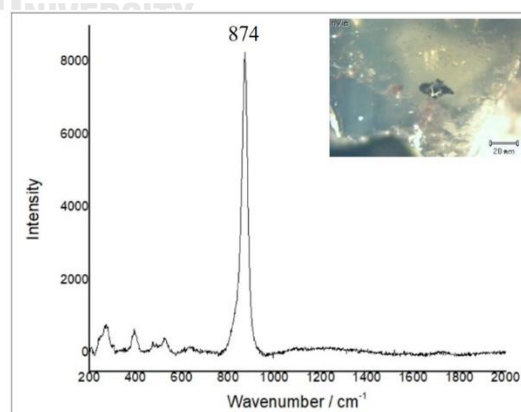


Figure A-118 Raman spectrum of a columbite observed in the sample DN63

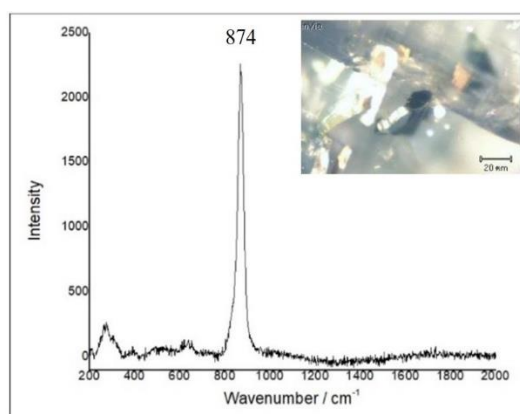


Figure A-119 Raman spectrum of a columbite observed in the sample DN64

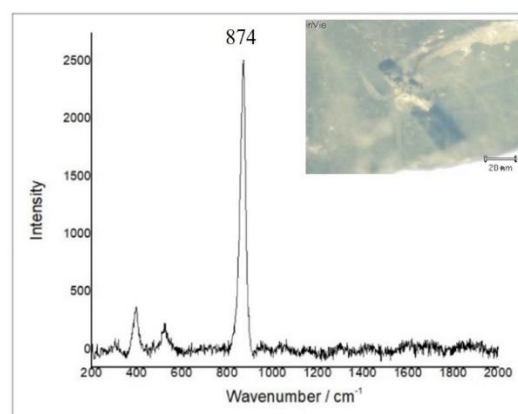


Figure A-120 Raman spectrum of a columbite observed in the sample DN65

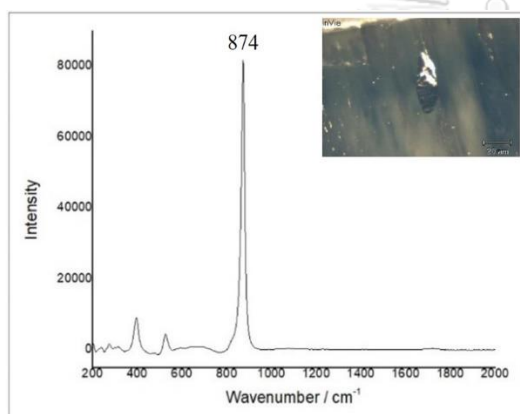


Figure A-121 Raman spectrum of a columbite observed in the sample DN66

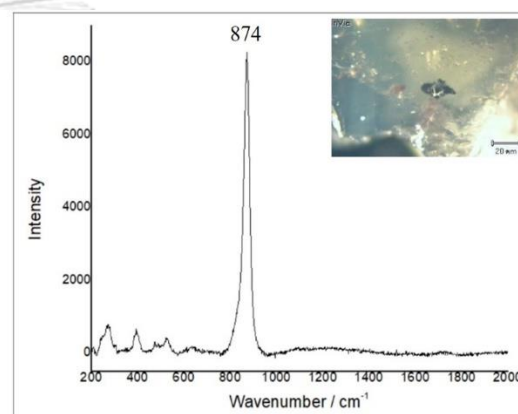


Figure A-122 Raman spectrum of a columbite observed in the sample DN68

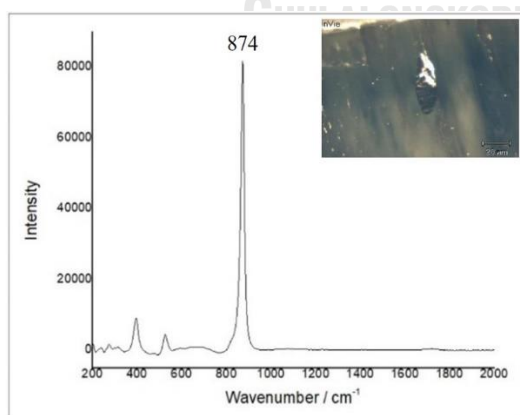


Figure A-123 Raman spectrum of a columbite observed in the sample DN75

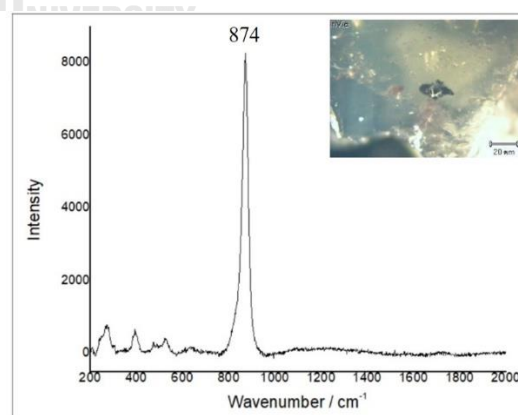


Figure A-124 Raman spectrum of a columbite observed in the sample DN76

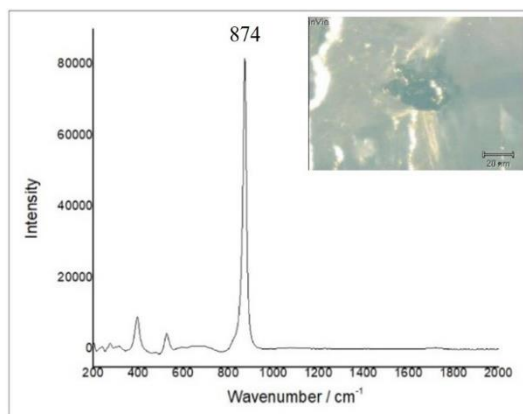


Figure A-125 Raman spectrum of a columbite observed in the sample DN78

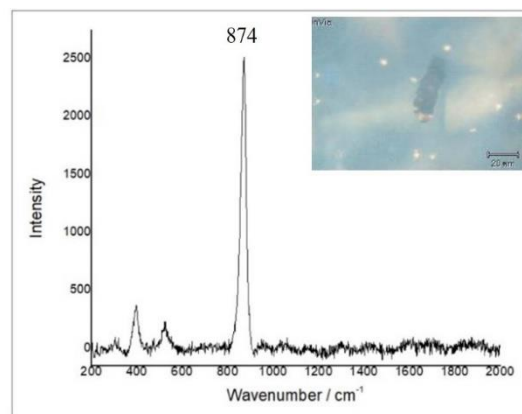


Figure A-126 Raman spectrum of a columbite observed in the sample DN80

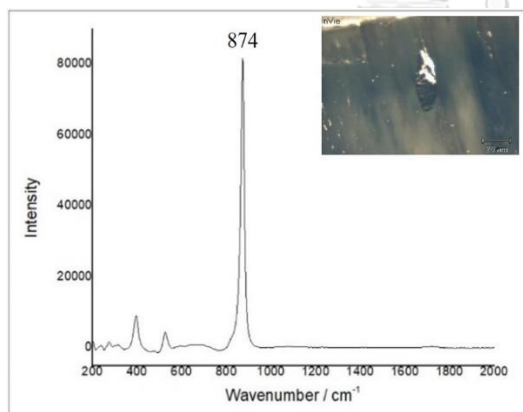


Figure A-127 Raman spectrum of a columbite observed in the sample DN81

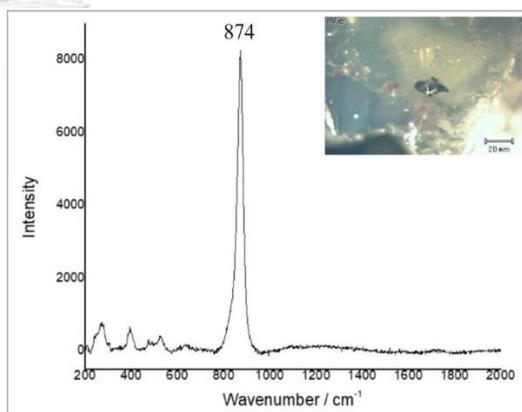


Figure A-128 Raman spectrum of a columbite observed in the sample DN83

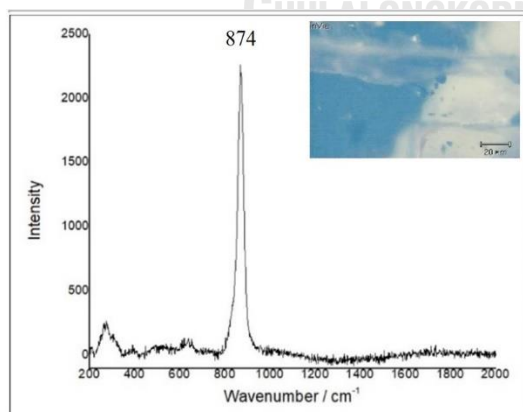


Figure A-129 Raman spectrum of a columbite observed in the sample DN84

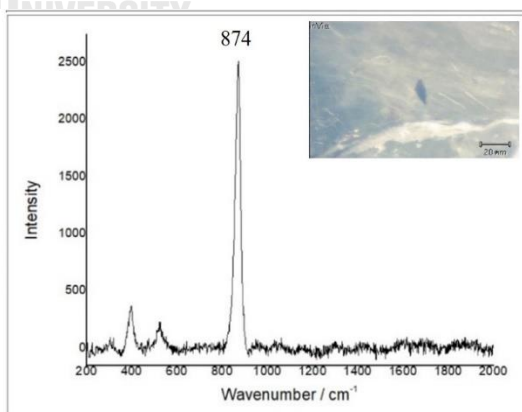


Figure A-130 Raman spectrum of a columbite observed in the sample DN85

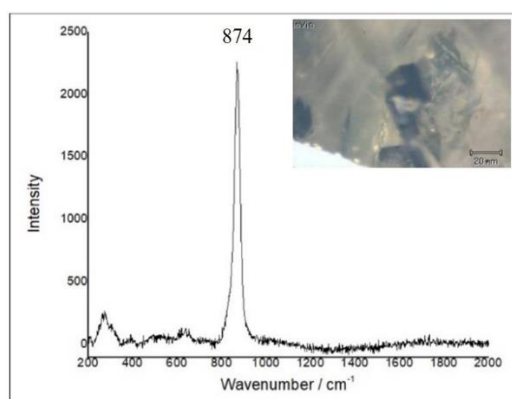


Figure A-131 Raman spectrum of a columbite observed in the sample DN87

b. Zircon

1) Binh Thuan area in Southern Vietnam

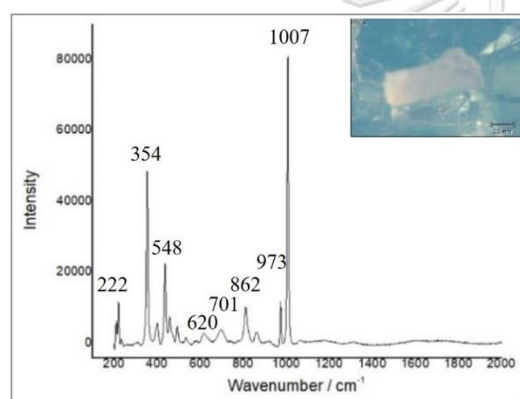


Figure A-132 Raman spectrum of a zircon observed in the sample PT04

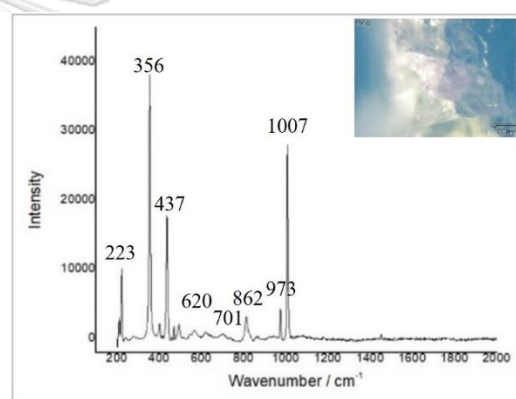


Figure A-133 Raman spectrum of a zircon observed in the sample PT05

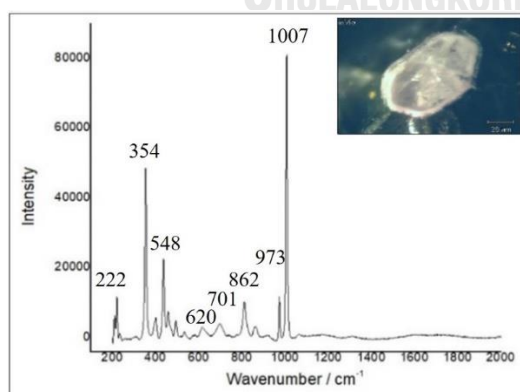


Figure A-134 Raman spectrum of a zircon observed in the sample PT12

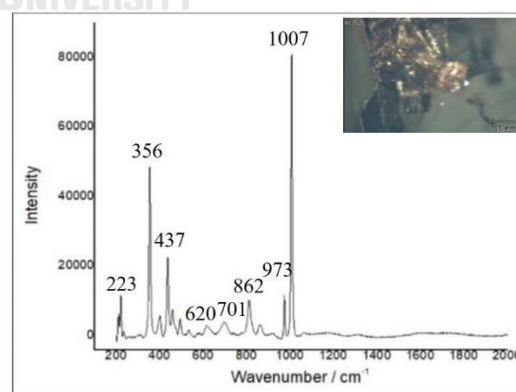


Figure A-135 Raman spectrum of a zircon observed in the sample PT13

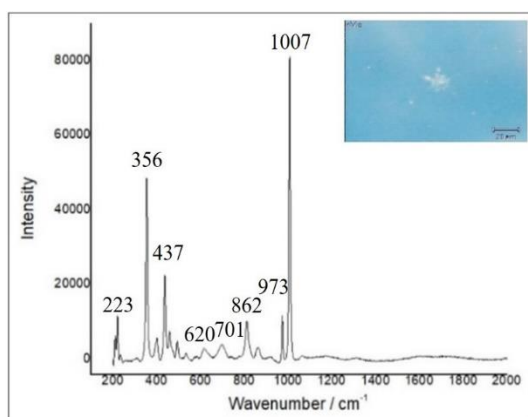


Figure A-136 Raman spectrum of a zircon observed in the sample PT15

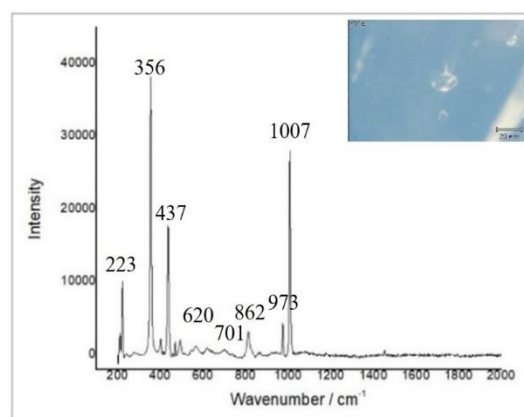


Figure A-137 Raman spectrum of a zircon observed in the sample PT16

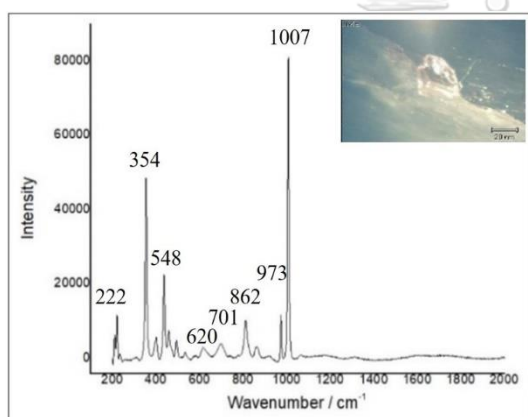


Figure A-138 Raman spectrum of a zircon observed in the sample PT26

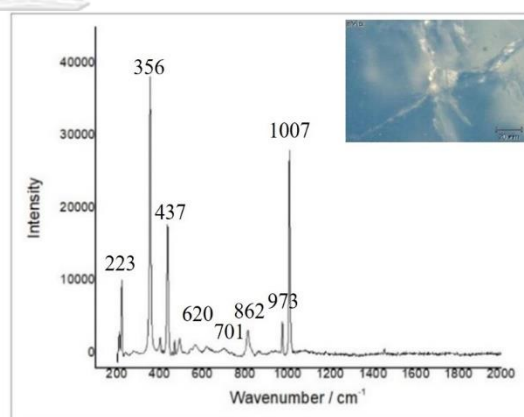


Figure A-139 Raman spectrum of a zircon observed in the sample PT36

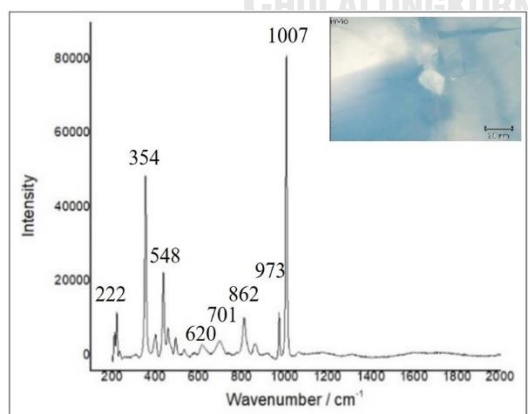


Figure A-140 Raman spectrum of a zircon observed in the sample PT44

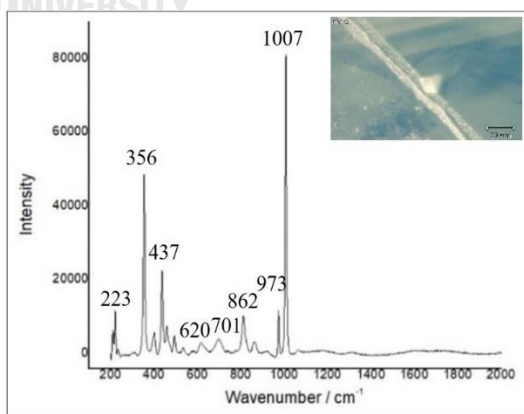


Figure A-141 Raman spectrum of a zircon observed in the sample PT45

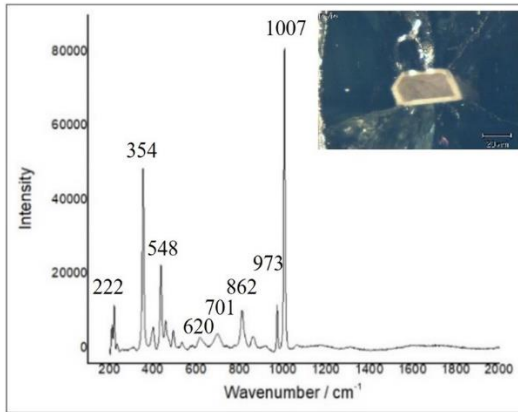


Figure A-142 Raman spectrum of a zircon observed in the sample PT47

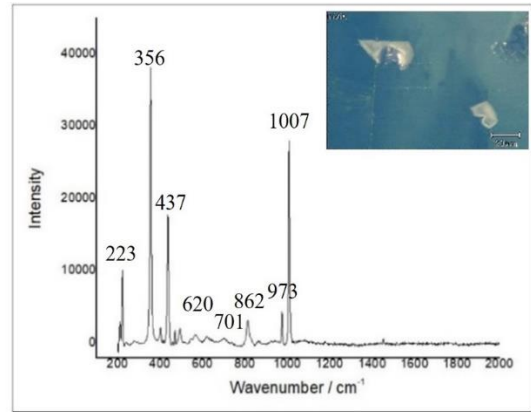


Figure A-143 Raman spectrum of a zircon observed in the sample PT53

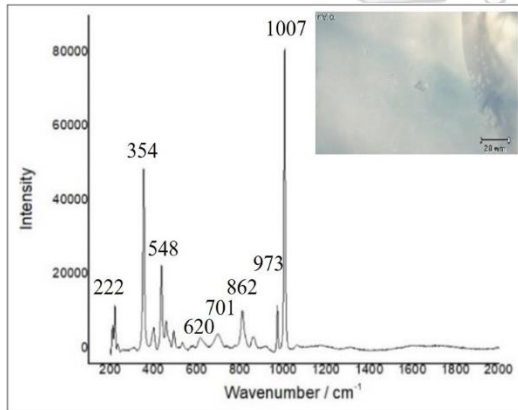


Figure A-144 Raman spectrum of a zircon observed in the sample PT59

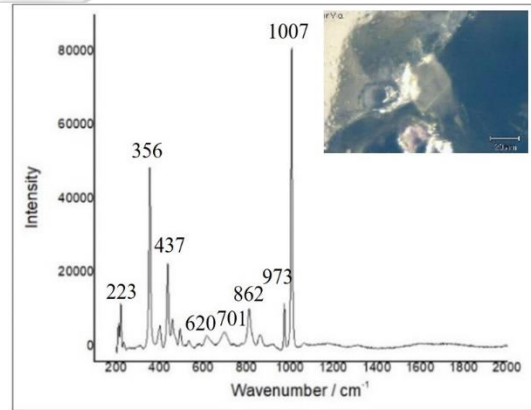


Figure A-145 Raman spectrum of a zircon observed in the sample PT61

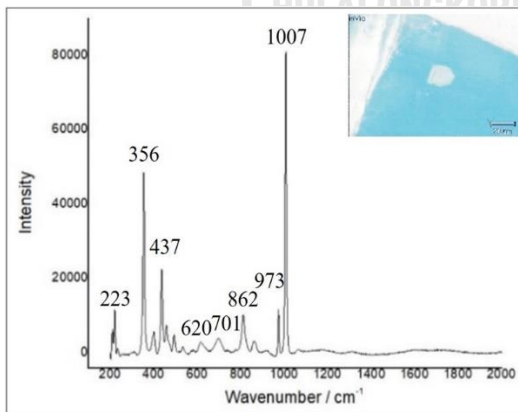


Figure A-146 Raman spectrum of a zircon observed in the sample PT65

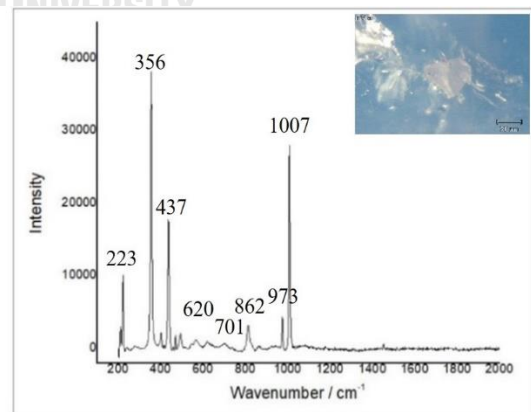


Figure A-147 Raman spectrum of a zircon observed in the sample PT66

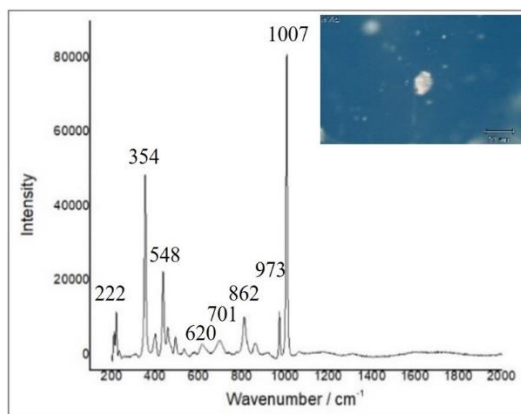


Figure A-148 Raman spectrum of a zircon observed in the sample PT69

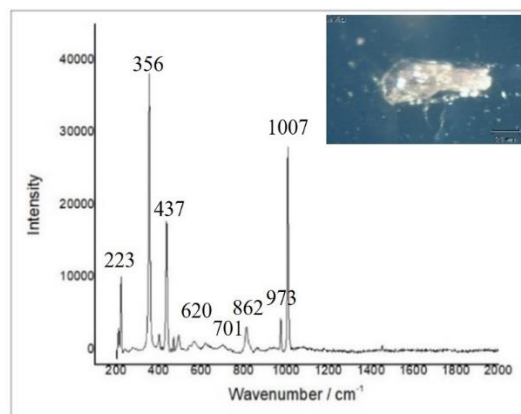


Figure A-149 Raman spectrum of a zircon observed in the sample PT70

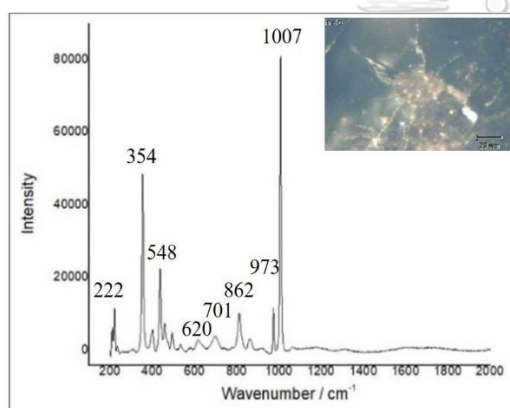


Figure A-150 Raman spectrum of a zircon observed in the sample PT80

2) Di Linh area in Southern Vietnam

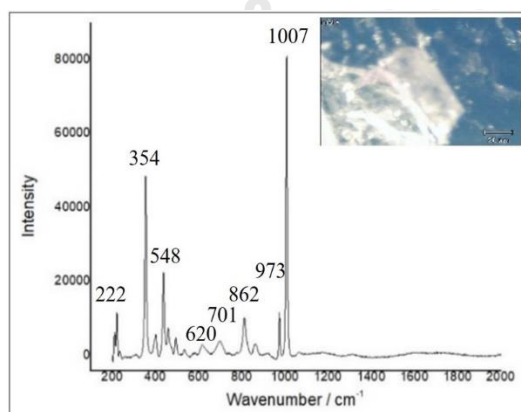


Figure A-151 Raman spectrum of a zircon observed in the sample DL01

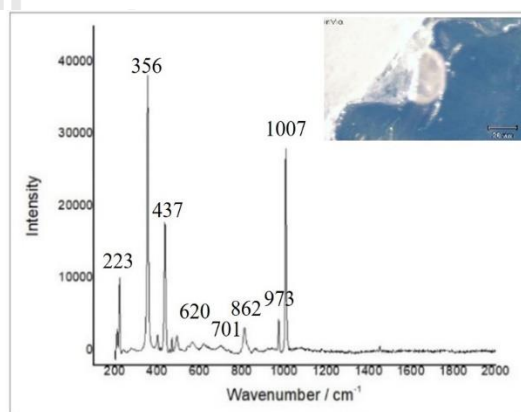


Figure A-152 Raman spectrum of a zircon observed in the sample DL02

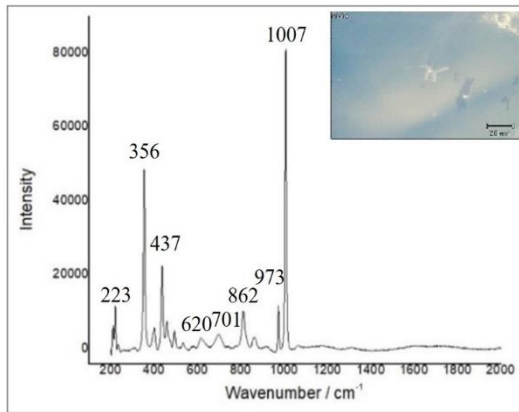


Figure A-153 Raman spectrum of a zircon observed in the sample DL03

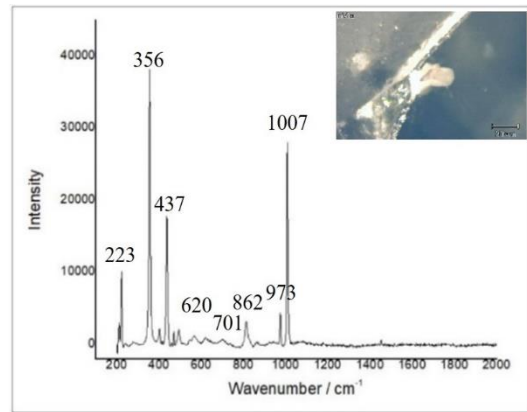


Figure A-154 Raman spectrum of a zircon observed in the sample DL04

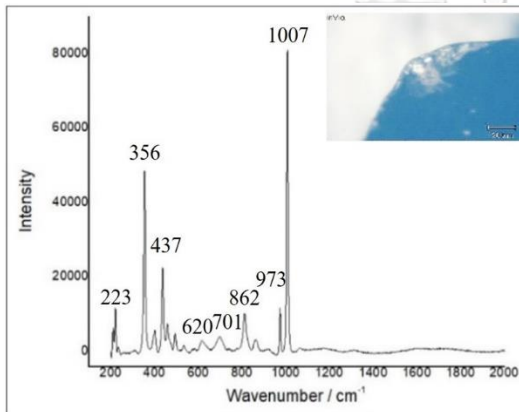


Figure A-155 Raman spectrum of a zircon observed in the sample DL13

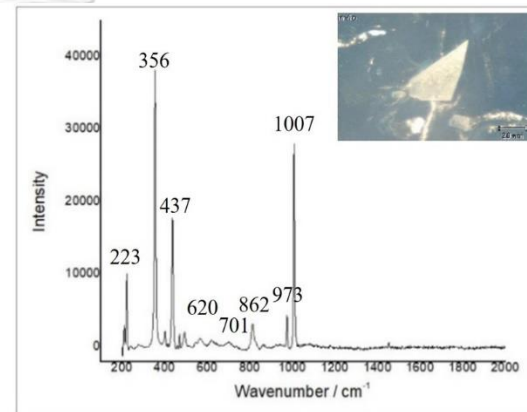


Figure A-156 Raman spectrum of a zircon observed in the sample DL18

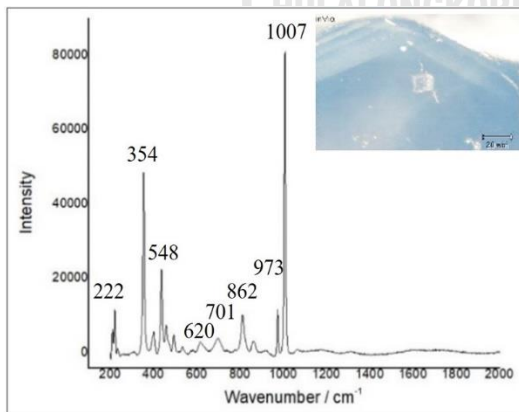


Figure A-157 Raman spectrum of a zircon observed in the sample DL20

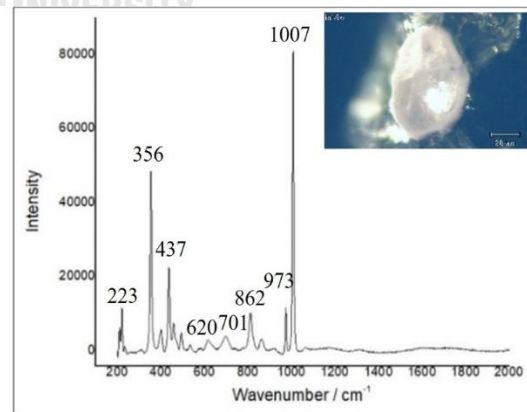


Figure A-158 Raman spectrum of a zircon observed in the sample DL26

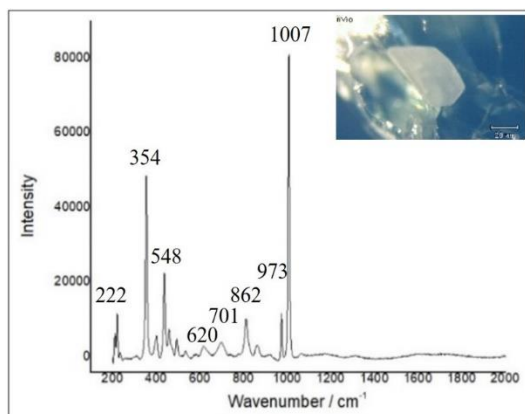


Figure A-159 Raman spectrum of a zircon observed in the sample DL40

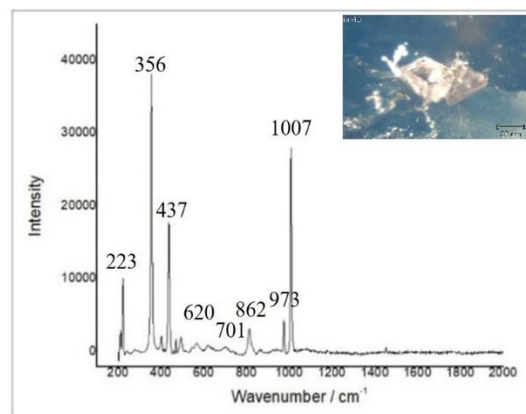


Figure A-160 Raman spectrum of a zircon observed in the sample DL43

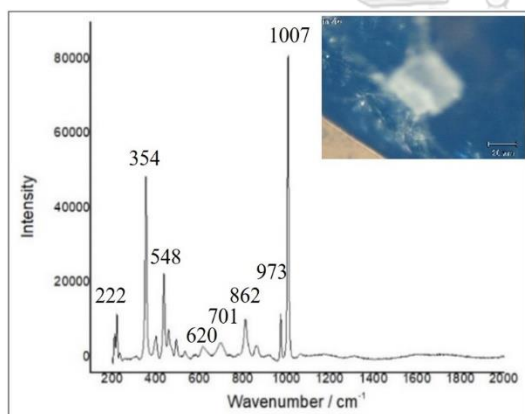


Figure A-161 Raman spectrum of a zircon observed in the sample DL44

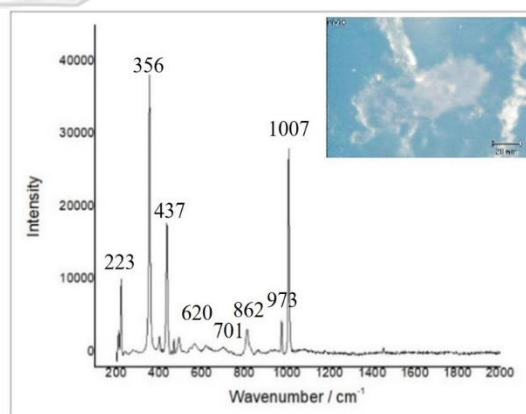


Figure A-162 Raman spectrum of a zircon observed in the sample DL46

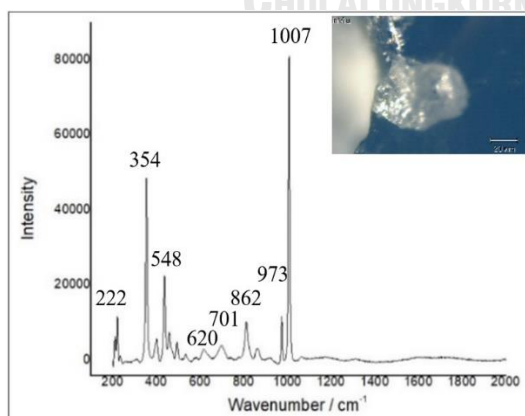


Figure A-163 Raman spectrum of a zircon observed in the sample DL47

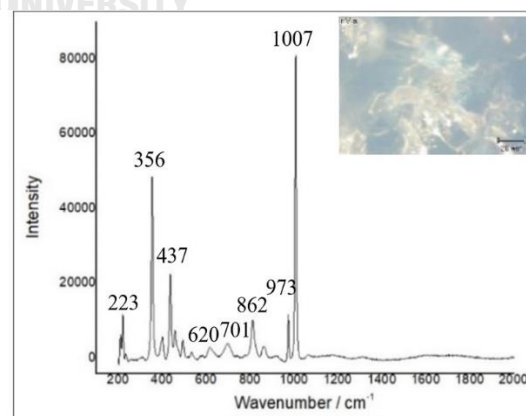


Figure A-164 Raman spectrum of a zircon observed in the sample DL48

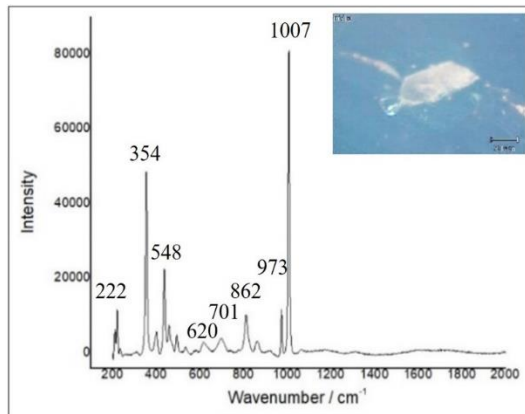


Figure A-165 Raman spectrum of a zircon observed in the sample DL58

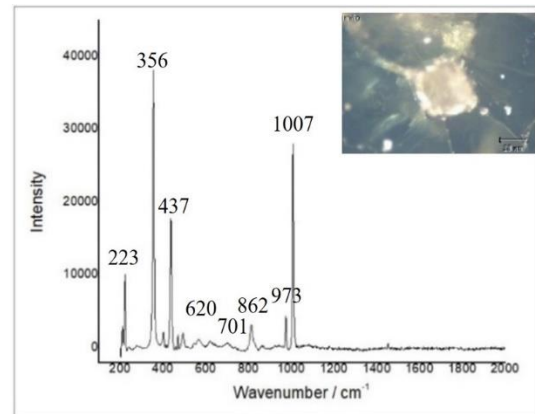


Figure A-166 Raman spectrum of a zircon observed in the sample DL60

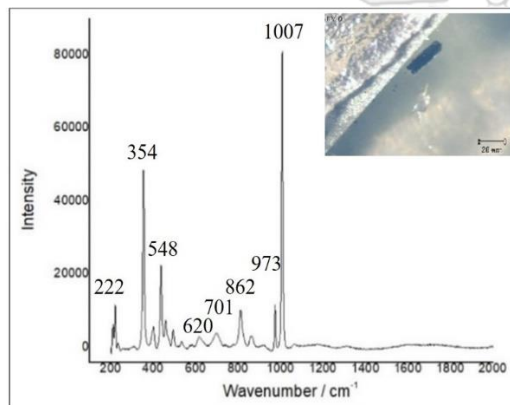


Figure A-167 Raman spectrum of a zircon observed in the sample DL61

3) Krong Nang area in Southern Vietnam

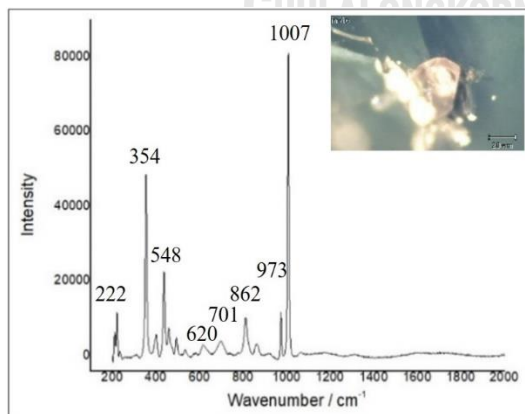


Figure A-168 Raman spectrum of a zircon observed in the sample KN08

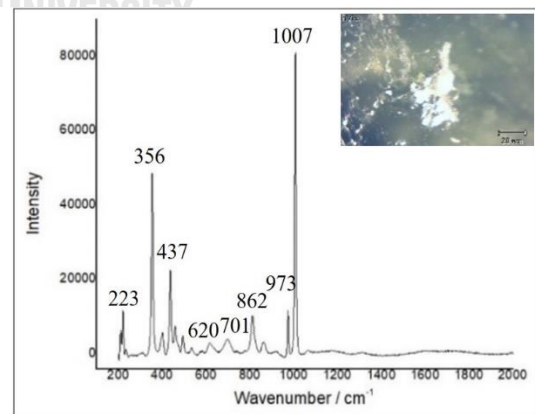


Figure A-169 Raman spectrum of a zircon observed in the sample KN12

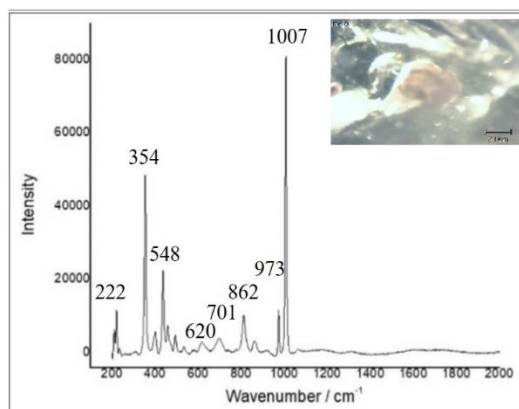


Figure A-170 Raman spectrum of a zircon observed in the sample KN13

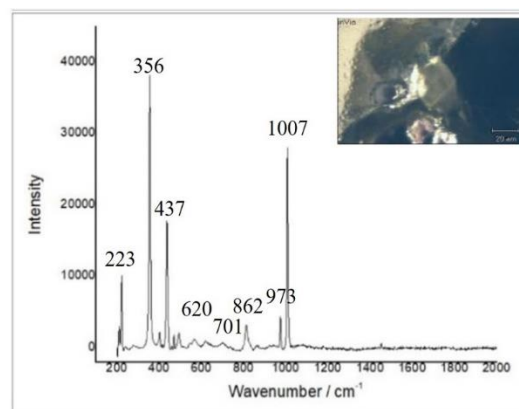


Figure A-171 Raman spectrum of a zircon observed in the sample KN14

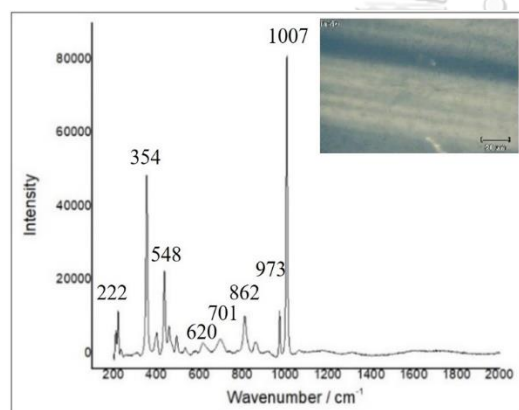


Figure A-172 Raman spectrum of a zircon observed in the sample KN15

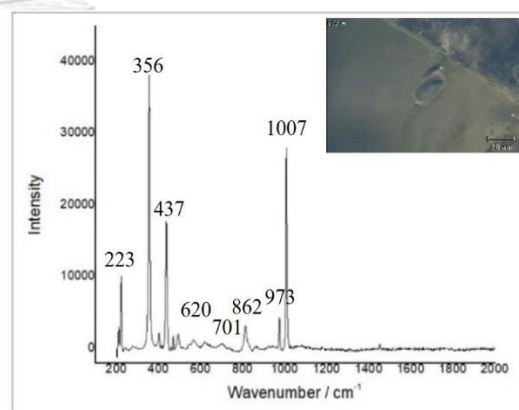


Figure A-173 Raman spectrum of a zircon observed in the sample KN27

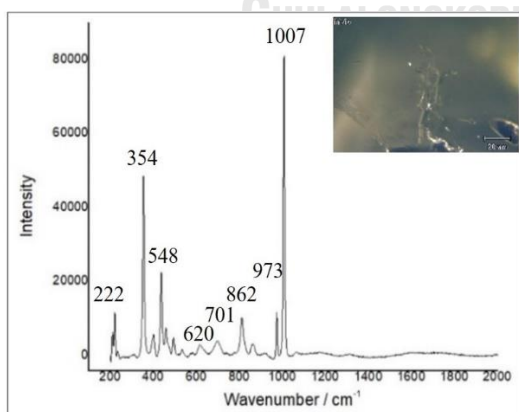


Figure A-174 Raman spectrum of a zircon observed in the sample KN35

4) Dak Nong area in Southern Vietnam

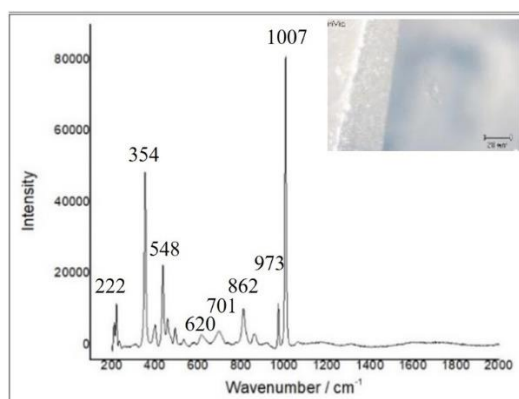


Figure A-175 Raman spectrum of a zircon observed in the sample DN04

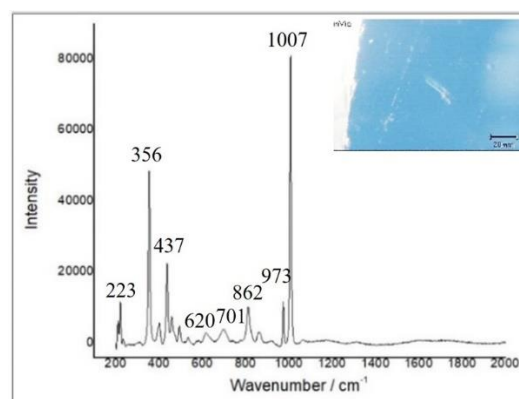


Figure A-176 Raman spectrum of a zircon observed in the sample DN05

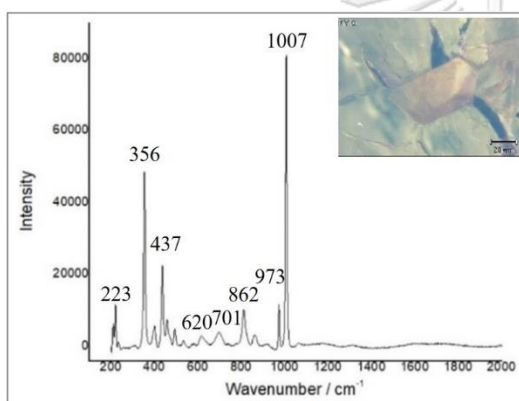


Figure A-177 Raman spectrum of a zircon observed in the sample DN06

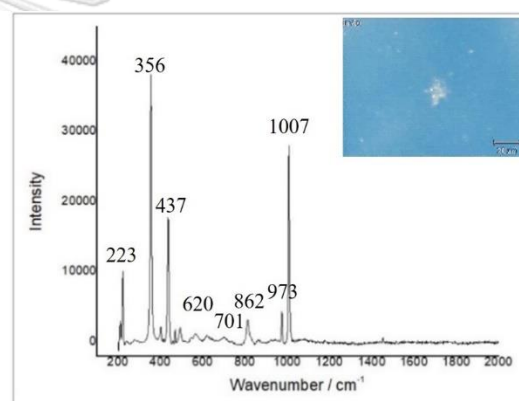


Figure A-178 Raman spectrum of a zircon observed in the sample DN14

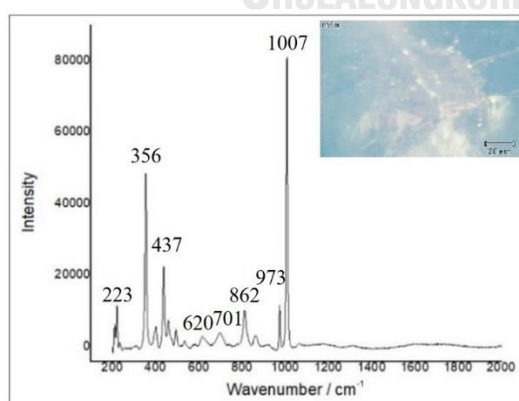


Figure A-179 Raman spectrum of a zircon observed in the sample DN15

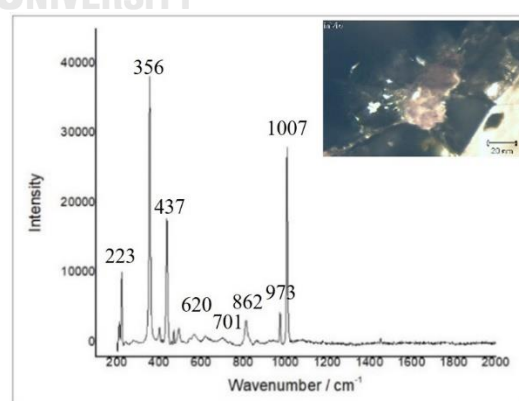


Figure A-180 Raman spectrum of a zircon observed in the sample DN20

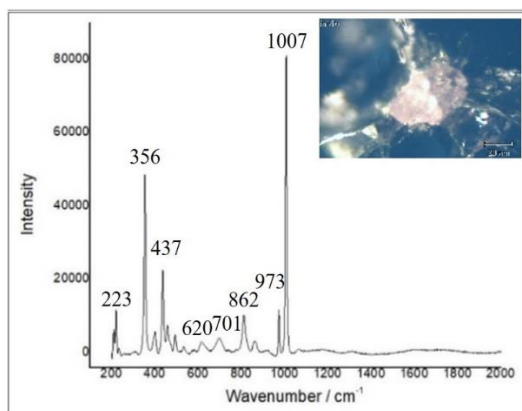


Figure A-181 Raman spectrum of a zircon observed in the sample DN21

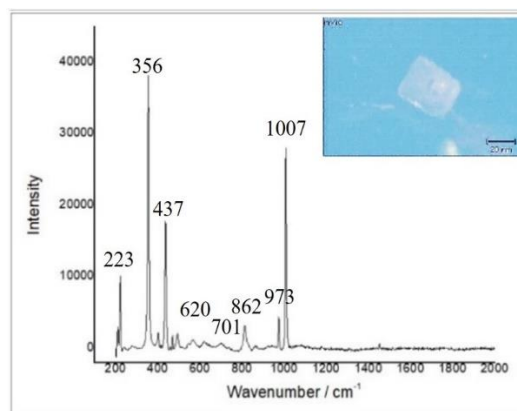


Figure A-182 Raman spectrum of a zircon observed in the sample DN22

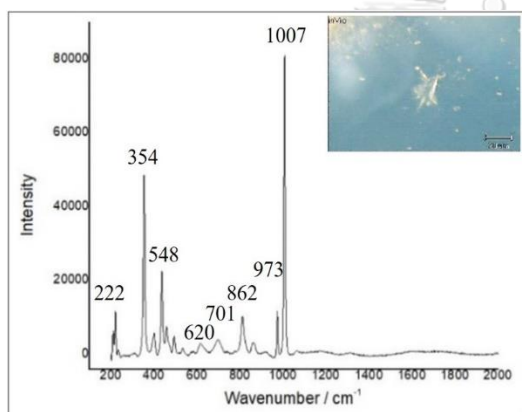


Figure A-183 Raman spectrum of a zircon observed in the sample DN23

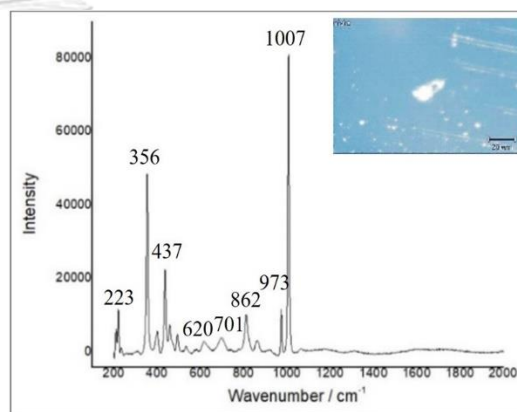


Figure A-184 Raman spectrum of a zircon observed in the sample DN24

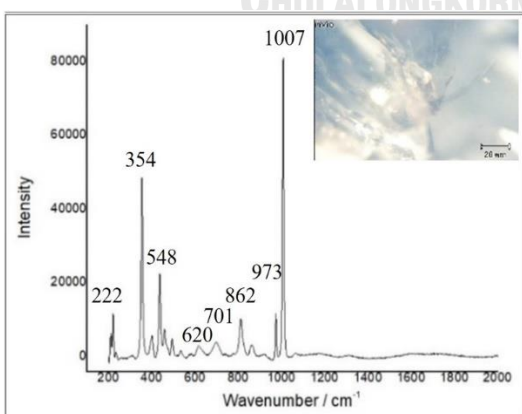


Figure A-185 Raman spectrum of a zircon observed in the sample DN25

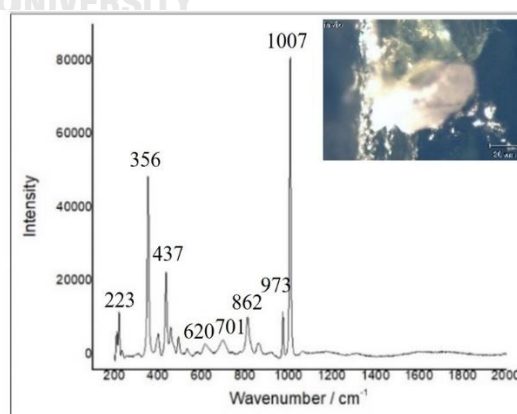


Figure A-186 Raman spectrum of a zircon observed in the sample DN29

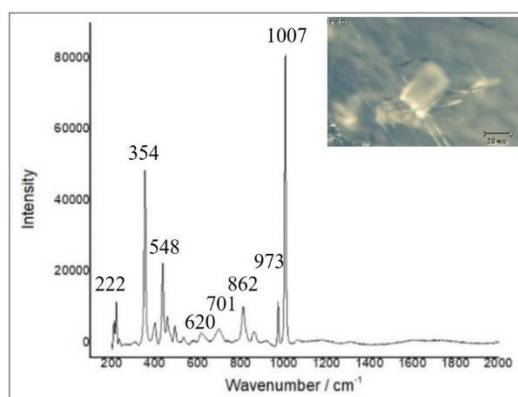


Figure A-187 Raman spectrum of a zircon observed in the sample DN31

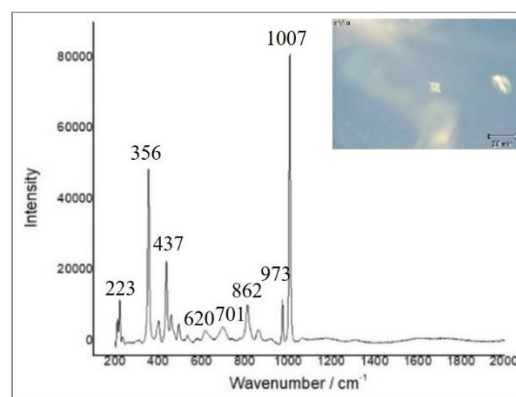


Figure A-188 Raman spectrum of a zircon observed in the sample DN32

c. Feldspar

1) Binh Thuan area in Southern Vietnam

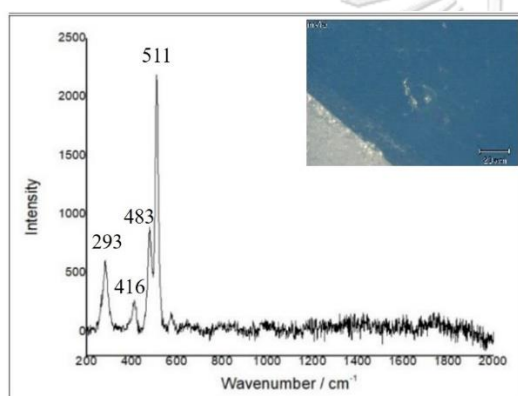


Figure A-189 Raman spectrum of a feldspar observed in the sample PT01

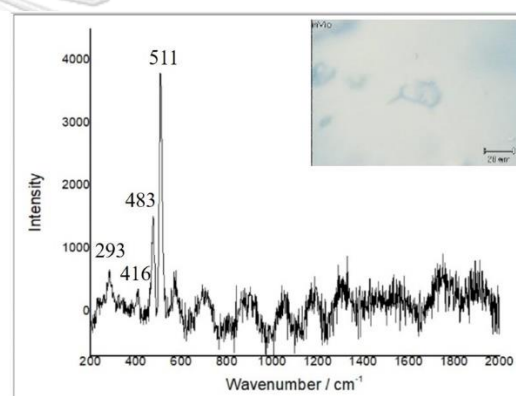


Figure A-190 Raman spectrum of a feldspar observed in the sample PT23

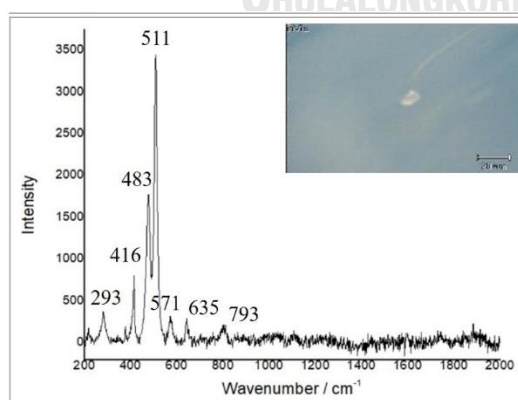


Figure A-191 Raman spectrum of a feldspar observed in the sample PT31

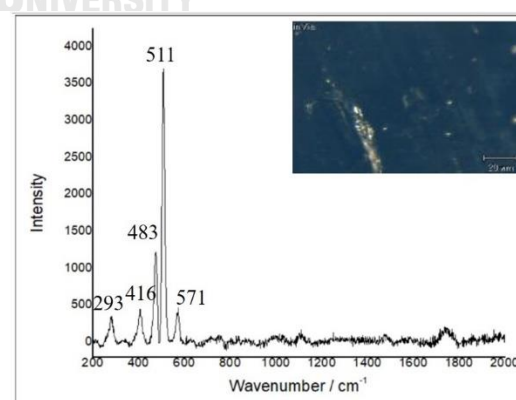


Figure A-192 Raman spectrum of a feldspar observed in the sample PT43

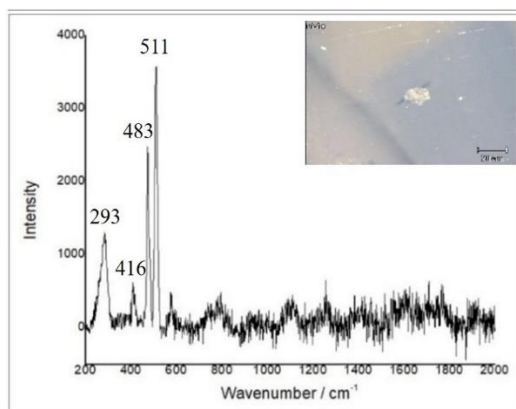


Figure A-193 Raman spectrum of a feldspar observed in the sample PT51

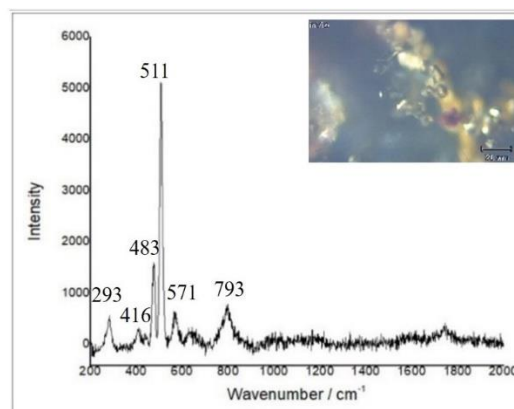


Figure A-194 Raman spectrum of a feldspar observed in the sample PT62

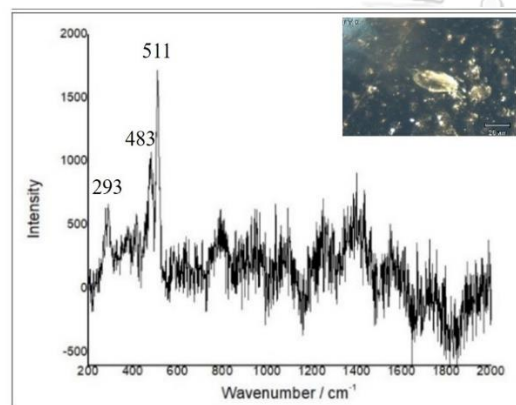


Figure A-195 Raman spectrum of a feldspar observed in the sample PT63

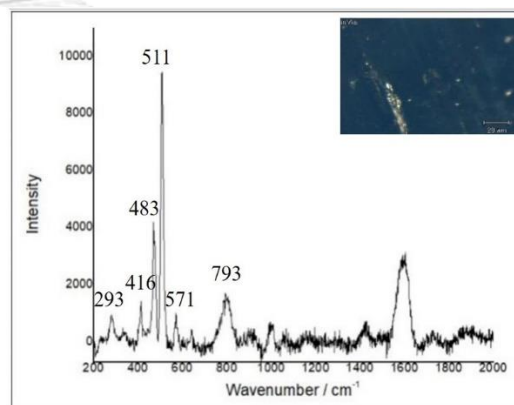


Figure A-196 Raman spectrum of a feldspar observed in the sample PT67

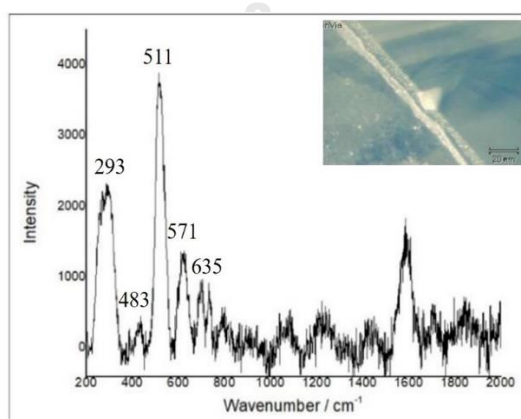


Figure A-197 Raman spectrum of a feldspar observed in the sample PT81

2) Di Linh area in Southern Vietnam

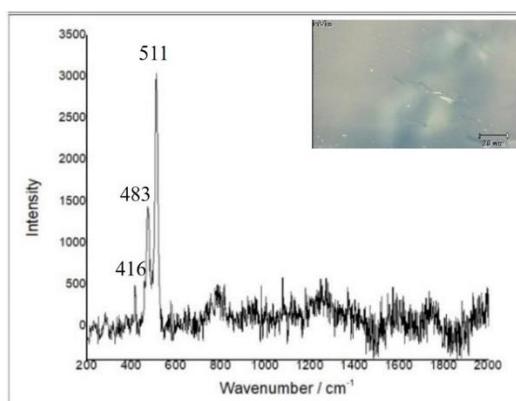


Figure A-198 Raman spectrum of a feldspar observed in the sample DL17

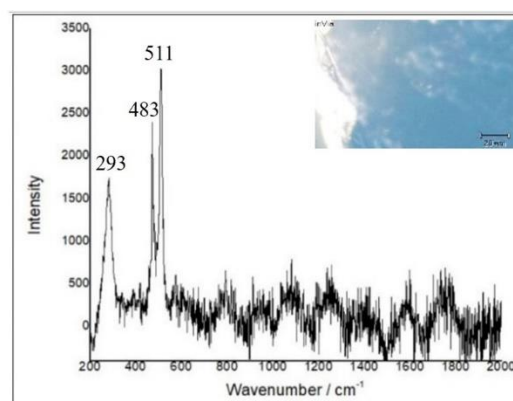


Figure A-199 Raman spectrum of a feldspar observed in the sample DL22

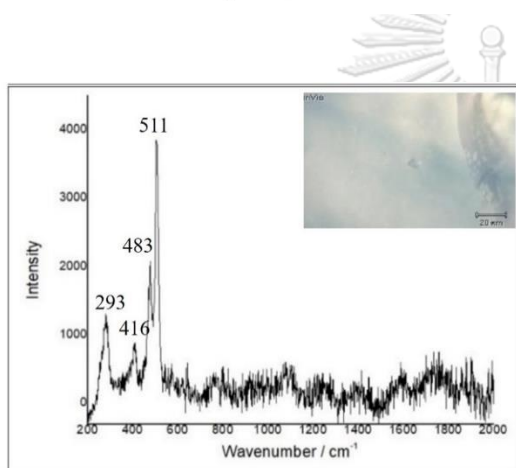


Figure A-200 Raman spectrum of a feldspar observed in the sample DL25

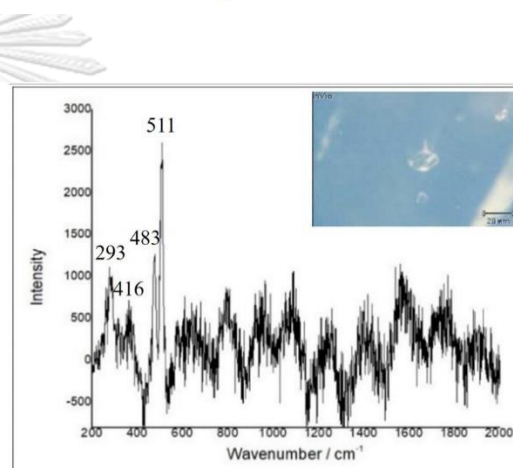


Figure A-201 Raman spectrum of a feldspar observed in the sample DL27

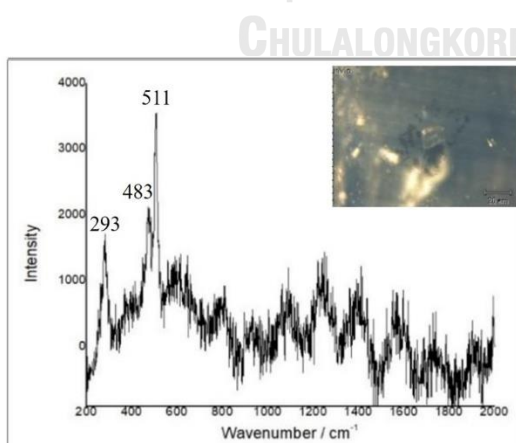


Figure A-202 Raman spectrum of a feldspar observed in the sample DL28

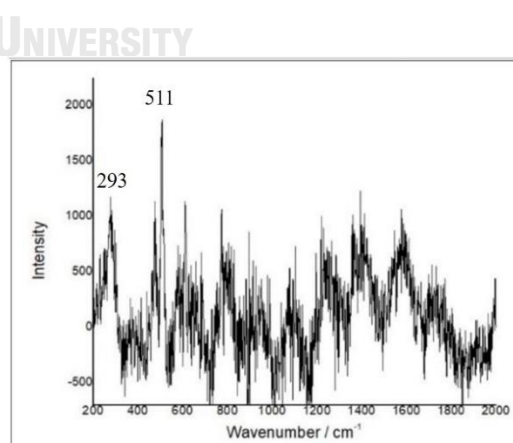


Figure A-203 Raman spectrum of a feldspar observed in the sample DL31

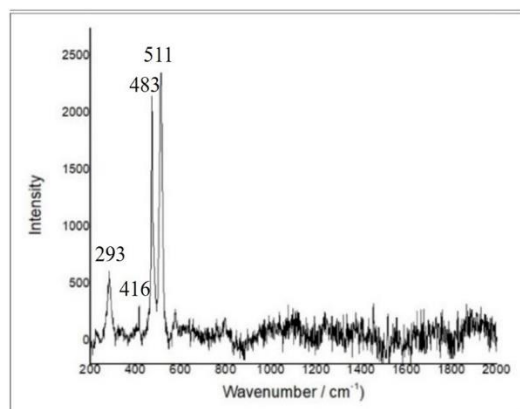


Figure A-204 Raman spectrum of a feldspar observed in the sample DL34

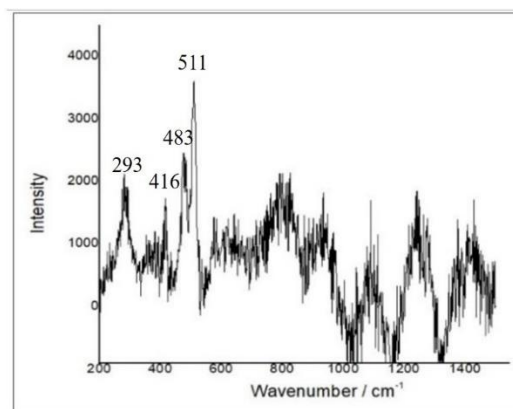


Figure A-205 Raman spectrum of a feldspar observed in the sample DL36

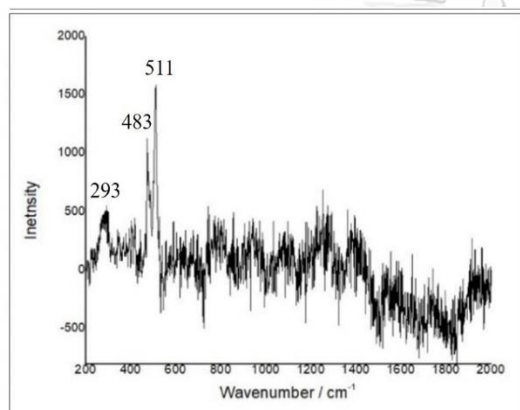


Figure A-206 Raman spectrum of a feldspar observed in the sample DL41

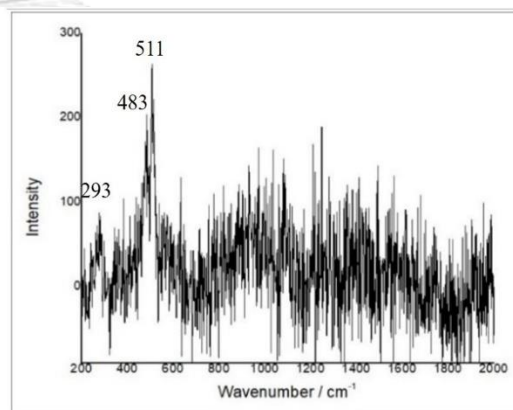


Figure A-207 Raman spectrum of a feldspar observed in the sample DL51

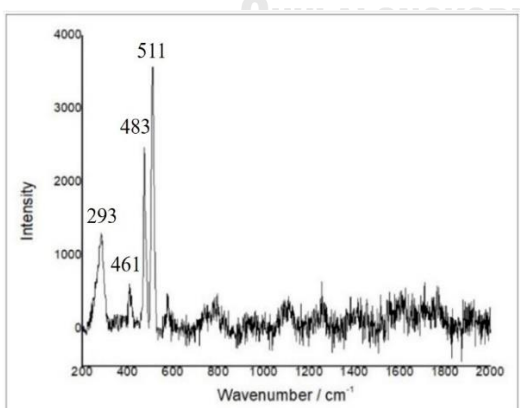


Figure A-208 Raman spectrum of a feldspar observed in the sample DL53

3) Krong Nang area in Southern Vietnam

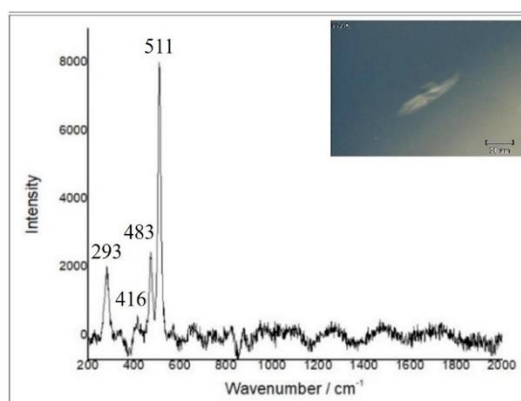


Figure A-209 Raman spectrum of a feldspar observed in the sample KN02

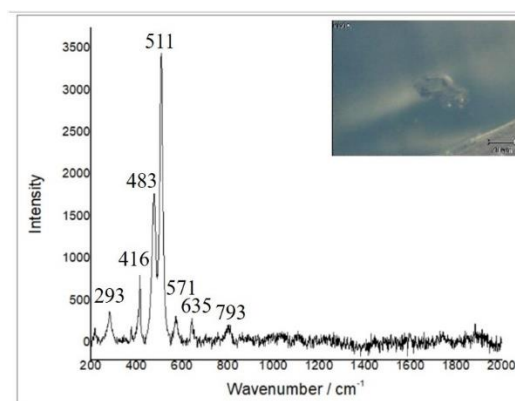


Figure A-210 Raman spectrum of a feldspar observed in the sample KN11

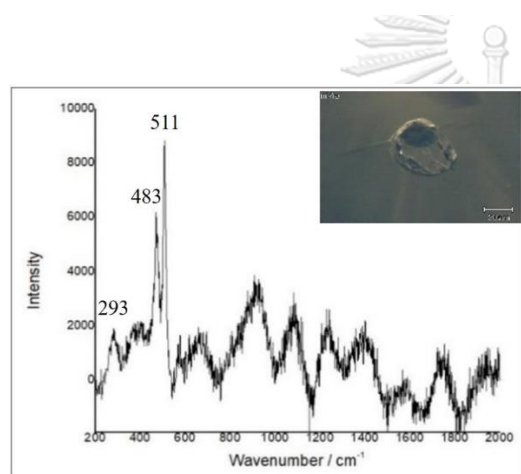


Figure A-211 Raman spectrum of a feldspar observed in the sample KN16

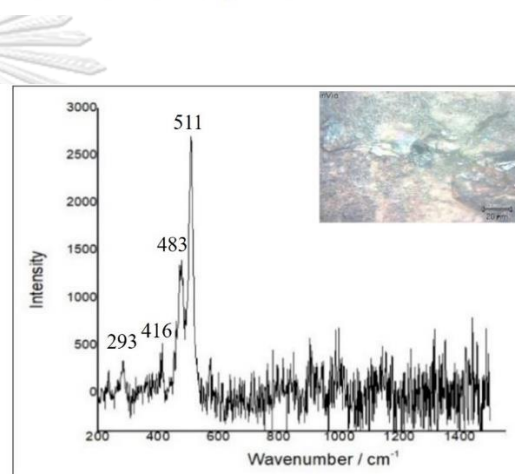


Figure A-212 Raman spectrum of a feldspar observed in the sample KN17

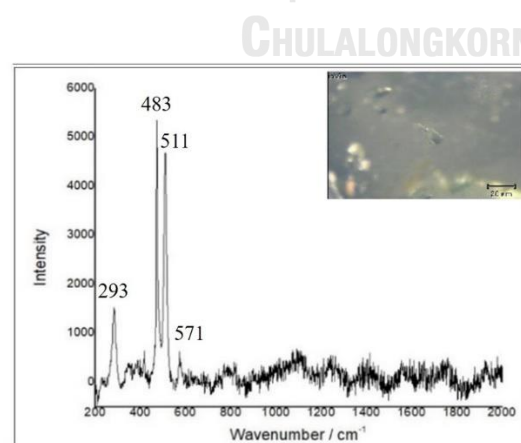


Figure A-213 Raman spectrum of a feldspar observed in the sample KN37

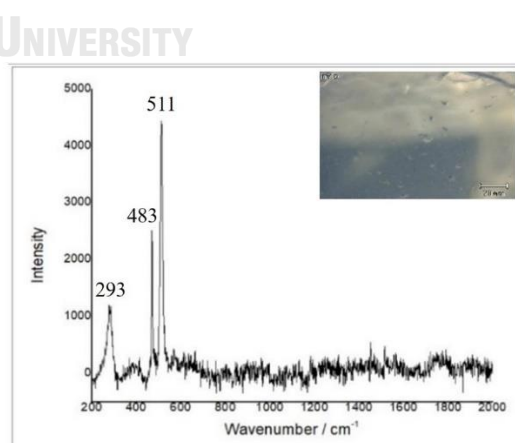


Figure A-214 Raman spectrum of a feldspar observed in the sample KN51

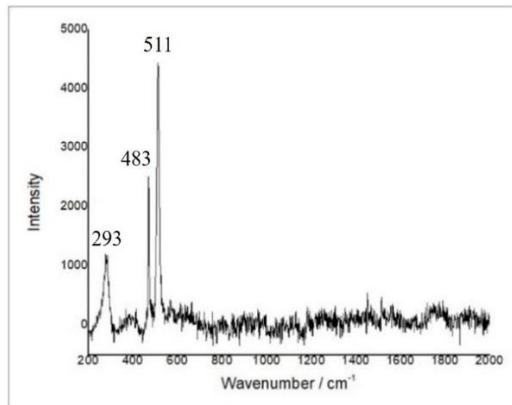


Figure A-215 Raman spectrum of a feldspar observed in the sample KN53

4) Dak Nong area in Southern Vietnam

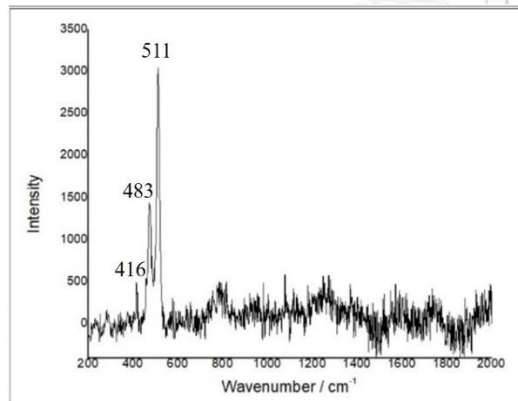


Figure A-216 Raman spectrum of a feldspar observed in the sample DN08

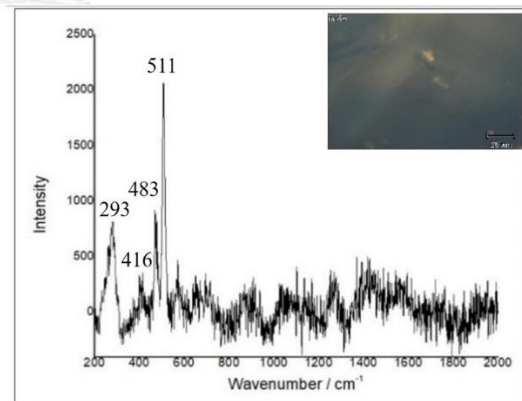


Figure A-217 Raman spectrum of a feldspar observed in the sample DN10

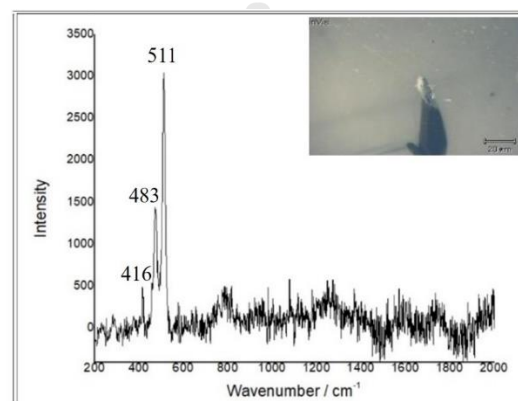


Figure A-218 Raman spectrum of a feldspar observed in the sample DN13

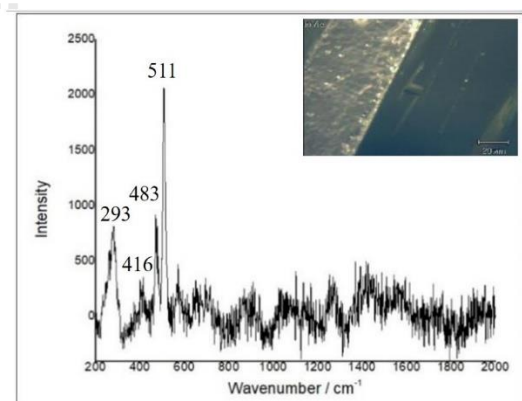


Figure A-219 Raman spectrum of a feldspar observed in the sample DN26

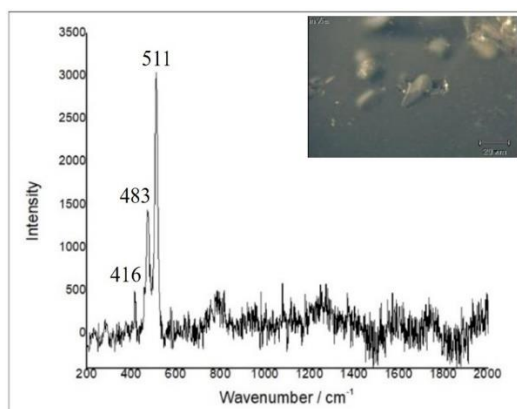


Figure A-220 Raman spectrum of a feldspar observed in the sample DN34

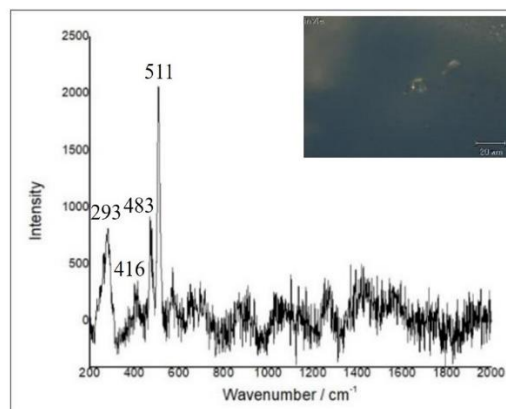


Figure A-221 Raman spectrum of a feldspar observed in the sample DN36

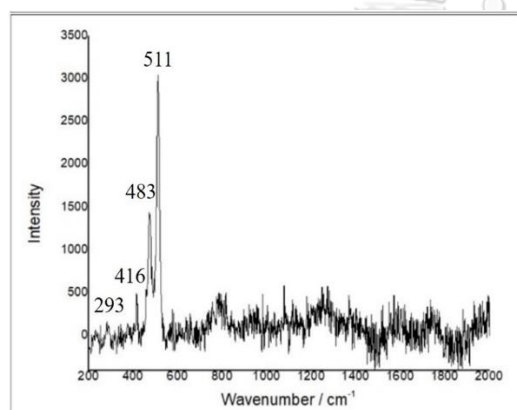


Figure A-222 Raman spectrum of a feldspar observed in the sample DN37

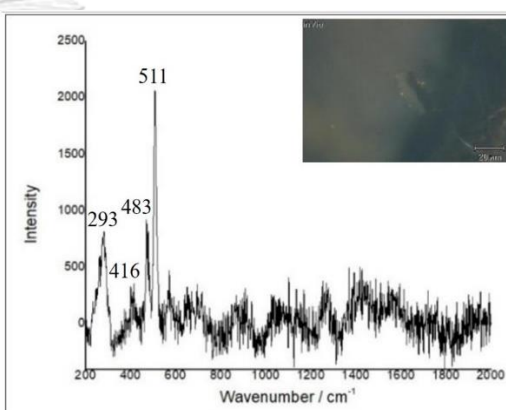


Figure A-223 Raman spectrum of a feldspar observed in the sample DN41

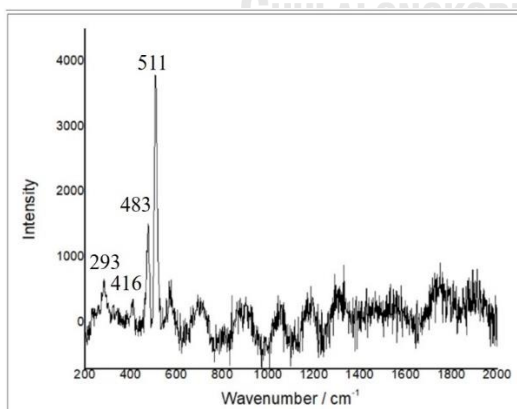


Figure A-224 Raman spectrum of a feldspar observed in the sample DN67

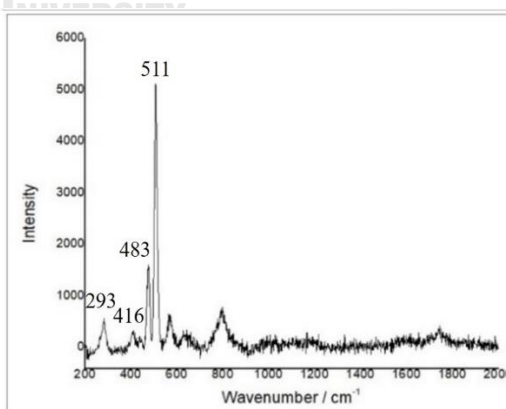


Figure A-225 Raman spectrum of a feldspar observed in the sample DN70

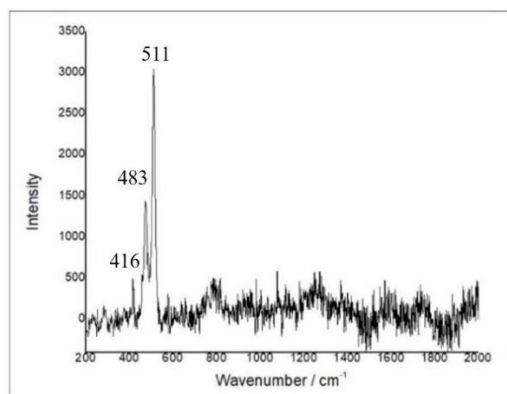


Figure A-226 Raman spectrum of a feldspar observed in the sample DN88

d. Wüstite

1) Binh Thuan area in Southern Vietnam

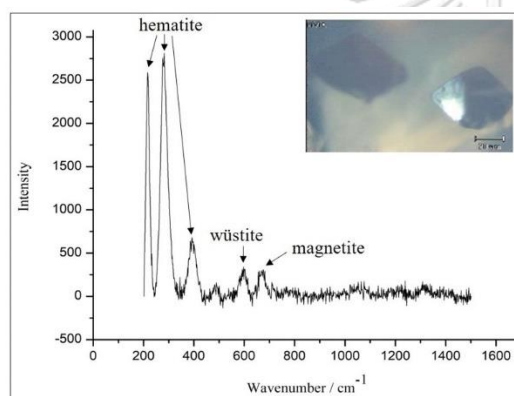


Figure A-227 Raman spectrum of a wüstite observed in the sample PT17

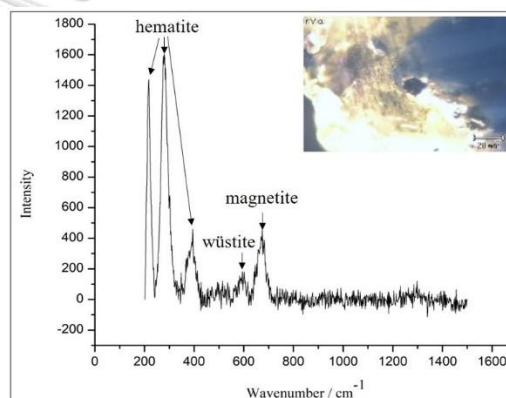


Figure A-228 Raman spectrum of a wüstite observed in the sample PT18

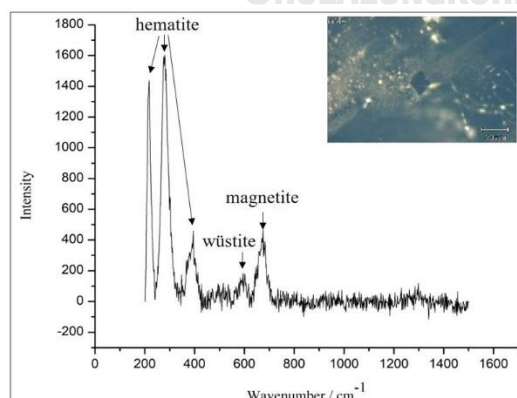


Figure A-229 Raman spectrum of a wüstite observed in the sample PT39

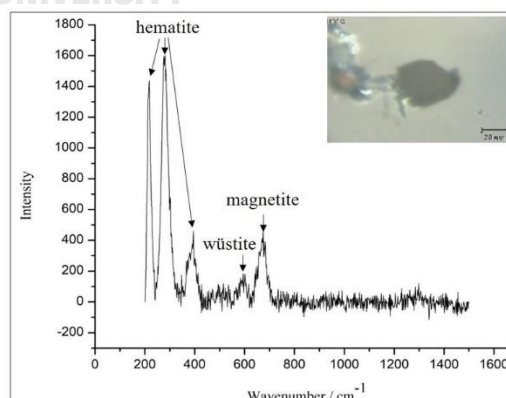


Figure A-230 Raman spectrum of a wüstite observed in the sample PT49

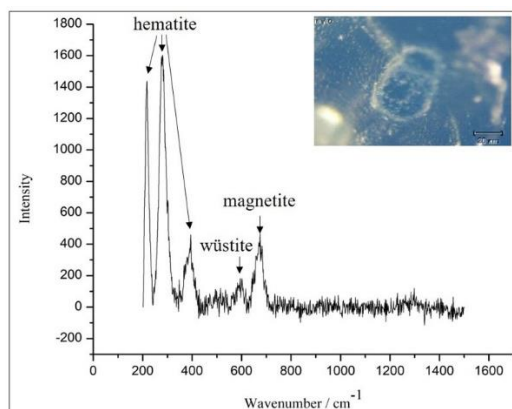


Figure A-231 Raman spectrum of a wüstite observed in the sample PT55

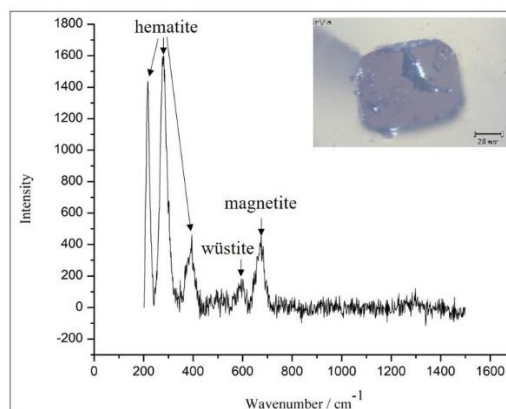


Figure A-232 Raman spectrum of a wüstite observed in the sample PT60

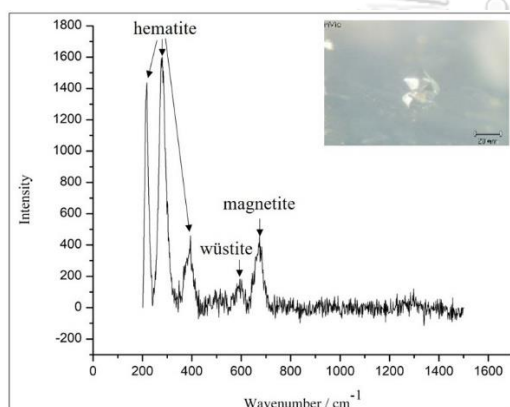


Figure A-233 Raman spectrum of a wüstite observed in the sample PT71

2) Di Linh area in Southern Vietnam

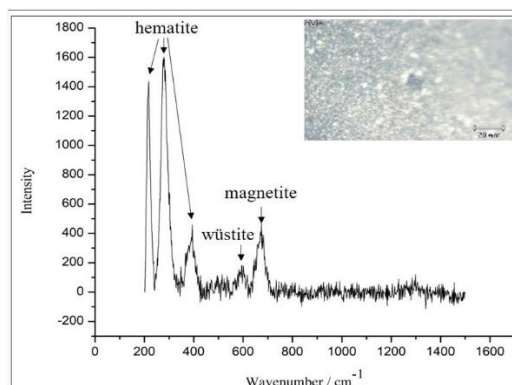


Figure A-234 Raman spectrum of a wüstite observed in the sample DL14

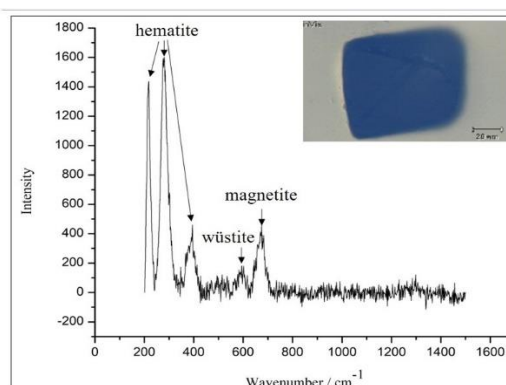


Figure A-235 Raman spectrum of a wüstite observed in the sample DL24

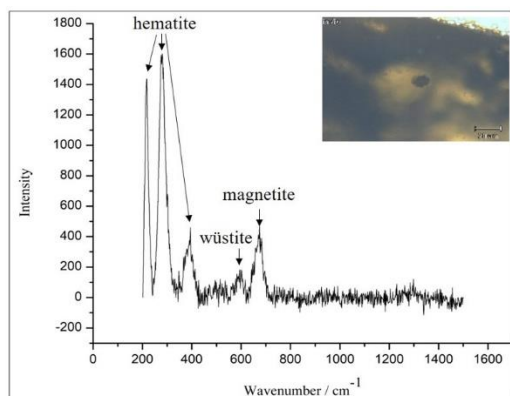


Figure A-236 Raman spectrum of a wüstite observed in the sample DL49

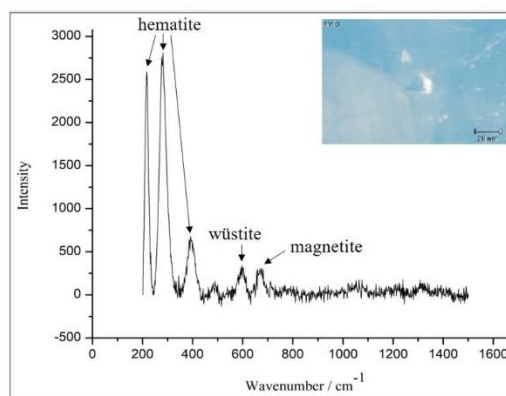


Figure A-237 Raman spectrum of a wüstite observed in the sample DL50

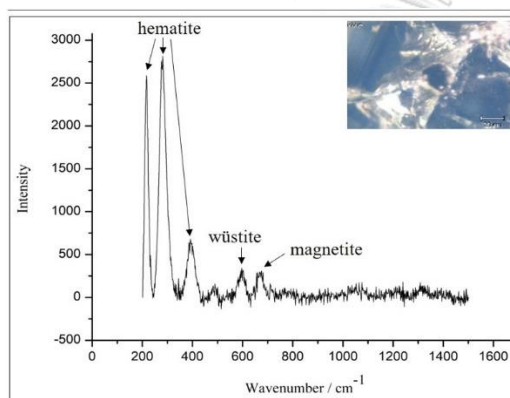


Figure A-238 Raman spectrum of a wüstite observed in the sample DL56

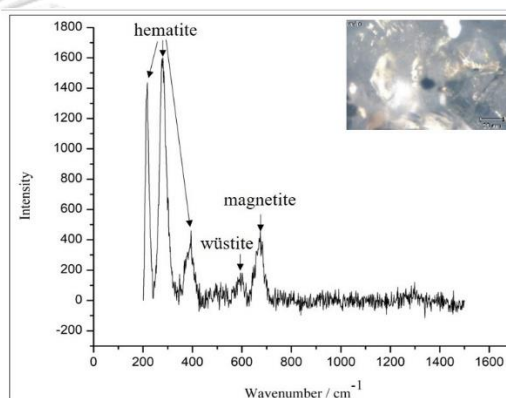


Figure A-239 Raman spectrum of a wüstite observed in the sample DL63

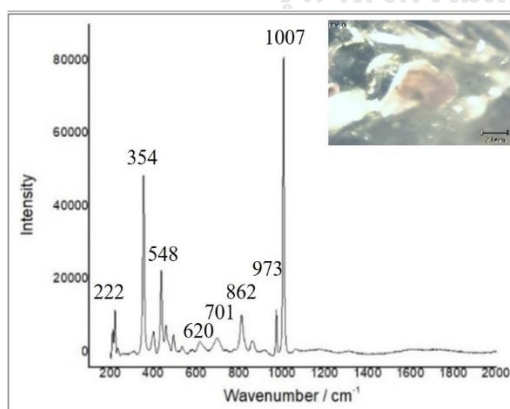


Figure A-240 Raman spectrum of a wüstite observed in the sample DL83

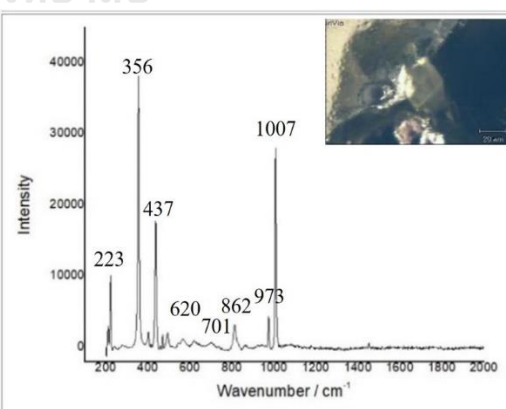


Figure A-241 Raman spectrum of a wüstite observed in the sample DL84

3) Krong Nang area in Southern Vietnam

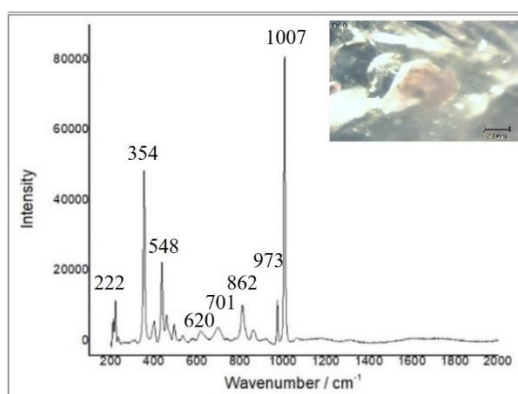


Figure A-242 Raman spectrum of a wüstite observed in the sample KN05

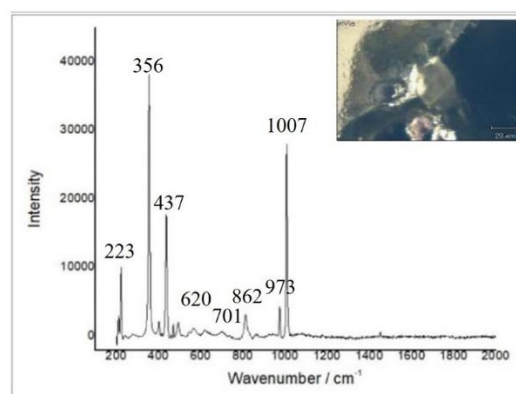


Figure A-243 Raman spectrum of a wüstite observed in the sample KN19

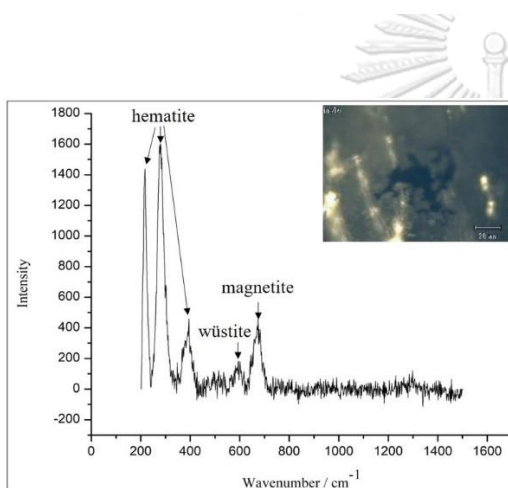


Figure A-244 Raman spectrum of a wüstite observed in the sample KN20

4) Dak Nong area in Southern Vietnam

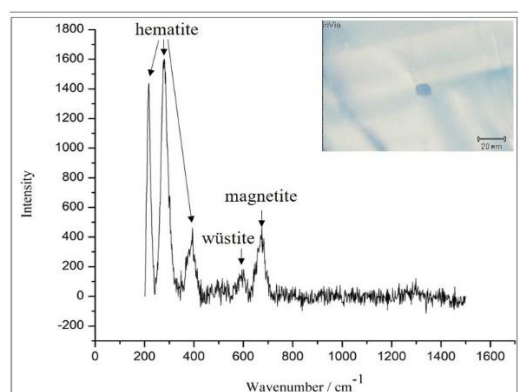


Figure A-245 Raman spectrum of a wüstite observed in the sample DN73

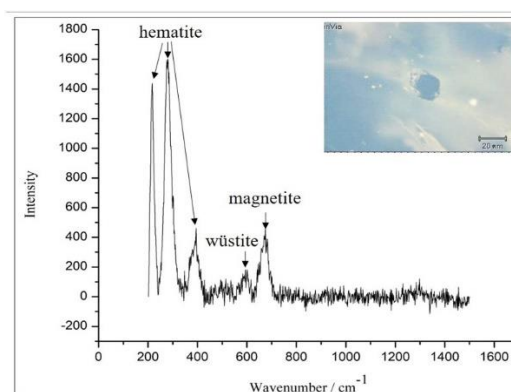


Figure A-246 Raman spectrum of a wüstite observed in the sample DN74

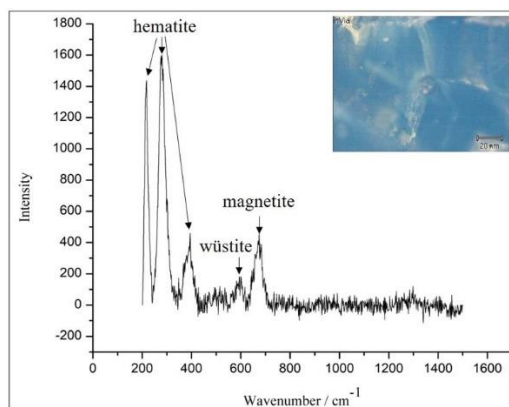


Figure A-247 Raman spectrum of a wüstite observed in the sample DN89

5) Pleiku area in Southern Vietnam

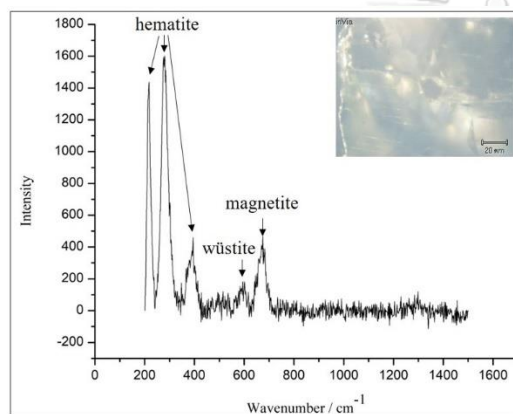


Figure A-248 Raman spectrum of a wüstite observed in the sample GL27

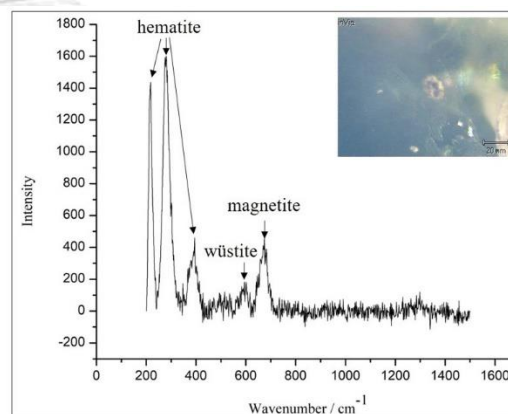


Figure A-249 Raman spectrum of a wüstite observed in the sample GL85

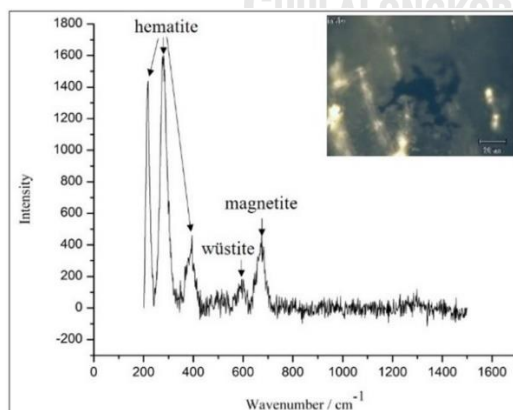


Figure A-250 Raman spectrum of a wüstite observed in the sample GL87

e. Spinel

1) Binh Thuan area in Southern Vietnam

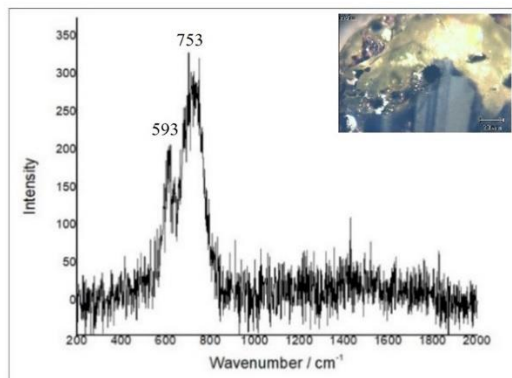


Figure A-251 Raman spectrum of a hercynite spinel observed in the sample PT07

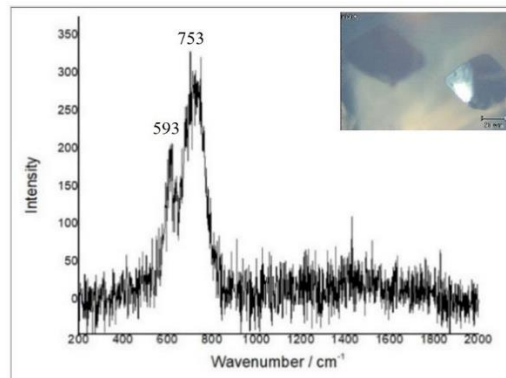


Figure A-252 Raman spectrum of a hercynite spinel observed in the sample PT17

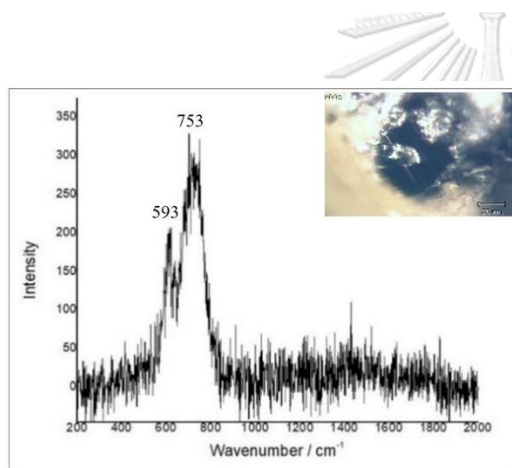


Figure A-253 Raman spectrum of a hercynite spinel observed in the sample PT22

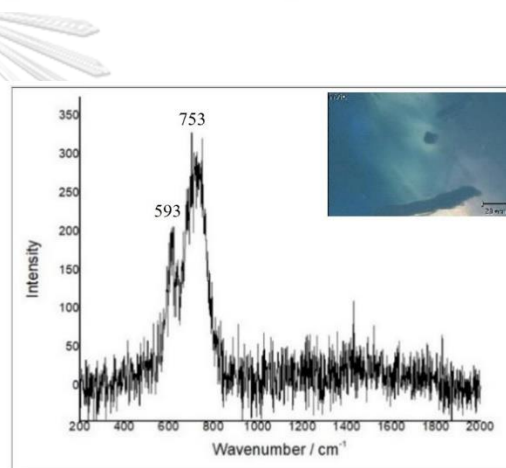


Figure A-254 Raman spectrum of a hercynite spinel observed in the sample PT34

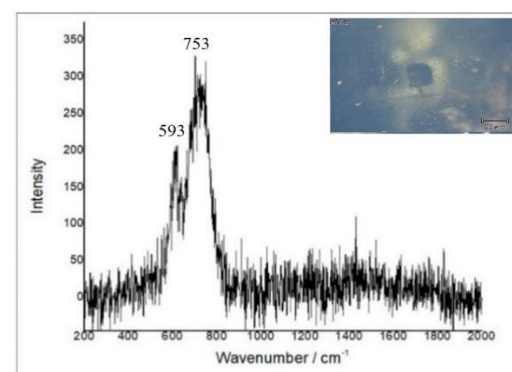


Figure A-255 Raman spectrum of a hercynite spinel observed in the sample PT46

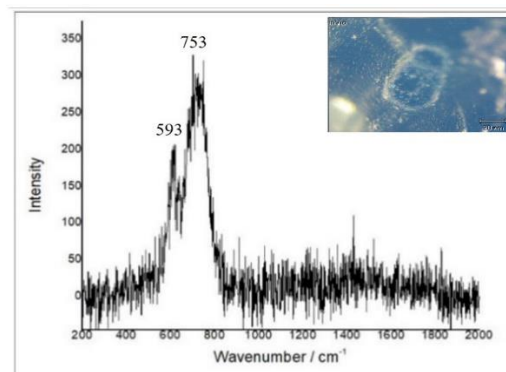


Figure A-256 Raman spectrum of a hercynite spinel observed in the sample PT55

2) Di Linh area in Southern Vietnam

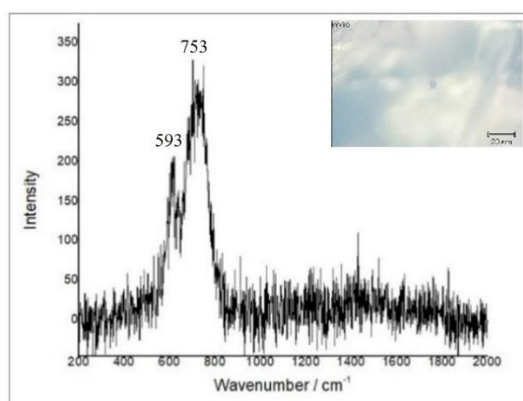


Figure A-257 Raman spectrum of a hercynite spinel observed in the sample DL62

3) Krong Nang area in Southern Vietnam

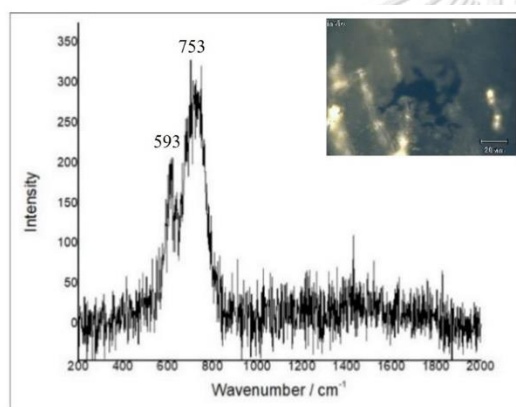


Figure A-258 Raman spectrum of a hercynite spinel observed in the sample KN20

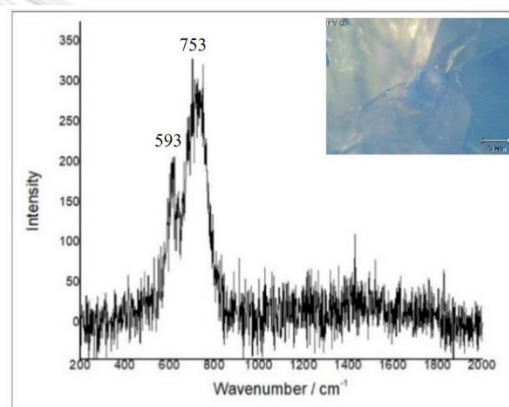


Figure A-259 Raman spectrum of a hercynite spinel observed in the sample KN42

CHULALONGKORN UNIVERSITY

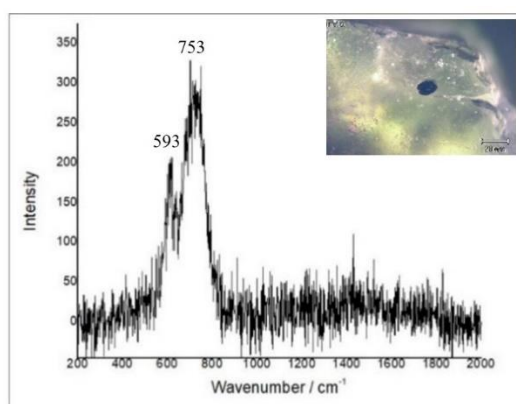


Figure A-260 Raman spectrum of a hercynite spinel observed in the sample KN43

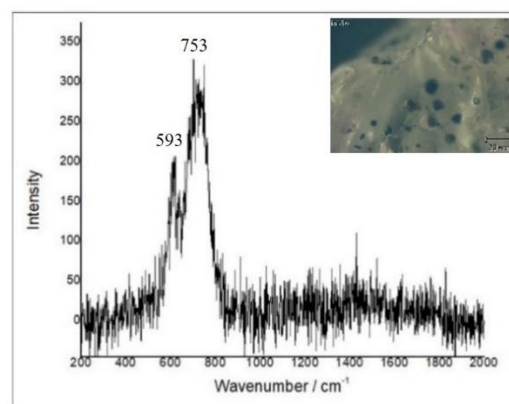


Figure A-261 Raman spectrum of a hercynite spinel observed in the sample KN47

4) Dak Nong area in Southern Vietnam

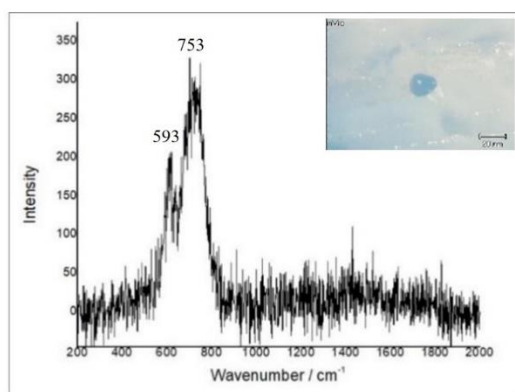


Figure A-262 Raman spectrum of a hercynite spinel observed in the sample DN12

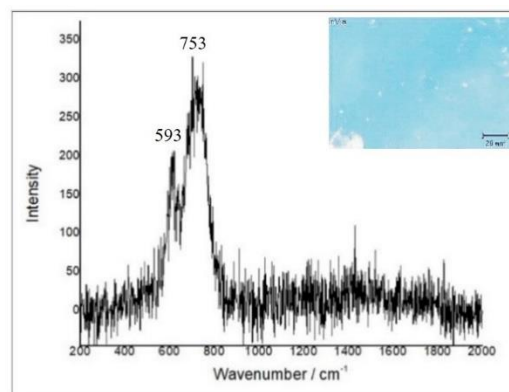


Figure A-263 Raman spectrum of a hercynite spinel observed in the sample DN16

5) Pleiku area in Southern Vietnam

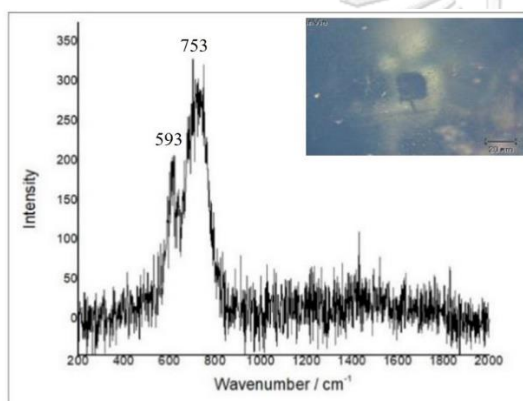


Figure A-264 Raman spectrum of a hercynite spinel observed in the sample GL07

f. Ilmenite

1) Di Linh area in Southern Vietnam

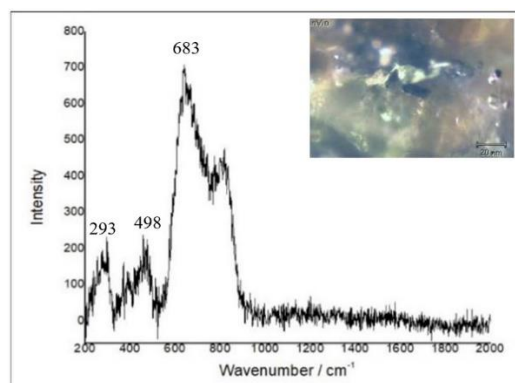


Figure A-265 Raman spectrum of an ilmenite observed in the sample DL23

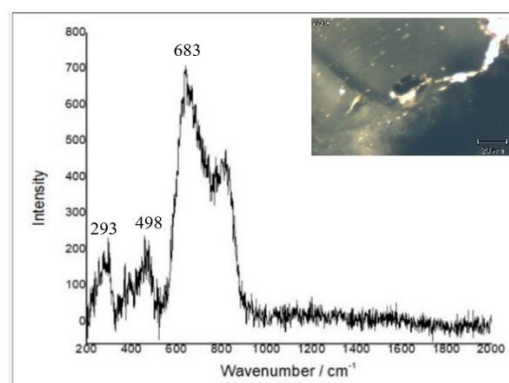


Figure A-266 Raman spectrum of an ilmenite observed in the sample DL85

2) Dak Nong area in Southern Vietnam

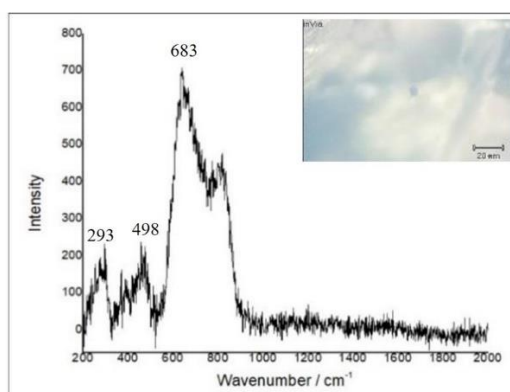


Figure A-267 Raman spectrum of an ilmenite observed in the sample DN39

3) Pleiku area in Southern Vietnam

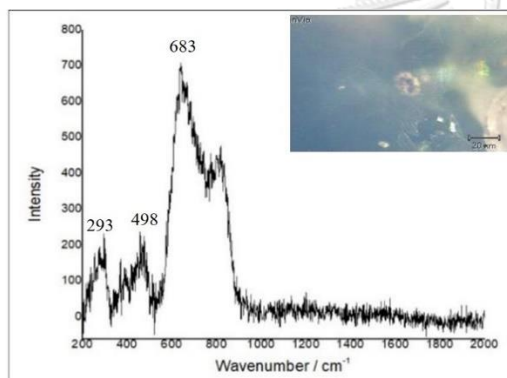


Figure A-268 Raman spectrum of an ilmenite observed in the sample GL23

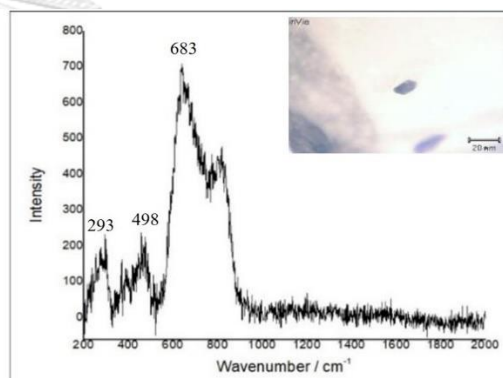


Figure A-269 Raman spectrum of an ilmenite observed in the sample GL28

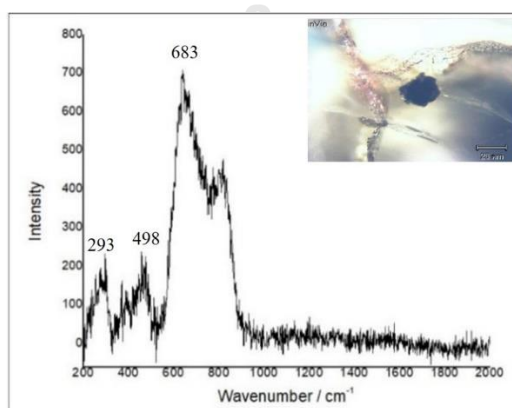


Figure A-270 Raman spectrum of an ilmenite observed in the sample GL86

g. Pyrochlore

1) Krong Nang area in Southern Vietnam

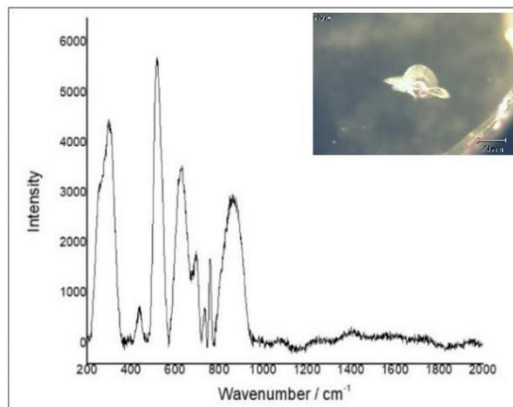


Figure A-271 Raman spectrum of a pyrochlore observed in the sample KN18

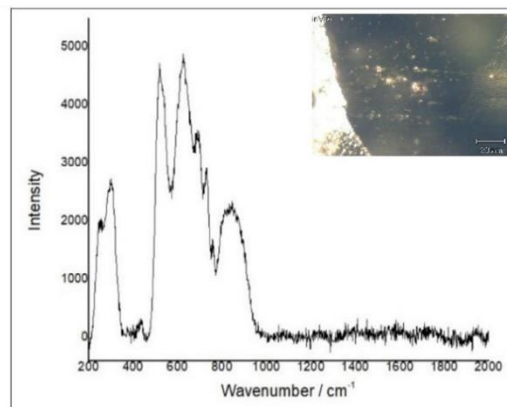


Figure A-272 Raman spectrum of a pyrochlore observed in the sample KN36

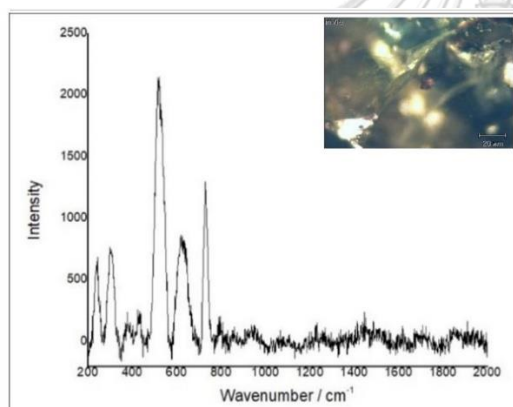


Figure A-273 Raman spectrum of a pyrochlore observed in the sample DN35

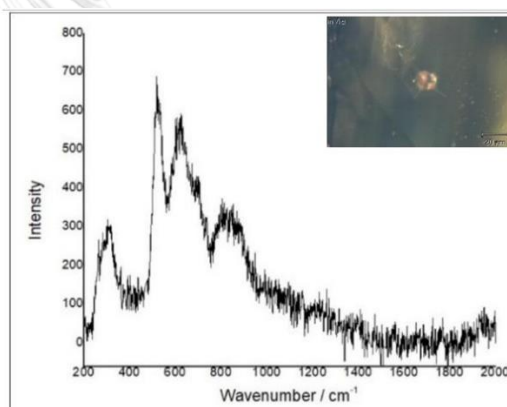
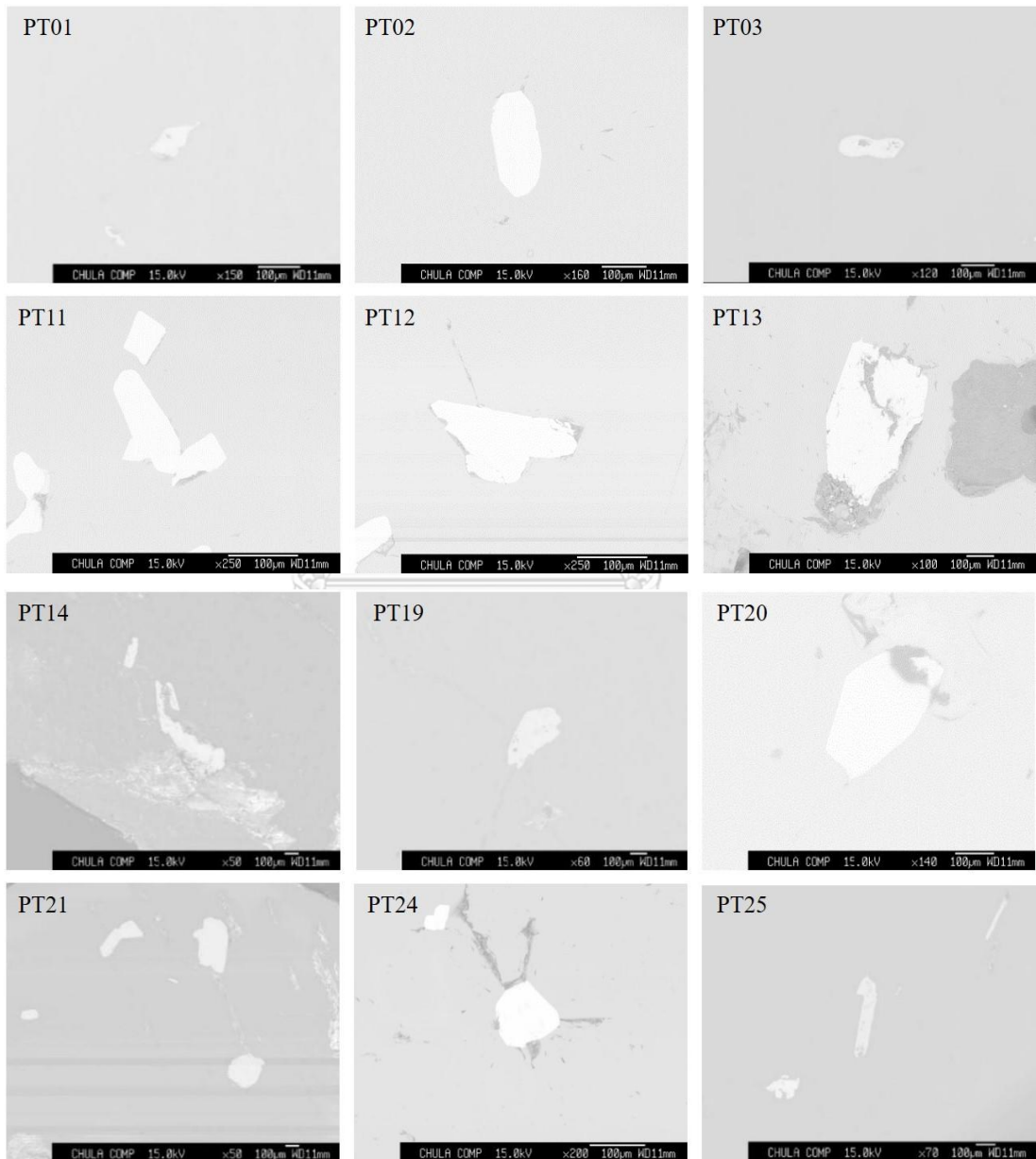


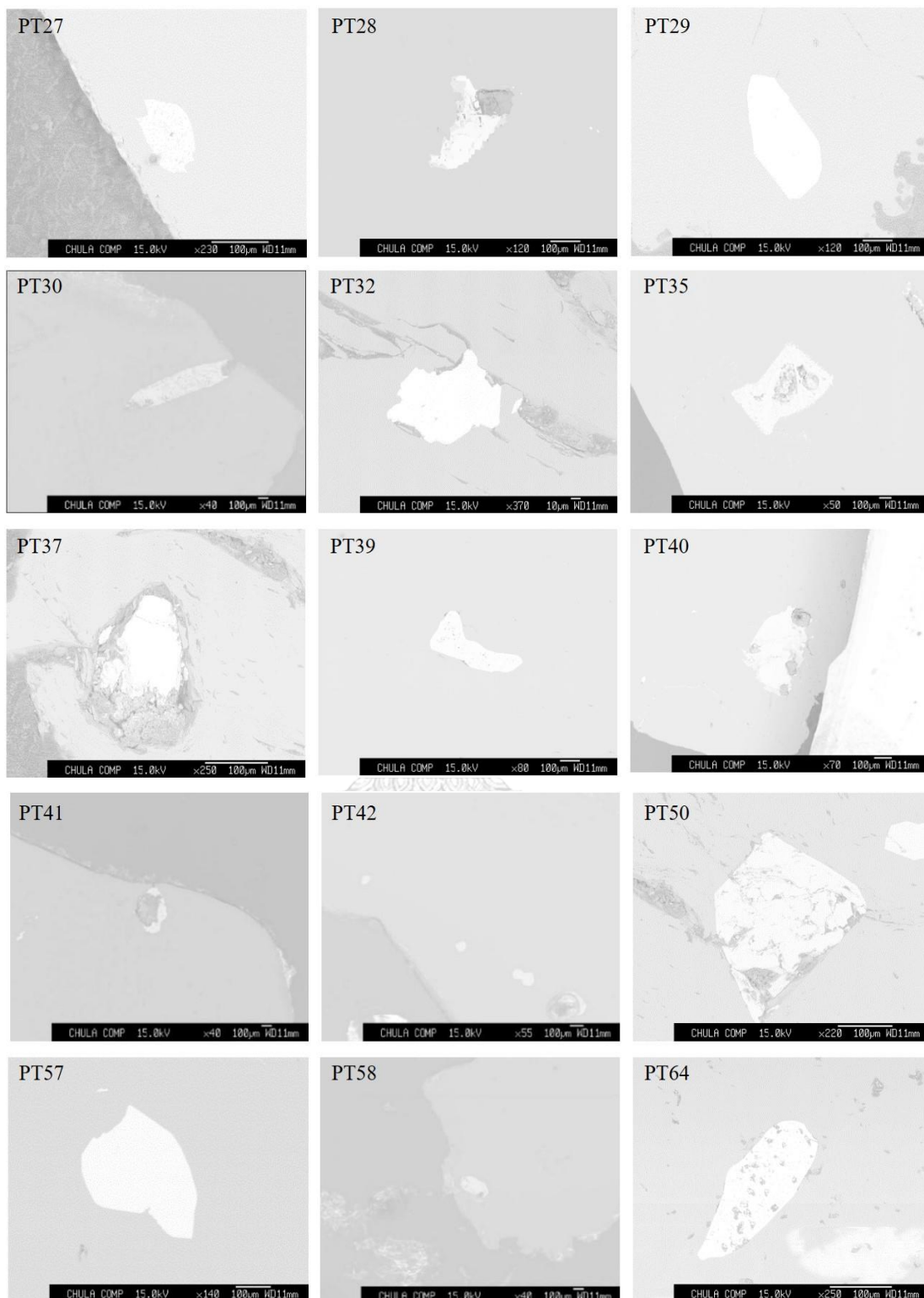
Figure A-274 Raman spectrum of a pyrochlore observed in the sample DN42

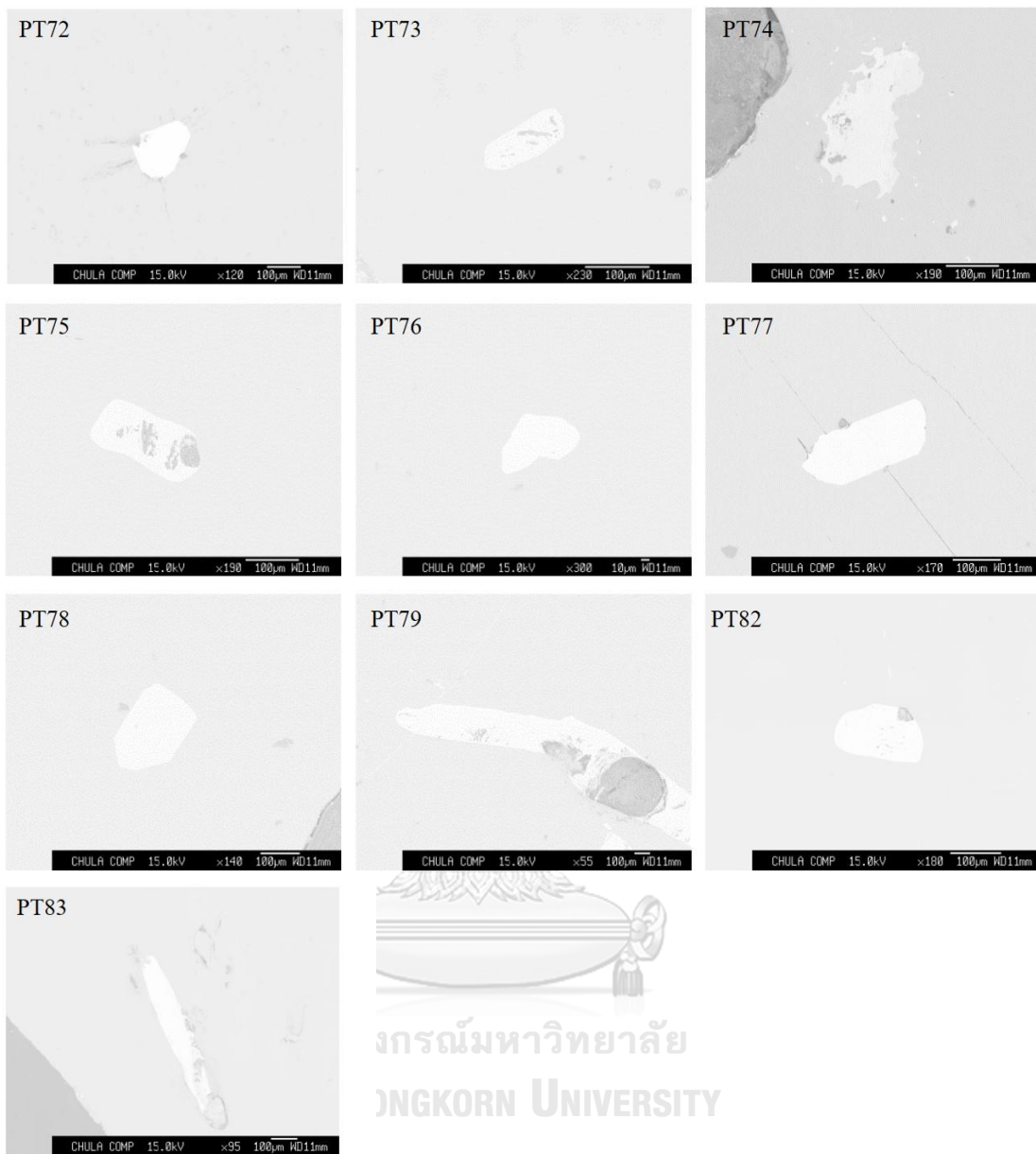
APPENDIX B
BACK SCATTERED ELECTRON (BSE) IMAGES OF MINERAL
INCLUSIONS

a. Columbite

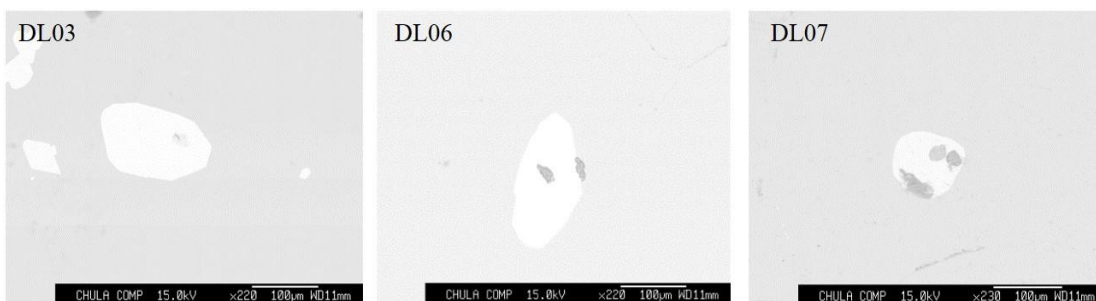
1) Binh Thuan area in Southern Vietnam

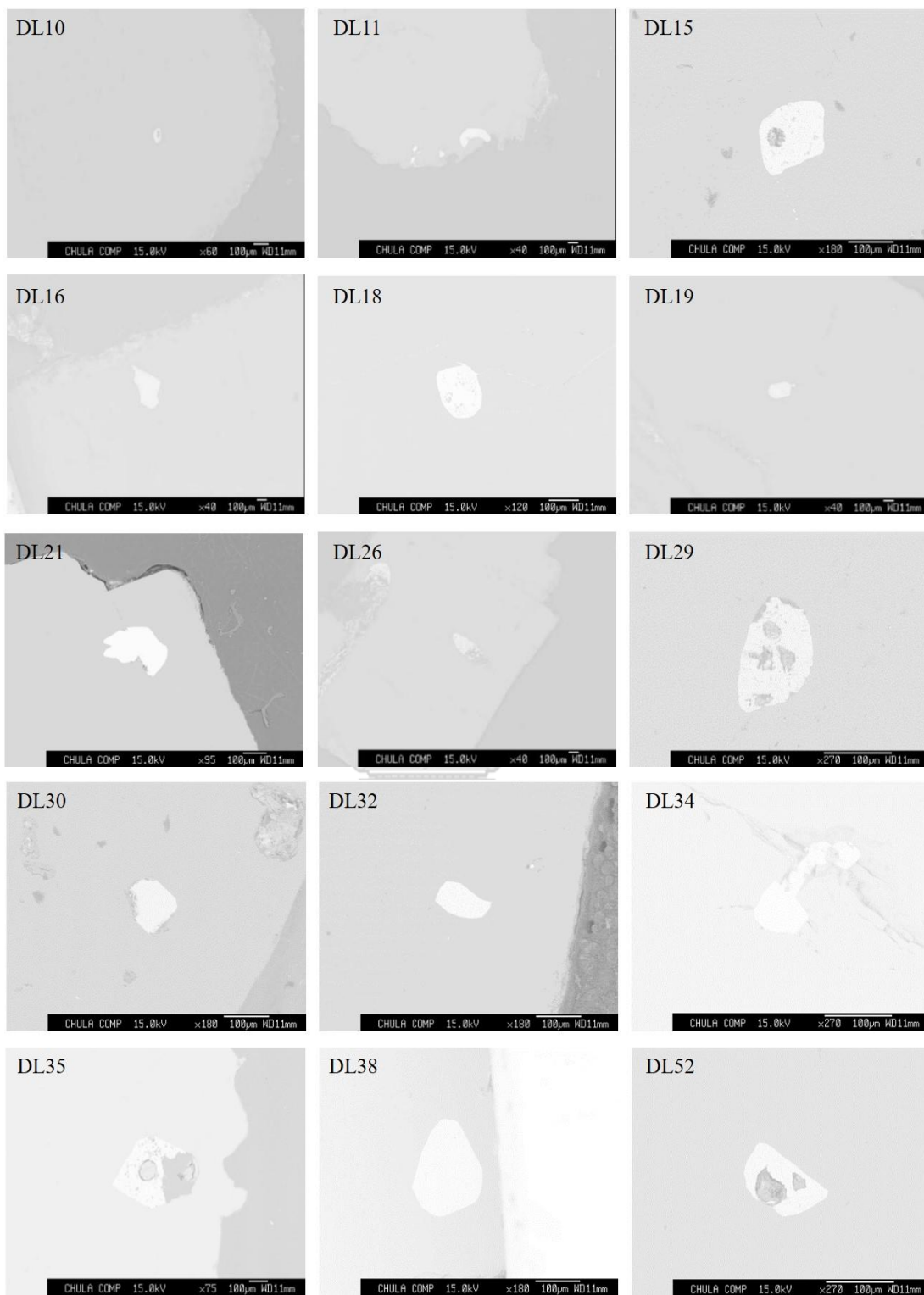


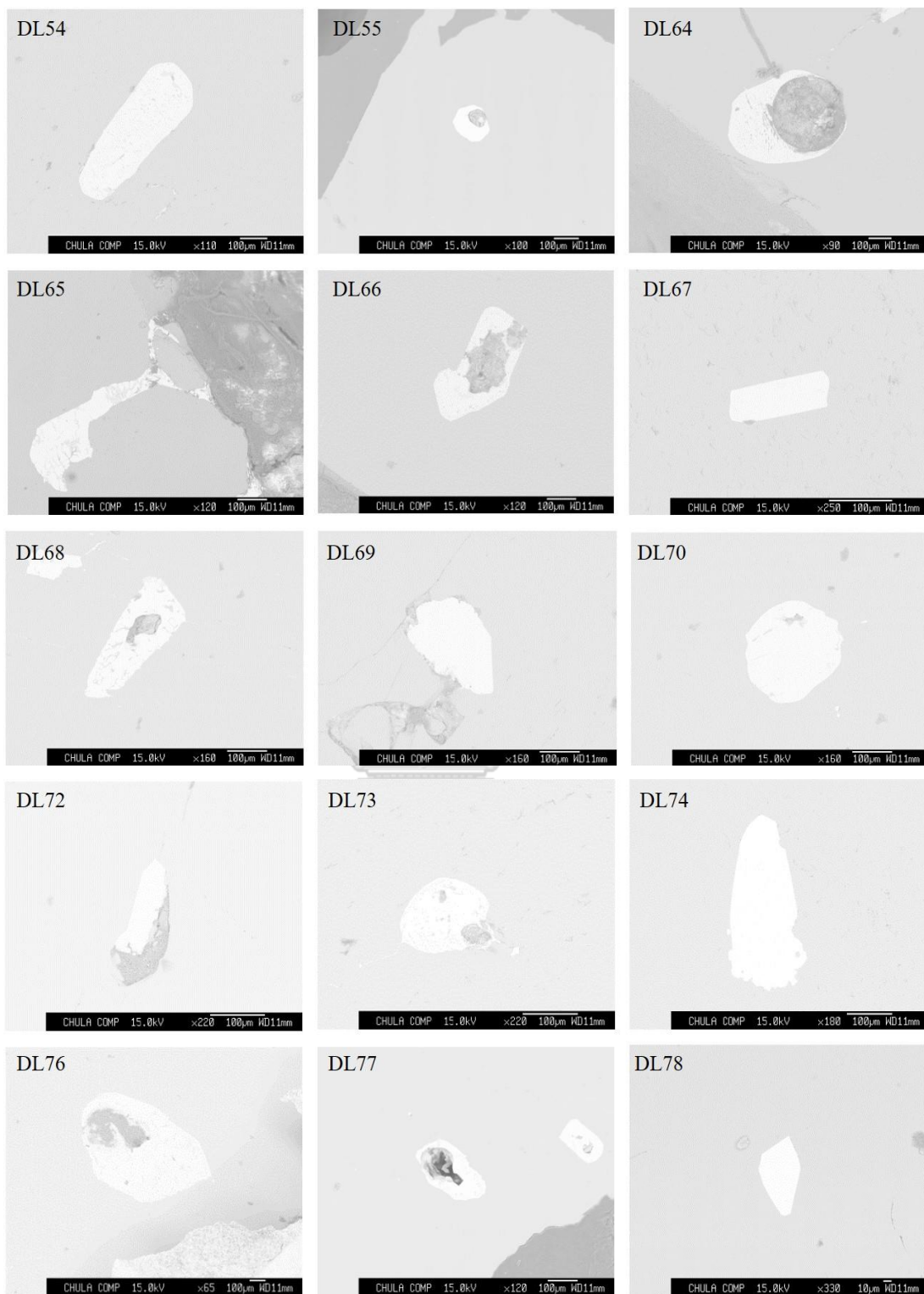


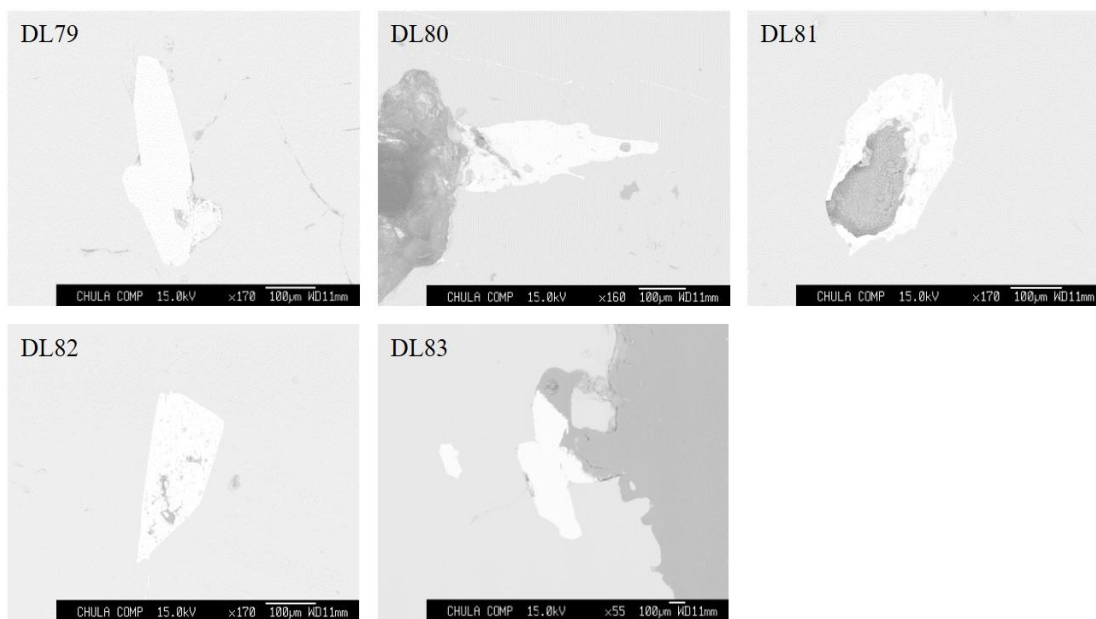


2) Di Linh area in Southern Vietnam

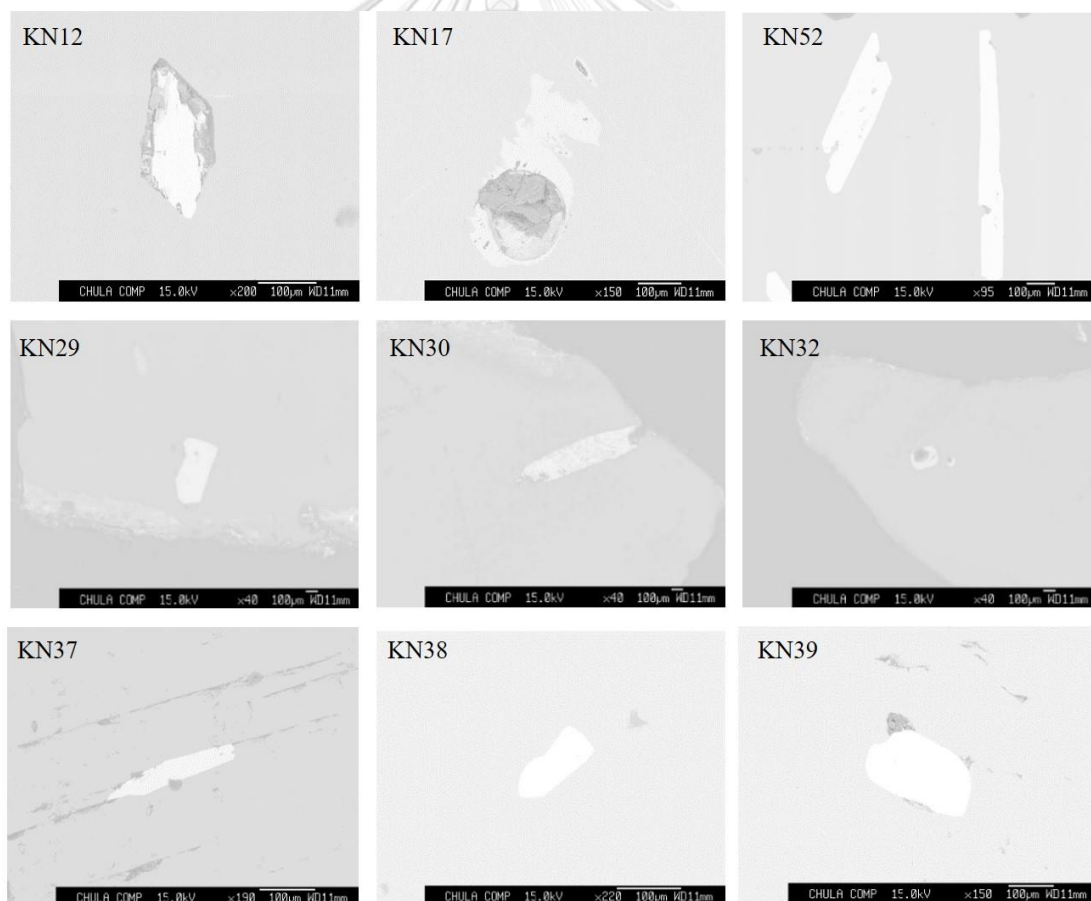


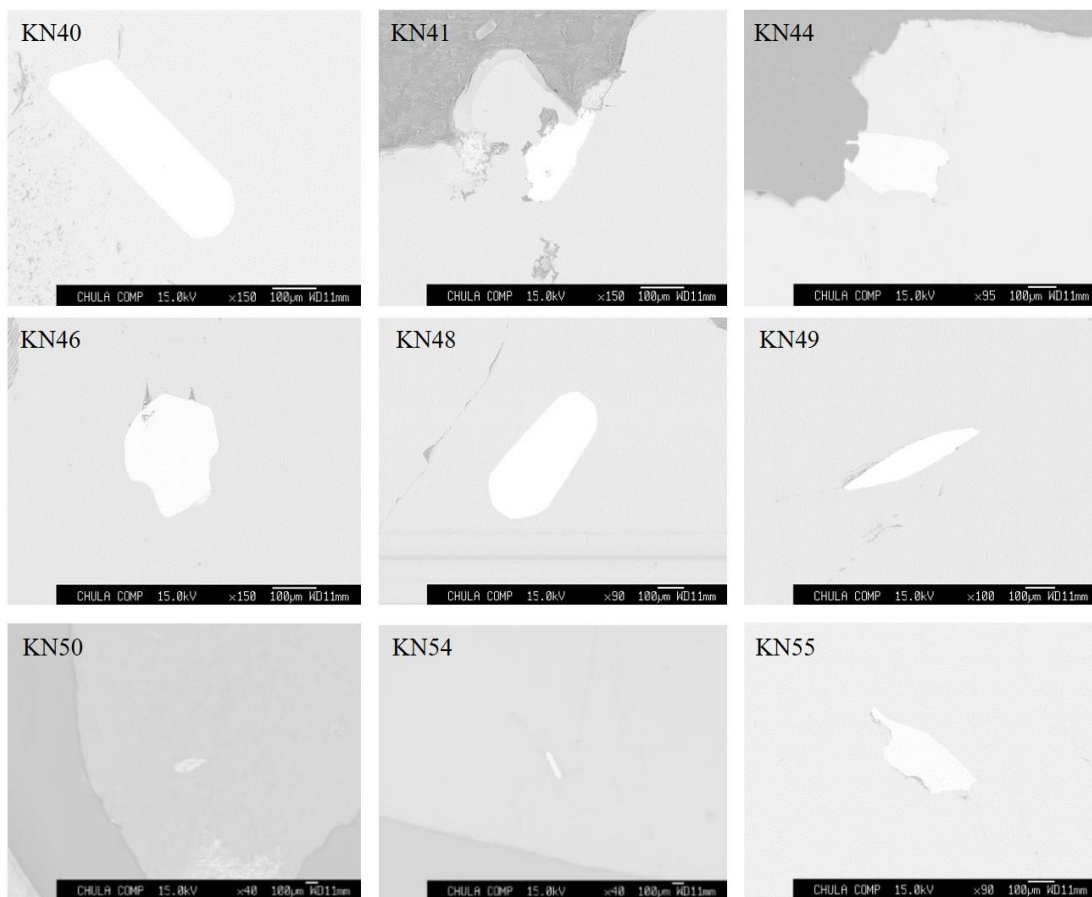




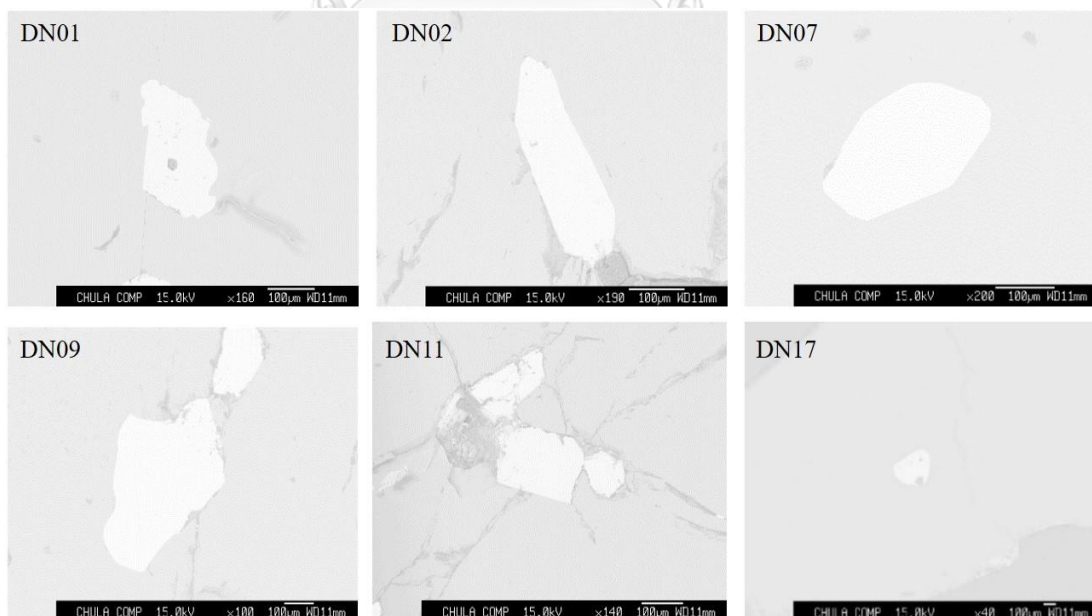


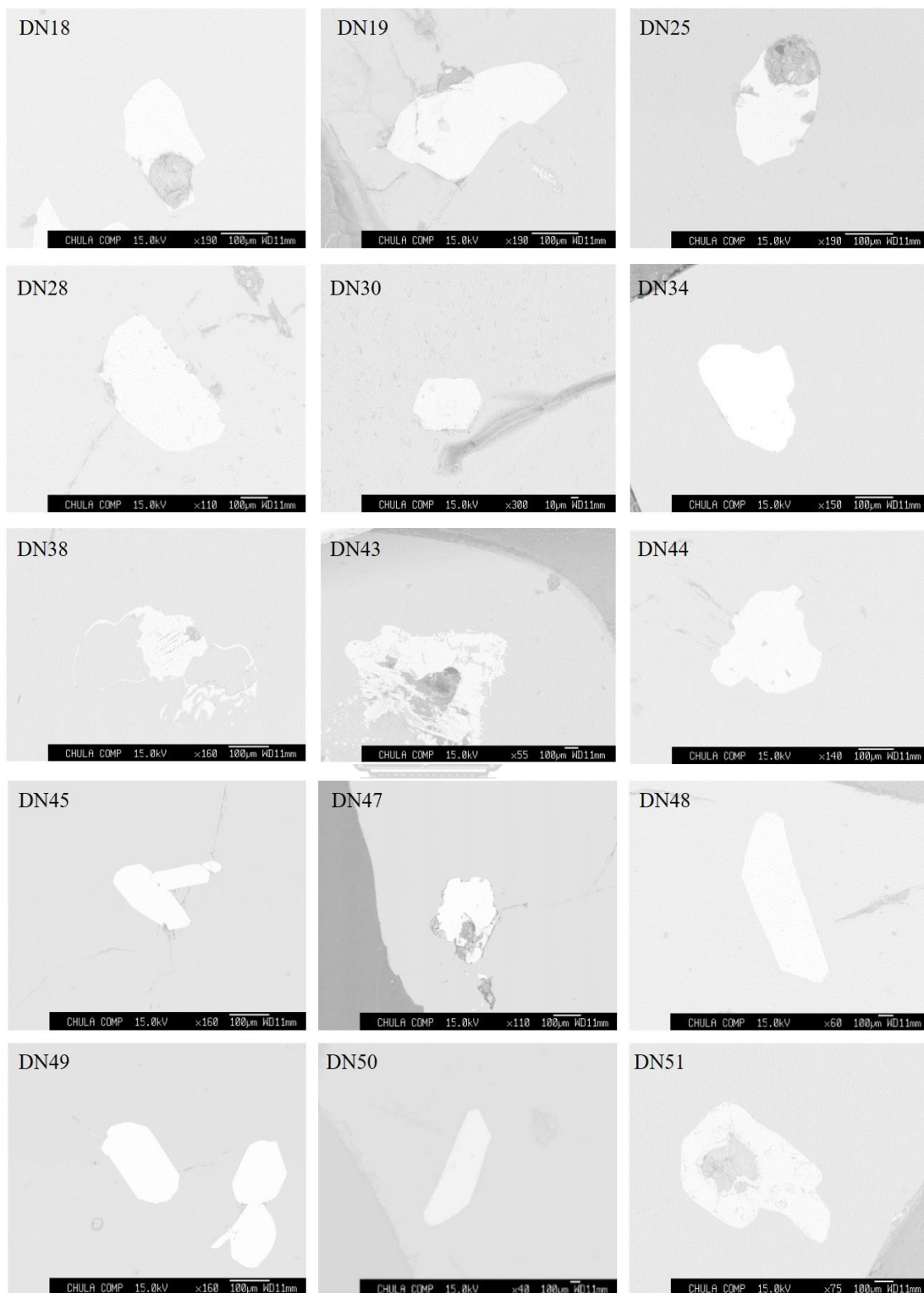
3) Krong Nang area in Southern Vietnam

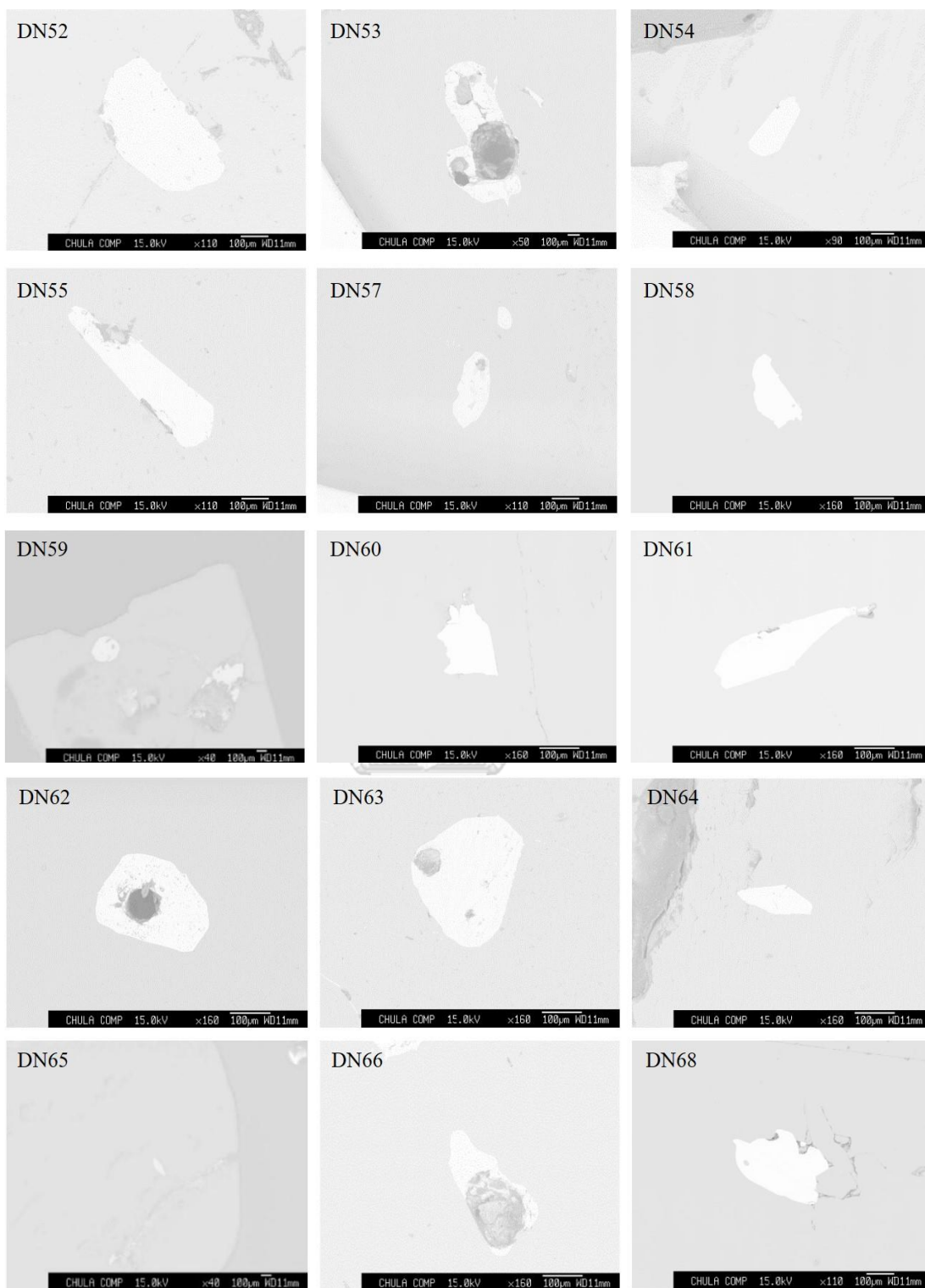


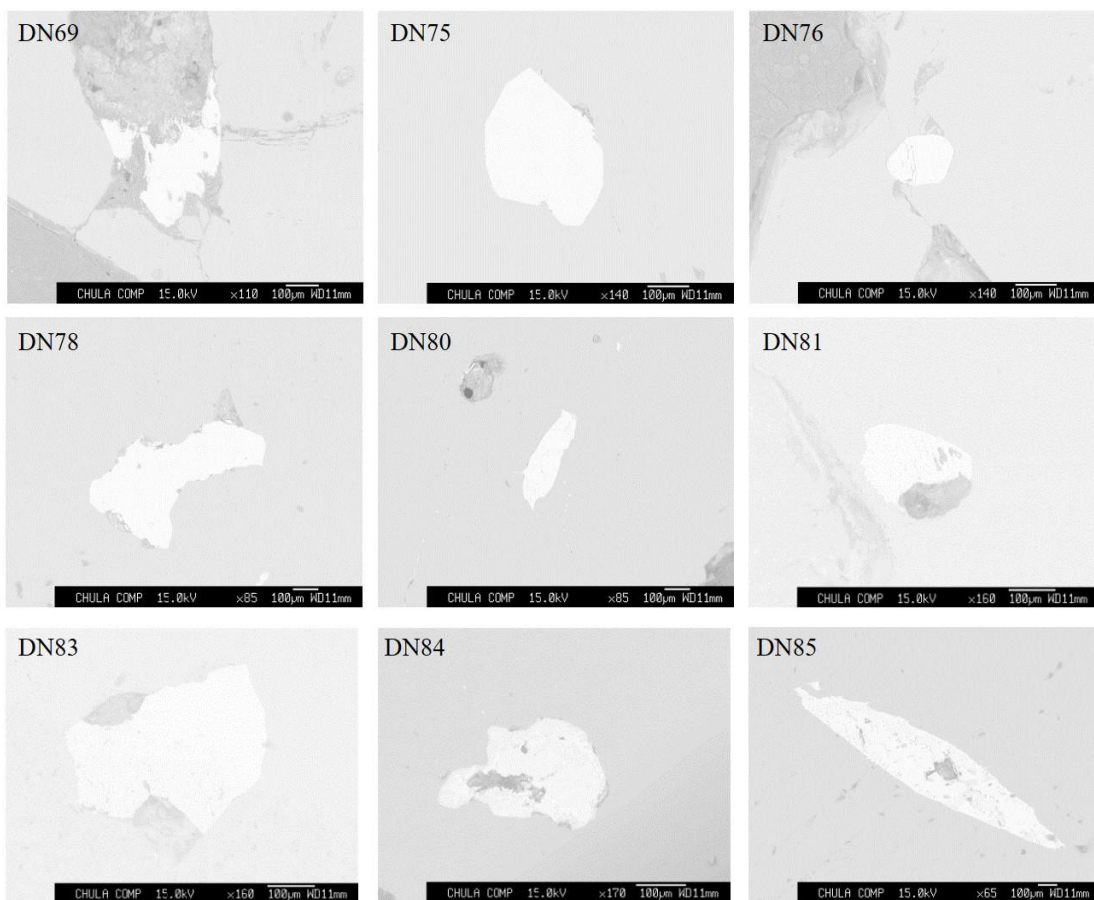


4) Dak Nong area in Southern Vietnam



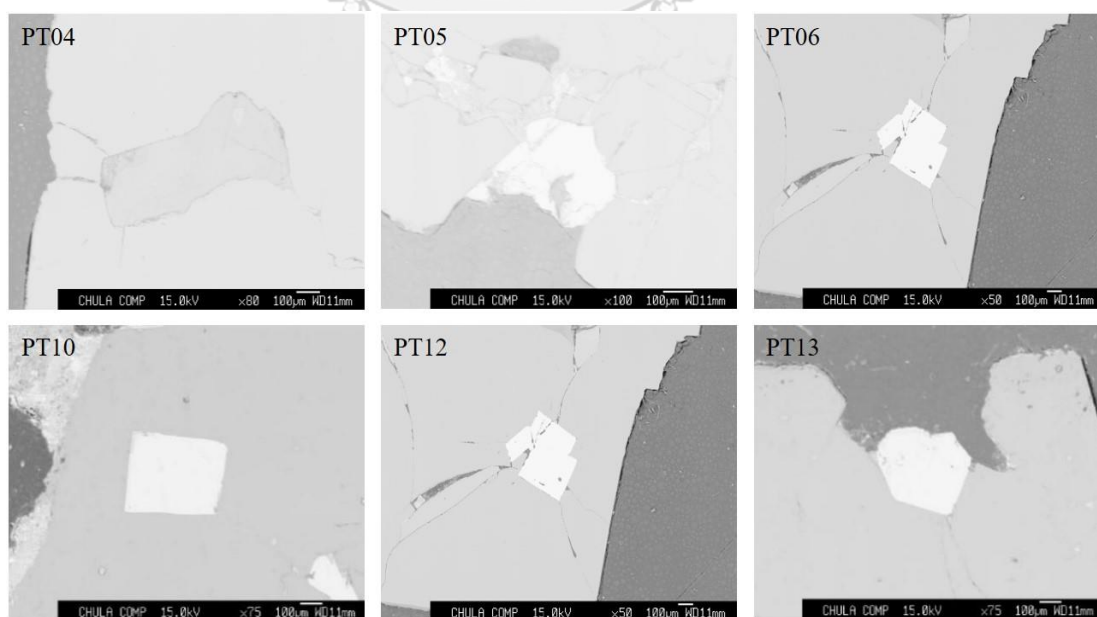


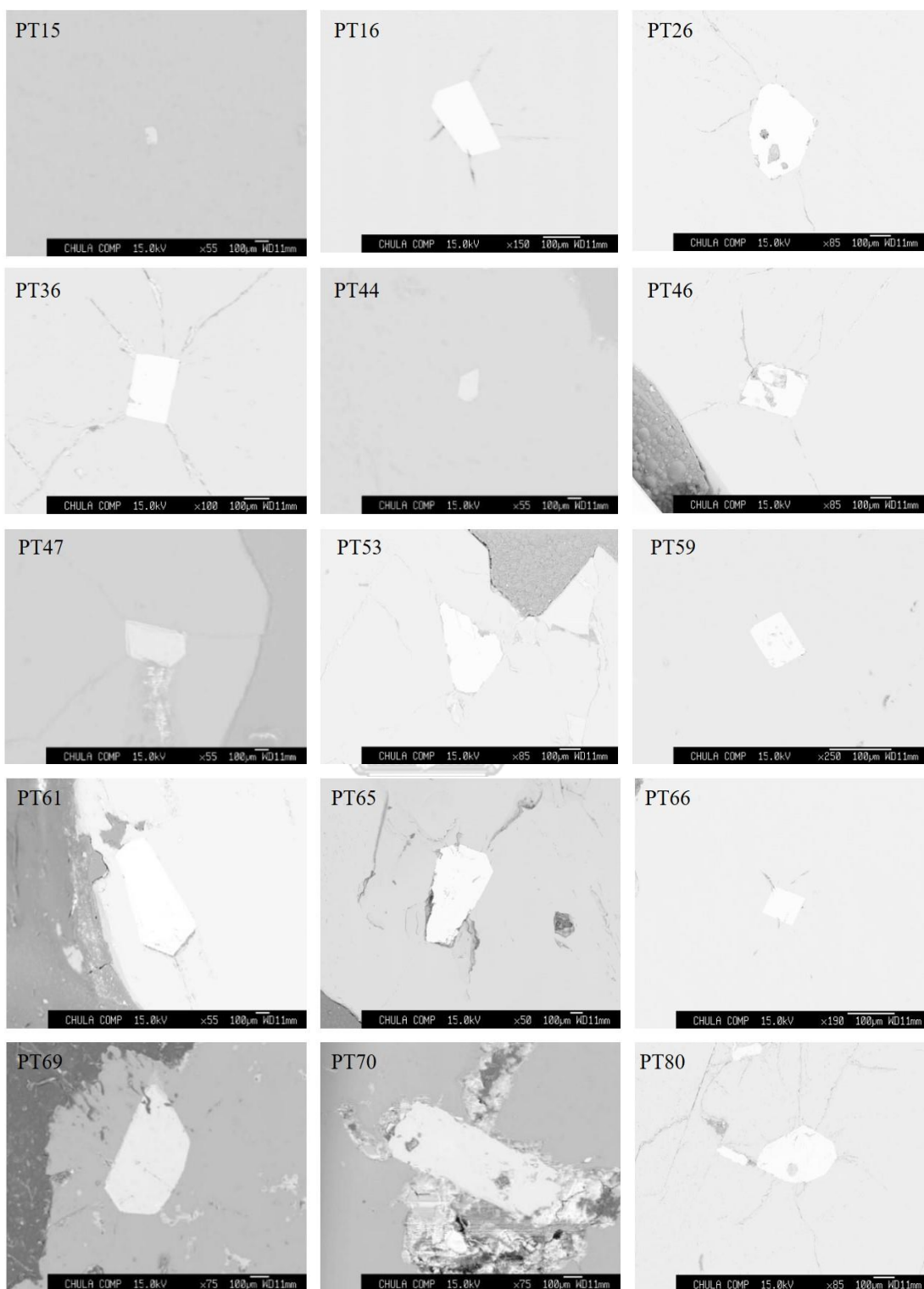




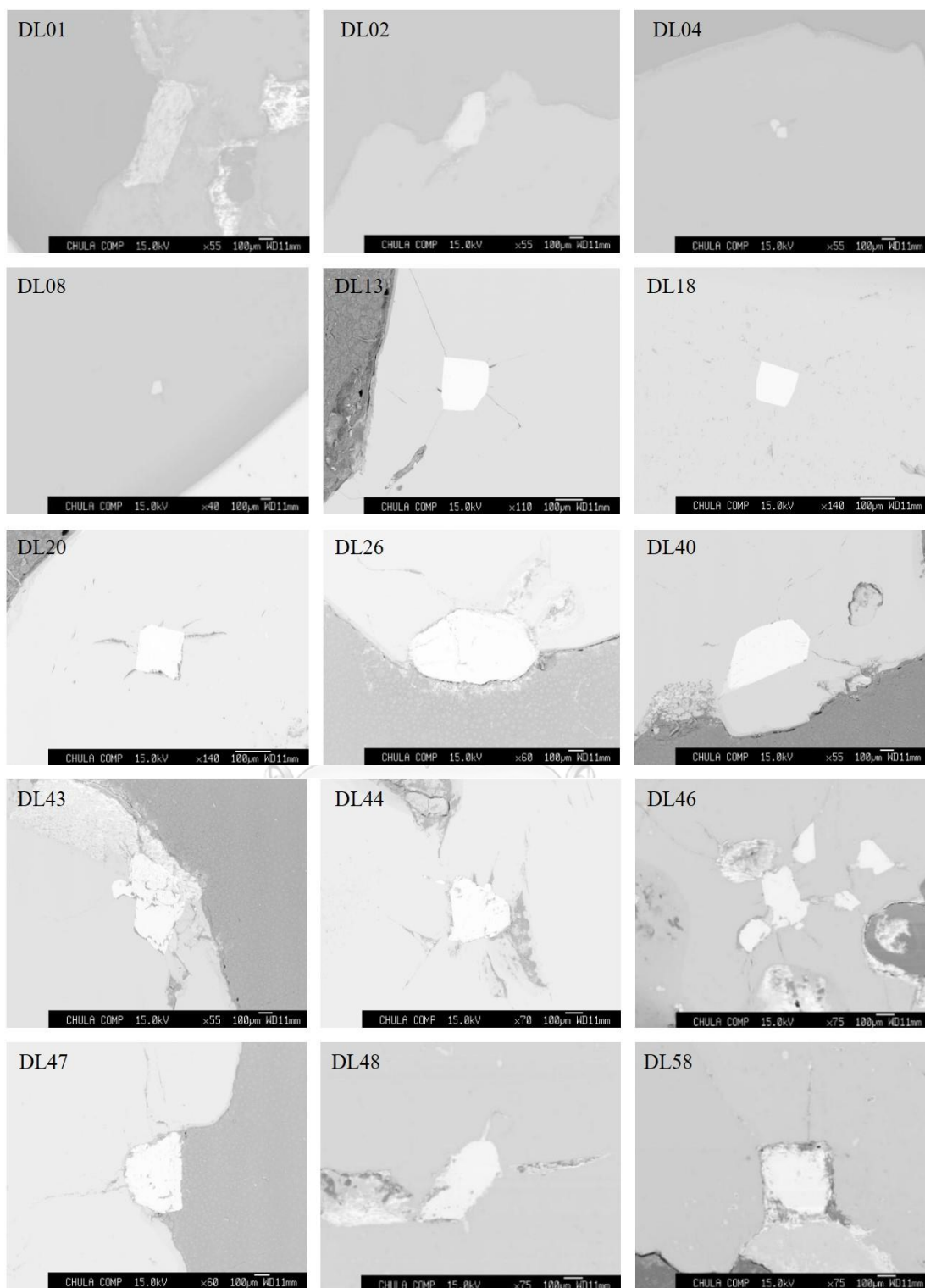
b. Zircon

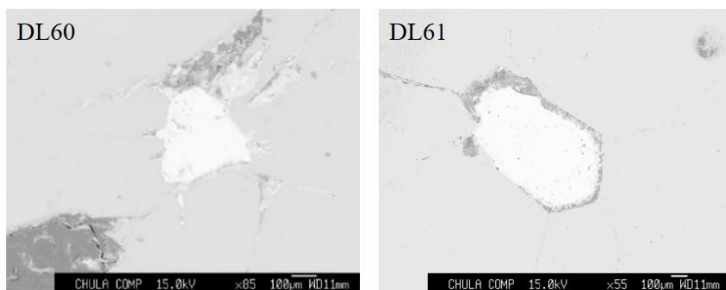
1) Binh Thuan area in Southern Vietnam



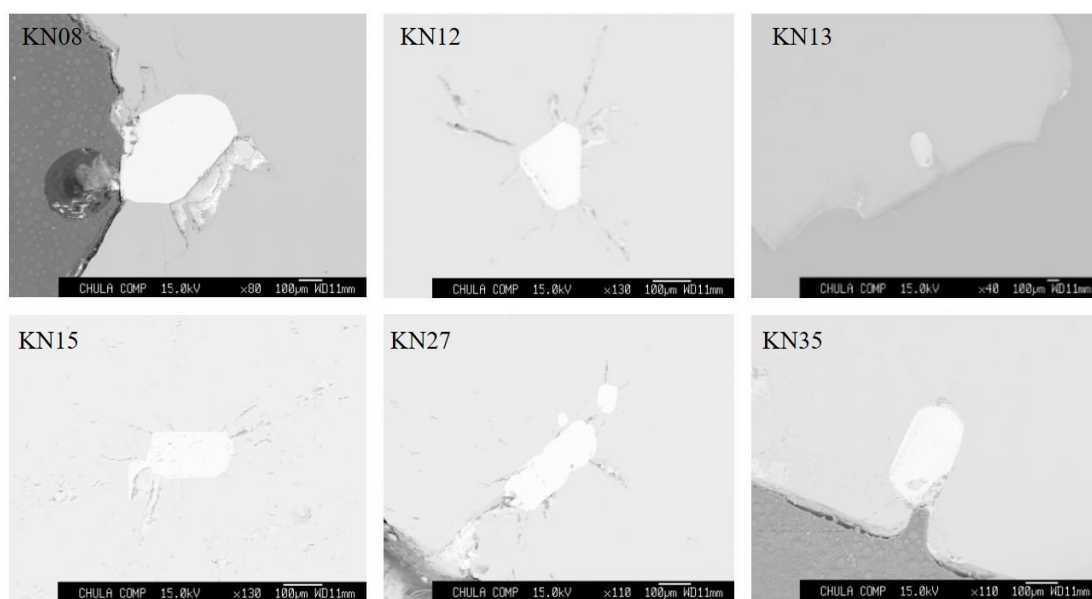


2) Di Linh area in Southern Vietnam

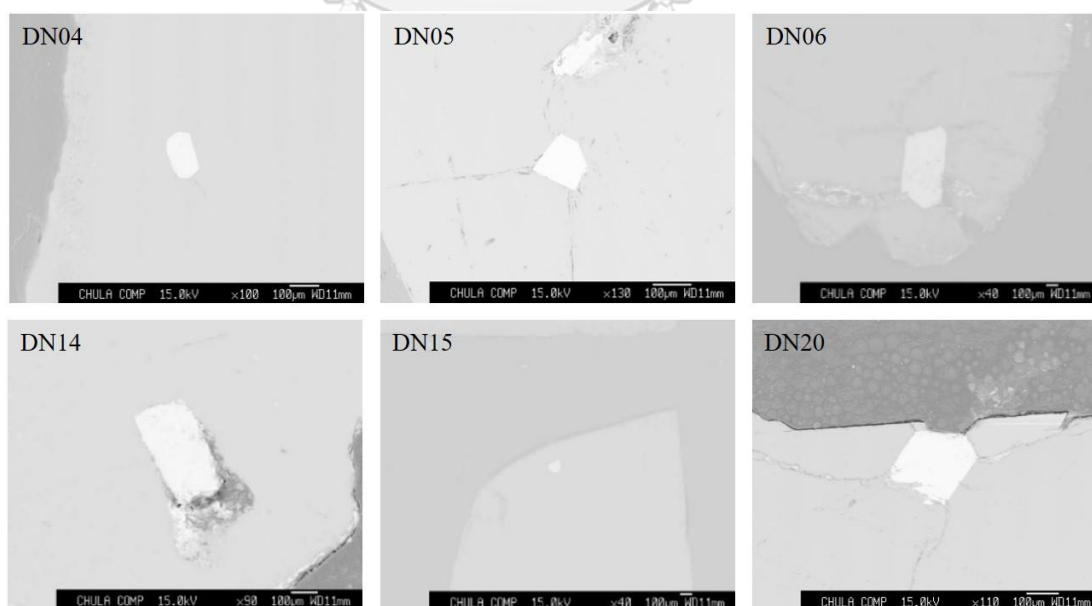


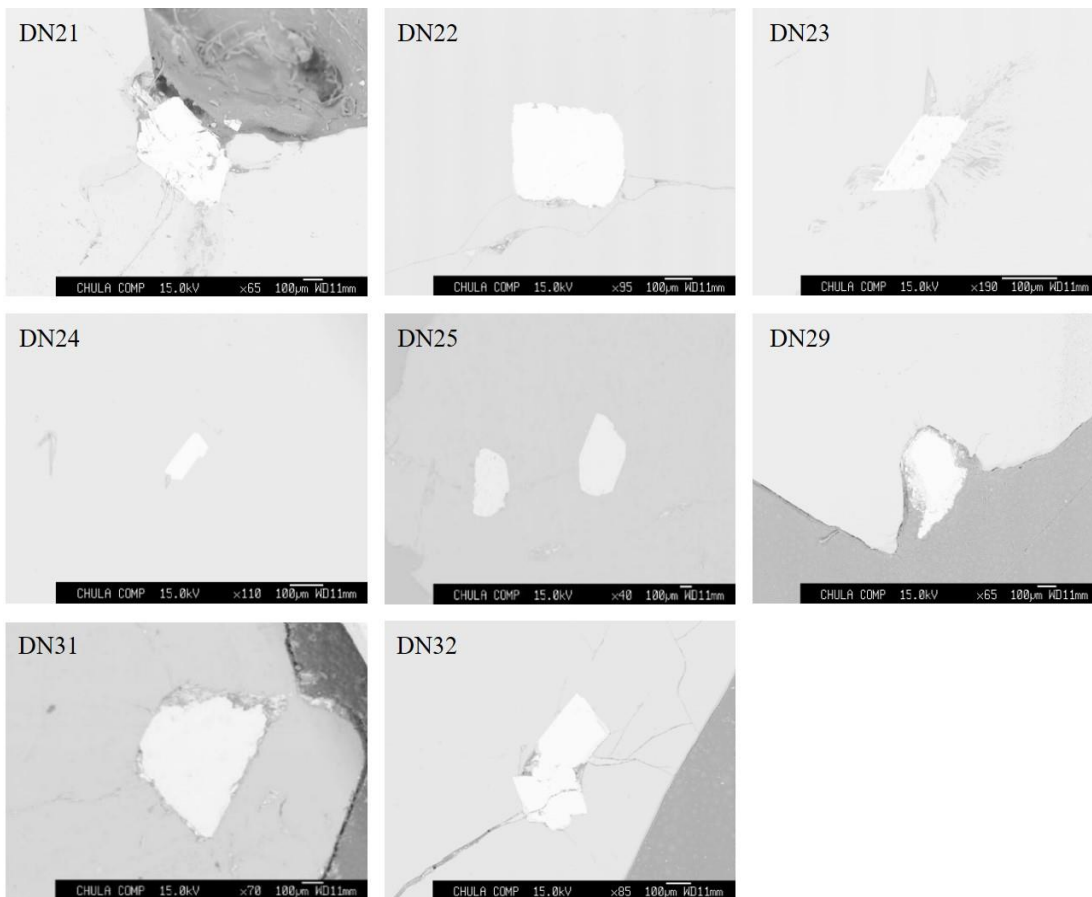


3) Krong Nang area in Southern Vietnam



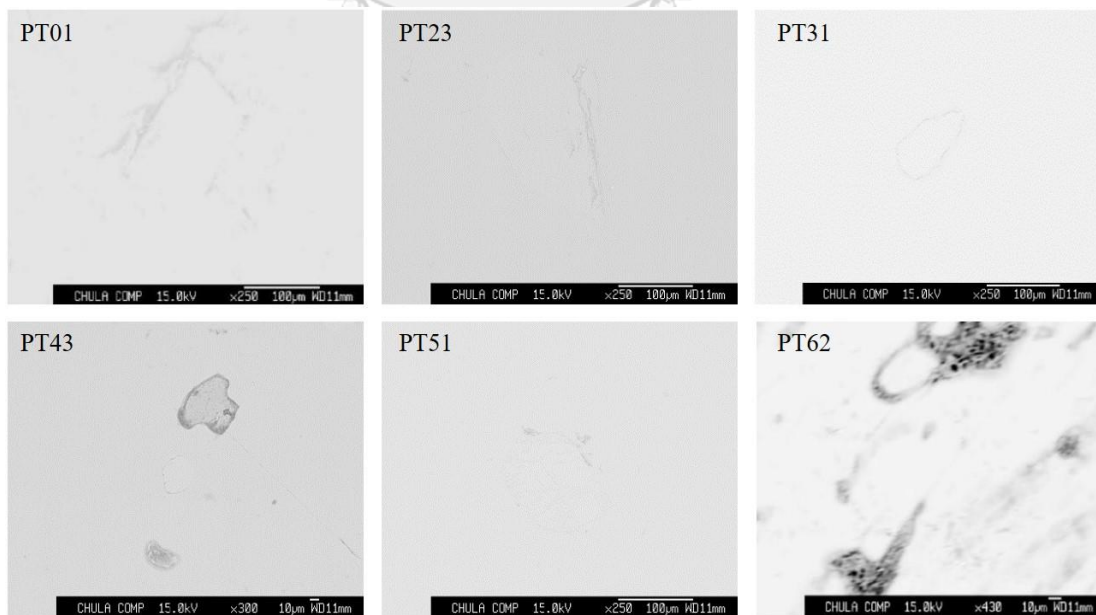
4) Dak Nong area in Southern Vietnam

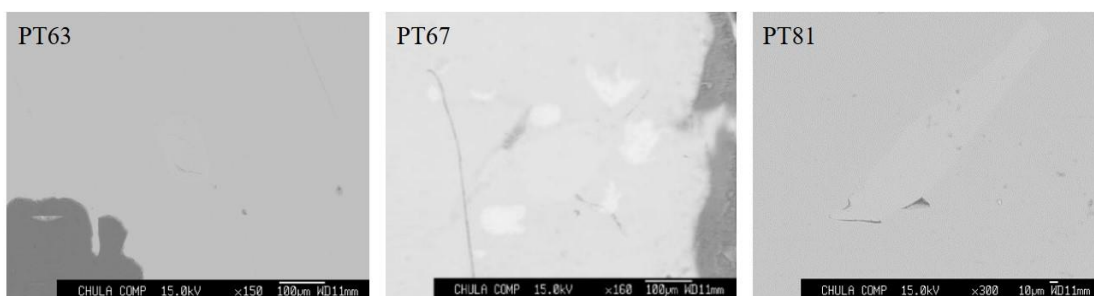




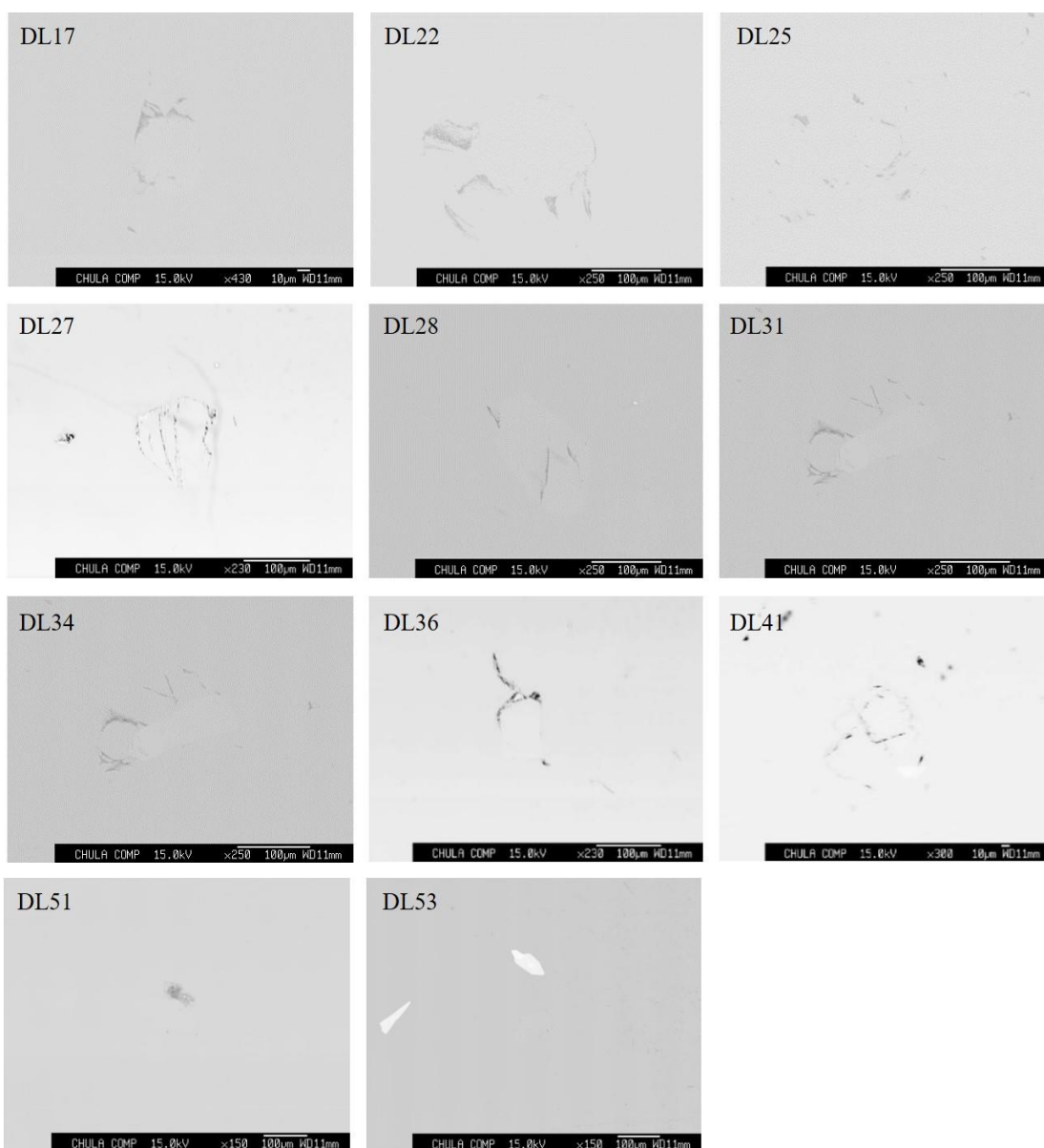
c. Feldspar

1) Binh Thuan area in Southern Vietnam

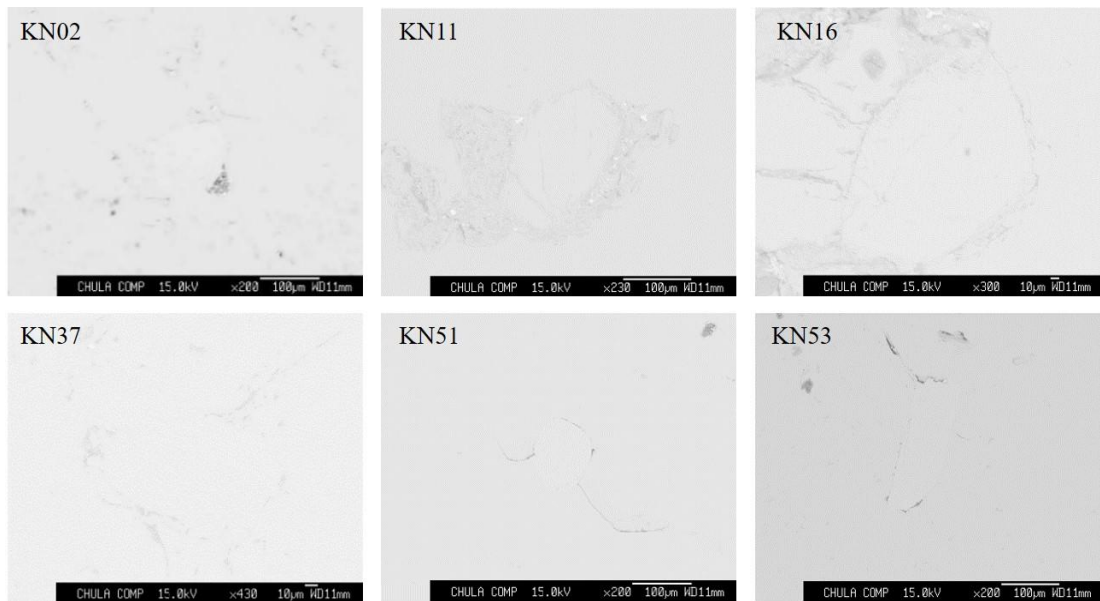




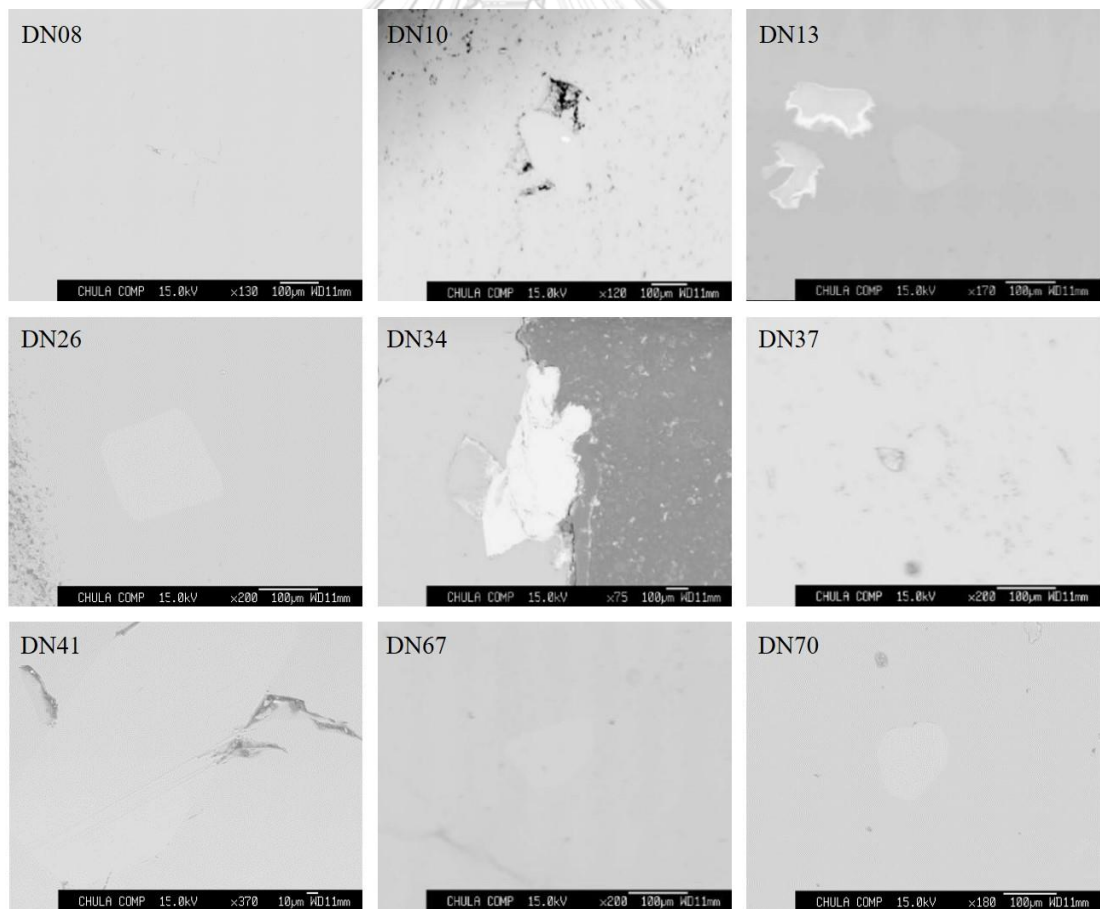
2) Di Linh area in Southern Vietnam

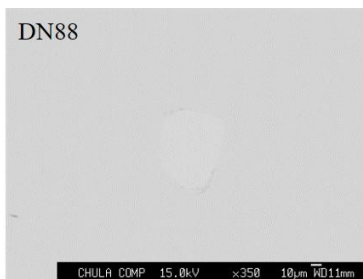


3) Krong Nang area in Southern Vietnam



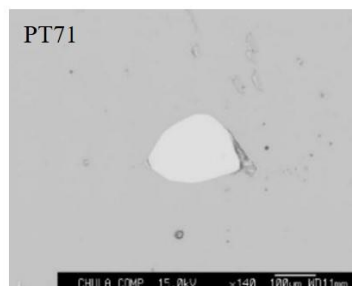
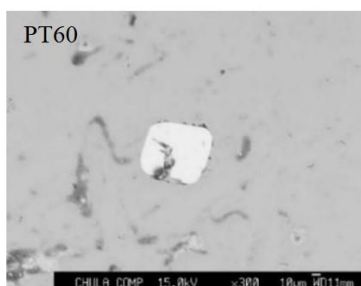
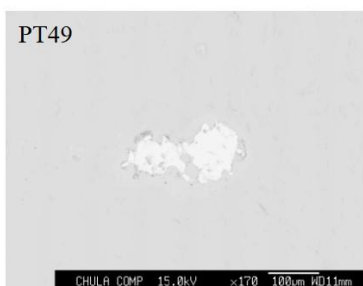
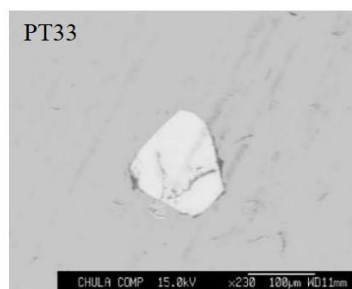
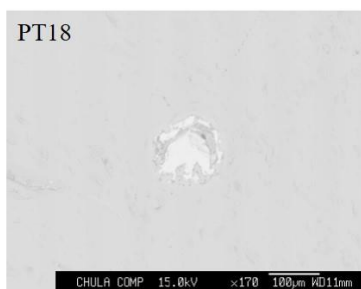
4) Dak Nong area in Southern Vietnam



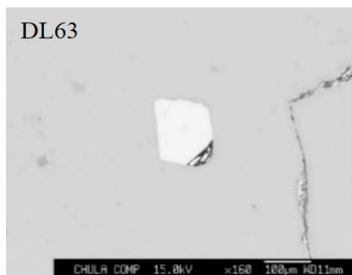
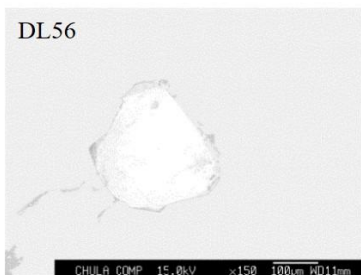
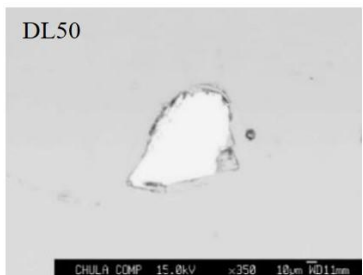
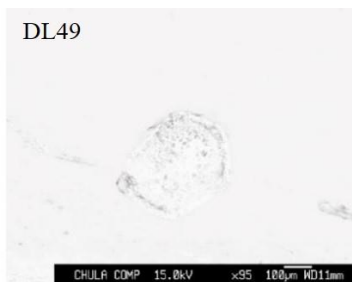
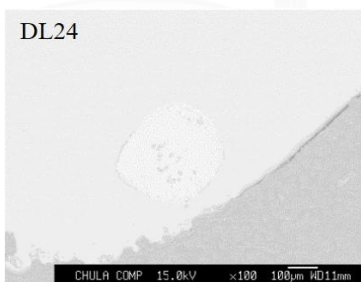
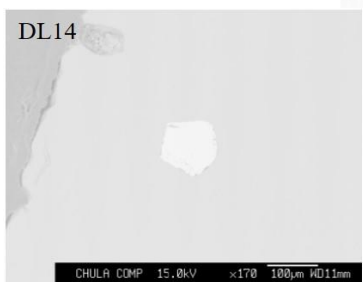


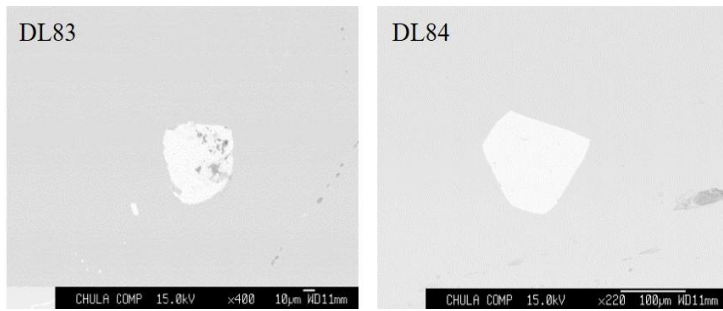
d. Wüstite

1) Binh Thuan area in Southern Vietnam

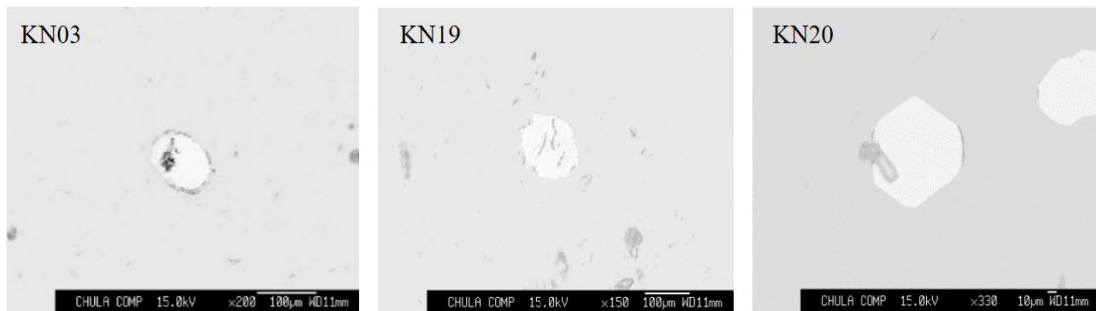


2) Di Linh area in Southern Vietnam

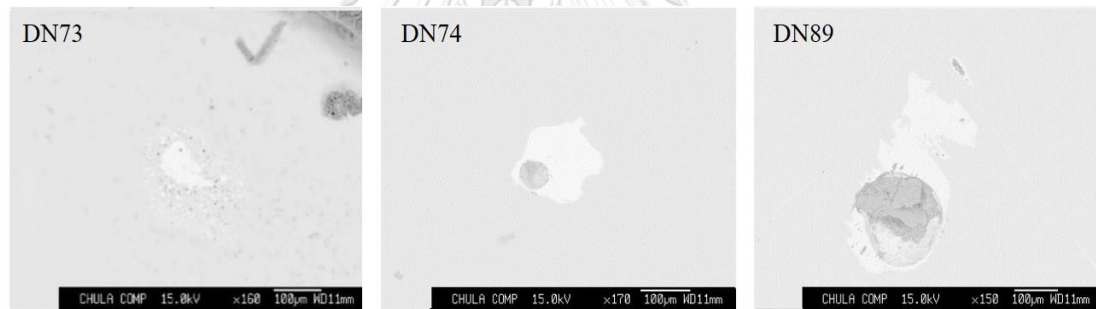




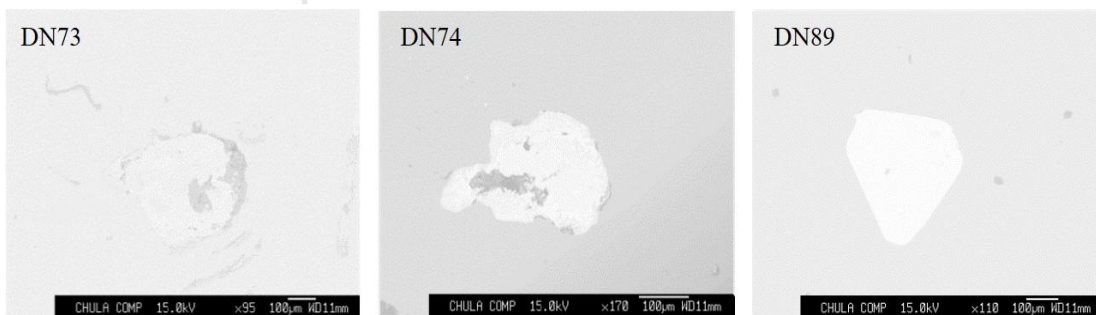
3) Krong Nang area in Southern Vietnam

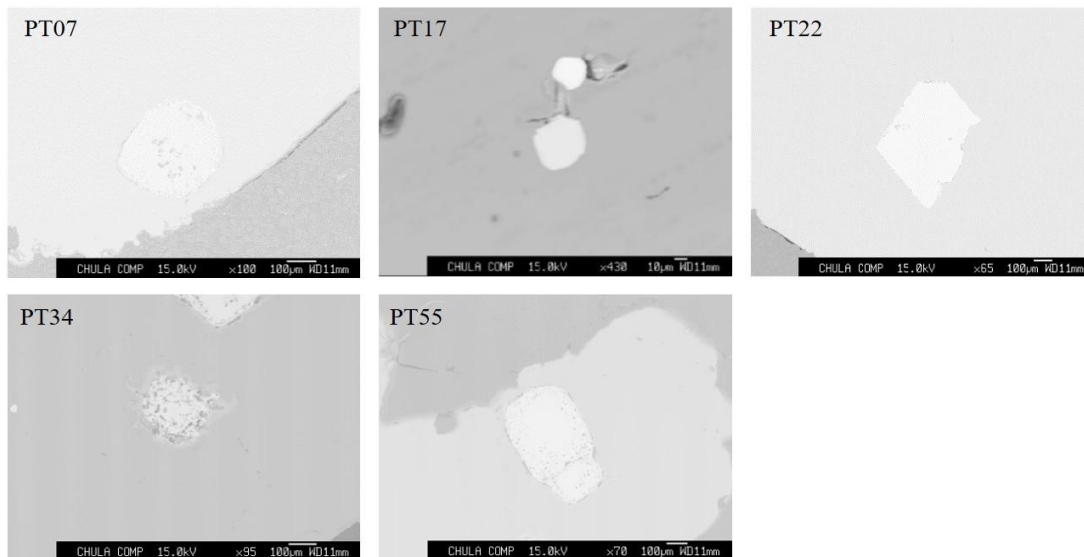
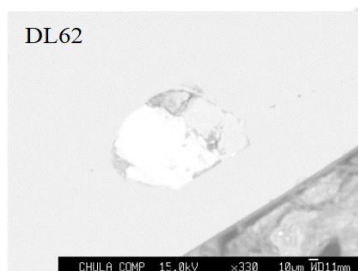
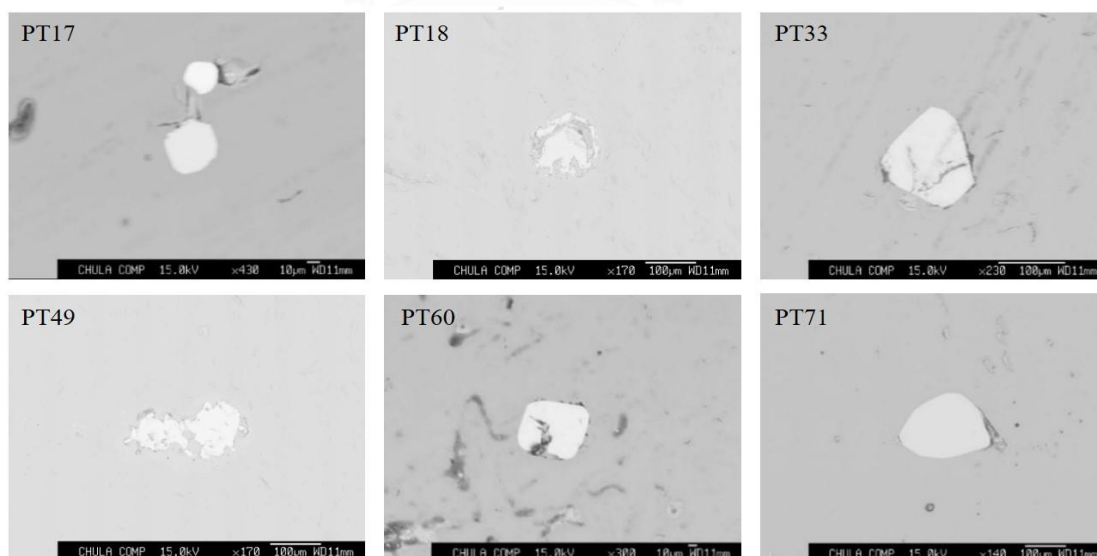


4) Dak Nong area in Southern Vietnam

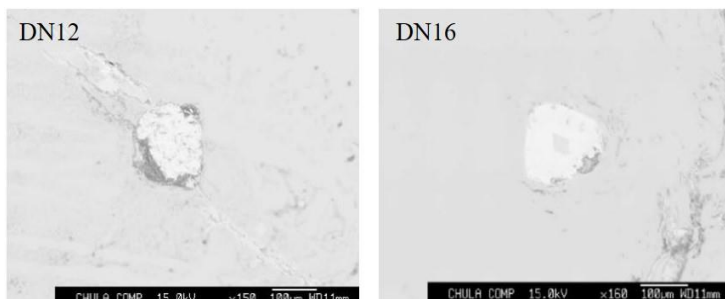


5) Pleiku area in Southern Vietnam

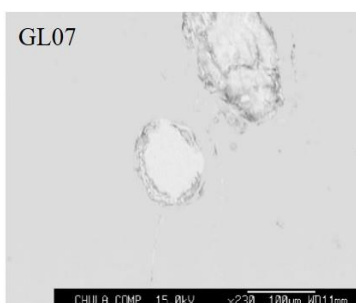


e. Spinel**1) Binh Thuan area in Southern Vietnam****2) Di Linh area in Southern Vietnam****3) Krong Nang area in Southern Vietnam**

4) Dak Nong area in Southern Vietnam

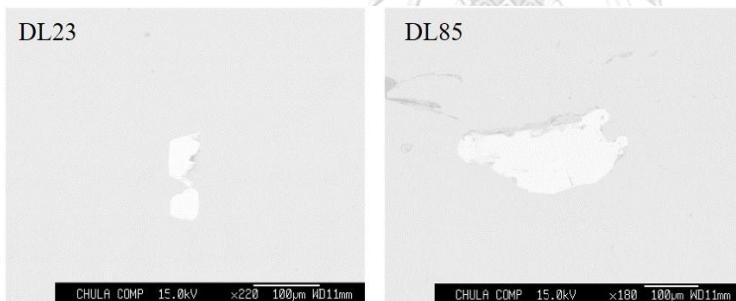


5) Pleiku area in Southern Vietnam

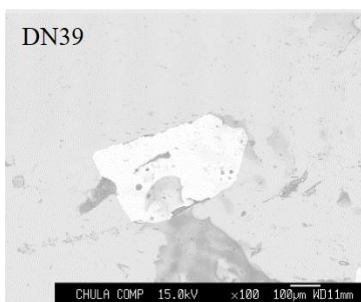


f. Ilmenite

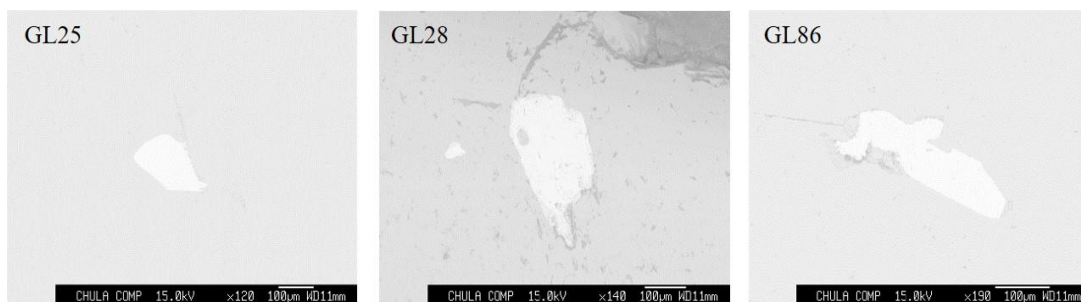
1) Di Linh area in Southern Vietnam



2) Dak Nong area in Southern Vietnam

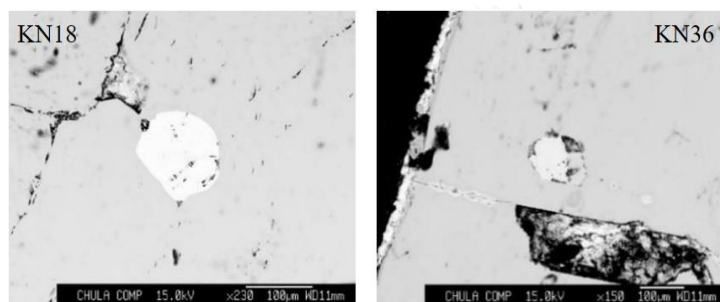


3) Pleiku area in Southern Vietnam



g. Pyrochlore

1) Krong Nang area in Southern Vietnam



2) Dak Nong area in Southern Vietnam



APPENDIX C

EPMA DATA

a. Columbite

Table C.1 Representative EPMA analyses of columbite inclusions found in sapphires from Binh Thuan.

	PT01	PT02	PT03	PT09	PT10	PT11	PT14	PT19	PT20	PT21	PT24	PT25	PT27
TiO ₂	7.11	4.09	6.81	6.96	7.86	0.00	1.96	6.33	2.22	3.47	5.13	5.68	6.80
FeO	16.66	19.77	16.06	14.40	16.34	15.96	13.09	15.01	19.72	15.77	15.00	15.37	16.71
MnO	3.53	4.83	3.02	2.54	2.45	3.77	5.67	3.08	7.62	3.14	5.00	4.43	6.39
MgO	0.12	0.19	0.09	1.12	1.08	0.00	1.23	0.13	0.30	1.02	0.08	0.35	0.23
CaO	0.01	0.03	0.04	0.15	0.02	0.00	0.00	0.35	0.01	0.03	0.00	0.01	0.02
Nb ₂ O ₅	68.79	68.84	69.65	68.21	68.98	76.98	76.18	67.80	66.51	74.07	73.53	68.73	66.44
Ta ₂ O ₅	1.14	0.92	1.47	1.54	0.92	3.78	1.25	4.39	1.40	1.35	0.32	4.44	0.75
ThO ₂	0.69	0.00	0.00	0.00	0.05	0.00	0.00	0.00	0.00	0.00	0.04	0.00	0.48
UO ₂	1.68	0.01	0.85	0.04	0.01	0.00	0.01	0.37	0.08	0.06	0.00	0.00	0.40
ZrO ₂	0.00	0.43	1.34	4.08	1.01	0.03	0.15	0.87	0.75	0.34	0.29	1.25	2.19
Y ₂ O ₃	0.00	0.06	0.01	0.00	0.04	0.00	0.00	0.02	0.14	0.00	0.00	0.00	0.00
Nd ₂ O ₃	0.00	0.00	0.29	0.00	0.00	0.00	0.00	1.06	0.00	0.00	0.00	0.00	0.00
Sm ₂ O ₃	0.00	0.00	0.00	0.00	0.02	0.00	0.00	0.00	0.00	0.00	0.00	0.00	0.06
Total	99.72	99.18	99.62	99.04	98.77	100.53	99.55	99.42	98.75	99.23	99.39	100.26	100.48
Formula 6(O)													
Ti	0.299	0.174	0.284	0.289	0.326	0.000	0.082	0.268	0.097	0.145	0.214	0.238	0.284
Fe	0.779	0.936	0.746	0.665	0.753	0.754	0.610	0.707	0.954	0.735	0.695	0.717	0.775
Mn	0.167	0.232	0.142	0.119	0.115	0.181	0.267	0.147	0.373	0.148	0.235	0.209	0.300
Mg	0.010	0.016	0.007	0.092	0.088	0.000	0.102	0.010	0.026	0.084	0.007	0.029	0.019
Ca	0.000	0.002	0.002	0.009	0.001	0.000	0.000	0.021	0.001	0.002	0.000	0.000	0.001
Nb	1.738	1.762	1.749	1.703	1.719	1.967	1.920	1.725	1.739	1.867	1.842	1.733	1.666
Ta	0.017	0.014	0.022	0.023	0.014	0.058	0.019	0.067	0.022	0.021	0.005	0.067	0.011
Th	0.009	0.000	0.000	0.000	0.001	0.000	0.000	0.000	0.000	0.000	0.001	0.000	0.006
U	0.021	0.000	0.010	0.000	0.000	0.000	0.000	0.005	0.001	0.001	0.000	0.000	0.005
Zr	0.000	0.012	0.036	0.110	0.027	0.001	0.004	0.024	0.021	0.009	0.008	0.034	0.059
Y	0.000	0.002	0.000	0.000	0.001	0.000	0.000	0.001	0.004	0.000	0.000	0.000	0.000
Nd	0.000	0.000	0.007	0.000	0.000	0.000	0.000	0.027	0.000	0.000	0.000	0.000	0.000
Sm	0.000	0.000	0.000	0.000	0.000	0.000	0.000	0.000	0.000	0.000	0.000	0.000	0.001
Total *	3.039	3.149	3.008	3.011	3.046	2.961	3.005	3.002	3.238	3.013	3.007	3.028	3.129
Mn/Mn+Fe	0.18	0.20	0.16	0.15	0.13	0.19	0.30	0.17	0.28	0.17	0.25	0.23	0.28
Ta/Ta+Nb	0.01	0.01	0.01	0.01	0.01	0.03	0.01	0.04	0.01	0.011	0.00	0.04	0.01

Table C.2 Representative EPMA analyses of columbite inclusions found in sapphires from Binh Thuan.

	PT28	PT29	PT30	PT32	PT35	PT37	PT39	PT40	PT41	PT42	PT50	PT57	PT58
TiO ₂	10.52	6.08	6.51	7.00	6.25	7.10	2.51	2.15	1.79	3.62	0.79	1.42	3.55
FeO	15.98	18.73	16.79	15.91	19.28	16.33	14.25	14.79	15.17	15.72	17.00	14.67	12.77
MnO	5.20	4.27	4.07	4.39	5.32	3.76	6.12	5.51	5.55	4.70	3.35	6.37	4.94
MgO	0.06	1.32	0.10	1.15	0.32	0.71	0.18	0.07	0.13	0.14	0.16	0.48	1.25
CaO	0.01	0.01	0.10	0.06	0.00	0.00	0.03	0.00	0.08	0.25	0.04	0.11	0.06
Nb ₂ O ₅	65.61	68.77	66.80	68.87	65.49	69.89	75.44	74.34	75.48	71.98	76.15	74.70	75.05
Ta ₂ O ₅	1.38	0.83	1.22	0.91	0.35	0.74	1.32	1.65	2.30	0.96	2.05	1.20	1.05
ThO ₂	0.03	0.01	1.73	0.00	0.00	0.01	0.00	0.00	0.00	0.00	0.00	0.00	0.00
UO ₂	0.06	0.03	0.96	0.03	0.03	0.01	0.10	0.06	0.06	0.20	0.04	0.13	0.06
ZrO ₂	0.44	0.59	0.17	0.40	2.96	0.08	0.20	0.84	0.11	1.47	0.10	0.60	0.48
Y ₂ O ₃	0.00	0.00	0.00	0.00	0.00	0.09	0.00	0.00	0.00	0.04	0.00	0.00	0.00
Nd ₂ O ₃	0.00	0.00	0.00	0.00	0.00	0.00	0.00	0.00	0.00	0.02	0.00	0.00	0.00
Sm ₂ O ₃	0.00	0.00	0.02	0.00	0.00	0.00	0.00	0.01	0.00	0.00	0.00	0.10	0.03
Total	99.29	100.63	98.49	98.72	100.00	98.71	100.15	99.41	100.67	99.10	99.67	99.76	99.22
Formula 6(O)													
Ti	0.434	0.251	0.279	0.292	0.262	0.296	0.105	0.091	0.075	0.153	0.033	0.060	0.148
Fe	0.734	0.860	0.800	0.738	0.898	0.757	0.665	0.698	0.709	0.740	0.804	0.691	0.593
Mn	0.242	0.199	0.196	0.206	0.251	0.177	0.289	0.263	0.263	0.224	0.161	0.304	0.232
Mg	0.005	0.108	0.009	0.095	0.027	0.059	0.015	0.006	0.011	0.011	0.013	0.040	0.103
Ca	0.001	0.000	0.006	0.003	0.000	0.000	0.002	0.000	0.005	0.015	0.002	0.007	0.003
Nb	1.629	1.707	1.721	1.727	1.650	1.752	1.902	1.896	1.907	1.831	1.947	1.902	1.883
Ta	0.021	0.012	0.019	0.014	0.005	0.011	0.020	0.025	0.035	0.015	0.031	0.018	0.016
Th	0.000	0.000	0.022	0.000	0.000	0.000	0.000	0.000	0.000	0.000	0.000	0.000	0.000
U	0.001	0.000	0.012	0.000	0.000	0.000	0.001	0.001	0.001	0.003	0.001	0.002	0.001
Zr	0.012	0.016	0.005	0.011	0.080	0.002	0.005	0.023	0.003	0.040	0.003	0.016	0.013
Y	0.000	0.000	0.000	0.000	0.000	0.003	0.000	0.000	0.000	0.001	0.000	0.000	0.000
Nd	0.000	0.000	0.000	0.000	0.000	0.000	0.000	0.000	0.000	0.001	0.000	0.000	0.000
Sm	0.000	0.000	0.000	0.000	0.000	0.000	0.000	0.000	0.000	0.000	0.000	0.002	0.001
Total *	3.078	3.154	3.071	3.086	3.175	3.056	3.005	3.003	3.008	3.034	2.996	3.042	2.993
Mn/Mn+Fe	0.25	0.19	0.20	0.22	0.22	0.19	0.30	0.27	0.27	0.23	0.17	0.31	0.28
Ta/Ta+Nb	0.01	0.01	0.01	0.008	0.00	0.01	0.01	0.01	0.02	0.01	0.02	0.01	0.01

Table C.3 Representative EPMA analyses of columbite inclusions found in sapphires from Binh Thuan.

	PT64	PT72	PT73	PT74	PT75	PT76	PT77	PT78	PT79	PT82	PT83
TiO ₂	6.62	2.24	12.04	5.61	6.84	4.14	6.23	4.70	6.31	10.68	2.33
FeO	16.06	14.51	15.29	15.00	16.88	17.27	17.55	17.09	15.09	15.35	15.16
MnO	3.41	8.37	4.27	5.01	4.84	4.78	4.52	6.06	5.27	6.74	8.67
MgO	1.62	0.24	0.08	0.08	1.46	0.37	1.47	0.85	1.37	0.03	0.20
CaO	0.01	0.06	0.00	0.00	0.03	0.00	0.05	0.00	0.08	0.00	0.04
Nb ₂ O ₅	69.62	72.15	66.03	73.92	68.40	68.73	68.82	68.00	69.46	66.09	71.94
Ta ₂ O ₅	0.83	1.04	0.46	0.20	0.55	0.73	0.72	0.75	0.72	0.80	0.95
ThO ₂	0.01	0.00	0.00	0.00	0.01	0.27	0.00	0.23	0.02	0.00	0.00
UO ₂	0.10	0.17	0.04	0.01	0.03	0.14	0.05	0.02	0.00	0.03	0.18
ZrO ₂	0.36	0.16	0.52	0.25	0.71	2.41	0.26	0.42	0.57	0.27	0.07
Y ₂ O ₃	0.00	0.00	0.15	0.00	0.05	0.08	0.00	0.06	0.11	0.00	0.00
Nd ₂ O ₃	0.00	0.00	0.00	0.00	0.00	0.00	0.00	0.00	0.00	0.00	0.00
Sm ₂ O ₃	0.01	0.00	0.00	0.00	0.00	0.10	0.00	0.01	0.00	0.00	0.00
Total	98.66	98.94	98.87	100.08	99.81	99.02	99.66	98.19	98.99	99.99	99.55
Formula 6(O)											
Ti	0.275	0.096	0.493	0.232	0.283	0.176	0.259	0.201	0.263	0.438	0.099
Fe	0.743	0.691	0.696	0.689	0.776	0.818	0.811	0.812	0.700	0.699	0.718
Mn	0.160	0.404	0.197	0.233	0.225	0.229	0.211	0.292	0.247	0.311	0.416
Mg	0.134	0.020	0.007	0.007	0.120	0.031	0.121	0.072	0.113	0.002	0.017
Ca	0.001	0.004	0.000	0.000	0.002	0.000	0.003	0.000	0.005	0.000	0.002
Nb	1.742	1.856	1.625	1.835	1.700	1.759	1.719	1.747	1.740	1.627	1.842
Ta	0.012	0.016	0.007	0.003	0.008	0.011	0.011	0.012	0.011	0.012	0.015
Th	0.000	0.000	0.000	0.000	0.000	0.003	0.000	0.003	0.000	0.000	0.000
U	0.001	0.002	0.000	0.000	0.000	0.002	0.001	0.000	0.000	0.000	0.002
Zr	0.010	0.004	0.014	0.007	0.019	0.067	0.007	0.012	0.015	0.007	0.002
Y	0.000	0.000	0.004	0.000	0.002	0.002	0.000	0.002	0.003	0.000	0.000
Nd	0.000	0.000	0.000	0.000	0.000	0.000	0.000	0.000	0.000	0.000	0.000
Sm	0.000	0.000	0.000	0.000	0.000	0.002	0.000	0.000	0.000	0.000	0.000
Total *	3.080	3.093	3.043	3.005	3.136	3.101	3.142	3.152	3.098	3.096	3.114
Mn/Mn+Fe	0.18	0.37	0.22	0.25	0.22	0.22	0.21	0.26	0.26	0.31	0.37
Ta/Ta+Nb	0.01	0.009	0.004	0.002	0.00	0.01	0.01	0.01	0.01	0.01	0.01

Table C.4 Representative EPMA analyses of columbite inclusions found in sapphires from Di Linh.

	DL03	DL06	DL07	DL10	DL11	DL15	DL16	DL19	DL21	DL26	DL29	DL30	DL32
TiO ₂	1.39	5.00	0.78	2.45	1.42	0.854	3.15	3.12	0.68	8.45	4.23	0.42	1.68
FeO	15.53	13.03	16.63	14.00	14.28	16.74	15.95	14.45	15.27	14.70	14.75	15.22	16.19
MnO	4.88	5.16	9.16	5.70	5.91	9.30	4.36	3.03	6.12	7.08	4.00	9.67	9.63
MgO	0.31	1.51	0.15	1.11	0.31	1.79	0.38	1.65	1.82	0.18	1.75	1.51	0.54
CaO	0.01	0.06	0.13	0.03	0.07	0.05	0.01	0.02	0.38	0.00	0.05	0.05	0.00
Nb ₂ O ₅	75.95	72.00	70.56	75.85	74.79	70.02	73.75	75.92	73.42	68.71	74.37	70.85	70.12
Ta ₂ O ₅	1.39	0.90	1.27	1.36	2.49	1.07	1.33	1.02	0.81	0.41	0.38	0.99	1.07
ThO ₂	0.00	0.00	0.06	0.00	0.00	0.09	0.00	0.00	0.00	0.00	0.00	0.00	0.01
UO ₂	0.02	0.22	0.02	0.06	0.00	0.04	0.03	0.00	0.06	0.09	0.02	0.00	0.06
ZrO ₂	0.16	0.61	0.39	0.38	0.41	0.28	0.51	0.16	1.07	0.39	0.41	0.08	0.46
Y ₂ O ₃	0.00	0.02	0.02	0.00	0.00	0.09	0.00	0.00	0.00	0.00	0.00	0.02	0.03
Nd ₂ O ₃	0.00	0.00	0.00	0.00	0.00	0.00	0.00	0.00	0.00	0.00	0.00	0.00	0.00
Sm ₂ O ₃	0.00	0.00	0.03	0.00	0.00	0.00	0.00	0.00	0.01	0.00	0.00	0.04	0.07
Total	99.64	98.51	99.17	100.94	99.68	100.33	99.46	99.38	99.63	100.01	99.96	98.84	99.85
Formula 6(O)													
Ti	0.059	0.209	0.034	0.102	0.060	0.036	0.133	0.130	0.029	0.348	0.175	0.018	0.072
Fe	0.731	0.607	0.800	0.645	0.675	0.792	0.747	0.668	0.718	0.673	0.676	0.729	0.770
Mn	0.233	0.243	0.446	0.266	0.283	0.445	0.207	0.142	0.292	0.328	0.186	0.469	0.464
Mg	0.026	0.125	0.012	0.091	0.026	0.151	0.031	0.136	0.153	0.015	0.143	0.129	0.046
Ca	0.001	0.003	0.008	0.001	0.004	0.003	0.000	0.001	0.023	0.000	0.003	0.003	0.000
Nb	1.932	1.812	1.836	1.888	1.909	1.789	1.868	1.898	1.867	1.700	1.843	1.835	1.802
Ta	0.021	0.014	0.020	0.020	0.038	0.016	0.020	0.015	0.012	0.006	0.006	0.015	0.017
Th	0.000	0.000	0.001	0.000	0.000	0.001	0.000	0.000	0.000	0.000	0.000	0.000	0.000
U	0.000	0.003	0.000	0.001	0.000	0.000	0.000	0.000	0.001	0.001	0.000	0.000	0.001
Zr	0.004	0.017	0.011	0.010	0.011	0.008	0.014	0.004	0.029	0.010	0.011	0.002	0.013
Y	0.000	0.001	0.001	0.000	0.000	0.003	0.000	0.000	0.000	0.000	0.000	0.001	0.001
Nd	0.000	0.000	0.000	0.000	0.000	0.000	0.000	0.000	0.000	0.000	0.000	0.000	0.000
Sm	0.000	0.000	0.001	0.000	0.000	0.000	0.000	0.000	0.000	0.000	0.000	0.001	0.001
Total *	3.006	3.033	3.170	3.024	3.007	3.245	3.021	2.995	3.123	3.081	3.042	3.203	3.186
Mn/Mn+Fe	0.24	0.29	0.36	0.29	0.30	0.36	0.22	0.18	0.29	0.33	0.22	0.39	0.38
Ta/Ta+Nb	0.01	0.01	0.01	0.01	0.02	0.01	0.01	0.01	0.01	0.004	0.003	0.01	0.01

Table C.5 Representative EPMA analyses of columbite inclusions found in sapphires from Di Linh.

	DL35	DL38	DL52	DL54	DL55	DL64	DL65	DL66	DL67	DL68	DL69	DL70	DL72
TiO ₂	8.31	1.18	1.27	0.95	2.86	6.98	6.94	6.30	7.30	0.75	1.20	0.28	6.97
FeO	19.17	16.18	17.34	16.62	16.45	16.15	14.41	14.50	17.32	13.69	14.38	14.28	16.68
MnO	2.08	9.52	9.48	8.73	6.22	5.57	5.74	4.78	4.69	9.90	10.58	14.64	4.57
MgO	1.13	0.70	0.95	0.97	1.69	0.58	1.32	2.05	1.20	1.76	1.83	0.16	0.61
CaO	0.64	0.05	0.02	0.00	0.07	0.06	0.02	0.00	0.00	0.02	0.03	0.01	0.03
Nb ₂ O ₅	66.96	70.45	69.90	70.45	70.08	68.70	68.03	69.67	66.48	72.83	71.44	68.54	67.90
Ta ₂ O ₅	0.10	1.81	0.97	0.67	1.52	0.55	1.80	1.15	0.89	0.67	0.97	1.76	0.73
ThO ₂	0.27	0.06	0.00	0.02	0.00	0.00	0.06	0.06	0.00	0.05	0.00	0.00	0.08
UO ₂	0.73	0.17	0.08	0.00	0.06	0.02	0.00	0.00	0.10	0.01	0.01	0.09	0.05
ZrO ₂	0.01	0.70	0.13	0.46	0.07	0.17	2.56	0.27	0.90	0.42	0.18	0.18	1.29
Y ₂ O ₃	1.08	0.04	0.00	0.00	0.00	0.00	0.06	0.00	0.02	0.02	0.05	0.00	0.01
Nd ₂ O ₃	0.00	0.00	0.00	0.00	0.00	0.00	0.00	0.00	0.00	0.00	0.00	0.00	0.00
Sm ₂ O ₃	0.65	0.08	0.00	0.00	0.00	0.00	0.00	0.00	0.00	0.01	0.01	0.00	0.00
Total	101.12	100.93	100.12	98.85	99.01	98.77	100.93	98.79	98.91	100.12	100.69	99.94	98.92
Formula 6(O)													
Ti	0.341	0.050	0.054	0.041	0.122	0.292	0.285	0.262	0.305	0.032	0.050	0.012	0.292
Fe	0.874	0.765	0.823	0.796	0.777	0.752	0.657	0.671	0.806	0.643	0.673	0.690	0.776
Mn	0.096	0.455	0.456	0.424	0.297	0.262	0.265	0.224	0.221	0.471	0.502	0.716	0.216
Mg	0.092	0.059	0.080	0.083	0.142	0.048	0.107	0.169	0.100	0.147	0.153	0.014	0.051
Ca	0.037	0.003	0.001	0.000	0.004	0.003	0.001	0.000	0.000	0.001	0.002	0.000	0.002
Nb	1.650	1.800	1.794	1.825	1.789	1.728	1.677	1.741	1.671	1.849	1.808	1.790	1.708
Ta	0.001	0.028	0.015	0.010	0.023	0.008	0.027	0.017	0.013	0.010	0.015	0.028	0.011
Th	0.003	0.001	0.000	0.000	0.000	0.000	0.001	0.001	0.000	0.001	0.000	0.000	0.001
U	0.009	0.002	0.001	0.000	0.001	0.000	0.000	0.000	0.001	0.000	0.000	0.001	0.001
Zr	0.000	0.019	0.004	0.013	0.002	0.005	0.068	0.007	0.024	0.012	0.005	0.005	0.035
Y	0.031	0.001	0.000	0.000	0.000	0.000	0.002	0.000	0.001	0.001	0.002	0.000	0.000
Nd	0.000	0.000	0.000	0.000	0.000	0.000	0.000	0.000	0.000	0.000	0.000	0.000	0.000
Sm	0.012	0.002	0.000	0.000	0.000	0.000	0.000	0.000	0.000	0.000	0.000	0.000	0.000
Total *	3.147	3.185	3.228	3.192	3.157	3.098	3.090	3.092	3.142	3.167	3.210	3.256	3.092
Mn/Mn+Fe	0.10	0.37	0.36	0.35	0.28	0.26	0.29	0.25	0.22	0.42	0.43	0.51	0.22
Ta/Ta+Nb	0.001	0.02	0.01	0.01	0.01	0.00	0.02	0.01	0.01	0.01	0.01	0.02	0.01



Table C.6 Representative EPMA analyses of columbite inclusions found in sapphires from Di Linh.

	DL73	DL74	DL76	DL77	DL78	DL79	DL80	DL81	DL82	DL83
TiO ₂	6.56	1.14	6.89	4.47	6.07	6.82	4.71	6.72	6.84	4.61
FeO	15.86	12.35	17.28	17.95	17.00	17.75	16.91	16.85	17.51	15.49
MnO	4.54	8.12	3.93	7.18	4.32	4.23	7.69	4.69	4.91	4.42
MgO	1.00	2.93	0.94	0.77	0.84	1.04	1.37	2.93	1.43	1.32
CaO	0.00	0.02	0.00	0.06	0.06	0.00	0.00	0.00	0.03	0.00
Nb ₂ O ₅	67.62	72.59	67.83	67.53	68.48	68.39	66.51	67.60	68.24	72.49
Ta ₂ O ₅	3.67	1.57	0.88	0.79	0.73	0.64	1.14	1.09	0.87	0.48
ThO ₂	0.00	0.00	0.00	0.02	0.00	0.02	0.00	0.00	0.01	0.01
UO ₂	0.03	0.00	0.06	0.00	0.04	0.05	0.04	0.03	0.00	0.08
ZrO ₂	0.81	0.26	0.77	0.00	2.02	1.30	0.51	0.18	0.32	0.10
Y ₂ O ₃	0.03	0.00	0.00	0.00	0.10	0.00	0.00	0.00	0.00	0.00
Nd ₂ O ₃	0.00	0.00	0.00	0.00	0.00	0.00	0.00	0.00	0.00	0.00
Sm ₂ O ₃	0.00	0.00	0.05	0.00	0.00	0.00	0.00	0.00	0.03	0.00
Total	100.12	98.98	98.63	98.75	99.65	100.25	98.87	100.10	100.18	99.00
Formula 6(O)										
Ti	0.274	0.048	0.289	0.190	0.253	0.282	0.200	0.276	0.283	0.192
Fe	0.736	0.581	0.806	0.851	0.788	0.815	0.799	0.770	0.804	0.720
Mn	0.213	0.387	0.185	0.345	0.203	0.197	0.368	0.217	0.228	0.208
Mg	0.082	0.246	0.078	0.065	0.069	0.085	0.115	0.239	0.117	0.110
Ca	0.000	0.001	0.000	0.003	0.003	0.000	0.000	0.000	0.002	0.000
Nb	1.695	1.846	1.710	1.730	1.715	1.698	1.698	1.669	1.693	1.821
Ta	0.055	0.024	0.013	0.012	0.011	0.010	0.018	0.016	0.013	0.007
Th	0.000	0.000	0.000	0.000	0.000	0.000	0.000	0.000	0.000	0.000
U	0.000	0.000	0.001	0.000	0.000	0.001	0.000	0.000	0.000	0.001
Zr	0.022	0.007	0.021	0.000	0.055	0.035	0.014	0.005	0.008	0.003
Y	0.001	0.000	0.000	0.000	0.003	0.000	0.000	0.000	0.000	0.000
Nd	0.000	0.000	0.000	0.000	0.000	0.000	0.000	0.000	0.000	0.000
Sm	0.000	0.000	0.001	0.000	0.000	0.000	0.000	0.000	0.001	0.000
Total [†]	3.078	3.140	3.104	3.196	3.101	3.122	3.212	3.192	3.149	3.062
Mn/Mn+Fe	0.22	0.40	0.19	0.29	0.20	0.19	0.32	0.22	0.22	0.22
Ta/Ta+Nb	0.03	0.01	0.01	0.01	0.01	0.01	0.01	0.01	0.01	0.004

Table C.8 Representative EPMA analyses of columbite inclusions found in sapphires from Dak Nong.

	DN01	DN02	DN07	DN09	DN11	DN17	DN18	DN19	DN28	DN30	DN38	DN43	DN44
TiO ₂	6.21	7.82	2.57	0.89	7.00	7.83	0.38	6.37	3.34	6.38	7.05	0.26	2.36
FeO	17.71	17.80	14.44	15.74	17.83	15.49	18.37	18.57	13.50	17.13	14.61	16.41	15.92
MnO	5.71	3.88	4.97	9.57	2.55	6.08	10.21	4.97	4.64	5.60	5.68	10.42	9.26
MgO	1.35	1.12	1.03	1.27	1.79	0.06	0.32	1.89	1.64	1.00	1.40	0.16	1.51
CaO	0.03	0.04	0.00	0.96	0.01	0.00	0.03	0.07	0.01	0.00	0.06	0.03	0.00
Nb ₂ O ₅	67.08	66.46	74.49	70.08	68.09	70.40	70.14	67.22	74.14	67.59	69.91	69.90	69.52
Ta ₂ O ₅	1.32	1.01	1.75	0.69	1.42	0.24	0.90	1.22	1.64	0.87	1.42	1.64	1.38
ThO ₂	0.00	0.00	0.00	0.00	0.00	0.00	0.04	0.04	0.00	0.00	0.03	0.00	0.00
UO ₂	0.00	0.13	0.03	0.00	0.02	0.00	0.00	0.03	0.07	0.02	0.06	0.00	0.10
ZrO ₂	0.69	0.56	0.15	0.39	0.00	0.58	0.22	0.08	0.32	0.38	0.32	0.06	0.33
Y ₂ O ₃	0.00	0.00	0.00	0.06	0.04	0.00	0.00	0.11	0.00	0.00	0.02	0.02	0.00
Nd ₂ O ₃	0.00	0.00	0.00	0.00	0.00	0.00	0.00	0.00	0.00	0.00	0.00	0.00	0.00
Sm ₂ O ₃	0.00	0.00	0.00	0.00	0.01	0.04	0.01	0.00	0.00	0.00	0.00	0.00	0.04
Total	100.10	98.82	99.42	99.65	98.75	100.71	100.63	100.57	99.30	98.97	100.55	98.90	100.42
Formula 6(O)													
Ti	0.258	0.327	0.108	0.038	0.292	0.321	0.016	0.263	0.140	0.268	0.289	0.011	0.100
Fe	0.820	0.827	0.676	0.748	0.827	0.705	0.876	0.853	0.628	0.799	0.666	0.796	0.748
Mn	0.268	0.183	0.235	0.460	0.120	0.280	0.493	0.231	0.218	0.265	0.262	0.512	0.440
Mg	0.112	0.093	0.086	0.107	0.148	0.005	0.027	0.155	0.136	0.084	0.113	0.014	0.127
Ca	0.002	0.002	0.000	0.059	0.000	0.000	0.002	0.004	0.000	0.000	0.003	0.002	0.000
Nb	1.678	1.668	1.884	1.800	1.706	1.731	1.808	1.669	1.863	1.705	1.722	1.834	1.765
Ta	0.020	0.015	0.027	0.011	0.021	0.003	0.014	0.018	0.025	0.013	0.021	0.026	0.021
Th	0.000	0.000	0.000	0.000	0.000	0.000	0.001	0.001	0.000	0.000	0.000	0.000	0.000
U	0.000	0.002	0.000	0.000	0.000	0.000	0.000	0.000	0.001	0.000	0.001	0.000	0.001
Zr	0.019	0.015	0.004	0.011	0.000	0.015	0.006	0.002	0.009	0.010	0.008	0.002	0.009
Y	0.000	0.000	0.000	0.002	0.001	0.000	0.000	0.003	0.000	0.000	0.001	0.001	0.000
Nd	0.000	0.000	0.000	0.000	0.000	0.000	0.000	0.000	0.000	0.000	0.000	0.000	0.000
Sm	0.000	0.000	0.000	0.000	0.000	0.001	0.000	0.000	0.000	0.000	0.000	0.000	0.001
Total *	3.176	3.131	3.021	3.235	3.116	3.061	3.244	3.201	3.019	3.144	3.087	3.197	3.211
Mn/Mn+Fe	0.25	0.18	0.26	0.38	0.13	0.28	0.36	0.21	0.26	0.25	0.28	0.39	0.37
Ta/Ta+Nb	0.01	0.01	0.01	0.01	0.01	0.002	0.01	0.01	0.01	0.01	0.01	0.01	0.01

Table C.9 Representative EPMA analyses of columbite inclusions found in sapphires from Dak Nong.

	DN48	DN49	DN48	DN49	DN50	DN51	DN52	DN53	DN54	DN55	DN57	DN58	DN59
TiO ₂	4.96	3.95	4.96	3.95	1.13	1.01	7.73	1.00	6.72	1.68	7.00	3.54	2.68
FeO	15.59	14.95	15.59	14.95	14.59	16.77	16.20	16.25	16.43	13.36	16.75	16.75	13.70
MnO	3.21	4.00	3.21	4.00	6.42	9.88	3.47	10.40	4.31	5.95	4.98	3.83	4.51
MgO	1.02	1.83	1.02	1.83	0.07	0.08	1.32	0.99	0.86	0.93	0.96	0.74	1.44
CaO	0.00	0.02	0.00	0.02	0.02	0.05	0.02	0.02	0.02	0.06	0.02	0.01	0.03
Nb ₂ O ₅	72.61	70.93	72.61	70.93	76.61	70.98	70.23	70.87	69.60	75.73	68.84	71.78	74.77
Ta ₂ O ₅	1.52	3.58	1.52	3.58	1.67	0.71	0.39	0.89	0.98	1.74	0.75	3.28	2.13
ThO ₂	0.00	0.00	0.00	0.00	0.00	0.06	0.05	0.00	0.05	0.00	0.00	0.00	0.00
UO ₂	0.06	0.04	0.06	0.04	0.05	0.00	0.01	0.04	0.01	0.04	0.00	0.17	0.07
ZrO ₂	0.26	0.24	0.26	0.24	0.10	0.01	0.68	0.45	0.00	0.14	0.08	0.11	0.11
Y ₂ O ₃	0.00	0.00	0.00	0.00	0.00	0.00	0.00	0.00	0.00	0.00	0.00	0.00	0.00
Nd ₂ O ₃	0.00	0.00	0.00	0.00	0.00	0.00	0.00	0.00	0.00	0.00	0.00	0.00	0.00
Sm ₂ O ₃	0.00	0.00	0.00	0.00	0.00	0.05	0.01	0.00	0.00	0.00	0.01	0.00	0.00
Total	99.23	99.54	99.23	99.54	100.65	99.60	100.12	100.90	98.98	99.62	99.38	100.20	99.43
Formula 6(O)													
Ti	0.207	0.166	0.207	0.166	0.048	0.043	0.316	0.042	0.280	0.071	0.291	0.149	0.112
Fe	0.724	0.698	0.724	0.698	0.682	0.803	0.736	0.765	0.762	0.626	0.774	0.784	0.639
Mn	0.151	0.189	0.151	0.189	0.304	0.479	0.160	0.496	0.203	0.282	0.233	0.181	0.213
Mg	0.085	0.152	0.085	0.152	0.006	0.007	0.107	0.083	0.071	0.078	0.079	0.062	0.120
Ca	0.000	0.001	0.000	0.001	0.001	0.003	0.001	0.001	0.001	0.003	0.001	0.000	0.002
Nb	1.822	1.791	1.822	1.791	1.937	1.836	1.725	1.804	1.745	1.918	1.719	1.815	1.885
Ta	0.023	0.054	0.023	0.054	0.025	0.011	0.006	0.014	0.015	0.026	0.011	0.050	0.032
Th	0.000	0.000	0.000	0.000	0.000	0.001	0.001	0.000	0.001	0.000	0.000	0.000	0.000
U	0.001	0.000	0.001	0.000	0.001	0.000	0.000	0.001	0.000	0.000	0.000	0.002	0.001
Zr	0.007	0.006	0.007	0.006	0.003	0.000	0.018	0.012	0.000	0.004	0.002	0.003	0.003
Y	0.000	0.000	0.000	0.000	0.000	0.000	0.000	0.000	0.000	0.000	0.000	0.000	0.000
Nd	0.000	0.000	0.000	0.000	0.000	0.000	0.000	0.000	0.000	0.000	0.000	0.000	0.000
Sm	0.000	0.000	0.000	0.000	0.000	0.001	0.000	0.000	0.000	0.000	0.000	0.000	0.000
Total *	3.018	3.059	3.018	3.059	3.006	3.184	3.070	3.218	3.078	3.009	3.111	3.045	3.007
Mn/Mn+Fe	0.17	0.21	0.17	0.21	0.31	0.37	0.18	0.39	0.21	0.31	0.23	0.19	0.25
Ta/Ta+Nb	0.01	0.03	0.01	0.03	0.01	0.01	0.003	0.01	0.01	0.01	0.01	0.03	0.02



b. Zircon

Table C.11 Representative EPMA analyses of zircon inclusions found in sapphires from Binh Thuan.

Sample no.	PT04	PT05	PT12	PT13	PT15	PT16	PT26	PT36	PT44	PT45	PT47	PT53
SiO ₂	34.13	31.95	34.04	34.02	32.48	32.20	33.20	31.19	32.43	33.86	32.52	34.44
TiO ₂	0.00	0.00	0.04	0.00	0.00	0.02	0.00	0.06	0.00	0.00	0.04	0.00
Al ₂ O ₃	0.03	0.00	0.02	0.02	0.00	1.00	0.00	0.28	0.03	0.01	0.01	0.01
FeO	0.02	0.08	0.00	0.00	0.00	0.00	0.00	0.31	0.02	0.00	0.04	0.00
MgO	0.00	0.00	0.01	0.00	0.00	0.00	0.01	0.02	0.00	0.01	0.00	0.02
CaO	0.00	0.00	0.00	0.00	0.02	0.00	0.02	0.01	0.02	0.00	0.01	0.00
Na ₂ O	0.00	0.00	0.00	0.00	0.01	0.09	0.00	0.04	0.00	0.00	0.00	0.00
K ₂ O	0.00	0.00	0.00	0.00	0.01	0.22	0.00	0.67	0.00	0.00	0.00	0.00
ThO ₂	0.03	0.02	0.96	0.26	0.05	0.77	0.27	0.13	0.34	0.09	0.10	0.26
UO ₂	0.10	0.09	0.77	0.64	0.07	0.59	0.73	0.17	0.31	0.34	0.46	0.26
ZrO ₂	63.06	64.68	61.06	61.53	64.27	62.82	61.94	63.78	63.87	62.02	63.01	63.22
HfO ₂	2.58	2.87	3.25	2.65	2.19	3.48	3.41	2.62	2.41	3.85	2.77	2.13
P ₂ O ₅	0.00	0.01	0.18	0.33	0.04	0.00	0.15	0.32	0.23	0.23	0.10	0.09
Y ₂ O ₃	0.06	0.03	0.07	0.00	0.00	0.03	0.07	0.28	0.22	0.03	0.16	0.13
Total	100.0	99.74	100.39	99.46	99.12	101.21	99.80	99.87	99.87	100.42	99.21	100.56
Formula 4(O)												
Si	1.039	0.992	1.041	1.041	1.007	0.988	1.025	0.971	1.001	1.033	1.010	1.041
Ti	0.000	0.000	0.001	0.000	0.000	0.000	0.000	0.001	0.000	0.000	0.001	0.000
Al	0.001	0.000	0.001	0.001	0.000	0.036	0.000	0.010	0.001	0.000	0.000	0.000
Fe	0.000	0.002	0.000	0.000	0.000	0.000	0.000	0.008	0.001	0.000	0.001	0.000
Mg	0.000	0.000	0.000	0.000	0.000	0.000	0.001	0.001	0.000	0.000	0.000	0.001
Ca	0.000	0.000	0.000	0.000	0.001	0.000	0.001	0.000	0.001	0.000	0.000	0.000
Na	0.000	0.000	0.000	0.000	0.000	0.005	0.000	0.003	0.000	0.000	0.000	0.000
K	0.000	0.000	0.000	0.000	0.000	0.008	0.000	0.027	0.000	0.000	0.000	0.000
Th	0.000	0.000	0.007	0.002	0.000	0.005	0.002	0.001	0.002	0.001	0.001	0.002
U	0.001	0.001	0.005	0.004	0.000	0.004	0.005	0.001	0.002	0.002	0.003	0.002
Zr	0.936	0.980	0.911	0.918	0.971	0.940	0.932	0.968	0.961	0.923	0.954	0.932
Hf	0.022	0.025	0.028	0.023	0.019	0.030	0.030	0.023	0.021	0.033	0.025	0.018
P	0.000	0.000	0.005	0.009	0.001	0.000	0.004	0.008	0.006	0.006	0.003	0.002
Y	0.001	0.001	0.001	0.000	0.000	0.001	0.001	0.005	0.004	0.000	0.003	0.002
Total ^a	2.001	2.001	1.999	1.998	2.000	2.019	2.000	2.028	2.000	1.999	2.001	2.001
Th/U	0.27	0.27	1.27	0.42	0.82	1.33	0.39	0.79	1.10	0.26	0.23	1.01
Hf/Zr	0.02	0.03	0.03	0.03	0.02	0.03	0.03	0.02	0.02	0.04	0.03	0.02

Table C.12 Representative EPMA analyses of zircon inclusions found in sapphires from Binh Thuan.

Sample no.	PT59	PT61	PT65	PT66	PT69	PT70	PT80
SiO ₂	34.40	32.48	34.13	31.95	34.04	34.02	32.48
TiO ₂	0.01	0.00	0.00	0.00	0.04	0.00	0.00
Al ₂ O ₃	0.00	0.00	0.03	0.00	0.02	0.02	0.00
FeO	0.03	0.00	0.02	0.08	0.00	0.00	0.00
MgO	0.01	0.03	0.00	0.00	0.01	0.00	0.00
CaO	0.00	0.02	0.00	0.00	0.00	0.00	0.02
Na ₂ O	0.00	0.03	0.00	0.00	0.00	0.00	0.01
K ₂ O	0.00	0.01	0.00	0.00	0.00	0.00	0.01
ThO ₂	0.18	0.05	0.03	0.02	0.96	0.26	0.05
UO ₂	0.30	0.11	0.10	0.09	0.77	0.64	0.07
ZrO ₂	63.34	63.01	63.06	64.68	61.06	61.53	64.27
HfO ₂	3.14	3.04	2.58	2.87	3.25	2.65	2.19
P ₂ O ₅	0.00	0.00	0.00	0.01	0.18	0.33	0.04
Y ₂ O ₃	0.10	0.00	0.06	0.03	0.07	0.00	0.00
Total	101.51	98.78	100.00	99.74	100.39	99.46	99.12
Formula 4(O)							
Si	1.037	1.013	1.039	0.992	1.041	1.041	1.007
Ti	0.000	0.000	0.000	0.000	0.001	0.000	0.000
Al	0.000	0.000	0.001	0.000	0.001	0.001	0.000
Fe	0.001	0.000	0.000	0.002	0.000	0.000	0.000
Mg	0.000	0.001	0.000	0.000	0.000	0.000	0.000
Ca	0.000	0.001	0.000	0.000	0.000	0.000	0.001
Na	0.000	0.002	0.000	0.000	0.000	0.000	0.000
K	0.000	0.000	0.000	0.000	0.000	0.000	0.000
Th	0.001	0.000	0.000	0.000	0.007	0.002	0.000
U	0.002	0.001	0.001	0.001	0.005	0.004	0.000
Zr	0.931	0.958	0.936	0.980	0.911	0.918	0.971
Hf	0.027	0.027	0.022	0.025	0.028	0.023	0.019
P	0.000	0.000	0.000	0.000	0.005	0.009	0.001
Y	0.002	0.000	0.001	0.001	0.001	0.000	0.000
Total *	2.001	2.002	2.001	2.001	1.999	1.998	2.000
Th/U	0.62	0.45	0.27	0.27	1.27	0.42	0.82
Hf/Zr	0.03	0.03	0.02	0.03	0.03	0.03	0.02

Table C.13 Representative EPMA analyses of zircon inclusions found in sapphires from Di Linh.

Sample no.	DL01	DL02	DL03	DL04	DL13	DL18	DL20	DL26	DL40	DL43	DL44	DL46	DL47	DL48	DL58	DL60	DL61
SiO ₂	31.98	32.67	32.81	33.80	33.81	34.34	32.90	33.25	33.91	33.92	32.59	33.64	33.90	33.58	31.69	33.36	32.37
TiO ₂	0.02	0.00	0.00	0.03	0.00	0.00	0.01	0.00	0.03	0.02	0.01	0.05	0.00	0.00	0.00	0.00	0.00
Al ₂ O ₃	0.00	0.00	0.00	0.00	0.00	0.00	0.01	0.00	0.03	0.00	0.00	0.01	0.03	0.00	0.27	0.01	0.02
FeO	0.00	0.02	0.00	0.00	0.00	0.04	0.10	0.03	0.00	0.03	0.00	0.09	0.03	0.00	0.02	0.10	0.10
MgO	0.00	0.02	0.00	0.02	0.00	0.00	0.00	0.00	0.00	0.01	0.00	0.02	0.00	0.03	0.02	0.01	0.01
CaO	0.01	0.01	0.02	0.01	0.01	0.00	0.00	0.01	0.00	0.01	0.00	0.01	0.00	0.00	0.04	0.00	0.00
Na ₂ O	0.00	0.00	0.00	0.03	0.00	0.00	0.00	0.00	0.00	0.00	0.00	0.00	0.00	0.00	0.00	0.00	0.00
K ₂ O	0.00	0.00	0.00	0.00	0.00	0.00	0.00	0.00	0.00	0.02	0.00	0.00	0.00	0.01	0.00	0.00	0.00
ThO ₂	0.31	0.84	0.82	0.06	0.76	0.11	0.71	0.05	0.35	0.22	1.40	0.16	0.06	0.02	0.63	0.41	0.42
UO ₂	0.35	0.40	1.04	0.24	1.03	0.12	0.77	0.10	0.34	0.19	1.73	0.15	0.03	0.01	1.35	0.45	0.48
ZrO ₂	63.30	63.19	61.04	62.22	61.00	62.20	61.90	62.78	61.20	62.27	61.00	62.80	62.46	62.64	61.69	62.69	62.72
HfO ₂	3.20	2.42	2.45	2.93	2.35	2.51	2.60	2.85	3.15	2.35	3.08	2.27	2.63	2.46	2.92	1.82	2.21
P ₂ O ₅	0.01	0.04	0.09	0.05	0.08	0.00	0.05	0.00	0.06	0.00	0.22	0.04	0.00	0.00	0.61	0.00	0.00
Y ₂ O ₃	0.00	0.11	0.21	0.11	0.30	0.27	0.35	0.03	0.14	0.09	0.56	0.07	0.17	0.01	0.32	0.04	0.04
Total	99.18	99.74	98.46	99.48	99.34	99.60	99.41	99.09	99.19	99.12	100.58	99.31	99.30	98.75	99.56	98.88	98.37
Formula 4(O)																	
Si	1.000	1.012	1.027	1.037	1.043	1.048	1.022	1.027	1.044	1.042	1.013	1.033	1.039	1.036	0.989	1.031	1.014
Ti	0.001	0.000	0.000	0.001	0.000	0.000	0.000	0.000	0.001	0.000	0.000	0.001	0.000	0.000	0.000	0.000	0.000
Al	0.000	0.000	0.000	0.000	0.000	0.000	0.000	0.000	0.001	0.000	0.000	0.000	0.001	0.000	0.010	0.000	0.001
Fe	0.000	0.001	0.000	0.000	0.000	0.001	0.003	0.001	0.000	0.001	0.000	0.002	0.001	0.000	0.000	0.003	0.003
Mg	0.000	0.001	0.000	0.001	0.000	0.000	0.000	0.000	0.000	0.001	0.000	0.001	0.000	0.001	0.001	0.001	0.001
Ca	0.000	0.000	0.001	0.000	0.000	0.000	0.000	0.000	0.000	0.000	0.000	0.000	0.000	0.000	0.001	0.000	0.000
Na	0.000	0.001	0.000	0.002	0.000	0.000	0.000	0.000	0.000	0.000	0.000	0.000	0.000	0.000	0.000	0.000	0.000
K	0.000	0.000	0.000	0.000	0.000	0.000	0.000	0.000	0.000	0.001	0.000	0.000	0.000	0.000	0.000	0.000	0.000
Th	0.002	0.006	0.006	0.000	0.005	0.001	0.005	0.000	0.002	0.002	0.010	0.001	0.000	0.000	0.004	0.003	0.003
U	0.002	0.003	0.007	0.002	0.007	0.001	0.005	0.001	0.002	0.001	0.012	0.001	0.000	0.000	0.009	0.003	0.003
Zr	0.965	0.954	0.932	0.931	0.917	0.925	0.937	0.946	0.919	0.932	0.924	0.940	0.934	0.942	0.939	0.945	0.958
Hf	0.029	0.021	0.022	0.026	0.021	0.022	0.023	0.025	0.028	0.021	0.027	0.020	0.023	0.022	0.026	0.016	0.020
P	0.000	0.001	0.002	0.001	0.002	0.000	0.001	0.000	0.002	0.000	0.006	0.001	0.000	0.000	0.016	0.000	0.000
Y	0.000	0.002	0.003	0.002	0.005	0.004	0.006	0.000	0.002	0.001	0.009	0.001	0.003	0.000	0.005	0.001	0.001
Total*	2.000	2.002	2.001	2.002	2.001	2.002	2.002	2.001	2.000	2.002	2.002	2.001	2.001	2.001	2.001	2.002	2.002
Th/U	0.90	2.14	0.80	0.25	0.76	0.93	0.94	0.58	1.04	1.18	0.83	1.10	2.39	1.92	0.48	0.94	0.89
Hf/Zr	0.03	0.02	0.02	0.03	0.02	0.02	0.02	0.03	0.03	0.02	0.03	0.02	0.02	0.02	0.03	0.02	0.02

Table C.14 Representative EPMA analyses of zircon inclusions found in sapphires from Krong Nang.

Sample no.	KN08	KN12	KN13	KN14	KN15	KN27	KN35
SiO ₂	33.62	33.06	33.43	33.24	33.84	33.52	34.15
TiO ₂	0.01	0.04	0.00	0.03	0.01	0.02	0.00
Al ₂ O ₃	0.01	0.00	0.00	0.03	0.00	0.03	0.02
FeO	0.00	0.02	0.10	0.06	0.00	0.07	0.01
MgO	0.00	0.00	0.00	0.00	0.00	0.00	0.00
CaO	0.00	0.00	0.01	0.00	0.00	0.00	0.00
Na ₂ O	0.00	0.00	0.00	0.00	0.00	0.00	0.00
K ₂ O	0.00	0.00	0.05	0.03	0.00	0.01	0.01
ThO ₂	0.07	0.03	0.03	0.20	0.32	0.14	0.06
UO ₂	0.15	0.04	0.06	0.61	0.30	0.05	0.22
ZrO ₂	62.47	63.41	63.29	61.50	63.98	62.85	62.74
HfO ₂	2.42	2.53	2.82	2.43	2.26	2.14	2.41
P ₂ O ₅	0.13	0.00	0.09	0.12	0.08	0.08	0.17
Y ₂ O ₃	0.03	0.11	0.07	0.42	0.05	0.47	0.15
Total	98.91	99.24	99.96	98.66	100.86	99.37	99.95
Formula 4(O)							
Si	1.035	1.020	1.024	1.031	1.026	1.029	1.039
Ti	0.000	0.001	0.000	0.001	0.000	0.000	0.000
Al	0.000	0.000	0.000	0.001	0.000	0.001	0.001
Fe	0.000	0.001	0.003	0.001	0.000	0.002	0.000
Mg	0.000	0.000	0.000	0.000	0.000	0.000	0.000
Ca	0.000	0.000	0.000	0.000	0.000	0.000	0.000
Na	0.000	0.000	0.000	0.000	0.000	0.000	0.000
K	0.000	0.000	0.002	0.001	0.000	0.000	0.000
Th	0.000	0.000	0.000	0.001	0.002	0.001	0.000
U	0.001	0.000	0.000	0.004	0.002	0.000	0.002
Zr	0.937	0.954	0.945	0.930	0.946	0.941	0.930
Hf	0.021	0.022	0.025	0.021	0.020	0.019	0.021
P	0.003	0.000	0.002	0.003	0.002	0.002	0.004
Y	0.000	0.002	0.001	0.007	0.001	0.008	0.002
Total ^a	1.999	2.001	2.003	2.003	2.000	2.003	2.000
Th/U	0.48	0.81	0.51	0.34	1.09	3.05	0.29
Hf/Zr	0.02	0.02	0.03	0.02	0.02	0.02	0.02

Table C.15 Representative EPMA analyses of zircon inclusions found in sapphires from Dak Nong

Sample no.	DN04	DN05	DN06	DN14	DN15	DN20	DN21	DN22	DN23	DN24	DN25	DN29	DN31	DN32
SiO ₂	33.44	32.56	31.04	32.54	32.56	32.07	33.41	31.38	32.56	32.07	32.74	32.91	32.43	32.15
TiO ₂	0.01	0.01	0.00	0.00	0.01	0.05	0.00	0.05	0.01	0.05	0.00	0.03	0.02	0.00
Al ₂ O ₃	0.00	0.01	0.04	0.03	0.01	0.00	0.00	0.00	0.01	0.00	0.00	0.00	0.30	0.02
FeO	0.00	0.00	0.02	0.03	0.00	0.00	0.00	0.00	0.00	0.00	0.00	0.02	0.02	0.07
MgO	0.01	0.00	0.00	0.00	0.00	0.00	0.00	0.00	0.00	0.00	0.00	0.00	0.01	0.00
CaO	0.00	0.00	0.00	0.00	0.00	0.00	0.00	0.00	0.00	0.00	0.00	0.02	0.05	0.00
Na ₂ O	0.00	0.00	0.00	0.00	0.00	0.00	0.00	0.00	0.00	0.00	0.00	0.00	0.00	0.01
K ₂ O	0.01	0.00	0.00	0.00	0.00	0.00	0.00	0.00	0.00	0.00	0.00	0.00	0.00	0.01
ThO ₂	0.60	0.06	0.13	0.07	0.06	0.10	0.12	0.43	0.15	0.10	0.46	0.17	0.31	0.03
UO ₂	0.35	0.15	0.20	0.13	0.15	0.02	0.10	0.46	0.06	0.02	0.55	0.03	1.40	0.09
ZrO ₂	63.57	64.33	65.26	63.59	64.33	63.69	63.03	64.44	64.33	63.69	63.87	63.44	61.44	62.78
HfO ₂	2.93	2.89	2.98	3.19	2.89	3.03	2.81	2.23	2.89	3.03	3.09	3.05	3.70	3.27
P ₂ O ₅	0.00	0.02	0.00	0.06	0.02	0.01	0.00	0.03	0.02	0.01	0.10	0.06	0.16	0.00
Y ₂ O ₃	0.05	0.04	0.00	0.00	0.04	0.10	0.01	0.10	0.04	0.10	0.02	0.02	0.08	0.00
Total	100.97	100.07	99.66	99.64	100.07	99.07	99.49	99.13	100.07	99.07	100.83	99.74	99.91	98.42
Formula 4(O)														
Si	1.021	1.004	0.973	1.007	1.004	1.001	1.028	0.984	1.004	1.001	1.006	1.015	1.008	1.008
Ti	0.000	0.000	0.000	0.000	0.000	0.001	0.000	0.001	0.000	0.001	0.000	0.001	0.000	0.000
Al	0.000	0.001	0.001	0.001	0.001	0.000	0.000	0.000	0.001	0.000	0.000	0.000	0.011	0.001
Fe	0.000	0.000	0.000	0.001	0.000	0.000	0.000	0.000	0.000	0.000	0.000	0.000	0.000	0.002
Mg	0.000	0.000	0.000	0.000	0.000	0.000	0.000	0.000	0.000	0.000	0.000	0.000	0.001	0.000
Ca	0.000	0.000	0.000	0.000	0.000	0.000	0.000	0.000	0.000	0.000	0.000	0.001	0.002	0.000
Na	0.000	0.000	0.000	0.000	0.000	0.000	0.000	0.000	0.000	0.000	0.000	0.000	0.000	0.001
K	0.000	0.000	0.000	0.000	0.000	0.000	0.000	0.000	0.000	0.000	0.000	0.000	0.000	0.000
Th	0.004	0.000	0.001	0.000	0.000	0.001	0.001	0.003	0.001	0.001	0.003	0.001	0.002	0.000
U	0.002	0.001	0.001	0.001	0.001	0.001	0.001	0.003	0.000	0.000	0.004	0.010	0.001	0.001
Zr	0.946	0.967	0.997	0.960	0.967	0.969	0.946	0.986	0.967	0.969	0.957	0.954	0.931	0.960
Hf	0.026	0.025	0.027	0.028	0.025	0.027	0.025	0.020	0.025	0.027	0.027	0.027	0.033	0.029
P	0.000	0.000	0.000	0.002	0.000	0.000	0.001	0.001	0.000	0.000	0.003	0.002	0.004	0.000
Y	0.001	0.001	0.000	0.000	0.001	0.002	0.000	0.002	0.001	0.002	0.000	0.000	0.001	0.000
Total*	2.001	2.000	2.001	2.000	2.000	2.001	2.000	2.000	2.001	2.001	1.999	2.000	2.003	2.002
Th/U	1.75	0.42	0.69	0.55	0.42	5.11	1.22	0.95	2.56	5.11	0.85	5.80	0.23	0.29
Hf/Zr	0.03	0.03	0.03	0.03	0.03	0.03	0.03	0.02	0.03	0.03	0.03	0.03	0.04	0.03

c. Feldspar inclusion

Table C.16 Representative EPMA analyses of feldspar inclusions found in sapphires from Binh Thuan.

Sample no.	PT01	PT23	PT31	PT43	PT51	PT62	PT63	PT67	PT81
SiO ₂	68.89	64.31	67.92	64.79	63.83	65.69	65.37	63.91	64.28
TiO ₂	0.00	0.00	0.00	0.00	0.00	0.06	0.02	0.00	0.01
Al ₂ O ₃	19.70	22.39	19.30	22.67	21.27	21.50	21.11	22.85	22.45
FeO	0.00	0.06	0.42	0.01	0.04	0.03	0.04	0.06	0.23
MnO	0.00	0.00	0.00	0.00	0.03	0.00	0.00	0.00	0.00
MgO	0.00	0.000	0.01	0.00	0.00	0.00	0.00	0.00	0.00
BaO	0.02	0.03	0.02	0.00	0.05	0.09	0.04	0.09	0.05
CaO	0.00	2.98	1.05	2.09	2.94	1.39	1.58	2.36	1.66
Na ₂ O	11.37	9.02	9.96	8.62	9.71	9.85	9.63	9.47	9.79
K ₂ O	0.32	1.43	1.05	1.38	0.95	0.97	1.00	1.18	1.43
Total	100.31	100.22	99.72	99.57	98.82	99.57	98.79	99.92	99.90
Formula 8(O)									
Si	2.998	2.841	2.989	2.861	2.861	2.901	2.908	2.828	2.846
Ti	0.000	0.000	0.000	0.000	0.000	0.002	0.001	0.000	0.000
Al	1.010	1.166	1.001	1.180	1.123	1.119	1.107	1.192	1.172
Fe	0.000	0.002	0.015	0.000	0.001	0.001	0.002	0.002	0.008
Mn	0.000	0.000	0.000	0.000	0.001	0.000	0.000	0.000	0.000
Mg	0.000	0.000	0.001	0.000	0.000	0.000	0.000	0.000	0.000
Ba	0.000	0.001	0.000	0.000	0.001	0.002	0.001	0.002	0.001
Ca	0.000	0.141	0.049	0.099	0.141	0.066	0.076	0.112	0.079
Na	0.959	0.772	0.849	0.738	0.844	0.843	0.831	0.813	0.841
K	0.018	0.081	0.059	0.078	0.054	0.055	0.057	0.067	0.081
Total *	4.986	5.003	4.965	4.957	5.027	4.987	4.981	5.015	5.028
Atomic (%)									
Na%	98.2	77.7	88.7	80.7	81.2	87.5	86.2	82.0	84.0
Ca%	0.0	14.2	5.2	10.8	13.6	6.8	7.8	11.3	7.9
K%	1.8	8.1	6.1	8.5	5.2	5.7	5.9	6.7	8.1

Table C.17 Representative EPMA analyses of feldspar inclusions found in sapphires from Di Linh.

Sample no	DL17	DL22	DL25	DL27	DL28	DL31	DL34	DL36	DL41	DL51	DL53
SiO ₂	65.38	65.05	65.25	65.66	65.94	65.08	62.30	65.56	65.32	64.72	62.84
TiO ₂	0.00	0.01	0.00	0.01	0.00	0.02	0.02	0.01	0.03	0.04	0.00
Al ₂ O ₃	23.48	23.88	23.35	23.72	21.42	23.57	23.73	21.51	21.71	22.45	22.70
FeO	0.03	0.08	0.02	0.03	0.09	0.01	0.19	0.07	0.08	0.02	0.12
MnO	0.00	0.00	0.00	0.00	0.00	0.00	0.00	0.00	0.00	0.00	0.00
MgO	0.01	0.00	0.01	0.00	0.02	0.00	0.00	0.00	0.00	0.00	0.00
BaO	0.00	0.00	0.06	0.03	0.11	0.02	0.06	0.05	0.02	0.02	0.00
CaO	1.72	1.08	1.47	1.09	1.62	1.13	1.64	1.94	2.04	2.39	1.67
Na ₂ O	8.74	8.93	8.60	7.63	9.19	8.20	10.76	9.24	9.50	10.09	10.27
K ₂ O	1.49	1.61	1.41	1.60	0.80	1.60	1.02	0.81	0.68	0.98	1.45
Total	100.85	100.64	100.16	99.76	99.18	99.62	99.72	99.20	99.38	100.70	99.05
Formula 8(O)											
Si	2.849	2.840	2.858	2.872	2.914	2.860	2.775	2.901	2.888	2.842	2.815
Ti	0.000	0.000	0.000	0.000	0.000	0.001	0.001	0.000	0.001	0.001	0.000
Al	1.206	1.228	1.205	1.223	1.116	1.221	1.245	1.122	1.131	1.162	1.198
Fe	0.001	0.003	0.001	0.001	0.003	0.000	0.007	0.003	0.003	0.001	0.005
Mn	0.000	0.000	0.000	0.000	0.000	0.000	0.000	0.000	0.000	0.000	0.000
Mg	0.000	0.000	0.001	0.000	0.001	0.000	0.000	0.000	0.000	0.000	0.000
Ba	0.000	0.000	0.001	0.000	0.002	0.000	0.001	0.001	0.000	0.000	0.000
Ca	0.080	0.050	0.069	0.051	0.077	0.053	0.078	0.092	0.097	0.112	0.080
Na	0.738	0.756	0.730	0.647	0.787	0.698	0.929	0.793	0.814	0.859	0.892
K	0.083	0.090	0.079	0.089	0.045	0.090	0.058	0.046	0.038	0.055	0.083
Total *	4.958	4.968	4.944	4.884	4.945	4.923	5.095	4.957	4.972	5.033	5.073
Atomic (%)											
Na%	81.9	84.4	83.2	82.1	86.6	83.0	87.2	85.2	85.8	83.7	84.5
Ca%	8.9	5.6	7.8	6.5	8.4	6.3	7.4	9.9	10.2	10.9	7.6
K%	9.2	10.0	9.0	11.3	5.0	10.7	5.4	4.9	4.0	5.4	7.9

Table C.18 Representative EPMA analyses of feldspar inclusions found in sapphires from Krong Nang.

Sample no.	KN02	KN11	KN16	KN17	KN37	KN51	KN53
SiO ₂	65.96	65.25	64.94	62.25	64.38	65.61	65.83
TiO ₂	0.02	0.00	0.02	0.01	0.01	0.01	0.01
Al ₂ O ₃	21.18	22.51	21.56	23.13	21.79	22.20	22.86
FeO	0.09	0.07	0.01	0.20	0.07	0.05	0.09
MnO	0.00	0.01	0.00	0.00	0.00	0.00	0.00
MgO	0.00	0.00	0.02	0.00	0.00	0.00	0.00
BaO	0.07	0.02	0.00	0.06	0.00	0.00	0.07
CaO	1.71	1.51	1.98	1.91	2.24	1.11	1.54
Na ₂ O	9.31	9.00	9.92	10.81	9.22	8.50	8.73
K ₂ O	1.51	1.35	1.32	1.26	1.44	1.21	1.70
Total	99.85	99.72	99.77	99.62	99.15	98.69	100.84
Formula 8(O)							
Si	2.910	2.875	2.876	2.783	2.868	2.905	2.872
Ti	0.001	0.000	0.001	0.000	0.000	0.000	0.000
Al	1.101	1.169	1.125	1.219	1.144	1.158	1.175
Fe	0.003	0.003	0.000	0.007	0.003	0.002	0.003
Mn	0.000	0.000	0.000	0.000	0.000	0.000	0.000
Mg	0.000	0.000	0.001	0.000	0.000	0.000	0.000
Ba	0.001	0.000	0.000	0.001	0.000	0.000	0.001
Ca	0.081	0.071	0.094	0.091	0.107	0.053	0.072
Na	0.796	0.769	0.852	0.937	0.796	0.729	0.738
K	0.085	0.076	0.075	0.072	0.082	0.069	0.095
Total *	4.979	4.963	5.024	5.111	4.999	4.915	4.957
Atomic (%)							
Na%	82.8	83.9	83.5	85.2	80.8	85.7	81.6
Ca%	8.4	7.8	9.2	8.3	10.9	6.2	8.0
K%	8.8	8.3	7.3	6.5	8.3	8.1	10.5

d. Spinel inclusion

Table C.19 Representative EPMA analyses of spinel inclusions found in sapphires from Southern Vietnam.

Sample no.	Binh Thuan				Di Linh		Dak Nong		Krong Nang		Pleiku			
	PT07	PT17b	PT22	PT34	PT55	PT71	DL62	DN12	DN16	KN20a		KN42	KN43	KN47
SiO ₂	0.02	0.00	0.00	0.25	0.00	3.50	0.01	0.00	0.00	0.00	0.00	0.00	0.00	0.02
TiO ₂	0.00	0.27	0.00	1.91	0.00	5.37	0.70	0.12	0.08	0.00	0.13	0.00	0.18	0.32
Al ₂ O ₃	61.12	61.02	61.18	61.58	60.94	10.08	60.76	60.99	60.93	61.07	60.31	60.68	60.11	60.02
Cr ₂ O ₃	0.01	0.00	0.00	0.00	0.00	0.05	0.09	0.00	0.00	0.07	0.00	0.02	0.00	0.00
FeO	33.40	35.38	33.35	35.53	34.62	77.49	33.87	33.99	34.18	33.84	34.96	32.24	33.77	33.87
MnO	0.06	1.47	0.53	1.44	0.46	0.96	0.34	0.00	0.89	0.81	0.05	0.28	1.18	0.98
MgO	4.55	0.56	4.60	0.08	4.07	0.06	4.62	4.02	4.29	4.61	3.17	5.26	4.31	5.23
CaO	0.00	0.00	0.00	0.00	0.01	0.00	0.18	0.12	0.38	0.00	0.00	0.63	0.00	0.00
ZnO	0.67	0.01	0.93	0.07	0.18	0.43	0.00	0.06	0.00	0.00	0.00	0.00	0.51	0.00
NiO	0.09	0.10	0.00	0.09	0.00	0.03	0.00	0.00	0.00	0.03	0.00	0.00	0.00	0.00
Total	99.91	98.81	100.58	100.95	100.27	97.96	100.58	99.29	100.74	100.43	98.61	99.11	100.06	100.45
Formula 32(O)														
Si	0.003	0.000	0.000	0.056	0.000	0.142	0.002	0.000	0.000	0.000	0.000	0.000	0.000	0.005
Ti	0.000	0.046	0.000	0.321	0.000	0.163	0.117	0.020	0.014	0.000	0.023	0.000	0.030	0.054
Al	16.071	16.433	16.018	16.194	16.040	0.480	15.886	16.134	15.975	16.003	16.153	16.025	15.881	15.763
Cr	0.002	0.000	0.000	0.000	0.000	0.002	0.016	0.000	0.000	0.012	0.000	0.004	0.000	0.000
Fe ³⁺	0.000	0.000	0.000	0.000	0.000	0.000	0.000	0.000	0.000	0.000	0.000	0.000	0.078	0.157
Fe ²⁺	6.232	6.762	6.196	6.630	6.466	2.618	6.285	6.380	6.359	6.152	6.645	6.042	6.253	6.155
Mn	0.012	0.285	0.100	0.272	0.087	0.033	0.064	0.000	0.168	0.129	0.009	0.053	0.224	0.186
Mg	1.514	0.191	1.524	0.026	1.355	0.003	1.529	1.344	1.421	0.000	1.072	1.758	1.440	1.739
Ca	0.000	0.000	0.000	0.000	0.002	0.013	0.030	0.020	0.062	0.000	0.000	0.104	0.000	0.000
Zn	0.111	0.002	0.152	0.012	0.030	0.000	0.000	0.015	0.000	0.000	0.000	0.000	0.122	0.000
Ni	0.017	0.018	0.000	0.016	0.000	0.001	0.000	0.000	0.000	0.006	0.000	0.000	0.000	0.000
Total*	23.960	23.737	23.991	23.526	23.980	3.454	23.929	23.913	23.999	23.993	23.901	23.986	24.029	24.059
ΣR ²⁺	7.885	7.259	7.973	6.956	7.940	2.668	7.907	7.759	8.010	7.979	7.726	7.957	8.040	8.080
ΣR ³⁺	16.076	16.479	16.018	16.571	16.040	0.786	16.022	16.154	15.989	16.014	16.175	16.029	15.989	15.979

Note. ΣR²⁺ = Fe²⁺+Mn+Mg+Zn+Cu+Ni; ΣR³⁺ = Si+Ti+Al+Cr+Fe³⁺.

e. Wüstite inclusion

Table C.20 Representative EPMA analyses of wüstite inclusions found in sapphires from Binh Thuan.

Sample no.	Wüstite (FeO)-Hercynite					Wüstite (FeO)
	PT18	PT33	PT49	PT60	PT71	PT17a
SiO ₂	0.34	0.00	0.04	0.00	3.50	0.27
TiO ₂	0.52	1.08	5.89	0.52	5.37	0.22
Al ₂ O ₃	10.14	11.43	12.88	12.24	10.08	0.12
Cr ₂ O ₃	0.06	0.00	0.03	0.05	0.05	0.03
FeO	86.45	82.57	77.29	81.98	77.49	95.46
MnO	1.57	1.57	2.38	2.31	0.96	1.81
MgO	0.05	0.29	0.15	0.36	0.06	0.88
CaO	0.00	0.41	0.82	0.63	0.43	0.00
ZnO	0.00	0.00	0.00	0.00	0.00	0.00
NiO	0.00	0.00	0.08	0.00	0.03	0.00
Total	99.13	97.33	99.47	98.10	97.96	98.78
Formula 4(O)						
Si	0.015	0.000	0.002	0.000	0.142	0.013
Ti	0.017	0.035	0.178	0.017	0.163	0.008
Al	0.513	0.580	0.612	0.614	0.480	0.007
Cr	0.002	0.000	0.001	0.002	0.002	0.001
Fe ³⁺	0.000	0.000	0.000	0.000	0.000	0.000
Fe ²⁺	3.105	2.972	2.604	2.917	2.618	3.811
Mn	0.057	0.057	0.081	0.083	0.033	0.073
Mg	0.003	0.018	0.009	0.023	0.003	0.062
Ca	0.000	0.000	0.000	0.000	0.000	0.000
Zn	0.000	0.013	0.024	0.020	0.013	0.000
Ni	0.000	0.000	0.003	0.000	0.001	0.000
Total *	3.711	3.675	3.514	3.676	3.454	3.975
$\sum R^{2+}$	3.165	3.061	2.721	3.044	2.668	3.946
$\sum R^{3+}$	0.546	0.615	0.793	0.632	0.786	0.029
% Wüstite	85	83	77	83	77	99
% Hercynite	15	17	23	17	23	1

Note. $\sum R^{2+} = Fe^{2+} + Mn + Mg + Zn + Ca + Ni$. $\sum R^{3+} = Si + Ti + Al + Cr + Fe^{3+}$.



Table C.21 Representative EPMA analyses of wüstite inclusions found in sapphires from Di Linh.

Sample no.	Wüstite (FeO)-Hercynite					Wüstite (FeO)		
	DL14	DL24	DL49	DL63	DL83	DL84	DL50	DL56
SiO ₂	0.00	0.01	0.01	0.00	0.05	0.03	0.02	0.15
TiO ₂	1.53	0.92	0.00	0.00	1.07	0.61	2.33	3.25
Al ₂ O ₃	6.66	11.24	7.01	10.17	12.05	10.68	0.21	0.27
Cr ₂ O ₃	0.04	0.02	0.01	0.06	0.00	0.02	0.02	0.04
FeO	89.29	77.75	84.50	86.83	77.78	86.25	96.45	95.31
MnO	1.49	1.29	0.00	0.00	1.36	0.18	0.41	0.35
MgO	0.29	0.17	0.03	0.00	0.35	0.51	1.36	0.40
CaO	0.36	0.68	0.00	0.01	0.52	0.91	0.00	0.00
ZnO	0.00	0.00	0.00	0.00	0.00	0.00	0.00	0.29
NiO	0.00	0.00	0.00	0.00	0.01	0.05	0.03	0.00
Total	99.66	92.07	91.56	97.07	93.18	94.24	100.84	100.06
Formula 4(O)								
Si	0.000	0.001	0.001	0.000	0.002	0.001	0.001	0.007
Ti	0.051	0.031	0.000	0.000	0.036	0.020	0.081	0.113
Al	0.346	0.601	0.397	0.529	0.631	0.538	0.011	0.015
Cr	0.001	0.001	0.000	0.002	0.000	0.001	0.001	0.001
Fe ³⁺	0.000	0.000	0.000	0.000	0.000	0.000	0.000	0.000
Fe ²⁺	3.291	2.950	3.400	3.203	2.887	3.081	3.708	3.681
Mn	0.056	0.050	0.000	0.000	0.051	0.007	0.016	0.014
Mg	0.019	0.011	0.002	0.000	0.023	0.032	0.093	0.027
Ca	0.012	0.023	0.000	0.000	0.017	0.029	0.000	0.000
Zn	0.000	0.000	0.000	0.000	0.000	0.000	0.000	0.014
Ni	0.000	0.000	0.000	0.000	0.000	0.002	0.001	0.000
Total *	3.776	3.667	3.801	3.734	3.647	3.710	3.912	3.872
ΣR ²⁺	3.378	3.034	3.402	3.203	2.978	3.151	3.818	3.736
ΣR ³⁺	0.398	0.634	0.398	0.531	0.669	0.560	0.094	0.136
%Wüstite	89	83	90	86	82	85	98	96
%Hercynite	11	17	10	14	18	15	2	4

Note. Σ R²⁺ = Fe²⁺+Mn+Mg+Zn+Ca+Ni. ΣR³⁺ = Si+Ti+Al+Cr+Fe³⁺.

Table C.22 Representative EPMA analyses of wüstite inclusions found in sapphires from Dak Nong, Krong Nang, and Pleiku.

Sample no.	Wüstite (FeO)-Hercynite								
	Dak Nong			Krong Nang			Pleiku		
	DN73	DN74	DN89	KN05	KN19	KN20a	GL27	GL85	GL87
SiO ₂	0.33	0.03	0.02	1.58	0.06	0.00	0.34	0.00	0.00
TiO ₂	4.43	0.84	1.57	6.62	1.24	0.00	0.00	1.33	0.85
Al ₂ O ₃	12.51	9.85	8.78	10.82	11.84	5.61	11.39	6.18	6.95
Cr ₂ O ₃	0.18	0.01	0.00	0.33	0.03	0.00	0.03	0.00	0.05
FeO	77.55	88.13	87.90	75.75	86.30	85.30	86.25	82.50	82.79
MnO	0.00	0.2	0.14	0.08	0.18	2.25	0.00	0.88	0.86
MgO	0.98	0.35	0.18	0.15	0.37	0.13	0.00	0.30	0.33
CaO	0.12	0.67	0.33	0.31	0.51	0.68	0.07	0.37	0.33
ZnO	0.43	0.00	0.00	0.12	0.00	0.00	0.00	0.00	0.00
NiO	0.02	0.02	0.00	0.10	0.00	0.01	0.05	0.02	0.00
Total	96.56	100.11	98.92	95.86	100.52	93.97	98.12	91.58	92.15
Formula 4(O)									
Si	0.014	0.001	0.001	0.065	0.002	0.000	0.015	0.000	0.000
Ti	0.138	0.027	0.051	0.206	0.039	0.000	0.000	0.048	0.030
Al	0.611	0.496	0.450	0.527	0.580	0.315	0.577	0.349	0.389
Cr	0.006	0.000	0.000	0.011	0.001	0.000	0.001	0.000	0.002
Fe ³⁺	0.000	0.000	0.000	0.000	0.000	0.000	0.000	0.000	0.000
Fe ²⁺	2.687	3.147	3.194	2.620	3.001	3.403	1.507	3.309	3.284
Mn	0.000	0.007	0.005	0.003	0.006	0.091	0.000	0.036	0.034
Mg	0.060	0.022	0.012	0.009	0.023	0.009	0.000	0.022	0.023
Ca	0.004	0.021	0.011	0.009	0.016	0.024	0.002	0.013	0.011
Zn	0.019	0.000	0.000	0.005	0.000	0.000	0.000	0.000	0.000
Ni	0.001	0.001	0.000	0.003	0.000	0.000	0.002	0.001	0.000
Total *	3.540	3.723	3.723	3.460	3.660	3.842	3.697	3.777	3.774
∑R ²⁺	2.771	3.198	3.222	2.649	3.046	3.527	1.511	3.381	3.352
∑R ³⁺	0.769	0.524	0.502	0.809	0.622	0.315	0.593	0.397	0.421
%Wüstite	78	86	87	77	83	92	84	89	89
%Hercynite	22	14	13	23	17	8	16	11	11

Note. $\sum R^{2+} = \text{Fe}^{2+} + \text{Mn} + \text{Mg} + \text{Zn} + \text{Ca} + \text{Ni}$. $\sum R^{3+} = \text{Si} + \text{Ti} + \text{Al} + \text{Cr} + \text{Fe}^{3+}$.

f. Ilmenite inclusion

Table C.23 Representative EPMA analyses of ilmenite inclusions found in sapphires from Dak Nong, Di Linh, and Pleiku.

Sample no.	Titanohematite			Titanomagnetite	
	Dak Nong	Di Linh	Pleiku	Pleiku	
	DN39	DL23	DL85	GL28	GL25
SiO ₂	0.11	0.10	0.00	0.08	0.17
TiO ₂	34.94	37.08	33.77	34.89	18.48
Al ₂ O ₃	0.02	1.50	0.58	1.14	3.25
Cr ₂ O ₃	0.00	0.04	0.12	0.05	0.00
FeO	61.43	61.58	63.48	63.00	76.12
MnO	0.14	0.06	0.05	0.09	0.64
MgO	0.00	0.18	0.64	0.07	0.06
CaO	0.80	0.00	0.00	0.00	0.00
ZnO	0.00	0.01	0.00	0.00	0.04
NiO	0.02	0.00	0.03	0.06	0.00
Total	97.46	100.54	98.67	99.38	99.11
Formula 4(O)					
Si	0.006	0.006	0.000	0.005	0.000
Ti	1.499	1.514	1.437	1.463	1.310
Al	0.001	0.096	0.039	0.075	0.435
Cr	0.000	0.002	0.005	0.002	0.001
Fe ³⁺	1.318	1.168	1.430	1.319	1.265
Fe ²⁺	1.612	1.629	1.573	1.618	1.411
Mn	0.007	0.003	0.002	0.004	0.042
Mg	0.000	0.014	0.054	0.006	0.006
Ca	0.049	0.000	0.000	0.000	0.000
Zn	0.000	0.000	0.000	0.000	0.000
Ni	0.001	0.000	0.001	0.003	0.000
Total *	4.494	4.431	4.541	4.494	4.471
ΣR ²⁺	1.668	1.646	1.630	1.630	1.459
ΣR ³⁺	2.825	2.785	2.911	2.864	3.012
%Ilmenite	53.1	54.4	49.4	51.1	24.0
%Magnetite	6.8	6.9	8.3	9.5	40.0
%hematite	38.7	33.7	39.8	35.5	35.5

Note. $\Sigma R^{2+} = Fe^{2+} + Mn + Mg + Zn + Ca + Ni$. $\Sigma R^{3+} = Si + Ti + Al + Cr + Fe^{3+}$.

g. Pyrochlore inclusion

Table C.24 Representative EPMA analyses of pyrochlore inclusions found in sapphires from Dak Nong and Krong Nang.

Sample no.	Dak Nong			Krong Nang	
	DN35	DN42	DN77	KN18	KN36
SiO ₂	0.23	0.16	0.37	0.55	0.33
TiO ₂	11.67	11.38	11.20	10.59	11.63
Al ₂ O ₃	0.00	0.00	0.00	0.00	0.00
FeO	1.68	1.00	1.38	1.54	1.57
MnO	0.37	0.41	0.19	0.08	0.03
CaO	6.86	6.41	6.63	6.26	6.89
Na ₂ O	4.33	5.11	4.73	4.44	5.24
K ₂ O	0.04	0.00	0.05	0.06	0.09
Nb ₂ O ₅	33.61	32.83	32.24	33.88	33.03
Ta ₂ O ₅	6.05	6.30	6.50	5.97	6.34
ThO ₂	7.88	8.00	7.31	7.00	7.61
UO ₂	22.28	20.48	23.06	23.83	22.32
ZrO ₂	0.08	0.00	0.15	0.01	0.02
Y ₂ O ₃	0.00	0.00	0.08	0.12	0.08
La ₂ O ₃	0.00	0.00	0.00	0.00	0.00
Ce ₂ O ₃	0.12	0.81	0.35	0.34	0.28
Nd ₂ O ₃	0.14	0.25	0.167	0.00	0.06
Sm ₂ O ₃	0.00	0.00	0.00	0.00	0.00
Pr ₂ O ₃	0.00	0.000	0.007	0.00	0.000
Gd ₂ O ₃	0.00	0.061	0.025	0.04	0.073
F	0.00	0.000	0.114	0.00	0.062
SrO	0.051	0.000	0.000	0.000	0.057
Total	95.41	93.18	94.54	94.71	95.70
Formula 6(O)					
Si	0.016	0.011	0.026	0.039	0.022
Ti	0.604	0.603	0.588	0.557	0.599
Al	0.000	0.000	0.000	0.000	0.000
Fe	0.097	0.059	0.081	0.090	0.090
Mn	0.022	0.024	0.011	0.005	0.002
Ca	0.506	0.483	0.496	0.468	0.506
Na	0.578	0.698	0.640	0.601	0.696
K	0.003	0.000	0.004	0.005	0.008
Nb	1.046	1.045	1.018	1.070	1.023
Ta	0.113	0.121	0.123	0.113	0.118
Th	0.123	0.128	0.116	0.111	0.119
U	0.341	0.321	0.358	0.370	0.340
Zr	0.003	0.000	0.005	0.000	0.001
Y	0.000	0.000	0.003	0.005	0.003
La	0.000	0.000	0.000	0.000	0.000
Ce	0.003	0.021	0.009	0.009	0.007
Nd	0.004	0.006	0.004	0.000	0.001
Sm	0.000	0.000	0.000	0.000	0.000
Pr	0.000	0.000	0.000	0.000	0.000
Gd	0.000	0.001	0.001	0.001	0.002
F	0.000	0.000	0.025	0.000	0.013
Sr	0.002	0.000	0.000	0.000	0.002
Total *	3.461	3.523	3.508	3.444	3.553

APPENDIX D

TRACE ELEMENT DATA OF ZIRCON INCLUSIONS

Table D.1 Trace element contents (ppm) of zircon inclusions in sapphire from Binh Thuan

Analysis (ppm)	PT05-1	PT05-2	PT08-1	PT13-1	PT52-1	PT53-1	PT53-2	PT68-1
P	426.47	488.04	326.84	163.26	190.54	182.09	189.12	186.68
Y	2868.13	3852.09	1870.56	1015.23	1275.32	1109.14	1516.93	1010.95
Nb	267.46	108.03	35.87	10.97	28.92	10.90	13.31	23.36
La	0.0035	0.0046	0.0064	bdl	0.8420	bdl	0.0037	0.0037
Ce	13.330	8.300	4.910	2.611	3.810	1.387	1.918	3.340
Pr	0.0523	0.0409	0.0307	0.0089	0.1304	0.0088	0.0118	0.0177
Nd	1.451	0.869	0.376	0.147	0.783	0.152	0.234	0.309
Sm	5.620	4.850	1.809	0.886	1.193	0.851	1.112	1.261
Eu	2.177	2.143	1.322	0.808	0.901	0.870	1.159	0.828
Gd	44.06	48.84	18.99	8.82	11.43	8.52	12.10	11.96
Tb	21.66	25.51	11.08	5.32	6.42	5.01	7.11	6.16
Dy	310.13	390.23	174.45	87.84	107.85	87.27	123.26	95.25
Ho	104.29	137.94	64.32	34.89	44.44	37.41	51.13	35.65
Er	442.14	615.22	296.48	175.47	231.29	203.96	263.42	168.00
Tm	89.21	127.55	61.72	40.67	54.52	48.81	60.87	37.01
Yb	721.34	1052.43	520.68	373.51	519.19	461.74	565.44	337.58
Lu	81.67	123.5	67.14	52.01	72.14	72.14	80.21	46.04
Hf (wt%)	2.68	2.57	1.78	1.80	1.98	2.02	1.96	2.32
Ta	92.45	36.47	11.47	3.82	7.58	4.24	5.11	9.10
Th	5198.78	2839.46	893.88	328.52	720.19	389.59	621.01	516.95
U	3586.87	2234.69	476.45	223.50	630.63	384.53	529.47	398.93
Total REE	1815.47	2511.92	1212.23	777.67	1048.52	923.12	1160.87	737.25
Th/U	1.45	1.27	1.88	1.47	1.14	1.01	1.17	1.30
U/Yb	4.97	2.12	0.92	0.60	1.21	0.83	0.94	1.18
Nb/Ta	2.89	2.96	3.13	2.87	3.82	2.57	2.60	2.57
Eu/Eu*	0.14	0.14	0.23	0.29	0.24	0.32	0.32	0.21

bdl = below detection limit.



Table D.2 Trace element contents (ppm) of zircon inclusions in sapphire from Di Linh.

Analysis (ppm)	DL04-4	DL09-1	DL26-1	DL26-2	DL43-2	DL45-1	DL46-2
P	486.39	412.78	325.35	208.50	189.57	384.70	347.90
Y	2152.97	1959.97	1317.53	855.27	1083.13	2958.54	4220.35
Nb	36.19	127.00	82.05	13.79	68.18	38.27	50.02
La	0.03	0.01	bdl	0.01	0.01	bdl	0.00
Ce	6.79	15.25	5.41	1.39	5.69	7.38	12.00
Pr	0.03	0.05	0.02	0.01	0.02	0.03	0.06
Nd	0.50	0.97	0.48	0.17	0.51	0.71	1.11
Sm	2.43	3.83	2.18	0.72	1.93	3.35	5.62
Eu	1.73	2.52	0.95	0.57	1.55	1.97	5.12
Gd	22.47	29.54	16.73	7.70	14.19	34.14	54.66
Tb	12.79	14.69	8.46	4.34	7.03	18.37	27.58
Dy	202.47	205.55	128.08	73.07	104.93	281.15	416.17
Ho	74.66	67.66	47.51	29.69	38.33	104.78	152.71
Er	344.21	284.02	224.87	153.29	182.07	483.38	672.98
Tm	73.64	56.24	50.46	37.00	40.33	101.97	134.11
Yb	640.79	455.03	465.81	354.84	362.75	869.08	1115.50
Lu	76.52	51.10	57.09	50.06	48.12	109.02	140.18
Hf (wt%)	1.75	1.85	2.79	2.53	2.06	2.30	1.84
Ta	10.52	39.88	47.38	5.19	26.34	14.52	18.72
Th	1100.88	3902.22	1821.65	359.79	2294.10	2162.18	3117.02
U	500.22	1169.92	1745.95	377.38	1224.58	1190.42	1129.58
Total REE	1446.27	1171.77	999.59	708.52	800.44	1996.96	2710.22
Th/U	2.20	3.34	1.04	0.95	1.87	1.82	2.76
U/Yb	0.78	2.57	3.75	1.06	3.38	1.37	1.01
Nb/Ta	3.44	3.18	1.73	2.66	2.59	2.64	2.67
Eu/Eu*	0.23	0.24	0.16	0.24	0.30	0.18	0.29

bdl = below detection limit.



Table D.3 Trace element contents (ppm) of zircon inclusions in sapphire from Krong Nang.

Analysis (ppm)	KN08-1	KN08-2	KN13-1	KN13-2	KN13-3	KN15-1
P	470.66	511.39	367.31	611.27	506.44	482.76
Y	1152.08	1194.74	1554.72	3220.31	2234.17	779.04
Nb	20.56	23.14	26.38	26.01	27.91	20.69
La	0.0027	0.0079	0.0033	bdl	0.0142	0.0428
Ce	1.621	1.651	5.070	7.030	5.900	1.221
Pr	0.0173	0.0184	0.0257	0.0299	0.0331	0.0190
Nd	0.244	0.257	0.344	0.581	0.581	0.319
Sm	0.802	0.676	1.807	3.010	2.540	0.935
Eu	0.602	0.592	1.190	2.235	1.694	0.425
Gd	6.11	5.74	16.04	31.02	22.19	6.66
Tb	3.82	3.91	8.69	17.34	12.24	3.35
Dy	73.96	76.25	136.67	275.23	192.24	56.50
Ho	36.36	38.25	52.35	107.79	75.09	25.38
Er	249.39	258.42	262.46	535.92	374.17	158.25
Tm	79.43	83.73	61.89	122.52	87.55	46.01
Yb	1008.86	1081.30	592.80	1145.31	838.47	538.72
Lu	175.84	179.34	80.45	156.11	112.45	101.69
Hf (wt%)	1.11	1.10	1.90	1.78	1.84	1.55
Ta	9.51	10.23	12.35	8.59	9.44	12.63
Th	410.23	377.95	877.20	1077.40	880.46	337.95
U	316.18	337.75	1165.76	1340.48	1106.94	387.13
Total REE	1633.24	1726.23	1211.1	2386.79	1712.92	936.17
Th/U	1.30	1.12	0.75	0.80	0.80	0.87
U/Yb	0.31	0.31	1.97	1.17	1.32	0.72
Nb/Ta	2.16	2.26	2.14	3.03	2.96	1.64
Eu/Eu*	0.27	0.30	0.22	0.23	0.23	0.17

Table D.4 Trace element contents (ppm) of zircon inclusions in sapphire from Dak Nong.

Analysis (ppm)	DN05-1	DN06-2	DN06-3	DN20-1	DN20-3	DN20-4	DN20-5	DN22-1	DN32-3
P	266.43	284.26	297.51	232.92	295.53	289.85	321.25	274.74	234.88
Y	1468.21	1082.58	1643.69	1074.27	1299.99	1280.83	1367.57	1860.92	1090.09
Nb	20.76	20.44	92.00	57.25	50.80	23.51	29.19	91.10	106.80
La	0.02	0.01	0.00	0.02	0.04	0.01	0.01	0.01	0.00
Ce	2.79	1.85	5.34	4.81	4.86	2.69	3.06	30.80	9.29
Pr	0.01	0.01	0.03	0.03	0.03	0.01	0.02	0.17	0.04
Nd	0.27	0.20	0.57	0.51	0.52	0.27	0.30	3.30	0.86
Sm	1.23	1.11	2.40	1.85	1.75	1.28	1.39	7.88	3.07
Eu	0.96	0.56	1.07	1.03	1.05	0.82	0.86	3.00	2.21
Gd	12.91	10.56	19.28	14.48	15.17	12.50	13.24	43.69	21.26
Tb	7.23	5.81	9.46	6.97	7.61	6.68	7.26	16.21	9.35
Dy	121.92	94.76	144.94	104.41	118.16	109.26	118.30	201.88	126.08
Ho	50.02	37.61	55.63	37.93	45.37	44.16	47.36	64.87	40.31
Er	258.30	188.84	269.60	180.07	223.73	225.89	240.74	264.23	165.94
Tm	60.40	44.11	59.99	39.25	50.80	52.85	56.79	51.48	32.92
Yb	566.33	415.91	544.91	352.23	474.38	502.27	542.85	432.17	271.81
Lu	80.77	57.72	73.78	47.05	64.14	70.89	75.78	50.92	32.06
Hf (wt%)	2.19	2.34	2.28	2.37	2.31	2.30	2.27	1.57	2.11
Ta	7.77	6.42	37.78	26.98	21.60	7.82	9.46	33.03	38.79
Th	753.05	567.39	2041.62	1433.67	1679.10	600.63	724.19	3510.55	4261.19
U	559.67	588.61	1481.11	1082.82	1154.16	608.81	687.23	1167.55	1856.08
Total REE	1155.94	853.25	1177.54	783.67	1000	1022.9	1100.69	1154.4	705.85
Th/U	1.35	0.96	1.38	1.32	1.45	0.99	1.05	3.01	2.30
U/Yb	0.99	1.42	2.72	3.07	2.43	1.21	1.27	2.70	6.83
Nb/Ta	2.67	3.18	2.44	2.12	2.35	3.01	3.09	2.76	2.75
Eu/Eu*	0.24	0.16	0.16	0.20	0.20	0.21	0.20	0.16	0.27



REFERENCES

- Akinin, V., Vysotskiy, S., Coble, M.A. and Aseeva, A., 2017. U–Pb age and geochemistry of zircon inclusions in sapphire: Alkali basaltic source of gems in placers of Primorye. *Doklady Earth Sciences*, 476: 1173-1176.
- Andersen, T., 2002. Correction of common lead in U–Pb analyses that do not report ^{204}Pb . *Chemical Geology*, 192: 59–79.
- Anh, H.T.H., Choi, S.H., Yu, Y., Hieu, P.T., Hoang, N.K. and Ryu, J., 2018. Geochemical constraints on the spatial distribution of recycled oceanic crust in the mantle source of late Cenozoic basalts, Vietnam. *Lithos*, 296: 382-395.
- Aspen, P., Upton, B.G.J. and Dickin, A.P., 1990. Anorthoclase, sanidine and associated megacrysts in Scottish alkali basalts: high-pressure syenitic debris from upper mantle sources? *European Journal of Mineralogy*, 2(4): 503-518.
- Barr, S. and MacDonald, A., 1981. Geochemistry and geochronology of late Cenozoic basalts of Southeast Asia: Summary. *Geological Society of America Bulletin*, 92(8): 1069-1142.
- Belousova, E., Griffin, W., O'Reilly, S. and Fisher, N., 2002. Igneous zircon: Trace element composition as an indicator of source rock type. *Contributions to Mineralogy and Petrology*, 143(5): 602-622.
- Benisek, A. and Finger, F., 1993. Factors controlling the development of prism faces in granite zircons: a microprobe study. *Contributions to Mineralogy and Petrology*, 114(4): 441-451.
- Bosshart, G., 1995. Sapphires and rubies from Laos, 25th International Gemmological Conference Program, Rayong, Thailand, pp. 23-26.
- Buddington, A.F., Fahey, J.J. and Vlisidis, A.C., 1955. Thermometric and petrogenetic significance of titaniferous magnetite. *American Journal of Science*, 253(9): 497-532.
- Buddington, A.F. and Lindsley, D.H., 1964. Iron-Titanium Oxide Minerals and Synthetic Equivalents. *Journal of Petrology*, 5(2): 310-357.
- Carter, A., Roques, D., Bristow, C. and Kinny, P., 2001. Understanding Mesozoic accretion in Southeast Asia: Significance of Triassic thermotectonism (Indosinian orogeny) in Vietnam. *Geology*, 29(3): 211-214.

- Cassidy, K., Groves, D. and Binns, R., 1988. Manganian ilmenite formed during regional metamorphism of Archean mafic and ultramafic rocks from Western Australia. *Canadian Mineralogist*, 26: 999-1012.
- Černý, P. and Ercit, T.S., 1985. Some recent advances in the mineralogy and geochemistry of Nb and Ta in rare-element granitic pegmatites. *Bulletin de Minéralogie*, 108: 499-532.
- Coenraads, R., 1992. Sapphires and rubies associated with volcanic provinces: inclusions and surface features shed light on their origin. *Australia Gemmology*, 18(3): 70-78.
- Coenraads, R., Sutherland, F. and Kinny, P., 1990. The origin of sapphires: U-Pb dating of zircon inclusions sheds new light. *Mineralogical Magazine*, 54(374): 113-122.
- Coldham, T., 1985. Sapphire from Australia. *Gem & Gemology*, 21(3): 130-146.
- Compston, W., 1999. Geological age by instrumental analysis; the 29th Hallimond Lecture. *Mineralogical Magazine*, 63(3): 297-311.
- Cynn, H., Sharma, S.K., Cooney, T.F. and Nicol, M., 1992. High-temperature Raman investigation of order-disorder behavior in the MgAl₂O₄ spinel. *Physical Review B Condensed Matter*, 45(1): 500-502.
- Deer, W.A., Howie, R.A. and Zussman, J., 2013. *An Introduction to the Rock-Forming Minerals*, Longman, Essex, UK, 696 pp.
- Droop, G.T.R., 1987. A general equation for estimating Fe³⁺ concentrations in ferromagnesian silicates and oxides from microprobe analyses, using stoichiometric criteria. *Mineralogical Magazine*, 51(361): 431-435.
- Elhlou, S., Belousova, E., Griffin, B., Pearson, N. and O'Reilly, S., 2006. Trace element and isotopic composition of GJ red zircon standard by Laser Ablation. *Geochimica et Cosmochimica Acta* 70(18): A158.
- Faria, D.L.A., Silva, S.V. and Oliveira, M.T.M., 1997. Raman microspectroscopy of some iron oxides and oxyhydroxides. *Journal of Raman Spectroscopy*, 28: 873-878.
- Flower, M., Hoang, N., Yem, N., Bao, N., McCabe, R. and Harder, S., 1992. Cenozoic magmatism in Indochina: lithosphere extension and mantle potential temperature. *Bulletin of the Geological Society of Malaysia*, 33: 211-222.

- Fuhrman, M.L., Frost, B.R. and Lindsley, D.H., 1988. Crystallization Conditions of the Sybille Monzosyenite, Laramie Anorthosite Complex, Wyoming. *Journal of Petrology*, 29: 699.
- Garnier, V., Ohnenstetter, D., Giuliani, G., Fallick, A.E., Trinh, P., Quang, V., Van, L. and Schwarz, D., 2005. Basalt petrology, zircon ages and sapphire genesis from Dak Nong, southern Vietnam. *Mineralogical Magazine*, 69(1): 21-38.
- Griffin, W., Powell, W.J., Pearson, N.J. and O'Reilly, S., 2008. GLITTER: data reduction software for laser ablation ICP-MS. *Short Course Series*, 40: 308-311.
- Gübelin, E.J., 1983. *Internal world of gemstones*. ABC Edition, Zurich.
- Guo, J., Griffin, W.L. and O'Reilly, S.Y., 1994. A cobalt-rich spinel inclusion in a sapphire from Bo Ploi, Thailand. *Miner. Mag*, 58: 247-258.
- Guo, J., O'Reilly, S.Y. and Griffin, W.L., 1996b. Corundum from basaltic terrains: a mineral inclusion approach to the enigma. *Contributions to Mineralogy and Petrology*, 122(4): 368-386.
- Guo, J., O'Reilly, S.Y. and Griffin, W.L., 1996c. Zircon inclusions in corundum megacrysts: I. Trace element geochemistry and clues to the origin of corundum megacrysts in alkali basalts. *Geochimica et Cosmochimica Acta*, 60(13): 2347-2363.
- Haggerty, S.E., 1991. Oxide mineralogy of the upper mantle, in "Oxide Minerals: Petrologic and Magnetic Significance", D.H. Lindley, ed. *Rev. Mineral.*, 25. Mineralogical Society of America, Washington, DC, pp. 355-416.
- Hanesch, M., 2009. Raman spectroscopy of iron oxides and (oxy)hydroxides at low laser power and possible applications in environmental magnetic studies. *Geophysical Journal International*, 177(3): 941-948.
- Hazen, R. and Jeanloz, R., 1984. Wüstite (Fe_{1-x}O): A review of its defect structure and physical properties. *Reviews of Geophysics*, 22(1): 37-46.
- Heaman, L., Bowins, R.J. and Crocket, J., 1990. The chemical composition of igneous zircon suites: implications for geochemical tracer studies. *Geochimica et Cosmochimica Acta*, 54(6): 1597-1607.
- Hoa, T.T., Phuong, N.T., Anh, T.T., Van, V.V., Y, N.V., Hoang, N., Thanh, H.H., Anh, P.L., Nien, B.A., Hung, T.Q., Dung, P.T., Lam, T.H., Hang, H.V., Anh, T.V.,

- Chuong, V.D., Hung, P.V., Quan, V.M. and eds., 2005. Study of forming conditions and distribution laws of precious and rare minerals related to magmatic activity in Central Vietnam and Tay Nguyen Highlands. State-level Project, code DTDL-2003/07, I: 347 pp (in Vietnamese).
- Hoang, N. and Flower, M., 1998. Petrogenesis of Cenozoic Basalts from Vietnam: Implication for Origins of a 'Diffuse Igneous Province'. *Journal of Petrology*, 39(3): 369-395.
- Hoang, N., Flower, M., Chi, C., Xuan, P., Quy, H. and Son, T., 2013. Collision-induced basalt eruptions at Pleiku and Buôn Mê Thuôt, south-central Viet Nam. *Journal of Geodynamics*, 69: 65–83.
- Hoang, N., Flower, M., Nguyen, X. and Nguyen, T., 1996. Trace element and isotopic compositions of Vietnamese basalts: Implications for mantle dynamics in the southeast Asian region. *Bulletin de la Societe Geologique de France*, 167(6): 785-795.
- Hogarth, D.D., 1977. Classification and nomenclature of the pyrochlore group. *American Mineralogist*, 62(5-6): 403-410.
- Huong, L.T.T., Vuong, B.T.S., Khoi, N.N., Satitkune, S., Wanthachaisaeng, B., Hofmeister, W., Haeger, T. and Hauzenberger, C., 2016. Geology, Gemmological Properties and Preliminary Heat Treatment of Gem-Quality Zircon from the Central Highlands of Vietnam. *Journal of Gemmology*, 35(4): 308-318.
- Hutchison, C., 2014. Tectonic evolution of Southeast Asia. *Bulletin of the Geological Society of Malaysia*, 60: 1-18.
- Hutchison, C.S., 1989. *Geological Evolution of South-east Asia*. Clarendon Press.
- Izokh, A.E., Smirnov, S.Z., Egorova, V.V., Anh, T.T., Kovyazin, S.V., Phuong, N.T. and Kalinina, V.V., 2010. The conditions of formation of sapphire and zircon in the areas of alkali-basaltoid volcanism in Central Vietnam. *Russian Geology and Geophysics*, 51(7): 719-733.
- Jackson, S., Pearson, N.J., Griffin, W. and Belousova, E., 2004. The application of laser ablation microprobe-inductively coupled plasma-mass spectrometry to in situ U-Pb zircon geochronology. *Chemical Geology*, 211: 11-37.

- Jobbins, E.A. and Berrangé, J.P., 1981. The Pailin Ruby and Sapphire Gemfield, Cambodia. *Journal of Gemmology*, 17: 555-567.
- Jozwiak, W., Kaczmarek, E., Maniecki, T., Ignaczak, W. and Maniukiewicz, W., 2007. Reduction behavior of iron oxides in hydrogen and carbon monoxide atmospheres. *Applied Catalysis A-general* 326(1): 17-27.
- Karsli, O., Aydin, F., Uysal, İ. and Sadiklar, M., 2008. Magma Interaction Processes Inferred from Fe-Ti Oxide Compositions in the Dölek and Sarıçiçek Plutons, Eastern Turkey. *Turkish Journal of Earth Sciences*, 17: 297-315.
- Keller, A.S. and Keller, P., 1986. The Sapphires of Mingxi, Fujian Province, China. *Gems & Gemology*, 22(1): 41-45.
- Keller, P.C., 1982. The Chanthaburi-Trat gem field, Thailand. *Gem & Gemology*, 18(3): 186-196.
- Khamloet, P., Pisutha-Arnond, V. and Sutthirat, C., 2014. Mineral inclusions in sapphire from the basalt-related deposit in Bo Phloi, Kanchanaburi, western Thailand: Indication of their genesis. *Russian Geology and Geophysics*, 55(9): 1087–1102.
- Lattard, D., 1995. Experimental evidence for the exsolution of ilmenite from titaniferous spinel. *American Mineralogist*, 80(9): 968-981.
- Lee, T., Lo, C.-H., Chung, S.-L., Chen, C.-Y., Wang, P.-L., Lin, W.-P., Hoang, N., Chi, C. and Yem, N., 1998. $^{40}\text{Ar}/^{39}\text{Ar}$ Dating Result of Neogene Basalts in Vietnam and its Tectonic Implication. *Mantle Geodynamics and Plate Interactions in East Asia*, AGU Monograph, 27: 317-330.
- Lepvrier, C., Vuong, N., Maluski, H., Thi, P. and Tich, V., 2008. Indosinian tectonics in Vietnam. *Comptes Rendus Geoscience* 340(2): 94-111.
- Levinson, A.A. and Cook, F.A., 1994. Gem corundum in alkali basalt: origin and occurrence. *Gem & Gemology*, 30(4): 253-262.
- Li, X.-H., Liang, X., Sun, M., Liu, Y. and Tu, X., 2000. Geochronology and geochemistry of single-grain zircons Simultaneous in-situ analysis of U-Pb age and trace elements by LAM-ICP-MS. *European Journal of Mineralogy*, 12(5): 1015-1024.
- Lindsley, D.H., 1991. Experimental studies of oxide minerals. *Reviews in Mineralogy and Geochemistry*, 25(1): 69-106.

- Liu, Y., Li, Q., Tang, G., Li, X.-H. and Yin, Q.-Z., 2015. Towards higher precision SIMS U-Pb zircon geochronology via dynamic multi-collector analysis. *Journal of Analytical Atomic Spectrometry* 30(4): 979-985.
- Long, P.V., Vinh, H., Garnier, V., Giuliani, G., Ohnenstetter, D., Lhomme, T., Schwarz, D., Fallick, A.E., Dubessy, J. and Trinh, P.T., 2004. Gem corundum deposits in Vietnam. *Journal of Gemmology* 29(3): 129-147.
- Mackay, D. and Simandl, G., 2015. Pyrochlore and columbite-tantalite as indicator minerals for specialty metal deposits. *Geochemistry: Exploration, Environment, Analysis*, 15(2-3): 167-178.
- Mbih, K.P., Meffre, S., Yongue, R.F., Kanouo, N.S. and Jay, T., 2016. Chemistry and origin of the Mayo Kila sapphires, NW region Cameroon (Central Africa): their possible relationship with the Cameroon Volcanic Line. *Journal of African Earth Sciences*, 118: 263-273.
- Metcalf, I., 1988. Origin and assembly of South-east Asian continental terranes. Geological Society, London, Special Publications, 37(1): 101-118.
- Metcalf, I., 1996. Pre-Cretaceous evolution of SE Asian terranes. Geological Society, London, Special Publications, 106(1): 97-122.
- Metcalf, I., 2009. Late Palaeozoic and Mesozoic tectonic and palaeogeographical evolution of SE Asia, in Buffetaut, E., Cuny, G., Le Loeuff, J., and Suteethorn, V., Eds., Late Palaeozoic and Mesozoic Ecosystems in SE Asia. The Geological Society of London, Special Publication, 315(1): 7-23.
- Metcalf, I., 2011. Palaeozoic-Mesozoic history of SE Asia. Geological Society of London Special Publications, 355(1): 7-35.
- Miyashiro, A., 1964. Oxidation and reduction in the Earth's crust with special reference to the role of graphite. *Geochimica et Cosmochimica Acta*, 28(5): 717-729.
- Nestola, F., Periotto, B., Anzolini, C., Andreozzi, G., Woodland, A., Lenaz, D., Alvaro, M. and Princivalle, F., 2015. Equation of state of hercynite, FeAl₂O₄, and high-pressure systematics of Mg-Fe-Cr-Al spinels. *Mineralogical Magazine*, 79(2): 285-294.

- Nguyen, T., Satir, M., Siebel, W. and Chen, F., 2004. Granitoids in the Dalat zone, southern Vietnam: Age constraints on magmatism and regional geological implications. *International Journal of Earth Sciences*, 93(3): 329-340.
- Ospitali, F., Sabetta, T., Tullini, F., Nannetti, M. and Lonardo, G., 2005. The role of Raman microspectroscopy in the study of black gloss coatings on Roman pottery. *Journal of Raman Spectroscopy*, 36(1): 18-23.
- Palke, A.C., Saeseaw, S., Renfro, N.D., Sun, Z. and McClure, S., 2019. Geographic origin determination of blue Sapphire. *Gems & Gemology*, 55(4): 536-579.
- Pin, C., Monchoux, P., Paquette, J.L., Azambre, B., Wang, R. and Martin, R., 2006. Igneous albitite dikes in orogenic Iherzolites, western Pyrenees, France: A possible source for corundum and alkali feldspar xenocrysts in basaltic terranes. II. Geochemical and petrogenetic considerations. *Canadian Mineralogist* 44(4): 843-856.
- Promwongnan, S. and Sutthirat, C., 2019b. Mineral Inclusions in Ruby and Sapphire from the Bo Welu Gem Deposit in Chanthaburi, Thailand. *Gems & Gemology*, 55(3): 354-369.
- Pupin, J.P., 2000. Granite genesis related geodynamics from Hf-Y in zircon. *Transactions of the Royal Society of Edinburgh: Earth Sciences*, 91: 245-256.
- Raman, R., Gleeson, B. and Young, D., 1998. Laser Raman spectroscopy: A technique for rapid characterisation of oxide scale layers. *Materials Science and Technology*, 14(5): 373-376.
- Rangin, C., Huchon, P., Le Pichon, X., Bellon, H., Lepvrier, C., Roques, D., Hoe, N.D. and Quynh, P.V., 1995. Cenozoic deformation of Central and South Vietnam. *Tectonophysics*, 251(1-4): 180-196.
- Rosa, M.L.S., Conceicao, H., Marinho, M.M., Macambira, M.J.B. and Marques, L.S., 2002. Geochronology of the South Bahia Alkaline Province (NE Brazil). *Geochimica et Cosmochimica Acta*, 66: A648.
- Rubatto, D. and Gebauer, D., 2000. Use of Cathodoluminescence for U-Pb Zircon Dating by Ion Microprobe: Some Examples from the Western Alps, In book: *Cathodoluminescence in Geosciences*, pp. 373-400.

- Saminpanya, S. and Sutherland, F., 2011. Different origins of Thai area sapphire and ruby, derived from mineral inclusions and co-existing minerals. *European Journal of Mineralogy*, 23(4): 683-694.
- Schollenbruch, K., Woodland, A.B. and Frost, D.J., 2010. The stability of hercynite at high pressures and temperatures. *Physics and Chemistry of Minerals*, 37(3): 137-143.
- Seifert, W., Thomas, R., Rhede, D. and Förster, H.J., 2010. Origin of coexisting wüstite, Mg-Fe and REE phosphate minerals in graphite-bearing fluorapatite from the Rumburk granite. *European Journal of Mineralogy*, 22: 495-507.
- Shebanova, O. and Lazor, P., 2003. Raman Study of Magnetite (Fe₃O₄): Laser-Induced Thermal Effects and Oxidation. *Journal of Raman Spectroscopy*, 34(11): 845-852.
- Shellnutt, J., Lan, C.-Y., Long, T., Usuki, T., Yang, H.-J., Mertzman, S., Iizuka, Y., Chung, S.-L., Wang, K.-L. and Hsu, W.-Y., 2013. Formation of Cretaceous Cordilleran and post-orogenic granites and their microgranular enclaves from the Dalat zone, southern Vietnam: Tectonic implications for the evolution of Southeast Asia. *Lithos*, 182-183: 229-241.
- Shore, M. and Fowler, A., 1996. Oscillatory zoning in minerals: A common phenomenon. *Canadian Mineralogist*, 34(6): 1111-1126.
- Smith, C.P., Kammerling, R.C., Keller, A.S., Peretti, A., Scarratt, K.V., Khoa, N.D. and Repetto, S., 1995. Sapphires from Southern Vietnam. *Gems and Gemmology*, 31(3): 168-186.
- Smyth, J., Jacobsen, S. and Hazen, R., 2000. Comparative crystal chemistry of dense oxide minerals. *Reviews in Mineralogy and Geochemistry*, 41(1): 157-186.
- Stacey, J.S.T. and Kramers, J.D., 1975. Approximation of terrestrial lead isotope evolution by a two-stage model. *Earth Planetary Science Letters*, 26(2): 207-221.
- Sutherland, F., Bosshart, G., Fanning, C., Hoskin, P.W.O. and Coenraads, R., 2002. Sapphire crystallization, age and origin, Ban Huai Sai, Laos: Age based on zircon inclusions. *Journal of Asian Earth Sciences*, 20(7): 841-849.
- Sutherland, F., Hoskin, P., Fanning, C. and Coenraads, R., 1998a. Models of corundum origin from alkali basaltic terrains: A reappraisal. *Contributions to Mineralogy and Petrology*, 133(4): 356-372.

- Sutherland, F., Schwarz, D., Jobbins, E.A., Coenraads, R. and Webb, G., 1998b. Distinctive gem corundum suites from discrete basalt fields: a comparative study of Barrington, Australia and West Pailin, Cambodia, Gemfields. *Journal of Gemmology*, 26(2): 65-85.
- Sutherland, F.L. and Coenraads, R.R., 1996. An unusual ruby-sapphire-sapphirine-spinel assemblage from the Tertiary Barrington volcanic province, New South Wales, Australia. *Mineralogical Magazine* 60 (401): 623-638.
- Sutherland, F.L., Coenraads, R.R., Abduriyim, A., Meffre, S., Hoskin, P.W.O., Giuliani, G., Beattie, R., Wuhler, R. and Sutherland, G.B., 2015a. Corundum (sapphire) and zircon relationships, Lava Plains gem fields, NE Australia: Integrated mineralogy, geochemistry, age determination, genesis and geographical typing. *Mineralogical Magazine*, 79(3): 545-581.
- Sutherland, F.L., Pilonen, P.C., Zaw, K., Meffre, S. and Thompson, J., 2015b. Sapphire within zircon-rich gem deposits, Bo Loei, Ratanakiri Province, Cambodia: trace elements, inclusions, U–Pb dating and genesis. *Australian Journal of Earth Sciences*, 62(6): 761-773.
- Sutherland, F.L., Zaw, K., Meffre, S., Giuliani, G., Fallick, A.E., Graham, L. and Webb, G.B., 2009. Gem-corundum megacrysts from east Australian basalt fields: Trace elements, oxygen isotopes and origins. *Australian Journal of Earth Sciences*, 56(7): 1003-1022.
- Sutthirat, C., Pisutha-Arnond, V., Khamloet, P. and Assawincharoenkij, T., 2020. Multistages of original sapphire formation related to basaltic magmatism in the Bo Phloi basaltic gem field, Kanchanaburi, Western Thailand: Evidence from trace elements and ages of zircons. *Journal of Asian Earth Sciences*, 187: 104068.
- Tan, W., Liu, P., He, H., Wang, C. and Liang, X., 2016. Mineralogy and Origin of Exsolution In Ti-Rich Magnetite From Different Magmatic Fe-Ti Oxide-Bearing Intrusions. *Canadian Mineralogist*, 54: 539-553.
- Taylor, S.R. and McLennan, S.M., 1985. The continental crust: Its composition and evolution. Blackwell Scientific Pub., Palo Alto, CA, 328 pp.
- Thibeau, R.J., Brown, C.W. and Heidersbach, R.H., 1978. Raman Spectra of Possible Corrosion Products of Iron. *Applied Spectroscopy*, 32(6): 532-535.

- Tri, T.V. and Khuc, V., 2011. *Geology and Earth Resources of Vietnam*. General Department of Geology and Minerals of Vietnam, Ha Noi, Publishing House for Science and Technology, 634 pp.
- Turnock, A.C. and Eugster, H., 1962. Fe Al Oxides: Phase Relationships below 1,000°C. *Journal of Petrology*, 3(3): 533-565.
- Upton, B., Finch, A. and Słaby, E., 2009. Megacrysts and salic xenoliths in Scottish alkali basalts: Derivatives of deep crustal intrusions and small-melt fractions from the upper mantle. *Mineralogical Magazine*, 73(6): 943-956.
- Vincent, E.A., 1960. Ulvöspinel in the Skaergaard intrusion, Greenland. *Neues Jahrbuch für Mineralogie - Abhandlungen*, 94: 993-1016.
- Vu, D.T.A., 2010. *Petrographical characteristics and genesis of Corundum in Vietnam*, University of Science, VNU-Hochiminh City, 120 pp.
- Vu, D.T.A., 2018. Gemological characteristics and the quality of sapphire from Krong H'Nang - Dak Lak. *Science and Technology Development Journal - Natural Sciences*, 1(T5): 263-269.
- Wang, A., Kuebler, K., Jolliff, B. and Haskin, L., 2004. Raman spectroscopy of Fe-Ti-Cr-Oxides, case study: martian meteorite EETA79001. *American Mineralogist*, 89: 665-680.
- Williams, I.S. and Claesson, S., 1987. Isotopic evidence for the Precambrian provenance and Caledonian metamorphism of high grade paragneisses from the Seve Nappes, Scandinavian Caledonides. *Contributions to Mineralogy and Petrology*, 97(2): 205-217.
- Zaw, K., Sutherland, F.L., Dellapasqua, F., Ryan, C.G., Yui, T., Mernagh, T.P. and Duncan, D., 2006. Contrasts in gem corundum characteristics, eastern Australian basaltic fields: Trace elements, fluid/melt inclusions and oxygen isotopes. *Mineralogical Magazine* 70: 669-687.

VITA

NAME Doan Thi Anh Vu

DATE OF BIRTH 23 March 1977

PLACE OF BIRTH Thua Thien - Hue province

INSTITUTIONS ATTENDED High school from Nguyen Du High School.
Bachelor's Degree (B.Sc. in Geology) from University of Science - Vietnam National University Ho Chi Minh City.
Master's Degree (M.Sc. in Geology) from University of Science - Vietnam National University Ho Chi Minh City.
Ph.D. candidate (Ph.D. in Geology) from Chulalongkorn University, Thailand.

HOME ADDRESS 58/3T Dong Nai Street, Ward 15, 10th District, Ho Chi Minh City, Vietnam

AWARD RECEIVED The Scholarship Program for ASIAN Countries of Chulalongkorn University.